ANALYSIS OF VTOL HANDLING QUALITIES REQUIREMENTS

PART II. LATERAL-DIRECTIONAL HOVER AND TRANSITION

SAMUEL J. CRAIG
ANTHONY CAMPBELL
Systems Technology, Inc.

*** Export controls have been removed ***

This document is subject to special export controls and each transmittal to foreign governments or foreign nationals may be made only with prior approval of the Handling Qualities Group, Control Criteria Branch, Air Force Flight Dynamics Laboratory, Wright-Patterson Air Force Base, Ohio 45433.

FOREWORD

This report presents the results of the second phase of an analytical effort to analyze and consolidate the available VTOL handling qualities data. This effort covers manual control aspects for the lateral/directional mode in the hover and transition flight regimes.

The work was performed by Systems Technology, Inc., Hawthorne, California, under the sponsorship of the Air Force Flight Dynamics Laboratory, Directorate of Laboratories, Air Force Systems Command, Wright-Patterson Air Force Base, Ohio. The research was conducted from July 1966 to June 1968 under Subcontract S-68-37 to the Cornell Aeronautical Laboratory as Part III of the VTOL Integrated Flight Control Systems Program (VIFCS), Contract No. AF33(615)-3736, Project 698DC, and the report was submitted for approval as STI TR-181-1. The RTD project engineer was Mr. Wilfred Klotzback and the CAL project engineer was Mr. Charles Chalk.

The authors gratefully acknowledge the technical and editorial contributions made by Mr. I. L. Ashkenas, and the efforts of the STI publication staff in assembling the report.

C. B. Westbrook
C. B. WESTBROOK
Chief, Control Criteria Branch
Flight Control Division

ABSTRACT

Analyses of available handling qualities data were performed to determine lateral/directional dynamic requirements for VTOL aircraft in hover and low speed flight.

The basis for this treatment is an examination of the pilot/vehicle as a closed-loop servo system. The quasi-linear pilot describing function is applied. The results of the studies suggest that the primary factors identifying satisfactory and unacceptable hover mode dynamic features are related to the closed-loop deficiencies.

Detailed consideration is made of the control task and piloting functions in transition flight. The results of this generic appraisal are evoked to confirm and justify preliminary lateral/directional requirement for control in transition.

CONTENTS

Page

I. INTRODUCTION. 1

II. MANUAL CONTROL REQUIREMENTS FOR LATERAL HOVER. 3

A. Lateral Dynamic Requirements 3

III. CONSIDERATION OF PRACTICAL CONTROL SYSTEM ASPECTS IN HOVER . . 26

A. Effects of Direct Force Control-Coupling Terms 26

B. Effects of Control System Dynamics and Nonlinearities . . 36

IV. ASPECTS OF LATERAL/DIRECTIONAL CONTROL IN LOW SPEED AND TRANSITION FLIGHT 61

A. Generic Aspects of Closed-Loop Manual Control in Transition 61

B. Consideration of Experimental Results 81

V. CONCLUDING REMARKS. 113

A. Preliminary Lateral Hover Dynamics Requirements 113

B. Lateral/Directional Control in Transition and Low Speed Flight. 114

C. Consideration of Future Experimental Programs. 114

REFERENCES. 115

APPENDIX A. PILOT/VEHICLE ANALYSIS FOR LATERAL HOVER A-1

APPENDIX B. EFFECTS OF CONTROL SYSTEM LAGS AND DELAYS ON CLOSED-LOOP SYSTEM. B-1

APPENDIX C. STABILITY DERIVATIVES FOR DIRECT FORCE CONTROL COUPLING ANALYSES IN HOVER C-1

APPENDIX D. SUMMARY OF AERODYNAMIC STABILITY DERIVATIVES FOR LATERAL/DIRECTIONAL STUDIES. D-1

APPENDIX E. CALCULATION OF CLOSED-LOOP RMS GUST RESPONSES FOR LATERAL/DIRECTIONAL MODE. E-1

APPENDIX F. SYSTEMS SURVEYS SHOWING EFFECTS OF RUDDER COUPLING TERMS, L_{δ_r}, OR MANUAL ATTITUDE CONTROL TASK F-1

FIGURES

Page

1. Satisfactory Handling Qualities Roll Rate Damping Requirements Implied from Transfer Function Factors. 8

2. Category I, Dynamic Requirements for Hover Mode 11

3. Correlation of Handling Quality Data with Suggested Boundaries . 14

4. Basic Oscillatory Mode Dynamic Requirements; Category II System, $1/T_E > 1/T_R$ 14

5. Comparison of Lateral Dynamic Requirements for Category II Augmentation Systems ($1/T_E > 1/T_R$) and Ref. 2 Data 17

6. Comparison of Lateral Dynamic Requirements for Category II Augmentation Systems ($1/T_E > 1/T_R$) with Experimental Data. . . 18

7. Oscillatory Mode Requirements for Category II ($1/T_E > 1/T_R$) Attitude Stabilized Systems; Comparison with Ref. 10 19

8. Hover Mode Dynamic Requirements for Attitude Augmentation Systems Composite of Categories I and II 21

9. Rate Ordering Command System Dynamic Requirements, Ref. 10 . . 24

10. Attitude Loop Control with Direct Force Control Coupling, $\theta \rightarrow \delta_{STK}$. 30

11. Position Loop Control with Direct Force Control Coupling, $x, \theta \rightarrow \delta_{STK}$. 32

12. Effect of Axial Force Control Term, X_δ/M_δ, Airspeed Closure . . 34

13. Effect of M_q and X_δ/M_δ on Airspeed Control; $X_\delta/M_\delta = -4$ ft. . . . 35

14. Elements of Control Feel System Characteristics 37

15. Effect of Actuator Lag ($1/T_c$) 40

16. Effects of Longitudinal Control Lag on Handling Qualities of XV-4B Aircraft 41

17. Effect of Transport Lag 43

18. Effect of Control System Backlash of Pilot/Vehicle Attitude Loop 44

19. Effect of Increasing Backlash on Amplitude of Predicted Limit Cycle (Satisfactory Case Example). 45

Page

20. Effect of Control System Threshold on Pilot/Vehicle Loop . . 47
21. Effect of Actuator Velocity Saturation on Pilot/Vehicle Loop . 48
22. Effect of Actuator Velocity Saturation of Stable Vehicle . . . 49
23. Effect of Valve Friction and Flow Forces on Effective Actuator Dynamics 51
24. Considerations of Valve Friction on Manual Control 52
25. Effect of SAS Saturation on Vehicle Dynamics 53
26. Experimental Effects of Pitch Rate Stabilization Authority on Handling Qualities 54
27. Effect of Stability Augmentation Authority Limits on Pilot Rating 56
28. Pilot Ratings versus Controlled Element Gain 57
29. Predicted Breakout Force Required to Produce Pilot Opinion Degradation from PR = 2.5 to PR = 7.3 for Ref. 2 Satisfactory Data 58
30. Breul Data — Unacceptable Case 59
31. Breakout Force That May Produce Limit Cycling 59
32. Manual Bank Angle Control in Initial Transition; XC-142A . . . 65
33. Manual Bank Angle Control in Midtransition; XC-142A 65
34. Manual Bank Angle Control in End Transition; XC-142A 65
35. Heading Control During Initial Transition 67
36. Heading Control During Midtransition 68
37. Heading Control During End Transition 69
38. Multiloop Lateral Displacement Control with Ailerons 73
39. Heading Control During Initial Transition 76
40. Heading Control During Midtransition 77
41. Heading Control During End Transition 78
42. Heading Control with Aileron Using Rudder Coordination; ψ, $\varphi \rightarrow \delta_a$, $\beta \rightarrow \delta_r$; Initial Transition (Hover) 80

Page

43. Heading Control with Aileron Using Rudder Coordination; $\psi, \varphi \rightarrow \delta_a, \beta \rightarrow \delta_r$; Midtransition 80

44. Heading Control with Aileron Using Rudder Coordination; $\psi, \varphi \rightarrow \delta_a, \beta \rightarrow \delta_r$; End Transition 81

45. Correlation of Lateral Numerator Damping Factor, $\zeta_\varphi \omega_\varphi$ (or $1/T_{\varphi_1}$), with Pilot Rating, taken from Ref. 20 84

46. Comparison of Handling Qualities Boundaries for Various Values of Dihedral Effect, Circuit Flying Task; from Ref. 22 86

47. Multiloop Heading Closure with Rudder for Moderate Dihedral $(L_v = -0.02)$ and Pilot Rating of 3-1/2 87

48. Regulatory Control of Heading; Multiloop; $\psi \rightarrow \delta_r, \varphi \rightarrow \delta_a$ . . 89

49. Lateral/Directional Control Cross-Coupling Handling Qualities Boundaries (Reproduced from Ref. 25). 93

50. Attitude Regulatory Closure with Rudder for High Proverse Yaw and Pilot Rating of 6-1/2 95

51. Heading Closure with Rudder for $N_{\delta_a} = 0$ and Pilot Rating of 3-1/2 96

52. Heading Closure with Rudder for Low Adverse Yaw and Pilot Rating of 3-1/2. 97

53. Heading Closure with Rudder for High Adverse Yaw and Pilot Rating of 6-1/2. 98

54. Basic Coordination Loop, Sideslip Control with Rudder, $\beta \rightarrow \delta_r$. 104

55. Effects of Sideslip Closure on Attitude Numerator 105

56. Bank Angle Control with Rudder Coordination, $\varphi \rightarrow \delta_a, \beta \rightarrow \delta_r$. 106

57. Effect of Sideslip Closure on Yaw Rate Numerator. 107

58. Coordination Control with Large Adverse Control Cross Coupling Terms, N_{δ_a} and L_{δ_r}. 108

59. Bank Angle Control with Large Proverse Control Coupling Terms . 110

A-1. Large Y_v, Attitude Rate Augmentation, φ/δ_a. A-12

A-2. Attitude Augmentation Block Diagram A-13

A-3. Classification Scheme for Attitude Augmentation System. . . . A-14

Page

A-4. Attitude Response Features of Category II ($1/T_E > 1/T_R$) Systems A-17

A-5. Comparison of Helicopter Attitude Loop Dynamics with and without Attitude Stabilization (Ref. 27); $\varphi \rightarrow \delta_a$ A-18

A-6. Effective Translation Augmentation, $Y_v \gg L_p$ and $1/T_R \doteq 1/T_\varphi \doteq Y_v$ A-20

A-7. Roll Attitude Loop Closure for Satisfactory Dynamics ($PR = 2.7$); $\varphi \rightarrow \delta_a$ A-28

A-8. Roll Attitude Loop Closure for Unacceptable Dynamics ($PR = 7.3$); $\varphi \rightarrow \delta_a$ A-29

A-9. Effect of Increased Attitude Loop Lead — Satisfactory Case; $\psi \rightarrow \delta_a$ A-30

A-10. Effect of Increasing Attitude Loop Lead — Unacceptable Case . . A-31

A-11. Lateral Position Loop Closure, Satisfactory Dynamics, $y, \varphi \rightarrow \delta_a$ (with and without Pilot Lead) A-32

A-12. Lateral Position Loop Closure, Unacceptable Dynamics, $y, \varphi \rightarrow \delta_a$ (with and without Pilot Lead) A-33

A-13. Roll Attitude Loop Closure for Large Lateral Side Force ($Y_v \gg 0$), $\varphi \rightarrow \delta_a$. A-34

A-14. Position Loop Closure with Large Lateral Side Force ($Y_v \gg 0$), $y, \varphi \rightarrow \delta_a$. A-35

A-15. Roll Attitude Closure for Category I System, $1/T_E < 1/T_R$, $\varphi \rightarrow \delta_a$ A-36

A-16. Position Loop Closure for Category I System, $1/T_E < 1/T_R$; $y, \varphi \rightarrow \delta_a$ A-37

A-17. Roll Attitude Control for Category II System, $1/T_E < 1/T_R$; $\varphi \rightarrow \delta_a$ A-42

A-18. Lateral Position Control for Category II System, $1/T_E > 1/T_R$; $y, \varphi \rightarrow \delta_a$ A-43

A-19. Roll Attitude Control of Category II System for Various Pilot Compensation Levels A-44

A-20. Lateral Position Loop Closure for Category II System; $y, \varphi \rightarrow \delta_a$ A-45

A-21. Position Closure with Attitude Augmentation System, $1/T_E > 1/T_R$, $\omega_d \geq 2.0$ rad/sec, $y \rightarrow \varphi_c$ A-46

A-22. Position Closure with Attitude Augmentation, $1/T_E > 1/T_R$, $\omega_d \geq 2.0$ rad/sec, $y \rightarrow \delta_a$ A-47

A-23. Roll Attitude Control, Translational Augmentation; Satisfactory Dynamics, $\varphi \rightarrow \delta_a$. A-48

A-24. Lateral Position Control, Translational Augmentation, Satisfactory Dynamics, y, $\varphi \rightarrow \delta_a$. A-49

A-25. Roll Attitude Control Translational Augmentation, Unacceptable Dynamics, $\varphi \rightarrow \delta_a$. A-50

A-26. Lateral Position Control, Translational Augmentation, Unacceptable Dynamics, y, $\varphi \rightarrow \delta_a$. A-51

A-27. Roll Attitude Gust Asymptotes $|N^{\varphi''}_{v_g}/\Delta''|$ (without Gust Filter). . A-57

A-28. Roll Attitude Power Spectrum (No Position Loop Lead) A-58

A-29. Control Power Spectrum $\Phi_{L_\delta \delta}$ (No Position Loop Lead). A-59

A-30. Lateral Displacement Gust Asymptotes $|N^{y''}_{v_g}/\Delta''|$ (without Gust Filter). A-61

A-31. Roll Attitude Power Spectrum (With Position Loop Lead). . . . A-62

A-32. Control Power Spectrum $\Phi_{L_\delta \delta}$ with Position Loop Lead. A-63

A-33. Estimated Effect of Position-Loop Compensation on Error Performance A-65

A-34. Roll Attitude Gust Asymptotes (without Gust Filter). A-67

A-35. Roll Attitude Gust Asymptotes (Comparison between Satisfactory and Unacceptable) A-68

A-36. Roll Attitude Response Spectra. A-69

A-37. Roll Attitude Response Spectra. A-70

A-38. Lateral Position Asymptotes for Various Levels of Y_v A-73

A-39. Lateral Position Response Spectra, Satisfactory Response . . . A-74

A-40. Lateral Position Response Spectra, Unacceptable Dynamics . . . A-75

F-1. Heading Closure with Rudder for $N_{\delta_a} = 0$, $L_{\delta_r} = -0.4$ and Pilot Rating of 3-1/2. . . . . F-2

F-2. Heading Closure with Rudder for $N_{\delta_a} = 0$, $L_{\delta_r} = -1.2$ and Pilot Rating of 6-1/2. . . . . F-3

F-3. Heading Closure with Rudder for $N_{\delta_a} = 0$, $L_{\delta_r} = +1.0$ and Pilot Rating of 6-1/2. . . . . F-4

TABLES

Page

I. Effective Lateral Controlled Element Forms for Conventional VTOL Systems . . . 5

II. Comparison Between Longitudinal and Lateral Criteria Covering Satisfactory and Unacceptable Rating Levels for Conventional VTOL Dynamic Features . . . 7

III. Attitude Augmentation System . . . 9

IV. Controlled-Element Forms for Translational Rate Augmentation [Position-Loop Feedback, $\delta_T/v = K_v(T_v s + 1)$] . . . 25

V. Control Structures and Feedback Function for Closed-Loop Tasks . . . 62

VI. Summary of RMS Responses for $\sigma_{v_g} = 1.0$ FT/SEC . . . 90

VII. Effect of Aileron Coupling on Heading Performance . . . 100

A-I. Open-Loop Parameters for Selected Cases . . . A-2

A-II. Open-Loop Properties for VTOL Configuration with Attitude Rate Augmentation $(1/T_E \leq 1/T_R)$ . . . A-3

A-III. Category I $(1/T_E \leq 1/T_R)$ Attitude Rate Augmentation System . . . A-4

A-IV. Category II $(1/T_E > 1/T_R)$ Attitude Augmentation Systems . . . A-5

A-V. Open-Loop Properties for VTOL Configuration with Translational Augmentation $(Y_v > L_p)$ . . . A-6

A-VI. Conventional Lateral Dynamic Configurations . . . A-7

A-VII. Conventional Lateral Dynamic Configurations . . . A-9

A-VIII. Lateral Dynamic Configurations . . . A-10

A-X. Summary of Gust Response Characteristics for Various Y_v/L_v Relations . . . A-71

C-I. Data for Control Coupling Studies by Gallagher, Ref. 16 . . . C-1

C-II. Data for Control Coupling Study by Bruel, Ref. 17 . . . C-2

D-I. Lateral/Dimensional Derivatives for the XC-142 . . . D-2

D-II. XC-142 Lateral/Directional Transfer Function for the Aileron and Rudder Controls . . . D-3

D-III. Lateral/Directional Derivatives and Transfer Function Factors . . . D-5

D-IV. Lateral/Directional Derivatives and Transfer Functions Control Coupling Study . . . D-6

SYMBOLS

b	Airplane wing span
c.g.	Center of gravity
dB	Decibel $\equiv 20 \log_{10} \lvert\ \rvert = \lvert\ \rvert_{dB}$
g	Acceleration due to gravity
G(s)	Open-loop transfer function; also specific transfer function if particularized by subscript(s)
$G(-\sigma)$ $G(j\omega)$	G(s) with s replaced by $-\sigma$ and $j\omega$, respectively; for $G(-\sigma) < 0$, values of $\lvert G(-\sigma) \rvert = 1$ identify real roots
h	Altitude perturbation
I	Moment of inertia
I_x, I_y, I_z	Moments of inertia about x-, y-, and z-axes, respectively
I_{xz}	Product of inertia in xz-plane
j	$\sqrt{-1}$
$j\omega$	The imaginary portion of the complex variable $s = \sigma \pm j\omega$
K	Bode gain of controlled element, particularized by subscript
K_M	Gain margin
K_{p_λ}	Pilot gain of λ degree of freedom
L	Integral scale of turbulence
L	Rolling moment/I_x which acts on the vehicle and arises from torques produced by the subscript
L_i'	$[L_i + (I_{xz}/I_x)N_i]/[1 - (I_{xz}^2/I_x I_z)]$ where i refers to any motion or input quantity
L_p	$\partial L/\partial p$, roll damping term
L_r	$\partial L/\partial r$
L_β or L_v	$\partial L/\partial \beta$ or $\partial L/\partial v$, moment due to sideslip angle or lateral velocity
m	Mass of aircraft

M	Pitching moment/I_y
M_q	$\partial M/\partial q$
M_u	$\partial M/\partial u$
M_w	$\partial M/\partial w$
M_δ	$\partial M/\partial \delta$
N_p	$\partial N/\partial p$
N_r	$\partial N/\partial r$
$N(s)$	Transfer function numerator
N_β or N_v	$\partial N/\partial \beta$ or $\partial N/\partial v$, yawing moment due to sideslip angle or lateral velocity
N_δ	$= \partial N/\partial \delta$, directional control sensitivity term
$N^{\lambda_1 \lambda_2}_{\delta_1 \delta_2}$	Coupling numerator relating output motion quantity to control deflection, particularized by subscripts
$N^{\lambda}_{\delta}(s)$	Numerator of transfer function relating output motion quantity to control deflection, particularized by subscripts
POR or PR	Pilot's rating
q	Dynamic pressure
q	Pitch rate, angular velocity about the y-axis, positive nose going up
r	Yaw rate, angular velocity about z-axis, positive nose right
RHP	Right half plane
rms	Root mean square
s	Laplace operator, $\sigma \pm j\omega$
S	Wing area
SAS	Stability Augmentation System
t	Time
$1/T$	Inverse time constant, particularized by subscript
T_E	Equalization time constant, attitude loop, $K_\theta/K_{\dot{\theta}}$

T_I	Human pilot lag time constant
T_L	Human pilot lead time constant
T_N	Human pilot neuromuscular time constant
T_u	Equalization time constant, position loop, K_{ax}/K_u
T_λ	Time constant of λ zero or pole
$T_{\lambda_i \lambda_j}$	Coupling numerator time constant for variables $\lambda_i \lambda_j$
u	Perturbation velocity along x-axis
u_g	Gust velocity along x-axis
U_o	Steady-state velocity along x-axis
v	Perturbation velocity along y-axis
V	Resultant velocity, $V = \sqrt{(U_o + u)^2 + v^2 + w^2}$
w	Perturbation velocity along z-axis
W	Vehicle weight
x	Horizontal displacement in direction of x-axis
X	Force in x-direction divided by aircraft mass
X_q	$= \partial X/\partial q$
X_u	$= \partial X/\partial u$
X_δ	$= \partial X/\partial \delta$
y	Lateral displacement in direction of y-axis
Y	Side force produced in y-direction
Y_f	Transfer function of filter
Y_p	$= \partial Y/\partial p$, side force due to rolling velocity
$Y_{p(\lambda)}$	Human pilot transfer function, particularized with respect to general variable
Y_r	$= \partial Y/\partial r$, side force due to yawing velocity
z	Vertical displacement in direction of z-axis, positive downward

Z	Force in z-direction divided by aircraft mass
Z_q	$= \partial Z/\partial q$
Z_u	$= \partial Z/\partial u$
Z_w	$= \partial Z/\partial w$
Z_δ	$= \partial Z/\partial \delta$
α	Angle of attack, $\doteq w/U_o$
β	Angle of sideslip, $= v/V$
γ	Perturbed flight path angle, $\theta - \alpha$
δ	Control deflection (positive: forward stick or stick right)
$\Delta(s)$	Denominator of airframe transfer functions; characteristic equation when set equal to zero
ζ	Damping ratio of linear second-order transfer function quantity, particularized by subscript
θ	Pitch angle
θ_1	Pitch angle response in 1 sec
λ	General variable (u, v, w, θ, φ, ψ, etc.)
λ_o	Thrust vector angle at trim condition
σ	Real part of s
σ_λ	Root-mean-squared value of λ
τ	Time delay
τ_e	Effective pilot time delay, τ plus neuromuscular time constant
φ	Phase angle, degrees
φ_M	Phase margin
Φ_λ	λ power spectrum
ω	Imaginary part of s
ω_c or ω_{c_o}	Crossover frequency
ω_{c_λ}	Crossover frequency of general closed-loop variable
ω_λ	Undamped natural frequency of λ zero or pole

Special Subscripts:

c	Command; crossover; controlled element (vehicle), collective
CL	Closed loop
e	Error, or elevator's pitch control (longitudinal cyclic)
eff	Effective
g	Gust
h	Altitude numerator for control input
hi	High frequency
o	Basic (unperturbed) condition
OL	Open-loop
p	Phugoid
p	Pilot
r	Yaw control (tail rotor or differential lateral cyclic)
R	Roll subsidence
s	Spiral
sp	Short-period
ss	Steady state
T	Throttle; thrust; lag
u	Airspeed numerator for control input

Special Superscripts:

$(\ )'$ $(\ )''$	Primes denoting loop closure. Primes on a transfer function or time constant indicate that it has been modified by inner-loop closures, the number of primes corresponding to the number of closures.
$(\dot{\ })$	Denotes derivative with respect to time, d/dt
$(\ddot{\ })$	Denotes second derivative with respect to time, d^2/dt^2

Mathematical Symbols:

$<$	Less than
$>$	Greater than
$<<$	Much less than
$>>$	Much greater than
$/$	Not (e.g., $\neq$, not equal to); divided by
$\doteq$	Approximately equal to
$\rightarrow$	Fed to; approaches
∂	Partial differential
λ/δ	Generalized transfer function, $\lambda(s)/\delta(s)$
$]$	Outer loop with inner loop(s) closed
$\measuredangle$	Angle
$\vert\ \vert$	Modulus
e	2.7183
×	Pole
⊙	Zero (root of numerator)
▮	Closed-loop root
$(1/T_i)$	First-order factors of transfer function
$[\zeta_i, \omega_i]$	Second-order factors of transfer function

Notational Rules for Closed-Loop Quantities:

1. The number of primes present indicates the number of loops closed previously.

2. The notation for the closed-loop factor is the same as that for the open-loop factor (plus a prime) when the closed-loop and open-loop forms are the same. In this case the origin of the closed-loop factor is always at hand (e.g., $\omega_d \rightarrow \omega_d'$, $\omega_\varphi \rightarrow \omega_\varphi'$, $T_R \rightarrow T_R'$, $T_{\varphi_1} \rightarrow T_{\varphi_1}'$, $T_{d_1} \rightarrow T_{d_1}'$, etc.)

3. When the closed-loop factors differ in form from their open-loop origins, several possibilities exist.

    a. For closed-loop factors which have the same form as, and are approaching, open-loop zeros, the closed-loop factor notation is that of the open-loop zeros (plus a prime). For example, open-loop quantities $(s + 1/T_s)$ and $(s + 1/T_{d_2})$, which couple to form a quadratic approaching the open-loop zeros of $(s^2 + 2\zeta_r\omega_r s + \omega_r^2)$, would give rise to a closed-loop factor ordinarily denoted as $(s^2 + 2\zeta_r'\omega_r's + \omega_r'^2)$.

    b. For closed-loop factors which differ in form from both the open-loop poles from which they depart and the open-loop zeros which they ultimately approach, a special notation is coined which ordinarily reflects the origin of the factor. For example, closed-loop factors which start from $s = 0$ and $s = -1/T_R$, couple to form a quadratic, and subsequently decouple to end finally at two real zeros, would be denoted $s^2 + 2\zeta_R'\omega_R's + \omega_R'^2$ in the quadratic region.

    c. Closed-loop factors which have no readily identified origin or end point, such as one starting at $s = 0$ and approaching $s = \infty$ as gain increases, are given a specially coined notation, e.g., $1/T_c'$.

4. When the application of these rules by rote would result in great confusion in the local context, a new form is substituted for the closed-loop factor involved. Primes, however, are always retained.

SECTION I

INTRODUCTION

Over the past two years, under the VTOL Integrated Flight Control Systems Program (VIFCS), a significant increase in the detailed understanding of flying quality requirements for VTOL aircraft has been obtained through application of pilot/vehicle closed-loop analyses. Such analyses, when correlated with available pilot rating (and commentary) data, established that longitudinal dynamic requirements for hover control were primarily related to closed-loop piloting functions. This led to the consolidation of the results of past handling quality experiments for this control mode and a preliminary prediction of the requirements for longitudinal control in hover (Ref. 1). Two recent VIFCS programs (Refs. 2 and 3) have provided some experimental validation of these requirements. Also it is noteworthy that the pilot compensation characteristics derived from the experimental data of Ref. 2 are in good agreement with these analytical predictions.

Encouraged by the success of these previous efforts, the analytical studies were extended to cover lateral/directional control aspects. This report presents the results of this second series of analyses which, again, covers both hover and transition flight regimes. Since these lateral/directional studies represent an extension of the longitudinal efforts reported in Part I (Ref. 1), much of the background justification and the procedures for application of the pilot/vehicle analysis techniques given therein are omitted here. For this reason it is suggested that the reader may find it desirable to refer to Part I occasionally for background.

Section II summarizes the basic manual control requirements defining satisfactory and unacceptable lateral hover dynamics. These requirements are identified in terms of vehicle dynamic characteristics and, where possible, their equivalence is expressed in terms of aerodynamic derivatives. The hover dynamic requirements identified cover the airframe without augmentation (e.g., conventional helicopter dynamic characteristics) and the airframe dynamics as modified by angular rate and position augmentation schemes and by translation augmentation schemes. The pilot/vehicle control situations associated with each level of augmentation are discussed briefly to support these requirements and as a means of gaining overall understanding.

Section III then expands the hover mode consideration by examining some effects of the nonidealized flight control system (i.e., including nonlinearities and control-coupling terms). Emphasis is placed on gaining insight to illustrate how such control system properties affect the closed-loop hover control.

The lateral/directional transition studies are presented in Section IV. These efforts start with detailed generic studies of the vehicle's stability and control characteristics as they change from hover to transition, and proceed to illustrate the piloting control problem associated with various closed-loop control tasks. The stability derivatives of a tilt-wing aircraft are used to provide a realistic basis for these analyses. With this background study of lateral/directional control in transition, the results from several handling quality experiments are examined and the closed-loop analyses are used to explain the root causes for the good and bad pilot rating.

Conclusions to be drawn from the results of these studies and recommendations for further experimentation are presented in Section V.

The appendices contain substantiating data which were considered too detailed and/or mathematical for presentation in the body of the report. Appendix A provides case studies and analytical treatments covering the dynamic requirements derived for the hover mode.

SECTION II

MANUAL CONTROL REQUIREMENTS FOR LATERAL HOVER

In the longitudinal studies of Part I (Ref. 1) it was established that the primary manual control problems in hover are associated with closed-loop pilot/vehicle deficiencies. Because the characteristics of the longitudinal and lateral modes in hover are dynamically equivalent, we would anticipate similar, if not identical, manual control requirements. That is, if we maintain the pilot model concept and adjustment rules as employed in the longitudinal study, the same or similar requirements would evolve for lateral control. Despite such expectations, it was considered desirable and necessary to proceed with a complete examination of the lateral closure aspects, and corresponding data, in order to:

1. Solidify preliminary predictions (based on longitudinal results) into a suitable set of lateral dynamic requirements.
2. Illustrate the detailed effects of various gust-sensitive derivatives on pilot compensation needs and error performance.
3. Study a broader cross section of dynamic features resulting from various augmentation schemes.
4. Consider the effects of flight control system properties and control cross-coupling terms.

A review of the above studies is accomplished in this section. For the detailed supporting analyses associated with these items the reader is referred to Appendix A.

A. LATERAL DYNAMIC REQUIREMENTS

To establish the dynamic requirements which identify satisfactory ($3 \le PR < 4$) and unacceptable ($6 \le PR \le 7$) boundaries for the lateral hover mode, a detailed survey was made of the dynamic characteristics experimentally tested in Refs. 2 through 10. The results of the survey including the dynamic characteristics, which are described by families of Bode plots representing both opinion levels, are given in Appendix A. This review of open-loop features follows the procedure developed and utilized in the longitudinal studies of Part I (Ref. 1). Essentially this involves a breakdown of the airframe dynamics into "effective vehicle" classifications. In making these distinctions, we again subdivided the dynamic features into controlled elements representing one of the following:

- Conventional VTOL systems (including subsidiary forms)
- Attitude augmentation systems
- Position- or translational-loop augmentation systems
- Combined attitude and translational systems.

The requirements derived from the survey for each controlled element classification are reviewed and some of the pertinent closed-loop implications are noted after first briefly considering the bases and form for their presentation.

1. Basis for Specification of Dynamic Requirements

An underlying problem associated with specifying dynamic requirements is finding an appropriate set of parameters or indices of merit. In general, for a given control task or piloting situation, suitable criteria should reflect consideration of:

- Pilot/vehicle performance merits (e.g., regulation errors, closed-loop responses, etc.)
- Closed-loop pilot effort and compensation requirements
- Vehicle only (i.e., open-loop) dynamics
  - Derivatives
  - Transfer function factors
  - Response time histories

For a given task, the vehicle (controlled element) dynamics determine the required pilot effort and compensation, and the resulting task performance. Thus criteria based on controlled-element dynamics are, perhaps, most inclusive of all the above considerations, for a given task. Furthermore, although the aspects of closed-loop control may really dominate a given situation the present state of art (e.g., Ref. 11) does not permit the use of pilot-related quantitative factors for the establishment of firm requirements. Nevertheless, a study of the closed-loop aspects is very instructive, can be used to make comparisions and extrapolations, and often reveals the underlying basis for the requirement on the vehicle-only dynamics (e.g., Ref. 1). Accordingly, while the main thrust of the data correlations is directed along the line of vehicle dynamic parameters, closed-loop studies are later invoked to provide understanding and a basis for extrapolation to different situations.

The remaining consideration on the use of vehicle dynamic parameters is whether to define the criteria in terms of the aerodynamic derivatives, the transfer function factors, or response time histories. In any case, the general suitability of the resulting criteria will depend on which form is more closely related to the true or primary causal effect. Furthermore, any such criteria will be subject to some conditional exceptions because of the approximations and assumptions involved in derivation of the key merit.

Based on the longitudinal analyses of Part I (Ref. 1), and the detailed lateral correlations in Appendix A, the transfer function factors are favored as the means of specifying the hover dynamic requirements. This selection stems from the fact that the dominant factors in the pilot opinion of the hover handling qualities do apparently involve the closed-loop aspects. However, for some of the simple controlled elements associated with conventional VTOL aircraft, the criteria will also be expressed in terms of the aerodynamic derivatives.

2. Conventional VTOL Lateral Dynamics and Simple Attitude-Rate Augmentation

The conventional lateral dynamics are those controlled elements which are specified by the vehicle's aerodynamic properties (see Table I). As such, the tie between the controlled element dynamics and the aerodynamic

TABLE I

EFFECTIVE LATERAL CONTROLLED ELEMENT FORMS
FOR CONVENTIONAL VTOL SYSTEMS

BASIC FEATURES AND SUBSIDIARY FORMS	PRIMARY CONTROL, ATTITUDE φ/δ	SECONDARY CONTROL, POSITION y/δ
1. Inertial Form (i.e., $Y_v = L_v = L_p = 0$)	$\frac{L_\delta}{s^2}$	$\frac{gL_\delta}{s^4}$
2. Angular Damping Form ($L_p \neq 0$, $Y_v = L_v = 0$)	$\frac{L_\delta}{s(s+1/T_R)}$	$\frac{gL_\delta}{s^3(s+1/T_R)}$
3. Aerodynamic Form (i.e., v and p terms not zero)	$\frac{L_\delta(s+1/T_{\varphi_1})}{(s+1/T_R)(s^2+2\zeta_d\omega_d s+\omega_d^2)}$	$\frac{gL_\delta}{s(s+1/T_R)(s^2+2\zeta_d\omega_d s+\omega_d^2)}$

where:

$$\frac{1}{T_R} \doteq -\frac{3}{4}L_p + \sqrt{\frac{L_p^2}{16} - \frac{gL_v}{2L_p}} \tag{1}$$

$$\frac{1}{T_{\varphi_1}} \doteq -Y_v \tag{2}$$

$$\omega_d \doteq \frac{gL_v}{-\frac{3}{4}L_p + \sqrt{\frac{L_p^2}{16} - \frac{gL_v}{2L_p}}} \tag{3}$$

$$2\zeta_d\omega_d \doteq -Y_v - \frac{L_p}{4} - \sqrt{\frac{L_p^2}{16} - \frac{gL_v}{2L_p}} \tag{4}$$

derivatives can be made with reasonable ease (Eqs. 1 through 4). In addition, the factors governing pilot/vehicle performance, such as rms errors and control activity, can be related both to specific derivatives and to the pilot activity (e.g., gain and lead).

The review of extant open-loop dynamic data presented in Appendix A shows that the dynamics features for the lateral mode which define satisfactory ($3 \leq PR \leq 4.0$) and unacceptable ($6.0 \leq PR \leq 7.0$) boundaries are essentially the same as the longitudinal. Table II shows the comparison between the longitudinal mode features from Ref. 1 and the present lateral study. The longitudinal criteria are identified by the subscripts p, sp, θ, u; the lateral by the subscripts d, R, φ, v.

The lateral dynamic boundaries differ from longitudinal only in the level of the aperiodic mode (roughly given by the rotary damping, L_p, e.g., Eq. 1) required for a satisfactory rating. Basically, the minimum acceptable roll subsidence mode inverse time constant is $1/T_R \geq 1.25\ \text{sec}^{-1}$ which corresponds approximately to a minimum effective airframe damping of $-L_p > 1.0\ \text{sec}^{-1}$. This level of rotary damping results in an oscillatory mode damping, ζ_d, always greater than zero. Such a level of oscillatory damping is apparently required to yield an acceptable rating regardless of whether or not motion cues are available in the simulation, whereas less stable dynamics are rated as satisfactory for longitudinal control when motion is available* (Ref. 1).

The satisfactory boundary level from Table II can be expressed in terms of the aerodynamic derivatives by the relationships of Eqs. 1 through 4. The results of this conversion are given in Fig. 1, which also shows the criteria values of $1/T_R = 1.25$, $\omega_d = 0.5$, $\zeta_d = 0$. Because the longitudinal and lateral modes are dynamically similar in hover the rotary damping, L_p, can be replaced by its longitudinal equivalent, M_q, and gL_v by $-gM_u$; thus, except for the slightly higher $1/T_R$ cutoff in Fig. 1, these requirements could apply equally as well to the longitudinal mode (see longitudinal counterpart to Fig. 1 in Ref. 1).

The unacceptable dynamics ($6 \leq PR \leq 7$) of Table II show essentially the same characteristics for both lateral and longitudinal control with the dominant features being the unstable oscillatory mode near 1 rad/sec (i.e., $\zeta_d < 0$). The higher frequency oscillatory mode stems primarily from the high lateral stability term gL_v although a very low angular damping, L_p, tends to increase ω_d (e.g., see Eq. 3).

---

*The damping differences noted here between the longitudinal and lateral requirements represent a statistical difference between the mean values; therefore, the discrimination between acceptable values of $1/T_{sp}$ and $1/T_R$ is subject to a low confidence level. Nevertheless, it is considered indicative of the trend for higher minimum satisfactory damping levels for the lateral axis.

TABLE II

COMPARISON BETWEEN LONGITUDINAL AND LATERAL CRITERIA COVERING SATISFACTORY AND UNACCEPTABLE RATING LEVELS FOR CONVENTIONAL VTOL DYNAMIC FEATURES

DYNAMIC PROPERTIES	SATISFACTORY $3 \leq PR \leq 4$	UNACCEPTABLE $6 \leq PR \leq 7$
Attitude Loop		
1. Oscillatory Mode		
a. Frequency, ω_p	$\omega_p < 0.5$ rad/sec	$\omega_p > 0.8$ rad/sec
b. Damping, ζ_p	$\zeta_p > 0$ (stable) or $\zeta_p\omega_p > 0.2$[*]	$\zeta_p < -0.15$ (unstable)
a. Frequency, ω_d	$\omega_d < 0.5$ rad/sec	$\omega_d > 0.8$
b. Damping, ζ_d	$\zeta_d > 0$	$\zeta_d\omega_d > 0.15$
2. Aperiodic Mode		
$1/T_{sp_2}$	$1/T_{sp_2} > 1$	$1/T_{sp_2} \doteq \omega_p$
$1/T_R$	$1/T_R > 1.25$	$1/T_R \doteq \omega_d$
3. Numerator Term $1/T_{\theta_1}$ or $1/T_{\varphi_1}$	$0 \doteq 1/T_{\theta_1}$ or $< 1/2\ \omega_p$ $0 \doteq 1/T_{\varphi_1}$ or $< 1/2\ \omega_d$	
4. Dominant vehicle asymptotic dynamic form near 2 rad/sec ω_{c_θ} or ω_{c_φ}	K/s	K/s^2
5. Phase margin near limiting ω_p or ω_d	$\varphi_M > 0$[†]	$\varphi_M \overline{<} -40^\circ$
6. Lowest frequency for stability, ω_{c_1}[‡]	$\omega_{c_1} < 1.0$[†]	$\omega_{c_1} \overline{>} 1.0$
Position Loop		
1. Dominant vehicle asymptotic dynamic form near 1 rad/sec ω_{x_c}, ω_{y_c}	K/s^3	K/s^4

[*] Requires moving-base or flight test simulation conditions (i.e., angular motion cues).

[†] Conditions required only for $\zeta_p\omega_p > -0.2$.

[‡] The lowest frequency for which the phase margin is zero.

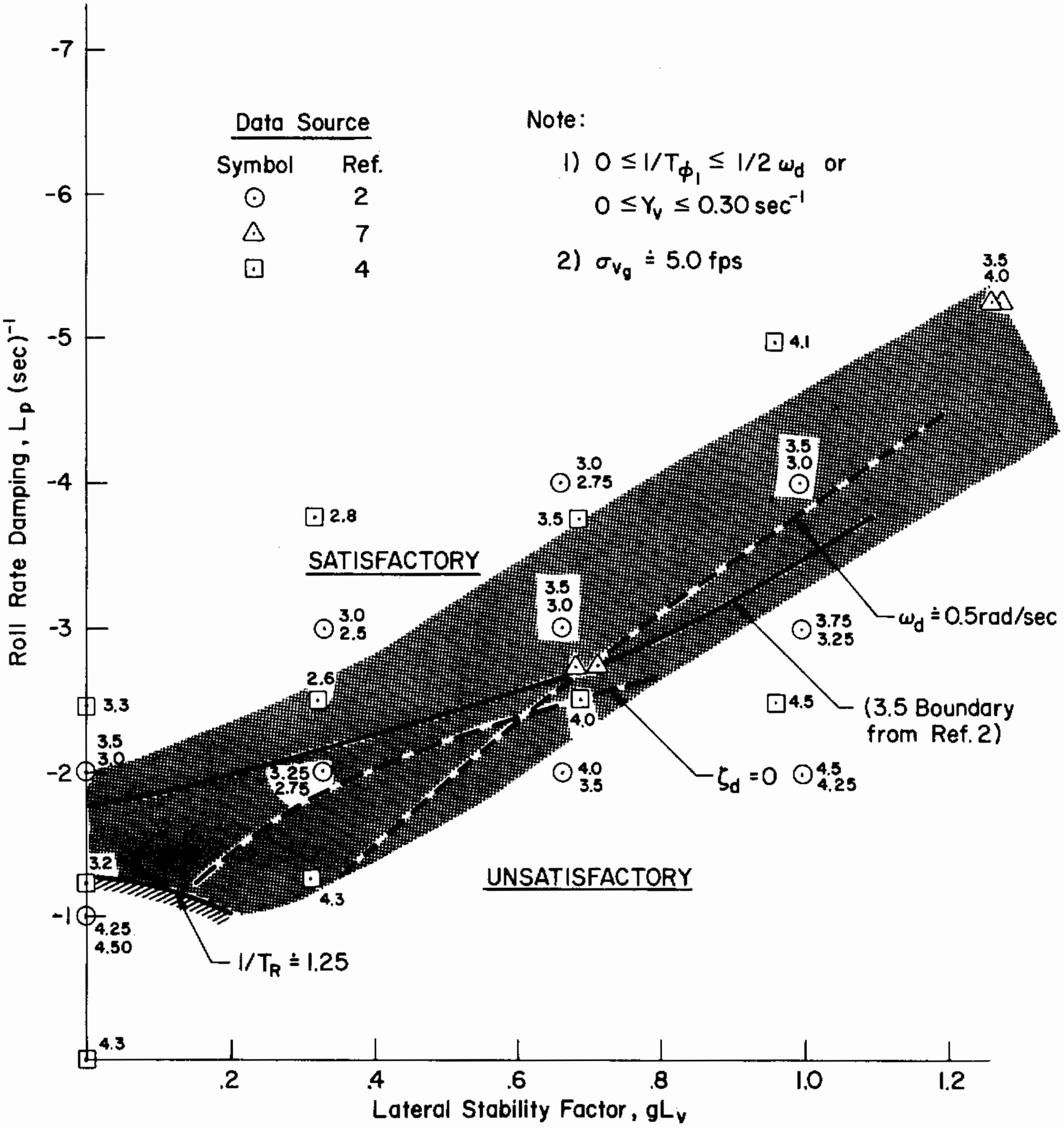

Figure 1. Satisfactory Handling Qualities Roll Rate Damping Requirements Implied from Transfer Function Factors

The above requirements also apply to the simple attitude-rate augmented aircraft because such augmentation simply increases the effective rotary damping. However, the consequence of attitude feedback and the means of expressing the boundaries (e.g., the s-plane presentation of the criteria is more appropriate) need further consideration, as summarized next.

3. Attitude Augmentation Systems

The effective controlled element forms for attitude augmentation systems may be subdivided into two categories. These categories are expressed by the ratio of the angular position feedback, K_φ, to the angular rate feedback, $K_{\dot{\varphi}}$ (i.e., $1/T_E = K_\varphi/K_{\dot{\varphi}}$) relative to the basic aircraft aperiodic mode (i.e., the unaugmented roll subsidence mode), $1/T_R$. Reference 1 discusses the longitudinal equivalent of such considerations in some detail and illustrates the changes in the controlled element dynamics resulting from the selection of $1/T_E$ greater or less than the airframe aperiodic mode ($1/T_{sp_2}$ or $1/T_R$ in the present case). The two resulting effective controlled element forms appropriate for lateral hover are presented in Table III below for reference.

TABLE III

ATTITUDE AUGMENTATION SYSTEM

BASIC FEATURES	PRIMARY CONTROL ATTITUDE, φ/δ	SECONDARY CONTROL LATERAL POSITION, y/δ
Category I $1/T_E \le 1/T_R$ $\omega_d' \le \omega_d$	$\dfrac{L_\delta(s+1/T_{\varphi_1})}{(s+1/T_R')(s^2+2\zeta_d'\omega_d's+\omega_d'^2)}$	$\dfrac{-gL_\delta}{s(s+1/T_R')(s^2+2\zeta_d'\omega_d's+\omega_d'^2)}$
Category II $1/T_E > 1/T_R$ $(s+1/T_{\varphi_1})/(s+1/T_R) \doteq 1$	$\dfrac{L_\delta}{s^2+2\zeta_d'\omega_d's+\omega_d'^2}$	$\dfrac{-gL_\delta}{s^2(s^2+2\zeta_d'\omega_d's+\omega_d'^2)}$

Basically, Category I systems have low stiffness and they exhibit responses equivalent to conventional VTOL dynamics. Thus the dominant response is that of attitude rate proportional to control input (i.e., $\varphi/\delta \doteq K/s$). The Category II, or high stiffness, system is dominated by the high frequency second-order mode and the command response to stick input is attitude (i.e., $\varphi/\delta \doteq K$). The separation of the dynamic categories according to the attitude response properties becomes fuzzy as effective augmentation lead, $1/T_E$, approaches $1/T_R$ and as the rotary damping, L_p, approaches zero. However, the method of classification for Category I and II systems remains valid regardless of the airframe aerodynamic derivatives. This is significant because we are concerned here with prescribing conditions under which a given set of handling quality requirements will apply.

The reader is further cautioned not to confuse the net derivatives L_φ and L_p with the feedback gain terms, K_φ and $K_{\dot{\varphi}}$. Generally, these terms are not equivalent since the inherent airframe stiffness or damping is lumped with similar artificially created terms when the derivatives L_φ and L_p are used.

With these comments as background, the dynamic requirements for attitude augmentation systems are reviewed. These were established initially by applying the governing closed-loop considerations determined as important for conventional VTOL dynamics. These closed-loop aspects were first derived in Ref. 1 for longitudinal control and are applied in Appendix A to cover lateral control. Essentially, this means that the same pilot compensation and performance merits (i.e., lead, crossover frequencies, etc.) predicted for the satisfactory conventional dynamics were used to define satisfactory regions for the attitude system. The confirmation of these predicted boundaries was then obtained from the experimental results in Refs. 2, 9, 10, 26, 27, 28. Data from these sources encompass both Category I and II systems. Again, detailed discussions of the documented results and verification of boundaries are contained in Appendix A.

a. Category I Systems ($1/T_E \leq 1/T_R$). Basic dynamic requirements for satisfactory hover control covering the Category I or rate-type damper systems are identified by the dynamic regions in the s-plane plot of Fig. 2. These open-loop dynamic characteristics constitute boundary or limiting pilot control situations. The regions identified by letter relate the dynamic characteristic to the appropriate closed-loop piloting factors as tabulated in Fig. 2.

Region A is generally where the unaugmented VTOL aircraft oscillatory dynamics fall and the handling qualities range from unsatisfactory to unacceptable. The most significant control deficiency in this region is the so-called "boxed in" situation (see Appendix A). This situation refers to the pilot's inability to improve closed-loop control by adopting lead compensation (anticipation). In fact, for these control elements (i.e., region A dynamics) we find that the pilot can improve his performance only by reducing his high frequency lags (e.g., the pilot's reaction time neuromuscular delay, τ_e). While significant reductions in such lags can be accomplished by the highly skilled pilot, particularly where motion cues are provided, the neuromuscular system dynamics do represent a physical upper limit on his control capabilities. Also, reductions in the pilot reaction time delay, τ_e, are accompanied by low frequency α-effects* (see

---

*The exact cause of these low-frequency aspects is not clear at this time. Recent evidence suggests that the effect is associated with time-varying pilot gain and remnant (see Ref. 35).

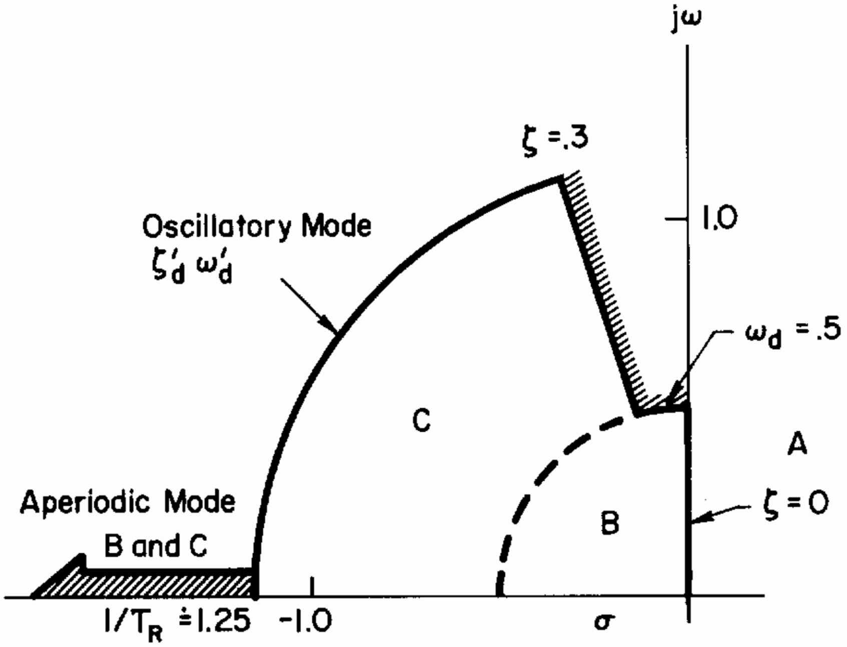
jω
ζ =.3
1.0
Oscillatory Mode
ζ′d ω′d
ωd =.5
C
A
Aperiodic Mode
B and C
B
ζ = 0
1/TR ≐1.25
-1.0
σ

REGION	PILOT CONTROL SITUATION
A	Unsatisfactory to unacceptable; lead compensation in attitude loop relatively ineffective ("boxed-in"); position-loop crossover marginal along $\zeta = 0.3$ boundary.
B & C	Satisfactory, multiloop control; small lead compensation in attitude $(T_{L_\varphi} \doteq T_R)$; adequate margins; outer-loop crossover at least 0.3 without lead.

Figure 2. Category I, Dynamic Requirements for Hover Mode

Ref. 1, Appendix D). The τ_e and α effects are inversely related; thus, an increase in low-frequency phase lags accompanies a decrease in the effective delay, τ_e. This conflict between low- and high-frequency phase lags for the pilot is graphically described as a "boxed-in" situation.

With progressive penetration of region A, the oscillatory mode divergence time decreases (i.e., the effective time constant, $\tau \doteq 1/-\zeta\omega$ increases) and the handling qualities ratings deteriorate very rapidly. In fact, as noted in the longitudinal studies (Ref. 1), the dynamic features in the crucial region of crossover are quite similar to those of a second-order "critical task" (Ref. 14). The critical task dynamics are designed to push the pilot to the limits of his neuromuscular and lead-generating capabilities. Any vehicle approaching such dynamics requires full-attention control and is accordingly considered hazardous to fly.

Region B, defined by $\omega_d = 0.5$ and $\zeta_d = 0$, is identified separately because this is where the oscillatory mode is normally located for moderate gain rate augmentation (i.e., L_p augmentation or a Category I feedback system where $1/T_E = 0$). With these simple angular rate damper schemes, the degree of positive damping for the oscillatory modes depends on the position of the numerator zero, $1/T_{\varphi_1}$, (see adjacent sketches) as well as on the rate feedback gain, $K_{\dot{\varphi}}$. In some cases, notably helicopters with large Y_δ terms, the value of $1/T_{\varphi_1}$ is negative (positive on the σ axis) and the oscillatory mode remains unstable regardless of the feedback gain (e.g., as shown in the sketch). The resulting low frequency oscillatory divergence causes the pilot only moderate concern and depending on the task (e.g., hovering without gust) such systems may be rated marginally satisfactory ($PR \doteq 4$). This appears particularly true when the corresponding aperiodic root, $1/T_R$, is significantly greater than 1.25 (see Fig. 1). However, a neutral or stable oscillatory mode is necessary to insure a satisfactory rating ($PR < 3.5$) for precision hover tasks involving moderate ($\sigma_{v_g} \doteq$ 5 fps) gust disturbances or IFR conditions. Thus, in Fig. 2, the boundary between satisfactory and unsatisfactory (i.e., $PR = 3.5$) is the $j\omega$ axis or neutral damping (i.e., $\zeta_d = 0$).

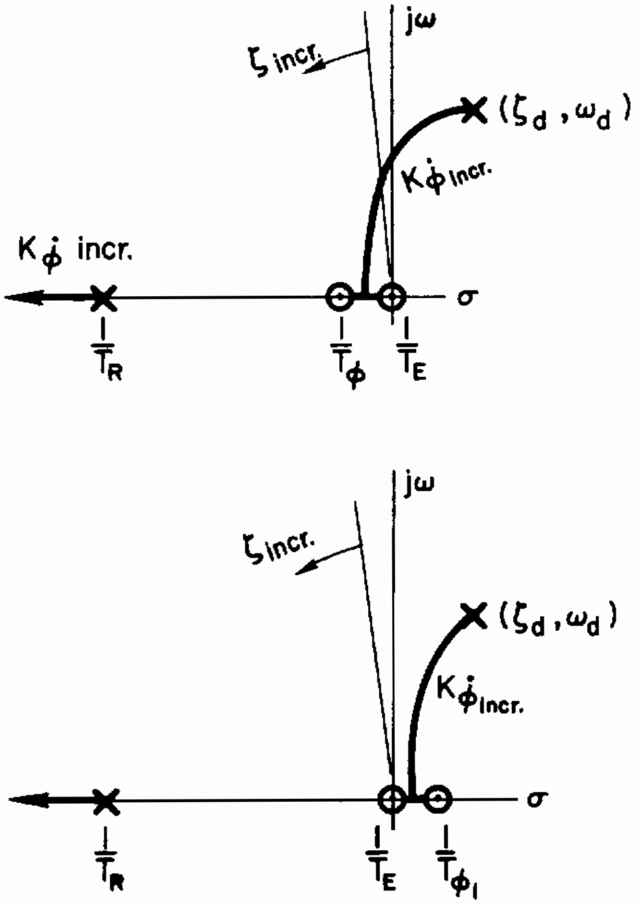

Typical Gain Loci for Rate Damper Systems (i.e., $1/T_E = 0$)

Region C covers the remaining Category I systems where $1/T_E < 1/T_R$ but greater than zero. The crucial boundary condition is that for $\zeta_d = 0.3$ which shows that the oscillatory mode roots must lie to the left for satisfactory manual control. As shown in Appendix A this requirement is directly related to that specifying a minimum position to attitude loop crossover frequency relationship (Fig. 2). The upper constant frequency boundary (ω_d = 1.25 rad/sec) of region C is more a practical implication than a rigid requirement. This is a consequence of the basic airframe frequency, ω_d, the effective augmenter lead, $1/T_E$, and the zero, $1/T_{\varphi_1}$. For example, we see from the sketch that increasing augmenter gain drives the poles (ζ_d, ω_d) to the centroid between $1/T_E$ and $1/T_{\varphi_1}$. Practical limits on ω_d suggest that "inherent aerodynamic" levels* of ω_d and $1/T_R$ are between 1 and 2 rad/sec, thus we can assume that for the Category I system the oscillatory roots will fall within region C of Fig. 2. Furthermore, as will be illustrated later, this region also conveniently provides an overlap of Category I and II requirements.

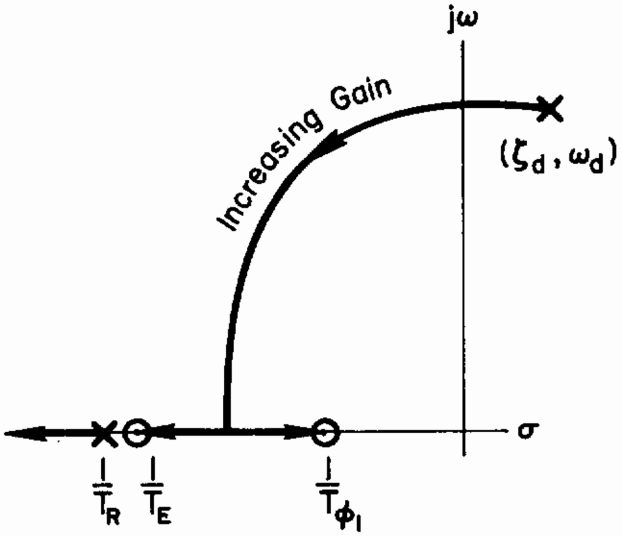

Excluding for this discussion simple rate augmentation systems (i.e., $1/T_E = 0$), we find good verification for these boundaries in the experimental results of Refs. 2, 3, and 27. In Fig. 3, these results are superimposed on the suggested boundaries. To emphasize the boundaries, the available data are segregated as to either PR > 3.5 or PR < 3.5. Detailed pilot ratings are given in Appendix A.

b. Category II Systems ($1/T_E > 1/T_R$). Category II requirements are shown in Fig. 4. For Category II systems only the oscillatory mode is specified since the second-order characteristics dominate. These regions are based on the closed-loop requirements inferred from the Category I and conventional dynamics studies. The various pilot control function and compensation regions identified in the figure are briefly outlined below.

---

*We use "inherent aerodynamics" to infer the absence of any mechanical augmentation schemes (e.g., gyro stabilizer bars) which might result in larger ω_d and $1/T_R$ values.

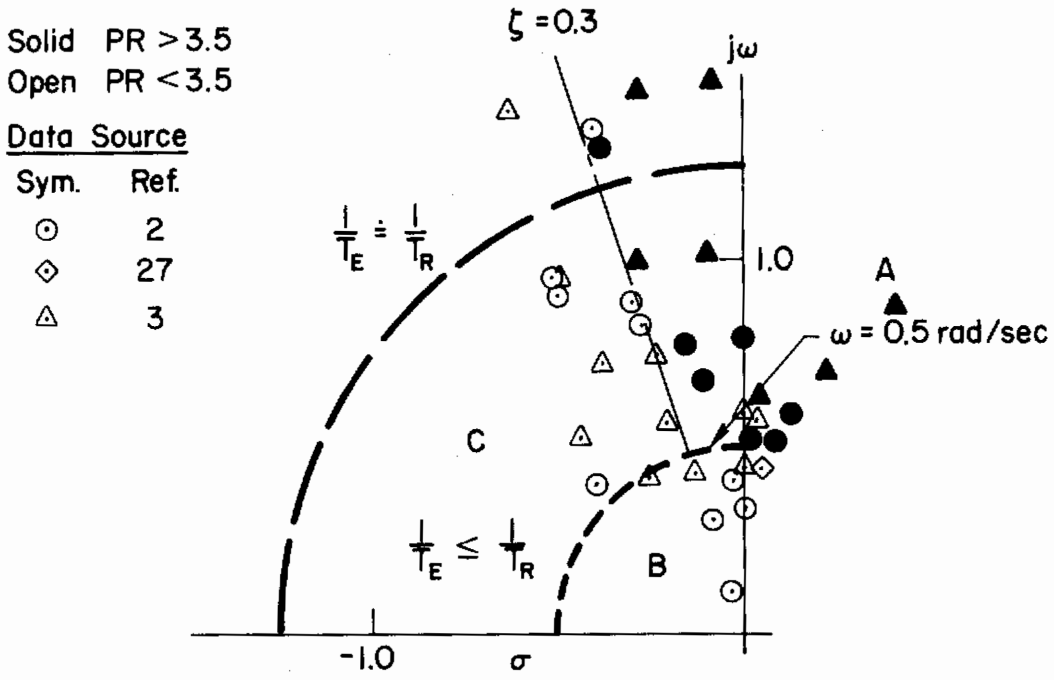

Figure 3. Correlation of Handling Quality Data with Suggested Boundaries

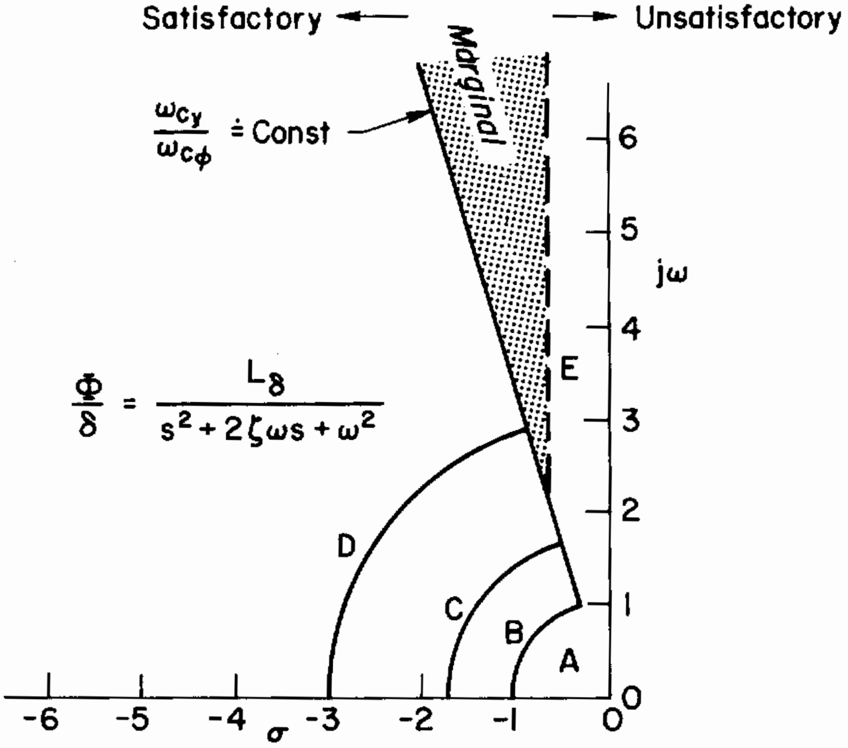

Figure 4. Basic Oscillatory Mode Dynamic Requirements; Category II System, $1/T_E > 1/T_R$

REGION	PILOT CONTROL SITUATION
A	Unacceptable: A multiloop control structure with large lead compensation ($T_L > 1$ sec) required in both attitude and position to obtain desired crossover frequencies ($\omega_{c_\varphi} \doteq 2.5$ rad/sec; $\omega_{c_y} \doteq 1$ rad/sec) with the compensation for a K/s-like outer-loop closure. Poor regulatory control of attitude disturbances due to low broadband gain features of inner loop. Due to low stiffness attitude dynamics appear as K/s^2 to the pilot.
B	Marginal Situation: Same loop structure required, but somewhat reduced pilot compensation ($T_L \doteq 1$ sec) in both loops. Regulatory control of attitude disturbances marginal due to poor error control. For this situation the broadband gain region is near the minimum of 6 dB for the crossover $\omega_{c_\varphi} \doteq 2.5$ rad/sec.
C	Satisfactory: Quasi-multiloop control structure with no lead or moderate pilot lead ($T_{L_\varphi} \doteq 1/\omega_{c_\varphi}$) required in the attitude loop. Moderate lead ($T_{L_y} \doteq 1$ sec) required in position closure. Regulatory control of attitude disturbance is good.
D	Satisfactory: Single-loop control of position with moderate lead ($T_{L_y} \leq 1$ sec) for a K/s-like crossover near $\omega_{c_y} \doteq 1$ rad/sec. Attitude command, φ_c, with stick required, otherwise pilot is gain or control power limited at higher frequencies ($\omega_\varphi > 3$ rad/sec).*
E	Unacceptable: Low attitude-loop damping restricts position-loop bandpass. Boundary suggested by desire to keep $\omega_{c_y}/\omega_{c_\varphi}$ approximately constant ratio. A marginal region exists between $\zeta \doteq 0.3$ (i.e., $\omega_{c_y}/\omega_{c_\varphi} = 0.3$) and $\zeta\omega = 0.75$.

Each region for the Category II systems identified above clearly places the pilot in a somewhat different closed-loop control situation. For this reason, it is worthwhile expanding on some of the key aspects of concern even though detailed considerations are given in Appendix A.

In regions A and B, the pilot is faced with a relatively low stiffness attitude system (i.e., $\omega_n < 1.7$ rad/sec) which although stable ($\zeta > 0$) requires excessive compensation to achieve reasonable performance in the presence of disturbances. Thus the key factor for these two regions is the level of attitude excitation. Without disturbances, a satisfactory rating (PR = 3.5) is normal, even for a zero stiffness system (e.g., hover-buggy, lunar landing craft, etc.), for VFR, motion-flight conditions.

---

*Attitude command refers to the mechanization features associated with systems in which a stick signal acts as a bias to the feedback signal.

Likewise, very large, high inertia vehicles which have low frequency dynamics could also be expected to fall in this region. Again, the degree that these vehicles can be disturbed will determine whether such low stiffness systems can approach a satisfactory handling quality level. However, considering the handling quality data surveyed, the "normal" vehicle response characteristics and disturbance levels tested, and the predicted pilot compensation required, it appears that the minimum vehicle stiffness falls between 1.7 and 1.0 rad/sec. A stiffness of 1.0 rad/sec can be inferred as an absolute minimum for most precision hover tasks. For these frequency conditions, the predicted "minimum broadband gain" for suppression of disturbances is -6 dB (i.e., with the pilot's crossover between 2 and 3.0 rad/sec).*

From a closed-loop or piloting control viewpoint regions C and D are somewhat similar and disturbance regulation is not a problem. Attitude response for control inputs can be the crucial factor for the higher stiffness system ($\omega > 3.0$ rad/sec) if control power is low. Attitude command systems are generally required to keep the response per inch of stick equal to or greater than about 0.1 rad in the first second. This response level has been suggested from several studies (e.g., Refs. 2, 8, and 20) for rate systems as well as attitude systems (Ref. 29).

Experimental verification for these requirements is evident from Figs. 5, 6, and 7. In these figures, the results of Refs. 2, 9, 10, and 27 are superimposed on the suggested boundaries. The results of Ref. 10 shown in Fig. 7 are particularly noteworthy as confirming the control functions and compensation features of regions A and B. Superimposed on the suggested boundaries and regions of Fig. 4 is the satisfactory Ref. 10 boundary ($PR \doteq 3.5$) derived from experimental testing of the attitude command system. The agreement between regions is remarkably good for the high frequency systems above regions A and B. Furthermore, region B, identified as marginal due to regulatory control from a closed-loop viewpoint, coincides with the observed changes in the satisfactory boundary ($PR \doteq 3.5$) when angular acceleration (simulated gust or ground effect) disturbances were introduced. Note also that in these experiments an attitude command feature was used to prevent the feedback signals from limiting the attitude response. For this reason, no upper limit on stiffness (i.e., frequency) was encountered in the Ref. 10 testing. However, inadequate control response was cited as restricting the pilot control in Ref. 26 (Fig. 6) which did not use an attitude command feature.

It appears reasonable, therefore, to conclude that the closed-loop factors previously identified do account for the restrictions imposed on the damping

---

*Suppression of external disturbances and minimization of errors are obtained in a closed-loop situation such that $G(j\omega) >> 1$ over the frequency range of the substantial input. The data suggest that a factor of two (6 dB) reduction over the frequency range below crossover is adequate.

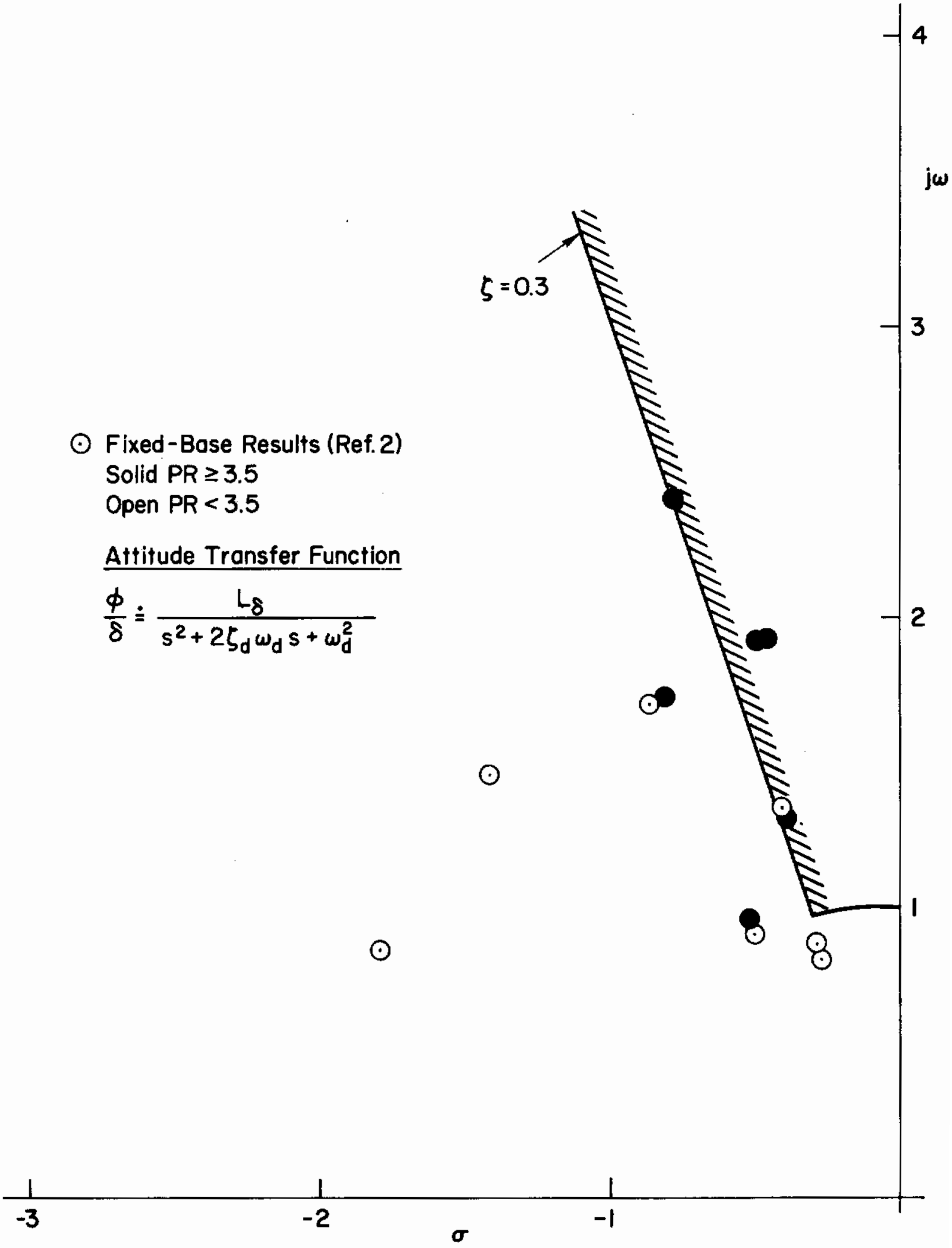

Figure 5. Comparison of Lateral Dynamic Requirements for Category II Augmentation Systems ($1/T_E > 1/T_R$) and Ref. 2 Data

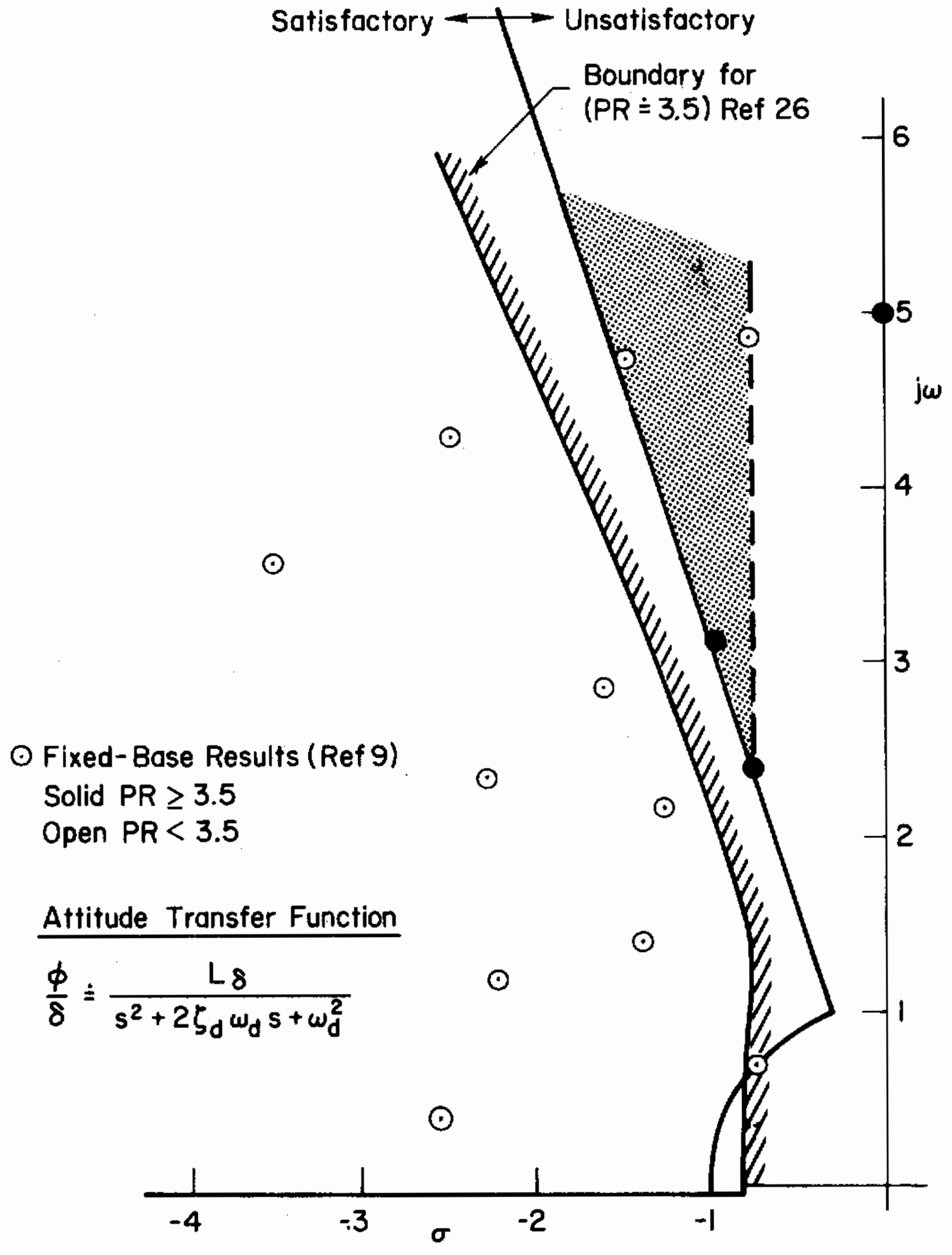

Figure 6. Comparison of Lateral Dynamic Requirements for Category II Augmentation Systems ($1/T_E > 1/T_R$) with Experimental Data

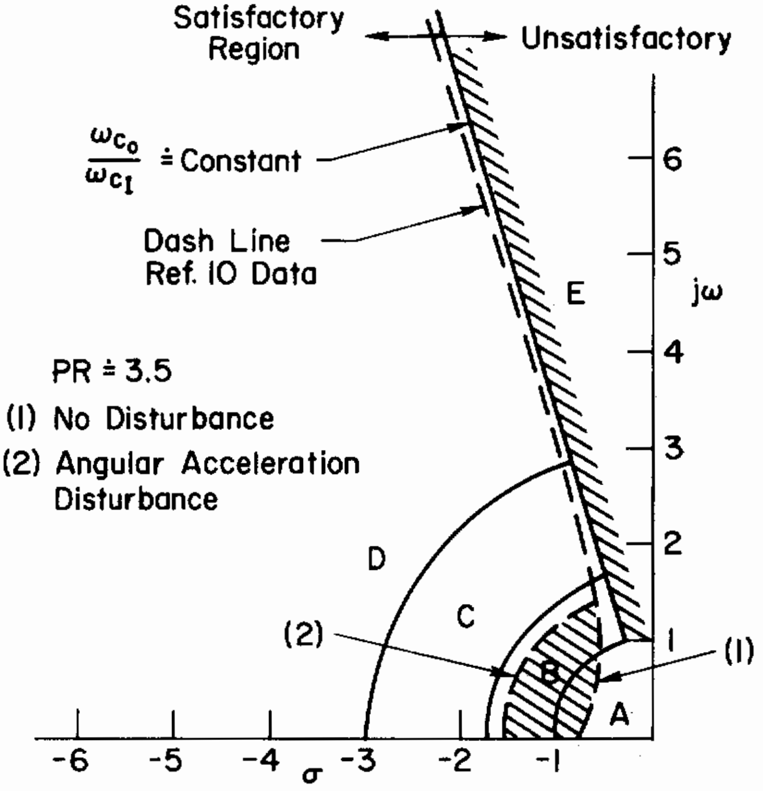

Figure 7. Oscillatory Mode Requirements for Category II ($1/T_E > 1/T_R$) Attitude Stabilized Systems; Comparison with Ref. 10

and frequency for attitude systems. Specifically, the handling quality merits indicate that the following restrictions are imposed:

1. A minimum frequency, $\omega_N \geq 1.7$ rad/sec for conditions where disturbances are expected. This is to insure a good broadband gain and pilot closure near ω crossover of 2-1/2 rad.

2. A minimum damping ratio, $\zeta \geq .3$, to prevent the inner loop from restricting the outer-loop pilot closure. This is in addition to the 2-1/2 rad/sec attitude bandwidth which is necessary also for good outer-loop control.

As a final point, we note from Fig. 8 that the oscillatory mode dynamic requirements for the two attitude augmentation system categories overlap and have a common $\zeta = 0.3$ boundary requirement. Furthermore, this uniformity of the oscillatory mode dynamics requirements can be considered to extend also to the basic vehicle case which, in essence, is a Category I system with zero gain and $1/T_E$. Accordingly it is feasible to specify the general satisfactory boundary as being either:

1. The aperiodic mode should have an effective inverse time constant $1/T_R > 1.25$ rad/sec, or
2. All oscillatory modes greater than 0.5 rad/sec shall have a damping ratio $\zeta > 0.3$. Frequencies below 0.5 rad/sec will be at least neutrally damped (i.e., $\zeta = 0$).

4. Other Augmentation Concepts

Based on the closed-loop criteria inferred, as above, the dynamic requirements can be extended to include more elaborate augmentation and command control schemes. However, at present, little confirmation of such predictions can be made except for two concepts for which limited experimental results are available; i.e.,

1. Command schemes employing rate ordering and attitude hold features.
2. Translational rate damping systems.

a. Rate Ordering, Attitude Hold. This system represents one form of command system which attempts to combine the desirable response characteristics of rate systems with the stiffness and regulatory features of the attitude stabilization schemes. These features can be achieved by the schematic arrangement shown in the block diagram below. In this concept,

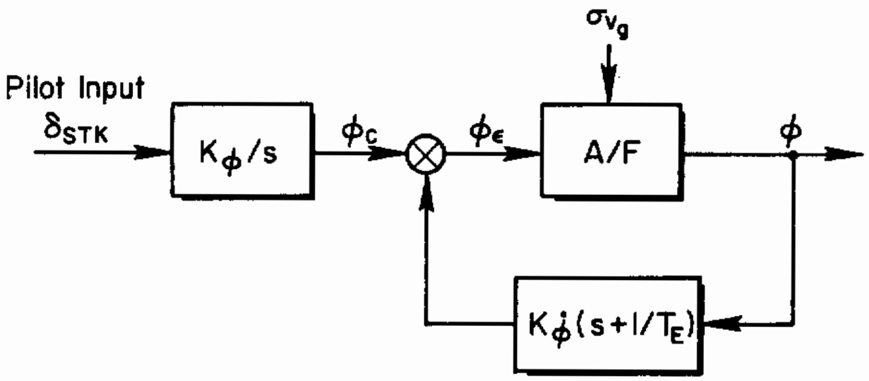

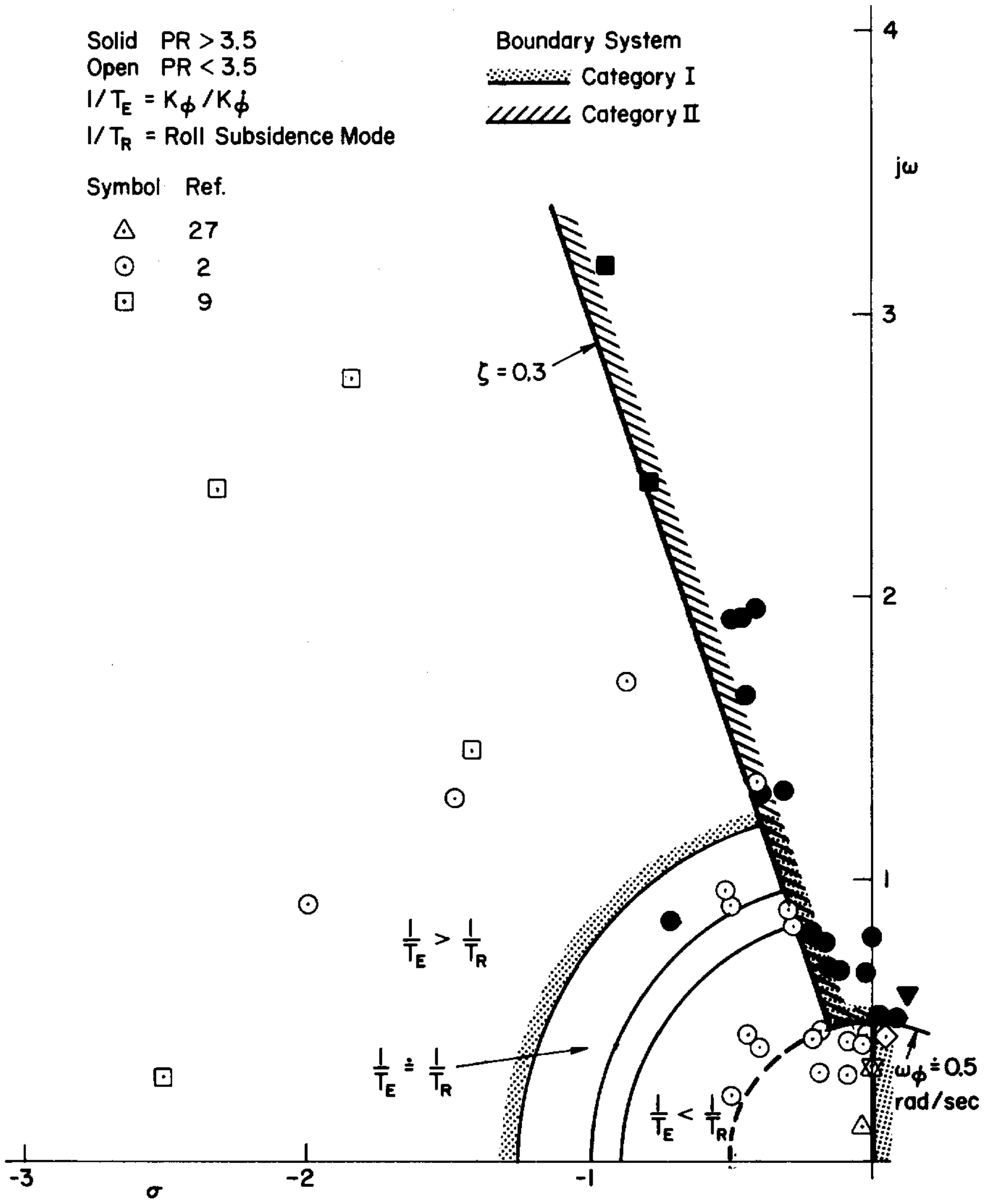

Figure 8. Hover Mode Dynamic Requirements for
Attitude Augmentation Systems Composite of Categories I and II

pilot control inputs are introduced as commands to the attitude stabilized vehicle through a rate network (an integrator). Thus, to the pilot the vehicle response to stick appears as angular rate. Without a stick command (i.e., stick neutral), the vehicle is stabilized in attitude and resists all external disturbances. These characteristics are depicted by the Bode sketch below.

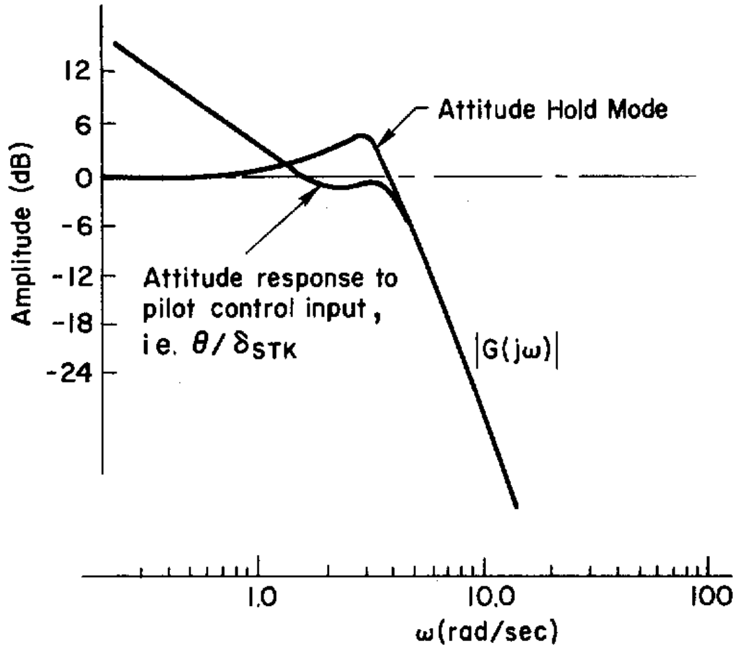

Bode Sketch of Rate Ordering Attitude Hold System

In hovering control the pilot is required to function within the multiloop framework because the stick is now an attitude rate ordering system; therefore he must function to control attitude as well as position in essentially the same series multiloop configuration as envisioned in Ref. 1 and shown below.

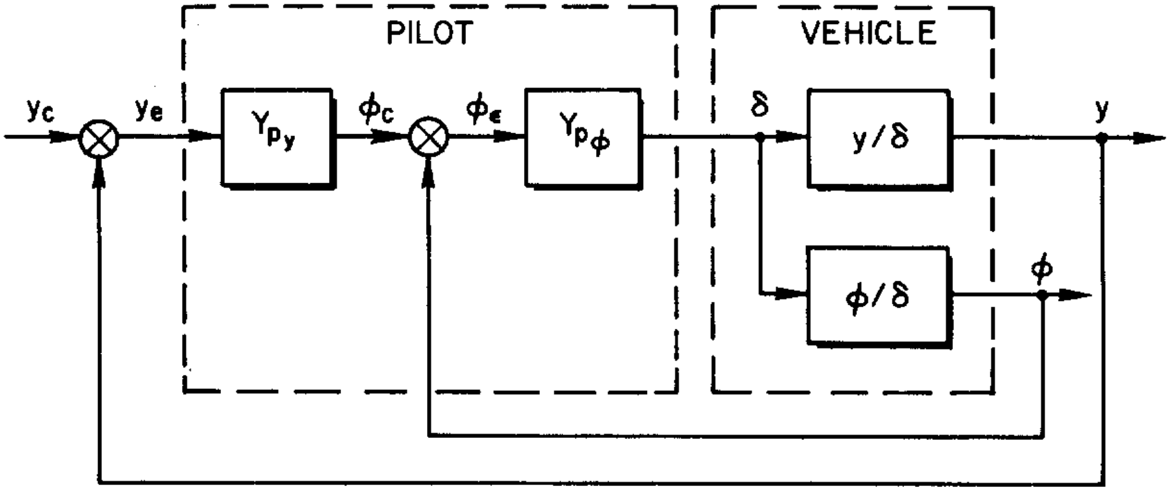

With this series arrangement a simple gain closure is quite satisfactory for closing the inner loop (i.e., the attitude loop) provided the control system bandpass and damping are adequate to permit meeting the requirements of $\omega_c > 2\text{-}1/2$ rad/sec. The primary restriction on the attitude stabilization frequency, ω_N, therefore, is that it be greater than 2.5 rad/sec. This is because values below this require the pilot to introduce excessive lead compensation. That is, the inherent K/s^3 character of the θ/δ_e transfer function for $\omega > \omega_N$ requires the pilot to generate a double lead to permit crossover near or greater than ω_N; and such compensation activities are opposed to good pilot ratings.

Another restriction on the crossover frequency is imposed by the damping ratio of the attitude stabilized mode, ζ_N, as sketched below. That is, to avoid instability the gain must be less than that corresponding to the amplitude peak at ω_N; thus the maximum crossover frequency, ω_c, approaches a value which is equal to $2\zeta_N\omega_N$.

Effect of Attitude Damping on Bandwidth

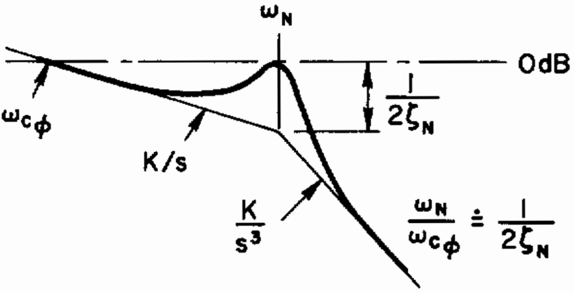

This simple approximation is valid only for damping ratios much less than critical, but with this restriction in mind; and with the previous requirement on $\omega_c > 2.5$ rad/sec we now obtain the requirement that ζ_N be greater than $1.25/\omega_N$.

The two requirements derived above; i.e.,

1. The effective attitude-stabilized frequency, ω_N, must be greater than 2-1/2 rad/sec
2. The effective damping of the second-order mode for the stabilization system must be such that $\zeta_N \geq 1.25/\omega_N$

are plotted as (dashed line) boundaries on Fig. 9. The experimentally derived 3.5 rating boundary values of Ref. 10, also shown (the actual experimental data points were not presented) are in quite good agreement. Note finally that the $\zeta = 0.3$ cutoff line shown in Fig. 8 for the "pure" attitude system does not apply since for the present rate command, attitude hold system the outer loop is characterized by two second-order breaks, one

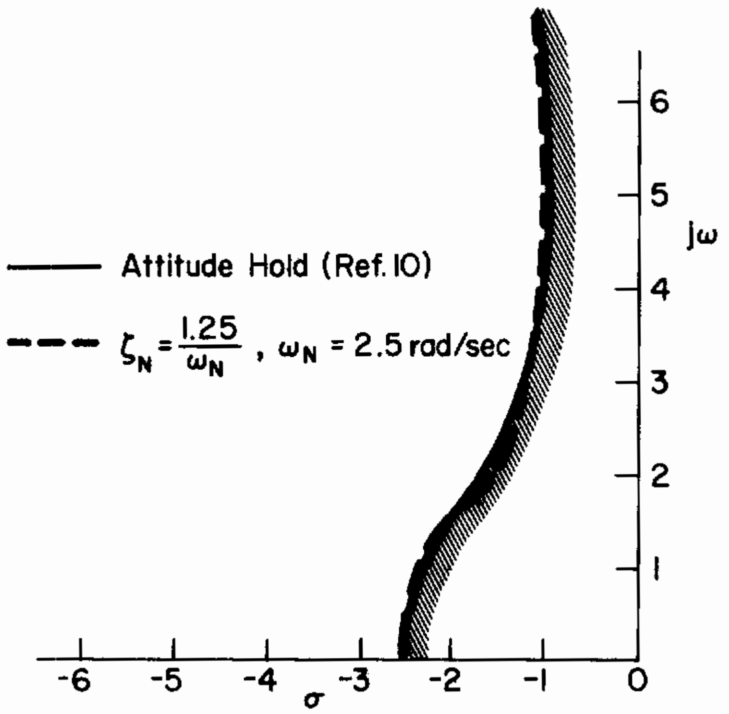

Figure 9. Rate Ordering Command System Dynamic Requirements, Ref. 10

at ω_c (the inner-loop pilot crossover) the other at ω_N, the attitude stabilization frequency. Thus the peaking at ω_N due to ζ_N does not interfere with the outer-loop crossover.

b. Translational Rate Augmentation.* Tentative estimates of the dynamic requirements for translation rate augmentation schemes (see Table IV) can be implied from closed-loop considerations. The estimations are confirmed to some degree by the large Y_v data tested by A'Harrah (Ref. 7), which are presented in Appendix A. The requirements for translation rate augmentation, again, stem basically from the lateral oscillatory mode damping considerations and the bandwidth requirements for good lateral position control. In fact, as shown in the closed-loop analyses of Appendix A, the interplay between controlled-element form, and pilot compensation needs affords the key to the translation system requirements. The pertinent controlled-element forms are given in Table IV. In Case 1, the augmented aperiodic mode, $1/T_R$, and the numerator zero, $1/T_{\varphi_1}$, are approximately equal (i.e., $Y_v \doteq 1/T'_{\varphi_1} \doteq 1/T'_R$) which means

---

*The translation rate augmentation as used here in effect changes the derivative Y_v by suitable feedback of translation or drift velocity, v, to a lateral-force producer.

TABLE IV

CONTROLLED-ELEMENT FORMS FOR TRANSLATIONAL RATE AUGMENTATION

[Position-Loop Feedback, $\delta_T/v = K_v(T_v s + 1)$]

BASIC FEATURES	PRIMARY CONTROL — ATTITUDE, φ/δ	SECONDARY CONTROL — POSITION, y/δ
Case 1 $1/T'_{\varphi_1} \doteq 1/T'_R$	$\dfrac{L_\delta}{s^2 + 2\zeta'_d\omega'_d s + \omega'^2_d}$	$\dfrac{gL_\delta}{s(s + 1/T'_R)(s^2 + 2\zeta'_d\omega'_d s + \omega'^2_d)}$
Case 2 $1/T'_{\varphi_1} \doteq \omega'_d < 1/T'_R$	$\dfrac{L_\delta(s + 1/T'_{\varphi_1})}{(s + 1/T'_R)(s^2 + 2\zeta'_d\omega'_d s + \omega'^2_d)}$	$\dfrac{gL_\delta}{s(s + 1/T'_R)(s^2 + 2\zeta'_d\omega'_d s + \omega'^2_d)}$

that the attitude controlled element looks like a second order system (i.e., Category II attitude system). In the second case, the augmented oscillatory mode, ω'_d, is nearly equal to the numerator zero, $1/T'_{\varphi_1}$. As a result, the attitude controlled element form more closely resembles the Category I attitude rate augmentation systems shown in Table III. Thus as noted previously in Ref. 1 for the longitudinal mode, the use of translation velocity feedback to a lateral force does not alter the general character of the loop dynamics. In fact, the two forms indicated are essentially the same as those resulting from the θ and $\dot{\theta}$ feedbacks. These similarities infer that the restrictions which relate to attitude control must be satisfied in addition to any which stem from position loop considerations. This conclusion is reasonably well confirmed by the adjacent sketch where the Ref. 7 data is compared to the attitude system requirements. Again open and solid symbols are used to emphasize good and bad dynamics, respectively.

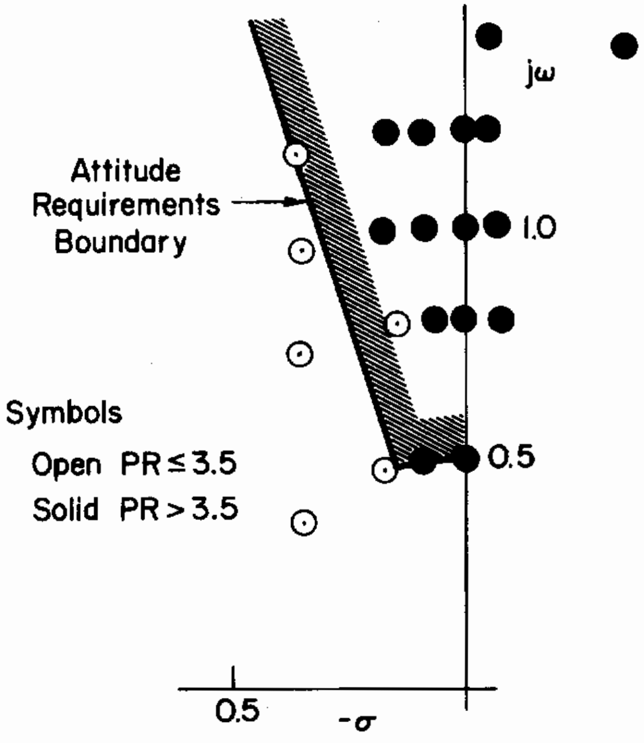

Tentatively, then, the results suggest that translational rate systems must meet either the Category I or II lateral attitude dynamic requirements.

SECTION III

CONSIDERATION OF PRACTICAL CONTROL SYSTEM ASPECTS IN HOVER

In the preceding discussions the flight control system and control surface response functions were assumed to have idealized dynamic properties. The actual manual flight control system can have dynamics which may appreciably alter the effective controlled element characteristics. Typically, the system between the pilot's manipulator and the control surface is nonlinear to some degree, although many of the more common effects can be closely approximated by simple linear relations. For example, actuator and control system properties are typically approximated by first-order lags. Other nonlinearities are strong functions of the forces on the manipulator, e.g., friction and detent or nonlinear bobweight forces; the former will be treated but the latter are beyond the scope of the present studies, which were directed at the system factors most important in closed-loop control in hover. Another set of considerations relates to control coupling between angular and translational terms. That is, the control forces applied to the airframe do not result in a pure angular acceleration response but a combination of both translational and angular. These couplings modify the numerator terms of the vehicle response to control inputs and may significantly affect the closed-loop pilot/vehicle control.

As the starting point for these discussions, the latter area, the control coupling term, is treated first. Generally, this is because there is more handling quality data available for analysis and thus provides a logical extension of the conventional hover control treated in Section II. In the remaining part of this section, we will examine the effects of the control system dynamics and nonlinearities. By necessity, a more theoretical viewpoint is taken here since there are little or no handling quality data. The prime purpose of these analyses is to show which control system properties could have significant handling qualities effects when typical VTOL hover dynamics are considered. Obviously then, the conclusions are not well substantiated, but are based on conventional nonlinear analysis techniques in combination with the closed-loop considerations evolved from the studies of Section II and Ref. 1. However, the background furnished by these studies has implication for future experimental efforts.

A. EFFECTS OF DIRECT FORCE CONTROL-COUPLING TERMS

Translatory control of the typical VTOL is generally obtained by direct tilting of the thrust vector (e.g., an attitude change); and direct force control-coupling is normally negligible. However, in order to reduce attitude control power requirements, it has been suggested by several sources (e.g., Refs. 16, 17, and 26) that the normal angular acceleration control should be supplemented to provide a substantial translational component. Several simulator programs have been undertaken to determine the best relation for such cross-coupling between angular and translation components for manual hover control. Generally, the results of these programs have been inconclusive as to the best relation of the cross-coupling components. In fact, in several incidences, control cross-coupling had a deteriorative effect on manual control. The alternative but more obvious reason for considering control coupling is that future VTOL vehicles such as the jet-lift configuration will probably have some degree of coupling, either by design or circumstance. In this case the question is, "What is an acceptable level of control coupling in hover?"

For the foregoing reasons, the effect of the translational coupling term, X_δ, on manual hover control was analyzed from the closed-loop viewpoint. Because of the close correspondence, in hover, between the longitudinal and lateral transfer functions and dynamics of interest, the conclusions are generally applicable to either mode. Several case configurations were analyzed, including situations rated by the pilots as satisfactory and unacceptable. These configurations were selected from the experimental results in Refs. 16 and 17. However, only two configurations are examined in detail to illustrate the consequence of control coupling.

a. Effects of Control Coupling Terms on Open-Loop Transfer Function. As a prelude to the closed-loop analyses it is worthwhile to consider generically how the open-loop attitude and position transfer function numerators are changed by including the coupling terms.

The effect of X_δ on the attitude response transfer function, θ/δ, is determined by the magnitude of M_u. This is evident from the transfer function shown below:

$$\frac{\theta}{\delta} = \frac{M_\delta\left(s - X_u + \dfrac{X_\delta M_u}{M_\delta}\right)}{s^3 - (X_u + M_q)s^2 + X_u M_q s + gM_u} = \frac{M_\delta\left(s + \dfrac{1}{T_{\theta_1}}\right)}{\left(s + \dfrac{1}{T_{sp_2}}\right)\left[s^2 + 2\zeta_p\omega_p s + \omega_p^2\right]}$$

For a vehicle with no aerodynamic derivatives sensitive to airspeed (e.g., M_u or X_u) the attitude response reduces to:

$$\frac{\theta}{\delta} = \frac{M_\delta}{s(s - M_q)}$$

For real values of M_u the numerator becomes a function of X_δ, M_u, and X_u:

$$N_\delta^\theta = M_\delta\left(s - X_u + \frac{M_u X_\delta}{M_\delta}\right)$$

With a stable speed stability term, positive M_u, the normally negative axial force to moment ratio, X_δ/M_δ,* moves the zero into the right half plane (RHP) as the product, $M_u X_\delta/M_\delta$, exceeds X_u.

The effect of X_δ on the position-loop transfer function is determined by the magnitude of (gM_δ/X_δ) and M_q as seen from the response numerator below:

$$N^{x}_{\theta_c} = X_\delta\left[s^2 - M_q s - \frac{gM_\delta}{X_\delta}\right] = X_\delta\left(s + \frac{1}{T_{x_1}}\right)\left(s + \frac{1}{T_{x_2}}\right)$$

These break up into a complex pair of zeros when X_δ is small or a real pair approaching $s(s-M_q)$ for X_δ very large with respect to M_δ. A root locus showing the zero locations is sketched below:

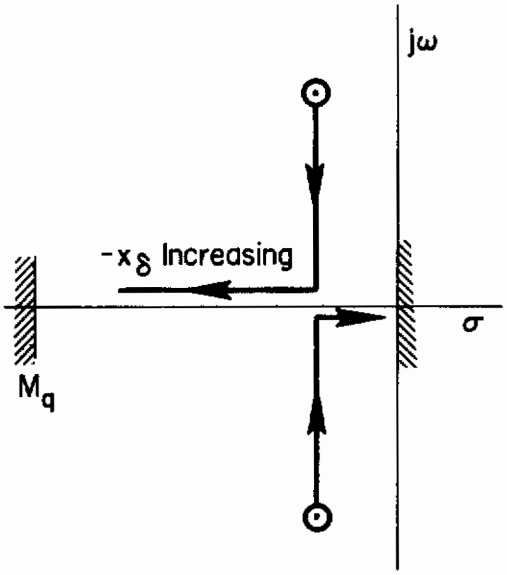

- Effect of increasing X_δ holding fixed M_q
- M_q determines the left-right zero position, ζω

▨ Limiting value of zeros

In summary, the above shows that the primary effect on the controlled element numerators, N^{θ}_{δ} and N^{x}_{δ} due to X_δ are

- The N^{θ}_{δ} zero, $1/T_{\theta_1}$ may become a nonminimum phase (RHP location) factor if X_δ or M_u is large.
- N^{x}_{δ} changes form and factors into two zeros which are either real or imaginary.

---

*X_δ/M_δ is negative since in a conventional helicopter a positive axial force as commanded by the stick produces a negative angular acceleration, since the thrust acts above the c.g.

b. Closed-Loop Effects. The two configurations selected for detailed examination here were chosen to illustrate that the consequence of control coupling on closed-loop control can involve either the attitude or position closures. The deciding factor, as will be shown later, is whether the speed stability term, M_u, is significant. The first case study considers the control situation when M_u is an important factor.

In Ref. 16, a variety of stabilization schemes in combination with a range of airframe dynamic characteristics (i.e., variation in M_u, M_q, etc.) were tested for a hover task. We have considered only the configurations employing simple rate damping (i.e., angular rate feedback). The attitude closure for the example case where M_u is important is shown in Fig. 10. This configuration was rated as marginal ($PR \doteq 4.0$) by the pilot, and as such represents the point at which increases in either M_u or X_δ caused rapid deterioration in pilot opinion.

Because of the nonminimum phase zero, $1/T_{\theta_1}$, the stable closure region is restricted to very low gains and, correspondingly, a low bandpass condition (i.e., $\omega_{c_\theta} << \omega_p$) results. While a simple gain closure (i.e., $Y_p = K_p e^{-\tau s}$) is illustrated in Fig. 10, it is obvious from the sketches shown below that the introduction of attitude lead, T_{θ_L}, will not improve

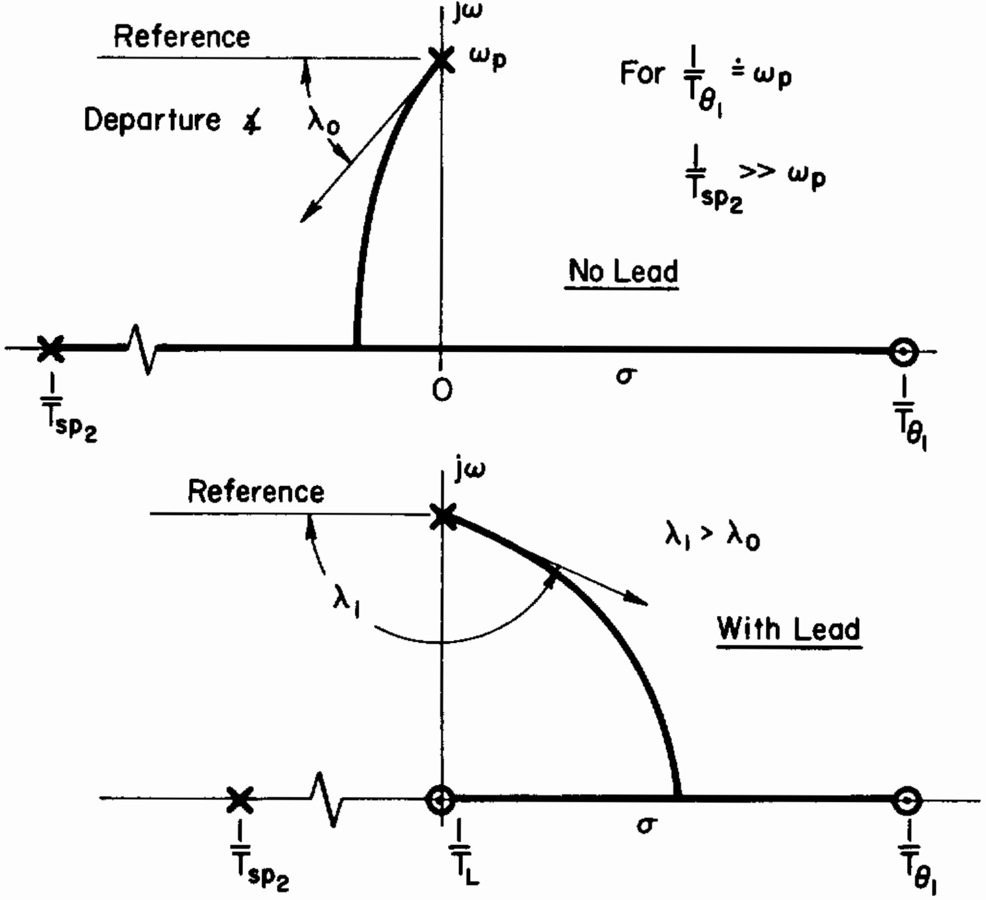

jω
Reference
ω_p
Departure ∡
λ_0
For $\frac{1}{T_{\theta_1}} \doteq \omega_p$
$\frac{1}{T_{sp_2}} >> \omega_p$
No Lead
0
σ
$\frac{1}{T_{sp_2}}$
$\frac{1}{T_{\theta_1}}$
jω
Reference
$\lambda_1 > \lambda_0$
λ_1
With Lead
σ
$\frac{1}{T_{sp_2}}$
$\frac{1}{T_L}$
$\frac{1}{T_{\theta_1}}$

Effect on Lead Compensation on Attitude Closure

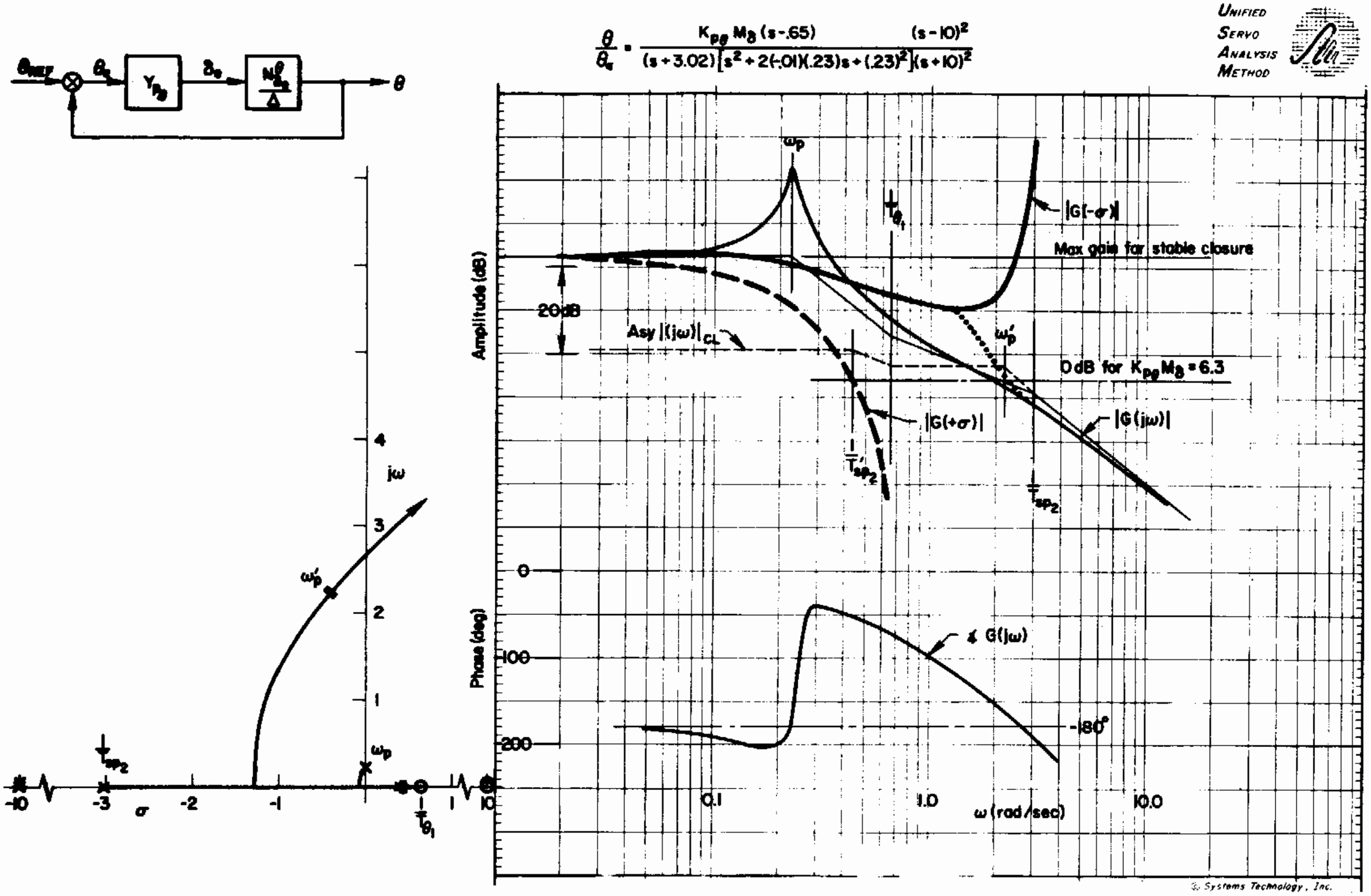

Figure 10. Attitude Loop Control with Direct Force Control Coupling, θ ⟶ δ_{STK}

the closure. In fact, because the additional zero supplied by $1/T_{\theta_L}$ adversely shifts the departure angle of loci from the phugoid, the stable gain region is reduced and is entirely eliminated as the lead becomes infinite (i.e., pure rate feedback, $1/T_{L_\theta} \equiv 0$). Thus the attitude-loop closure is relatively deficient because of the low frequency divergence which results.

The outer position-loop closure is shown in Fig. 11. Here a simple gain closure, not shown but easily visualized by removing the small pilot lead, $T_{L_x} = 1/2.75$, results in a stable multiloop control situation with an outer-loop crossover frequency of $\omega_{c_x} \doteq 1.0$ rad/sec.* The N_δ^x zeros which are due to X_δ account for the K/s features shown in the Bode diagram and enable this loop to be gain-stabilized. A small lead, T_{L_x}, to cancel the adverse phase contribution of the pilot delay term, $e^{-\tau s}$, provides an extended K/s region for crossover and additional phase margin, as can be seen in Fig. 11.

The closed-loop control situation described by the outer-loop survey is controllable, but the restriction imposed on pilot compensation to maintain a stable inner-loop, attitude, closure with adequate bandwidth apparently confirms the marginal pilot rating.

A rapid deterioration in the closed-loop control situation and corresponding degraded opinion is predictable from the above if either M_u or X_δ increases. This is evident because the consequence of such increases is to make the numerator zero, $1/T_{\theta_1}$ more unstable (further in the right half plane). A stable closure of the attitude loop becomes exceedingly difficult, and to obtain the desired crossover frequency the closed-loop divergent mode will increase (i.e., the time to double amplitude becomes smaller). Because of this unstable situation, the pilot must eventually rely entirely on the final outer-loop position closure to stabilize the system.

The second case of interest is the situation when M_u is negligible. This condition was examined in the simulator program of Ref. 17. In this study, X_δ was varied to simulate the relatively small amount such as obtainable through M_δ gearing changes or in going from one type of helicopter to another. The test vehicle was an inertial body with rate damping (i.e., M_q) but without velocity derivatives (i.e., $X_u = M_u = Z_u = 0$). Because the pilot's evaluation task was to accelerate to a specific speed, not position, the u/δ loop is therefore analyzed, the corresponding transfer function being:

$$\frac{u}{\delta} = \frac{(s^2 - M_q s)X_\delta - gM_\delta}{s^3 - (X_u + M_q)s^2 + X_u M_q s + gM_u}$$

---

*The advantage of X_δ is obvious from the position-loop amplitude feature of the x/x_e Bode, since the desired K/s-like characteristics are evident after closure of the attitude inner loop. The low frequency divergence or nonminimum phase characteristics are of course neglected.

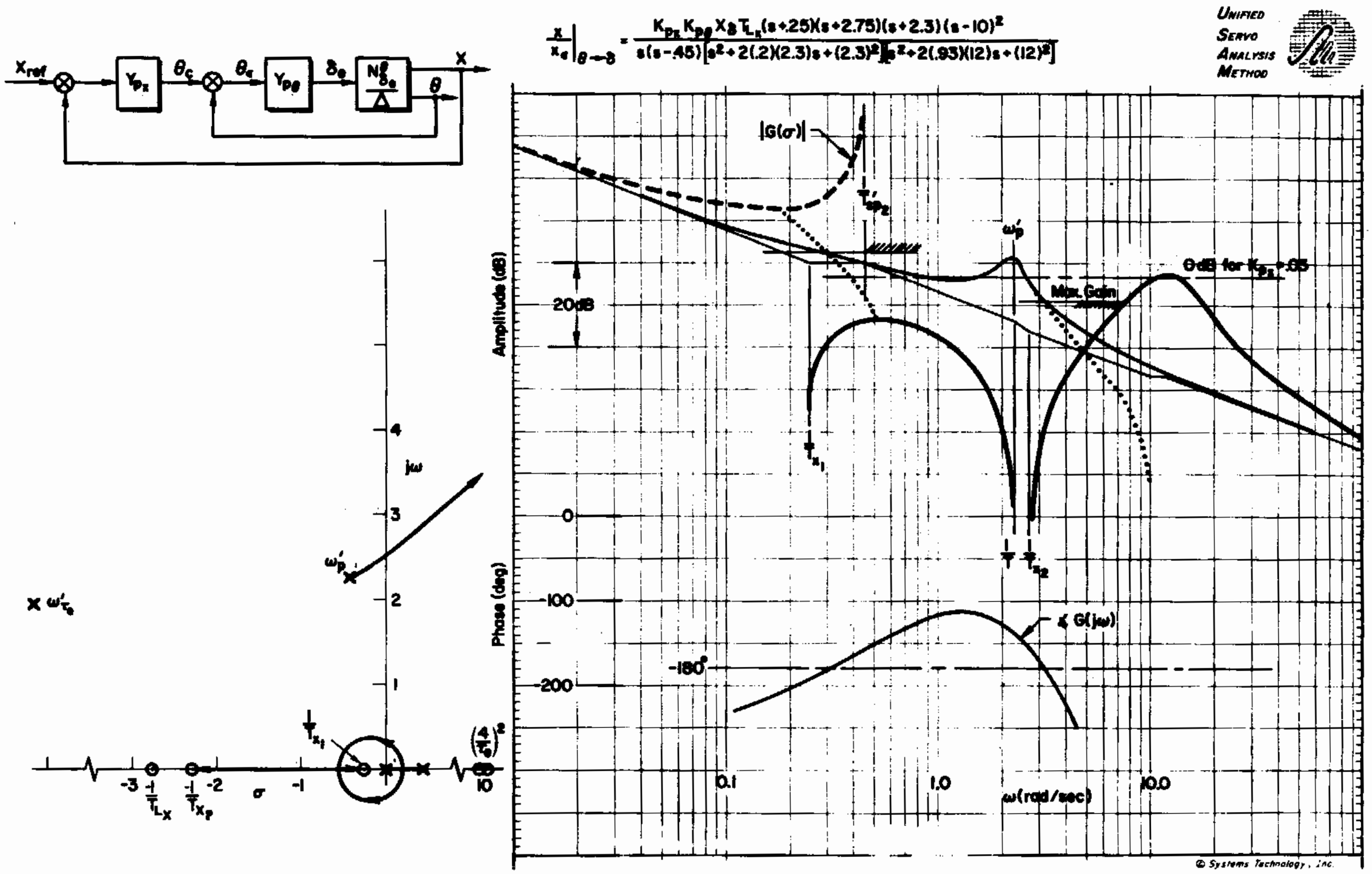

Figure 11. Position Loop Control with Direct Force Control Coupling, x, θ ⟶ δ_{STK}

As shown earlier, this zero-M_u, X_u case reduces the attitude transfer function to nearly a pure integrator where changing X_δ has no effect. The speed or position-loop, however, retains the X_δ zeros found to be helpful in position control for the "aerodynamic" vehicle analyzed above. Since X_δ does not change the inner numerator term, N_δ^θ, it cannot affect the θ-closure; thus the effects of X_δ are here confined to the outer speed loop closure. Figure 12 shows sketches of the outer loops as X_δ/M_δ is increased from 0 to −10 to −20 ft/rad, respectively. For a given gain margin, the crossover frequency is a maximum at the midvalue of X_δ. For the larger X_δ value the crossover frequency is reduced and the zeros are approaching the real axis. The possibility of reduced crossover frequency for the outer loop becomes the factor potentially influencing the vehicle control. That is, the secondary "hump" in the Bode plot intersecting the 0 dB line corresponds to a "nuisance" mode at a frequency of 2-3 rad/sec superimposed on vehicle response.

When both X_δ/M_δ and M_q are lowered (see Fig. 13), the oscillatory zeros and poles are biased more toward the RHP, introducing an "ω_φ/ω_d" effect commonly appearing in a conventional aircraft's lateral/directional mode (e.g., Ref. 28). For small X_δ this mode is at a high enough frequency as not to be objectionable, and the increased crossover frequency due to X_δ again improves the pilot ratings. Increasing X_δ beyond this apparent optimum reduces the crossover frequency again. The low damping of this zero also results in a possible instability for a certain closure range. This ω_φ/ω_d-like restriction on the position-loop closure was reflected in the pilot ratings of Ref. 17. The ratings initially improved with X_δ, then rapidly degraded as the level was increased beyond the apparent optimum.

In summary, from the results shown here, we conclude that the effects of X_δ will be generally detrimental to the manual hover control task although they do tend to improve position control. This is apparently due to the difficulty the pilot experiences in closing the attitude control loop in a stable region.

To minimize the adverse effects of X_δ on the attitude loop, speed stability, M_u, must be small and the damping terms, $-X_u$ and $-M_q$, large. When M_u is large, excessive pilot compensation is necessary unless X_u is substantially increased or the attitude control function is performed by separate augmentation schemes.

When the speed derivatives are zero ($M_u = X_u = 0$), the magnitude X_δ may restrict control due to a possible "ω_φ/ω_d" interaction of the x-loop zeros and the closed-inner loop poles set by the pilot or by an augmentation system.

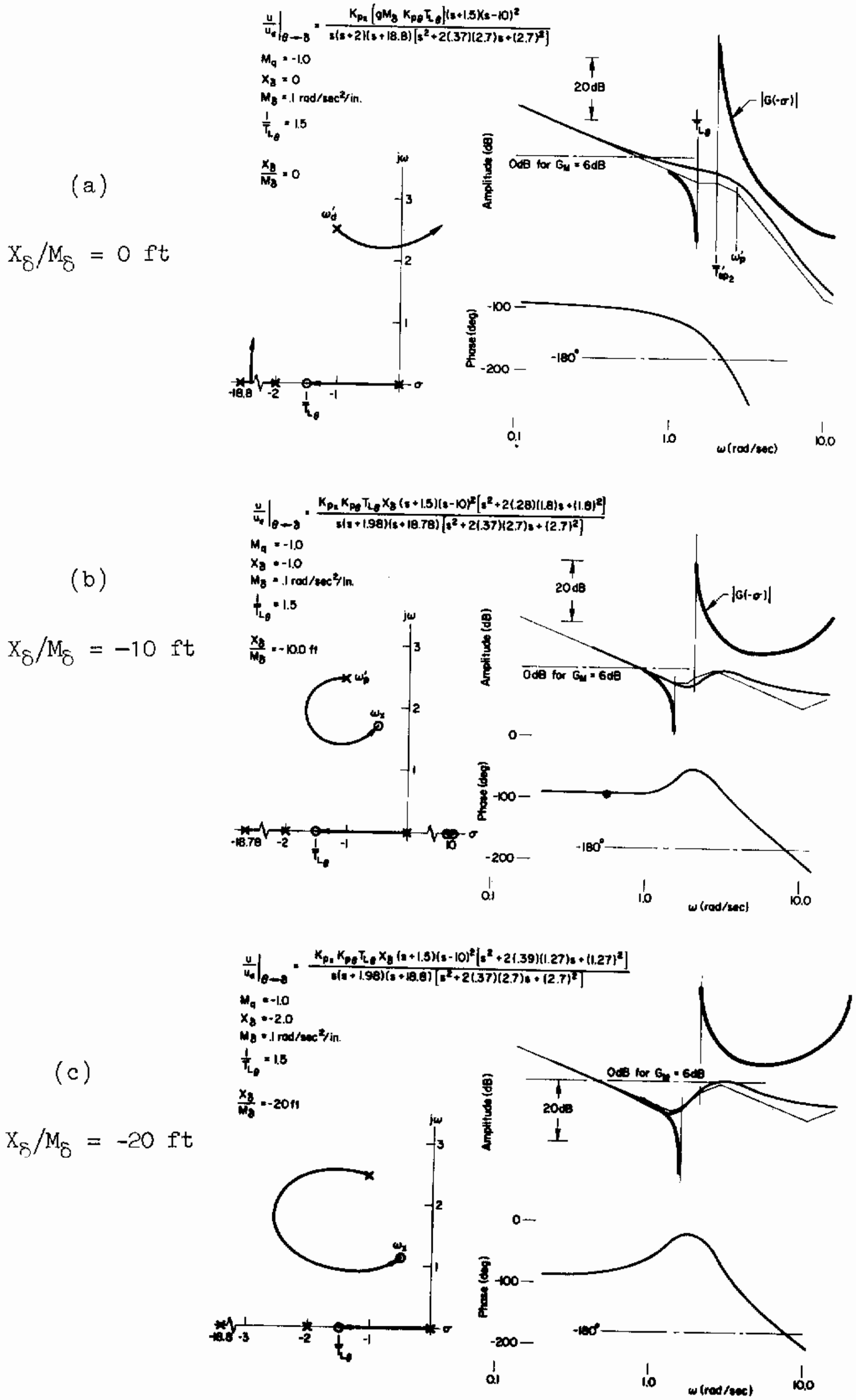

Figure 12. Effect of Axial Force Control Term, X_δ/M_δ, Airspeed Closure

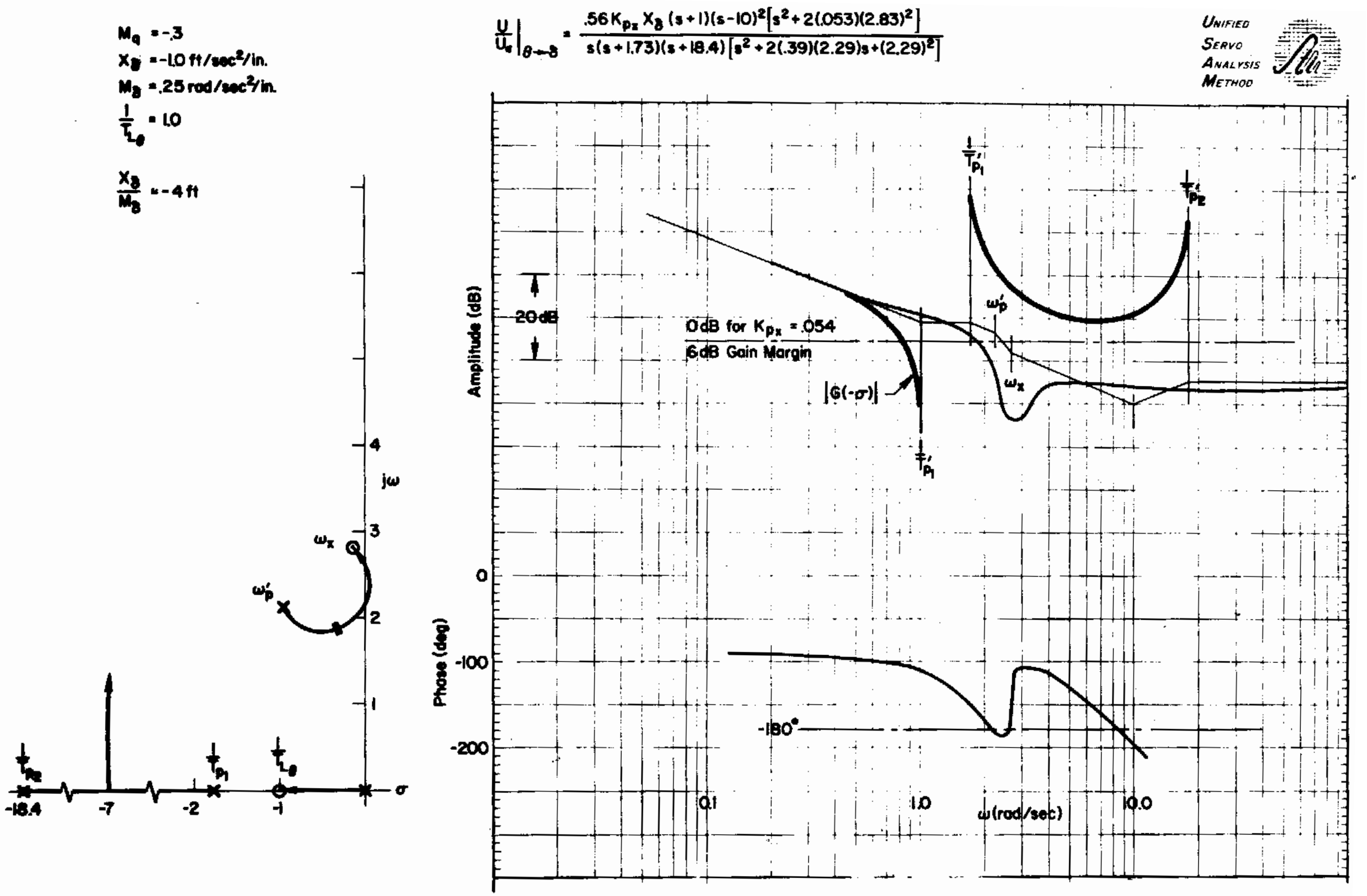

Figure 13. Effect of M_q and X_δ/M_δ on Airspeed Control; $X_\delta/M_\delta = -4$ ft

B. EFFECTS OF CONTROL SYSTEM DYNAMICS AND NONLINEARITIES

The preceding discussion of control coupling terms has assumed "ideal" control system characteristics. In this subsection, we will consider the effects that typical control system properties have on the manual control situation.

Figure 14 (extracted from Ref. 14) shows a simplified control system identifying some of the more detailed characteristics present in manual control systems. Several of the nonlinearities were chosen for examination together with other effects such as actuator lag and high frequency dynamic modes. The specific control systemproperties studied in this analysis are:

1. Effects of actuator lag
2. Effects of high frequency dynamics
3. Control system backlash
4. Control system threshold, including control feel system breakout forces
5. Actuator velocity saturation
6. Valve friction and flow forces
7. Stability augmenter authority limits

Two airframe dynamic configurations, representing a satisfactory and an unacceptable handling quality rating were chosen as the basic controlled elements in these analyses. These hover configurations are listed below for reference and were selected from the conventional VTOL dynamics analyzed in Appendix A. The closed-loop pilot/vehicle system without the adverse control system features is viewed as the base condition. With this as a starting point, we show how inclusion of nonlinearities or other control system features can adversely affect the closed-loop control situation. From such considerations we attempt to judge, where possible, just what level of the characteristic will cause a significant deterioration in the pilot opinion or handling qualities.

CASE	AERODYNAMIC CHARACTERISTICS			DYNAMIC FACTORS			
	Y_v	L_v	L_p	$1/T_{\varphi_1}$	$1/T_R$	ζ	ω
Satisfactory (PR = 2.7)	−0.037	−0.01	−2.50	0.037	2.55	−0.018	0.36
Unacceptable (PR = 7.3)	−0.037	−0.04	−1.25	0.037	1.70	−0.239	0.87

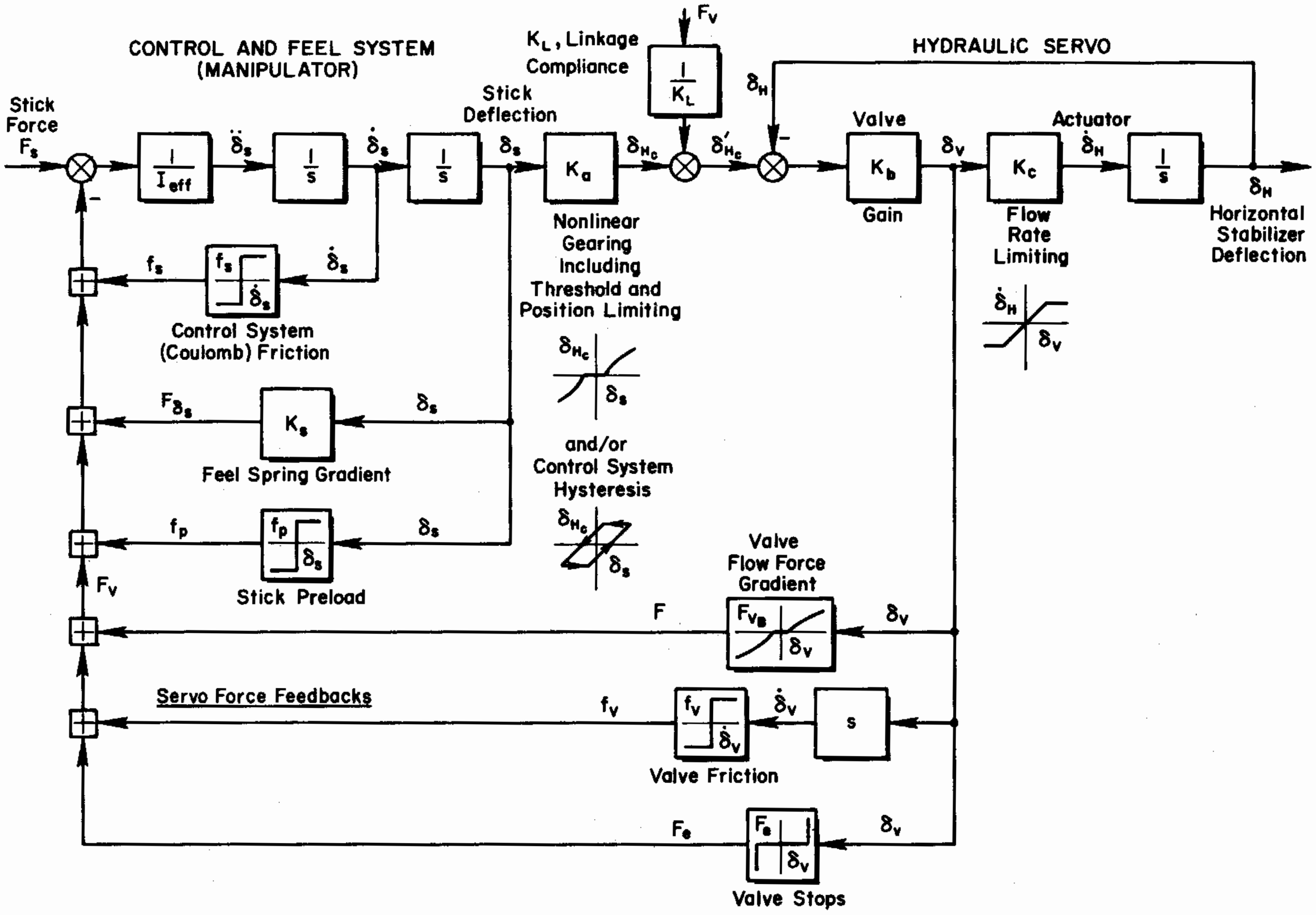
CONTROL AND FEEL SYSTEM
(MANIPULATOR)
HYDRAULIC SERVO
Stick
Force
F_s
$\frac{1}{I_{eff}}$
$\ddot{\delta}_s$
$\frac{1}{s}$
$\dot{\delta}_s$
$\frac{1}{s}$
Stick
Deflection
δ_s
K_a
δ_{H_c}
K_L, Linkage
Compliance
F_V
$\frac{1}{K_L}$
δ'_{H_c}
δ_H
Valve
K_b
Gain
δ_V
K_c
Flow
Rate
Limiting
Actuator
$\dot{\delta}_H$
$\frac{1}{s}$
δ_H
Horizontal
Stabilizer
Deflection
Nonlinear
Gearing
Including
Threshold and
Position Limiting
and/or
Control System
Hysteresis
f_s
Control System
(Coulomb) Friction
F_{δ_s}
K_s
Feel Spring Gradient
f_p
Stick Preload
F_V
Valve
Flow Force
Gradient
F_{V_B}
F
Servo Force Feedbacks
f_V
$\dot{\delta}_V$
s
Valve Friction
F_e
Valve Stops

Figure 14. Elements of Control Feel System Characteristics

1. Effects of Actuator Lag, T_c

A general sensitivity expression is derived in Appendix B to show the effect of the actuator lag on the closed-loop roots. Since the inner-loop closure requires the highest bandpass, the expression as developed considers only this closure. The primary effect of the lag from a closed-loop viewpoint is to reduce the effective bandwidth of this closure. This effect is shown by the migration of the closed-loop oscillatory mode, ω_d' (approximately equal to the crossover frequency, ω_c) as sketched below. As values of actuator lag become very large the roots of the dominant ω_d' mode become coincident with

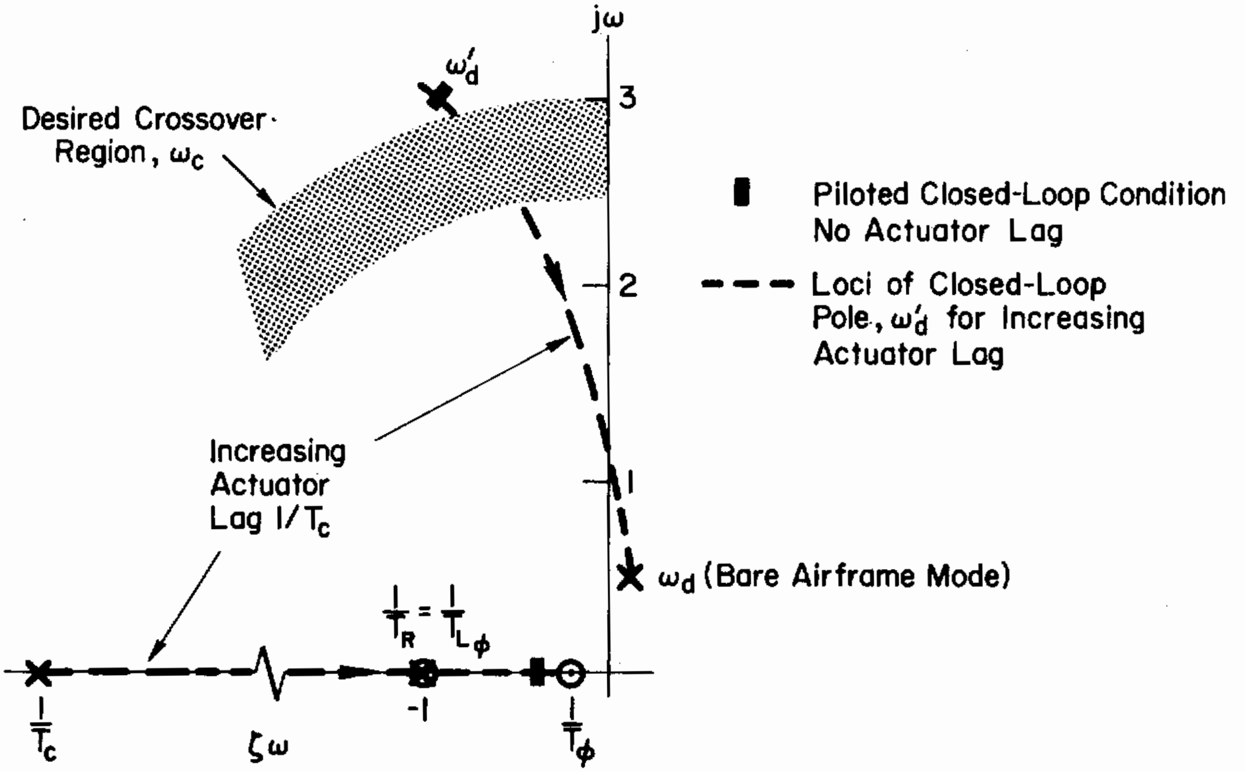
jω
ω_d'
3
Desired Crossover Region, ω_c
▮ Piloted Closed-Loop Condition No Actuator Lag
– – – Loci of Closed-Loop Pole, ω_d' for Increasing Actuator Lag
2
Increasing Actuator Lag $1/T_c$
1
ω_d (Bare Airframe Mode)
$\frac{1}{T_R} = \frac{1}{T_{L\phi}}$
-1
$\frac{1}{T_c}$
$\zeta\omega$
$\frac{1}{T_\phi}$

Sketch of Closed-Loop Roots as a Function of Actuator Lag, $1/T_c$
(Attitude Loop Only)

the Dutch roll roots of the "basic" vehicle. This is logical since, if the actuator is viewed as an extremely low pass filter, then pilot command inputs are essentially completely attenuated and the system reverts to basic vehicle open-loop characteristics. The desired inner-loop crossover frequency region ($\omega_c \geq 2.5$ rad/sec) is shown as a band on the sketch. When actuator lag becomes greater than some nominal value, the pilot is required to change his compensation to maintain the desired crossover frequency, ω_c, and a stable attitude closure. This provides the basis for estimating the level at which the lag will affect handling qualities. As noted in previous discussions and shown in Appendix A, we can assume that a significant degradation in pilot opinion will occur if values of pilot's attitude loop lead time constant greatly exceed 1 sec and/or the lead is ineffective as a means of compensation. We will apply these simple rules to estimate the effects of actuator lag on the satisfactory and unacceptable cases. Root locus sketches are used in the following discussions for clarity; however, the conclusions are based on detailed system surveys.

a. Satisfactory Case. For the satisfactory dynamics (i.e., $\omega_d \leq 0.5$ rad/sec and $\zeta \doteq 0$), the frequency* of the actuator lag must be ten times greater than the bare airframe Dutch roll frequency $\lfloor (1/T_c)/\omega_d > 10:1 \rfloor$ to ensure that no significant deterioration in pilot opinion will occur. This is shown by the root locus traces in Fig 15a which illustrate how the closed-loop attitude root ω_d' changes for various combinations of lags and pilot lead compensation. Basically, if no adjustment in compensation is assumed as the lags increase, the closed-loop performance deteriorates (i.e., both bandpass and damping decrease). However, for the condition where $1/T_c \doteq 10\,\omega_d$, a lead of approximately 1 sec ($T_L = 1.0$) will compensate for the system lag and the closed-loop performance will be maintained. For larger actuator lags the closed-loop situation cannot be restored without additional pilot compensation (e.g., increased lead, T_{L_φ}, and/or reduced pilot effective delay, τ_e). This is obvious from the figure, since the closed-loop roots are of lower frequency for the larger lags.

Limited verification of these predicted effects is shown by the Ref. 2 data reproduced in Fig. 16. Here the estimated T_c's for which a significant change in PR is predicted ($1/T_c \doteq 10\,\omega_d$) are superimposed on the actual (longitudinal) data. For the two dynamic conditions tested, the predicted values coincide with the onset ($\Delta PR \doteq 0.5$) of pilot rating degradation.

b. Unacceptable Case. When the basic airframe dynamics are unacceptable, the closed-loop performance trends with increasing lag are essentially the same as for the satisfactory case. This is shown in Fig. 15b, where we again note that the bandwidth decreases when the pilot's lead compensation remains constant (i.e., $1/T_{L_\varphi} = 1/T_R$). Moreover, the relative improvement in the closed-loop frequency and damping when lead corresponding to $T_{L_\varphi} = 1$ is used is far less than for the acceptable cases. However, Fig. 15 does indicate that if the lag break "frequency" is, again, approximately 0.1 of the bare airframe frequency ω_d [i.e., $(1/T_c)/\omega_d > 10:1$] the closed-loop situation is nearly unchanged; we infer therefore that there would be no significant deterioration in pilot opinion for such values of T_c.

Unfortunately there are no data, as of this writing, to check this conclusion for the case in question. However, the unacceptable bare airplane oscillatory frequency is about 0.85 rad/sec (see Fig. 15b) which is about halfway between the frequencies corresponding to the two conditions shown in the data of Fig. 16. Except for the difficulty of easily identifying ΔPR's of 0.5 for basic ratings of 6.5 (see Ref. 11) we would therefore anticipate similar results for the unacceptable case in question.

2. Effects of High Frequency Dynamics

High frequency dynamic modes associated with the control system, hydraulic actuator or basic airframe can be approximated by an overall transport lag

---

*Bandwidth and crossover frequency are assumed equivalent to the closed-loop roots for simplicity.

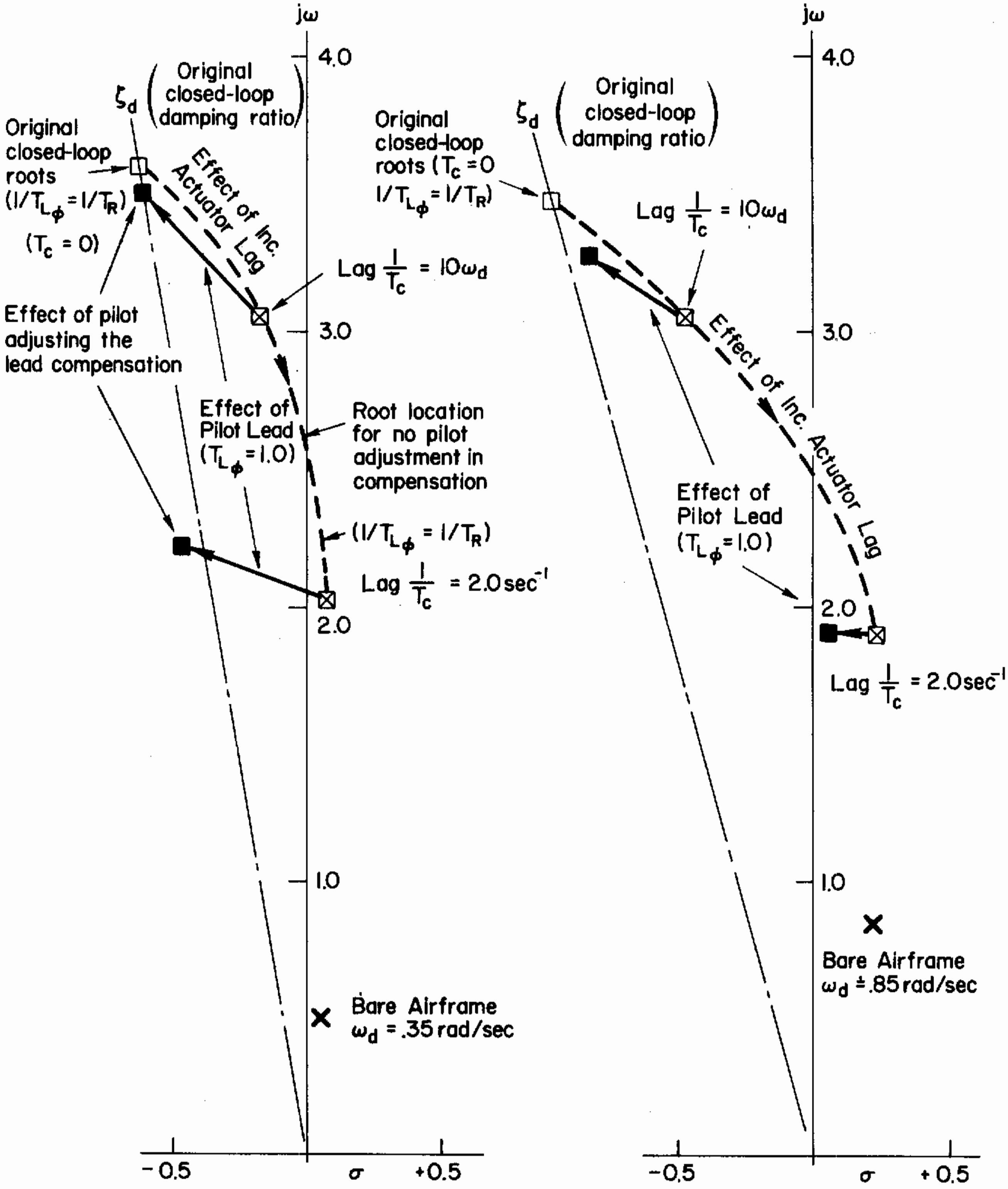

a) Satisfactory Case

b) Unacceptable Case

Figure 15. Effect of Actuator Lag ($1/T_c$)

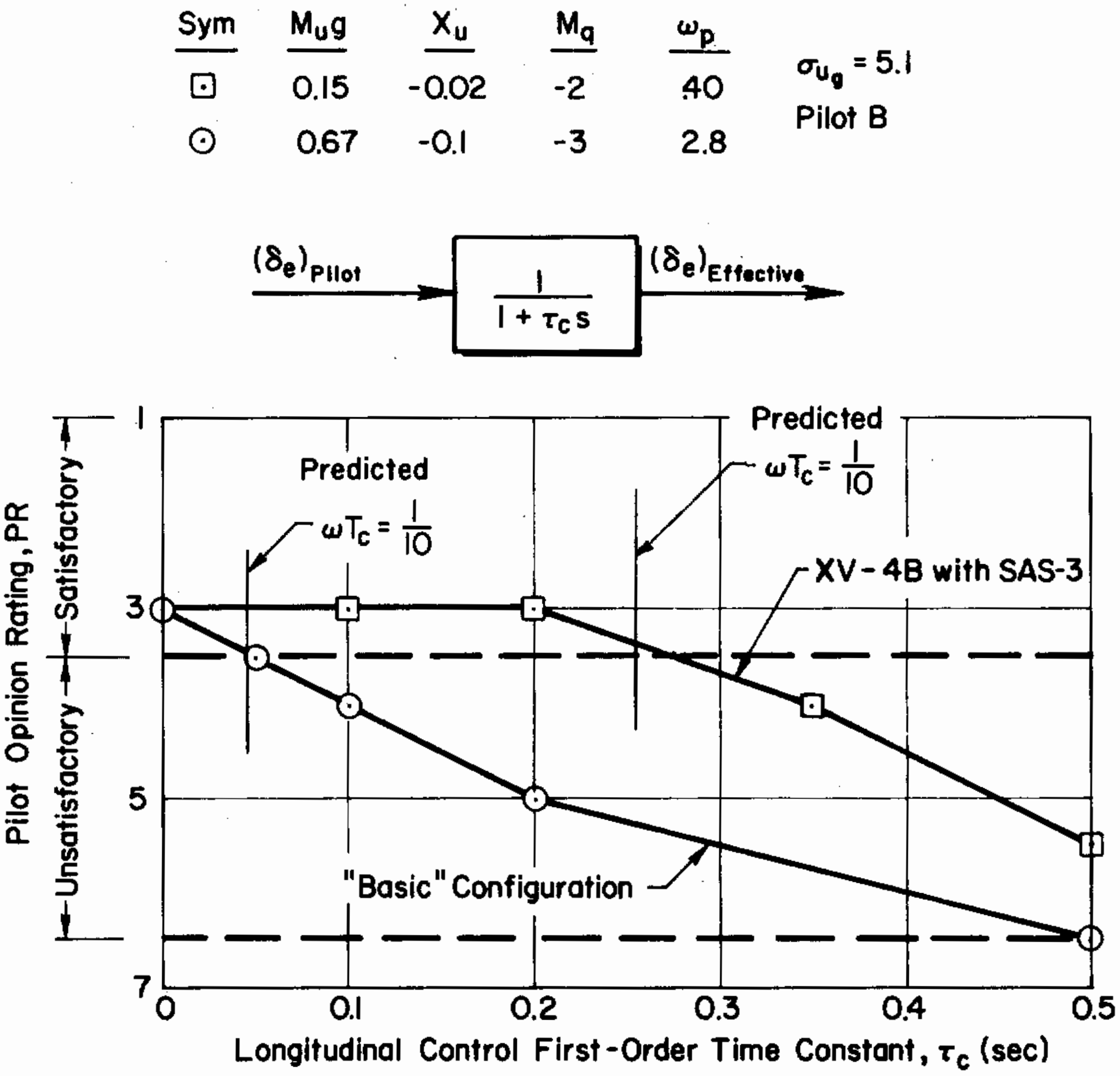

Sym	$M_u g$	X_u	M_q	ω_p
⊡	0.15	-0.02	-2	40
⊙	0.67	-0.1	-3	2.8

Figure 16. Effects of Longitudinal Control Lag on Handling Qualities of XV-4B Aircraft

$e^{-\tau_c s}$. This approximation, based on the assumption that high frequency dynamic modes exhibit negligible attentuation but significant phase lag in the frequency range of interest, is used in the analyses to follow.

a. Satisfactory Case. Figure 17a illustrates how the dominant closed-loop roots for the satisfactory case are affected by increasing values of transport lag (τ). The major effects are reductions in bandpass and damping ratio. Lead generation on the part of the pilot can restore the original performance of the system for values of τ less than approximately 0.6 sec without pilot opinion degradation (i.e., $T_L \geq 1$). If a nominal transport delay of 0.4 sec is attributed to the pilot then the effective additional delay due to high frequency dynamics and other sources must be limited to 0.2 sec in order to avoid significant opinion degradation.

b. Unacceptable Case. The effect of increasing transport lag on the dominant mode of the unacceptable case is shown on Fig. 17b. Reduction of bandpass and damping ratio is again evident. In this case however pilot lead is ineffective in restoring system performance. Thus in order to improve the system dynamic performance the pilot is forced to abandon the conventional technique of lead generation, and to adopt some other tactic such as reduction of his basic reaction time delay (τ_e). This implies that he is operating close to the performance limits of his neuromuscular system and as a consequence pilot opinion will undergo rapid degradation.

The nature of the dynamics for the unacceptable case therefore makes this situation much less tolerant of variations in system parameters (such as transport lag) than is the case for the satisfactory rated dynamics. Such intolerance to variations in system parameters appears to be one of the hallmarks of configurations which receive unacceptable ratings. This feature can be extremely useful in preliminary analysis for delineating "crucial" configurations likely to receive a poor pilot rating.

3. Control System Backlash

Effects of control system backlash are shown on the gain-phase plot of Fig. 18. The linear portion of the loop $G(j\omega)$ is plotted (with ω a parameter along the plot) for satisfactory and unacceptable cases; the $-1/N$ function, the negative inverse of the nonlinear describing function is plotted for increasing values of the oscillatory amplitude and is frequency-independent. The intersection of $G(j\omega)$ and $-1/N$ produces a limit cycle condition at the corresponding $G(j\omega)$ frequency and the $-1/N$ amplitude (e.g., see Ref. 31). Changes in the linear system gain shift the $G(j\omega)$ plot up and down relative to the $-1/N$ plot; and the Fig. 18 levels of gain used are considered representative of expected pilot adaptation in the absence of any backlash. The predicted limit cycle for the unacceptable case occurs at a higher frequency and larger amplitude than the satisfactory case. It is evident from Fig. 18 that reduction in pilot gain for the satisfactory case does not significantly alter the characteristics of the limit cycle until very low values of gain are reached. For the unacceptable case, however, a much smaller reduction in pilot gain produces a rapid increase in limit cycle amplitude. This

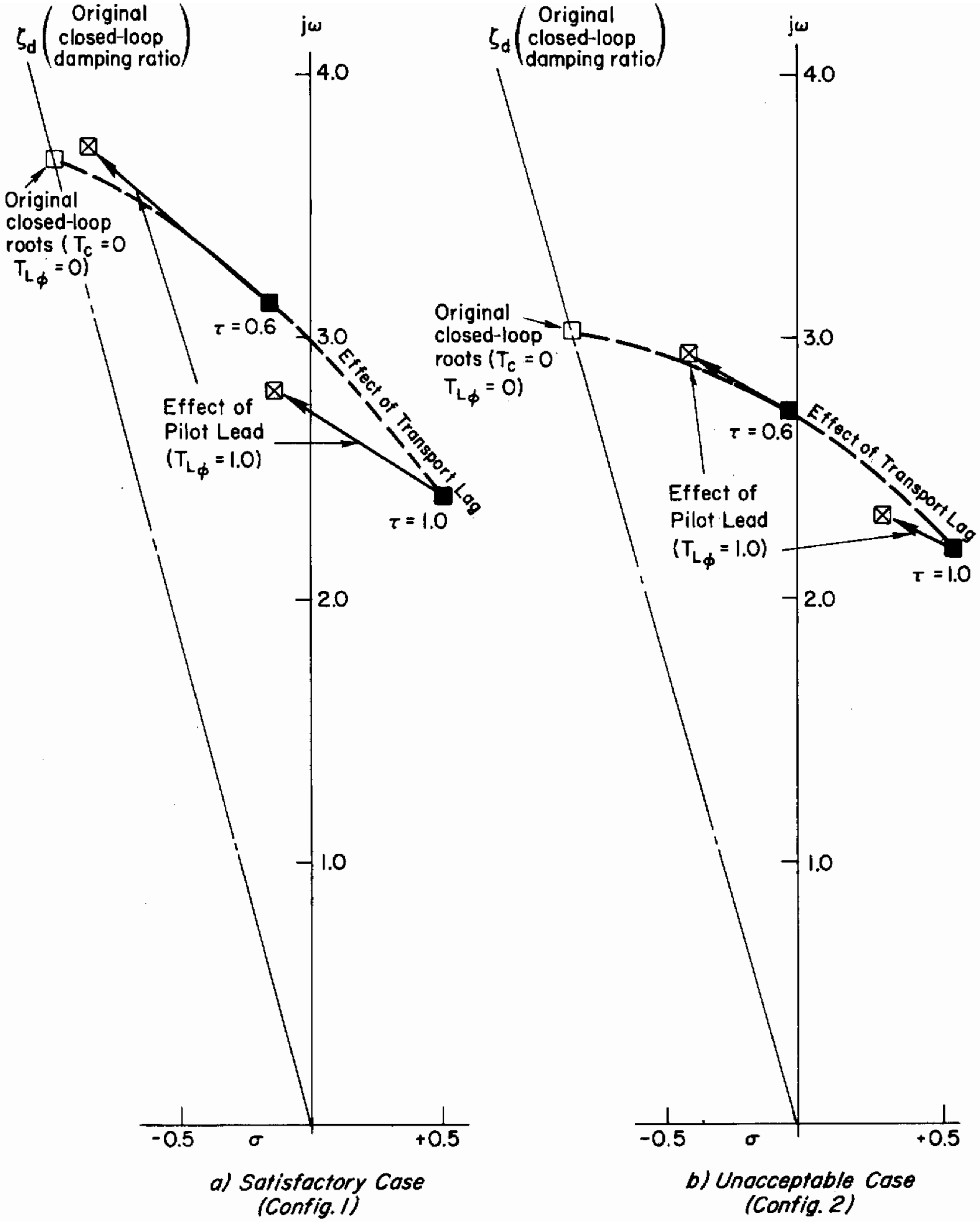

Figure 17. Effect of Transport Lag

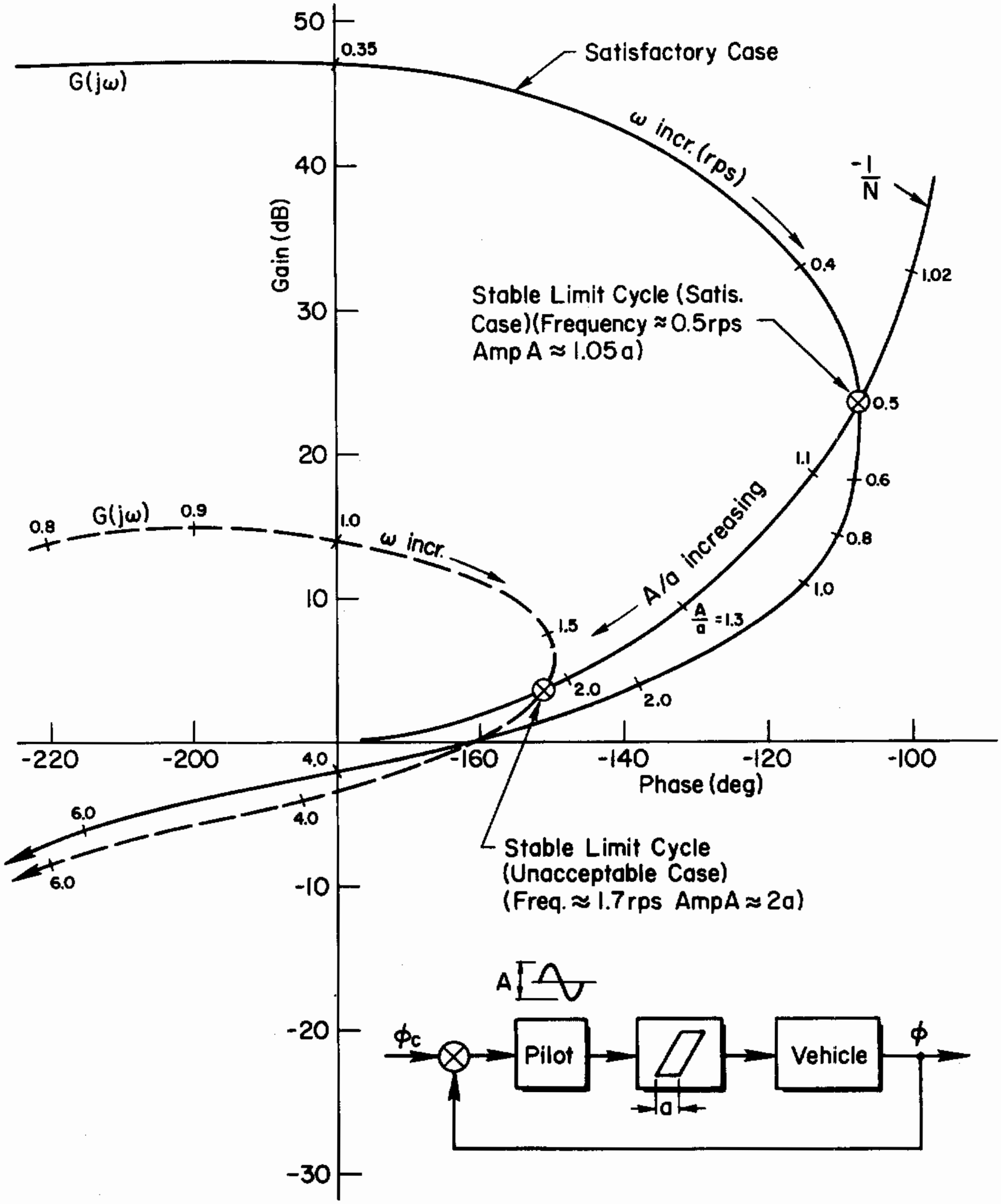

Figure 18. Effect of Control System Backlash on Pilot/Vehicle Attitude Loop

is primarily due to the narrower stable gain region in the unacceptable case which resulted initially from the higher value of Dutch roll frequency. Of course, increases in gain will rapidly drive the linear system unstable; i.e., when the amplitude of $G(j\omega)$ at -180° of phase is greater than 0 dB.

For the limit cycle predicted in the satisfactory case, amplitude of aircraft oscillation (attitude and displacement) were calculated for various values of backlash magnitude (see Fig. 19). Experimental data from the simulator investigation of Ref. 2 provides pilot rating and comments for various levels of control system backlash. Vehicle dynamics for the test vehicle of Ref. 2 and for the satisfactory case in this analysis are similar.

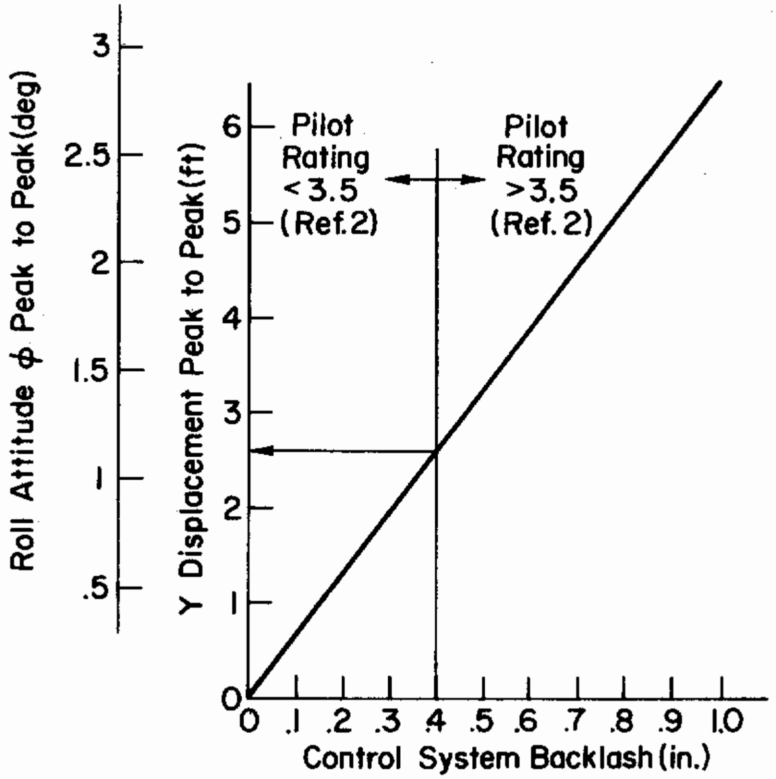

Figure 19. Effect of Increasing Backlash on Amplitude of Predicted Limit Cycle (Satisfactory Case Example)

From Ref. 2 data when the levels of backlash exceeded 0.4 in. the pilot rated the flying qualities as unsatisfactory. At this level of backlash the pilot also commented that precision control of attitude was difficult and that the aircraft exhibited a tendency to oscillate in position. The calculated limit cycle amplitudes for a backlash value of 0.4 in. are of the order of $\pm 0.5^\circ$ attitude and ±1.3 ft in lateral position (see Fig. 19). Frequency of the predicted limit cycle was in the region of 0.5 rad/sec. Since it has already been shown in Ref. 1, and inferentially demonstrated by the correlations in Section II, that typical crossover frequencies for the attitude loop are in the region 2 to 3 rad/sec and for the position loop 0.5 to 1 rad/sec, it would appear that the predicted limit cycle would be more troublesome to the pilot in controlling position. Also, a lateral displacement of the aircraft of ±1.3 ft is in the region of average error for control in a hovering task and as such would be readily discernible to the pilot in the Ref. 2 simulations. A logical deduction, therefore, is that the observed downrating was primarily due to the resulting position wander.

On the other hand, for the unacceptable case studied, the predicted limit cycle amplitudes are $\pm 2^{\circ}$ in roll and ±0.4 ft in lateral displacement. The decrease in lateral displacement amplitude is due to its significant attenuation at the higher frequency of the predicted limit cycle. This suggests that, as the limit cycle frequency increases, the emphasis as regards system degradation would be shifted from position control to attitude control. Unfortunately there are no specific experimental data to support this deduction.

4. Control System Threshold

Effects of control system threshold are shown in Fig. 20. The same value of threshold magnitude will produce a larger amplitude and higher frequency limit cycle in the unacceptable case compared with the satisfactory case. This is primarily due to the smaller stable gain region in the unacceptable case which results from the higher Dutch roll frequency of the basic vehicle.

It is evident that reduction of pilot gain in the satisfactory case does not alter the characteristics of the limit cycle significantly until low values of gain are reached. In the unacceptable case, however, reduction of pilot gain produces a rapid increase in the limit cycle amplitude. A given value of control system threshold, therefore, is much more likely to produce deterioration of pilot opinion in the unacceptable case than in the satisfactory case.

Unfortunately there are no available experimental data which bear directly on these predictions.

5. Actuator Velocity Saturation

Effects of actuator velocity saturation are shown on Fig. 21. The predicted limit cycles for both satisfactory and unacceptable cases are unstable; that is, whenever the rate saturation limit is exceeded, the amplitude of the oscillation in the pilot/vehicle loop tends to increase. Increased amplitude produces increased phase lag because of the saturation effect and the oscillation amplitude tends to diverge. The fundamental reason for this divergence lies in the characteristics of the basic airframe. Because the basic vehicle has an unstable Dutch roll mode the response characteristic exhibits a single crossover with the saturation function $-1/N$. If the basic vehicle were stable the characteristics would be similar to those shown in Fig. 22. Residual oscillations tend to converge toward the stable limit cycle point resulting in an oscillation of finite amplitude. In the Fig. 22 case the system can be designed so that the limit cycling is either eliminated or is small enough to be negligible.

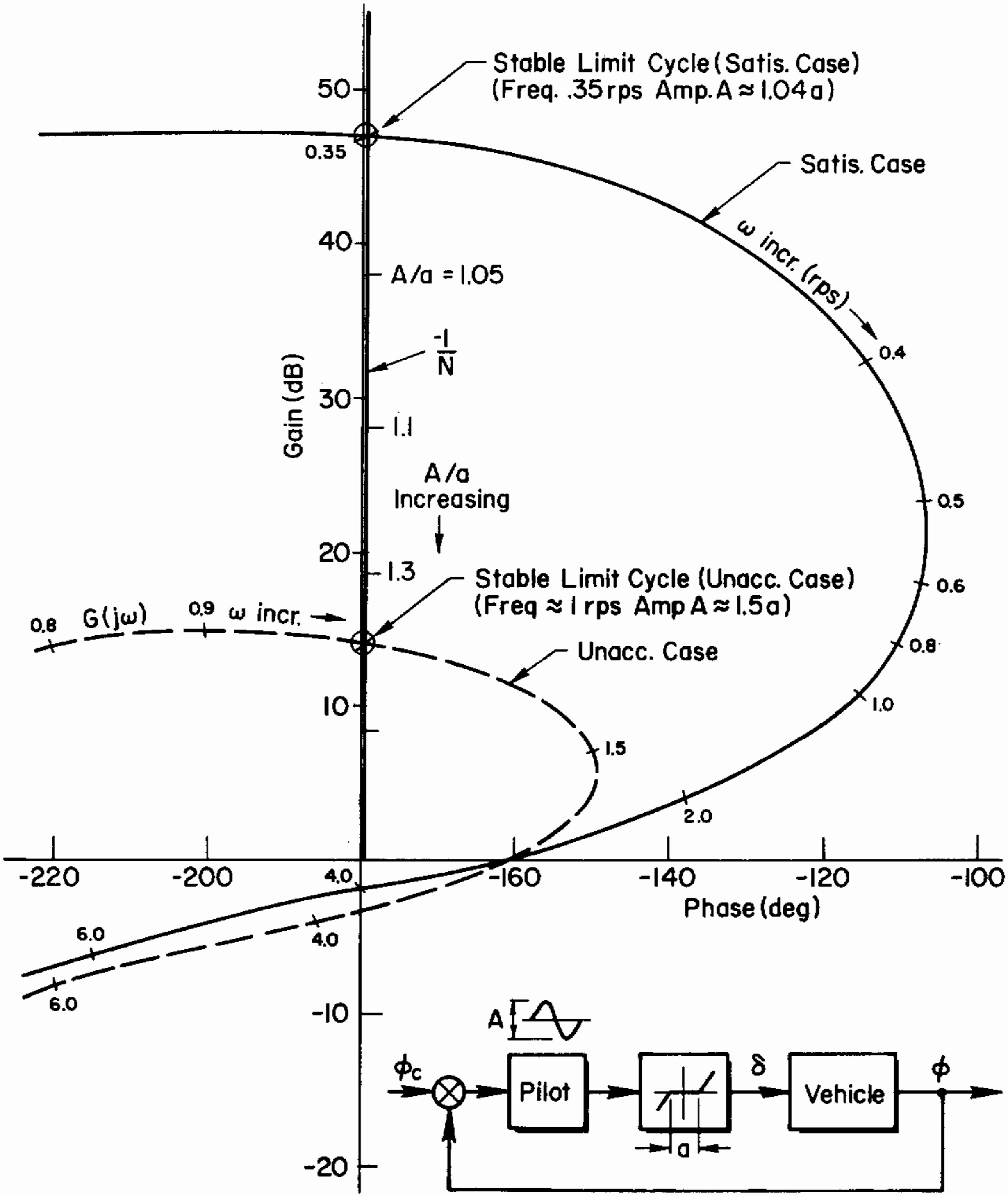

Figure 20. Effect of Control System Threshold on Pilot/Vehicle Loop

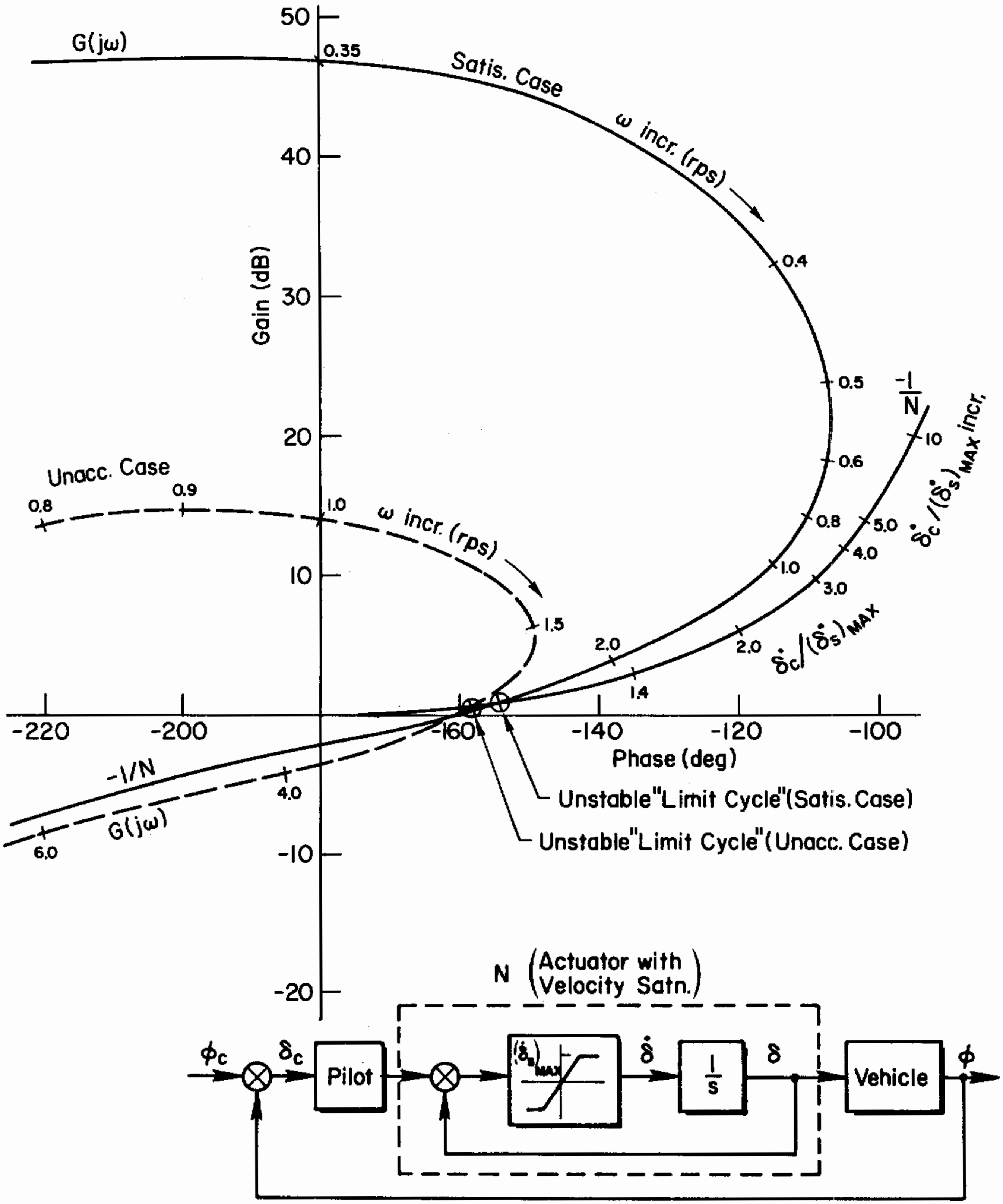

Figure 21. Effect of Actuator Velocity Saturation on Pilot/Vehicle Loop

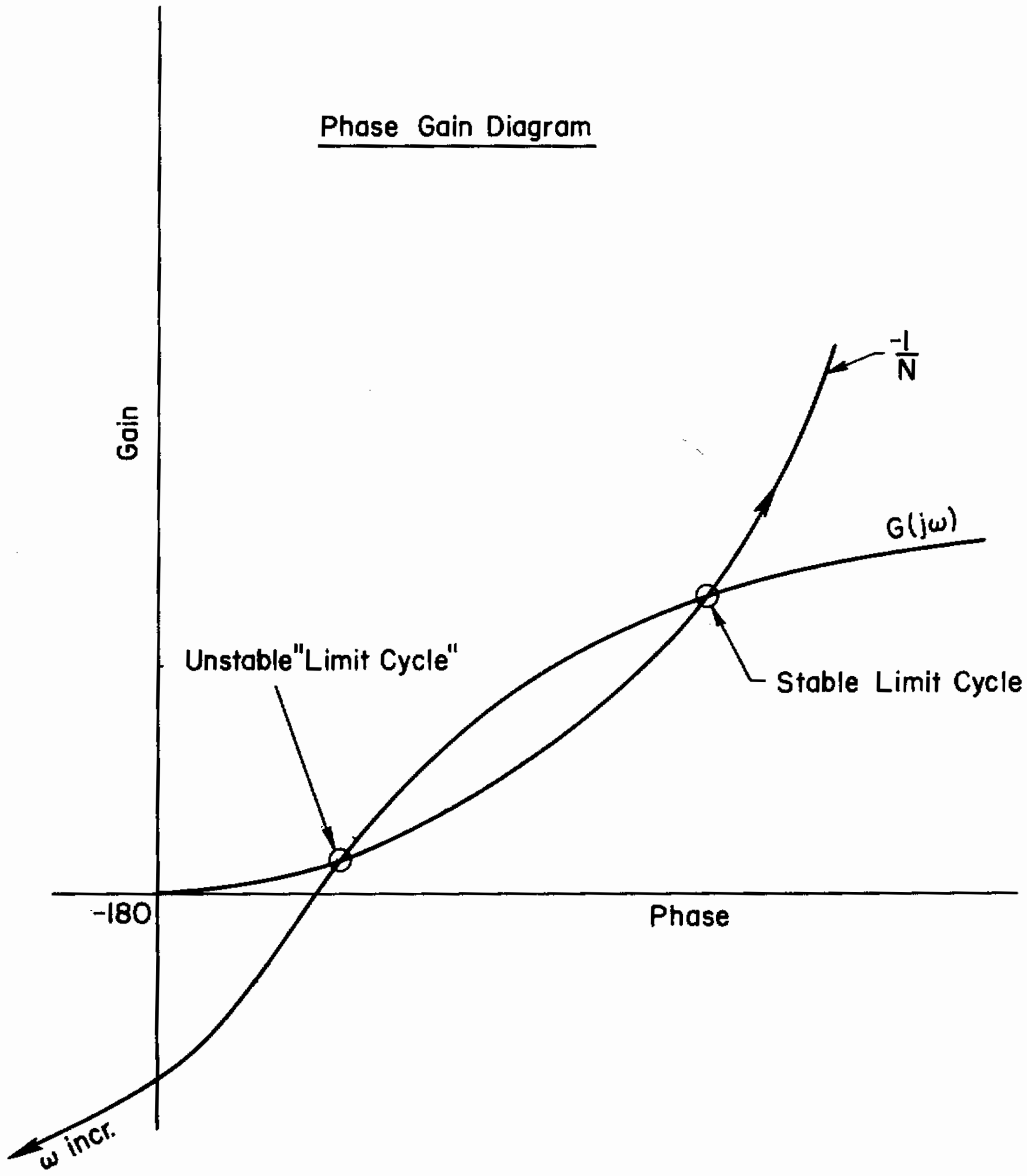
Phase Gain Diagram
Gain
$-\frac{1}{N}$
$G(j\omega)$
Unstable "Limit Cycle"
Stable Limit Cycle
-180
Phase
ω incr.

Figure 22. Effect of Actuator Velocity Saturation for Stable Vehicle

It would appear, therefore, that if the damping of the basic vehicle modes is not positive the actuator rate must be set to avoid saturation and attendant divergence problems.

6. Valve Friction and Flow Forces

Effects of valve friction and Bernoulli flow forces were estimated using a simplified model of the type shown in Fig. 23. Bernoulli flow forces were assumed to be a linear function of valve displacement. The resultant effect is to increase the time constant of the actuator and, therefore, to reduce the actuator bandpass [time constant is increased from $T = 1/K_V$ to $T_e = (K_L + K_B)/K_L K_V$, see Fig. 23]. Thus the effect of Bernoulli flow forces on the pilot/vehicle loop is similar to the effect of increasing actuator lag which was discussed previously.

Applying describing function techniques, effects of valve friction reduce to an effective acceleration feedback loop, the feedback gain being a function of amplitude (see Fig. 23). The major effect of this feedback is to increase the phase lag of the actuator as input amplitude to the nonlinear element decreases (see Fig. 24a). Increased phase lag for the satisfactory case (Fig. 24b) tends to decrease both the maximum phase margin and the stable gain region. Thus as values of valve friction increase, the satisfactory case tends to exhibit characteristics similar to the unacceptable case indicating a trend towards poorer pilot opinion. Maximum phase margins are already small for the unacceptable case and additional phase lag due to valve friction will be even more detrimental than for the satisfactory case.

7. Stability Augmenter Authority Limits

Stability augmenter authority limits effectively reduce the SAS feedback gain as a function of amplitude. As amplitudes of vehicle angular rate increase beyond some fixed level of saturation, the vehicle dynamics tend toward the unaugmented characteristics as in Fig. 25. It is possible therefore to specify saturation values, as a function of angular rate amplitude, which will provide a minimum desired level of augmentation.

Effect of pitch rate stabilization authority was studied experimentally in Ref. 2 (see Fig. 26). Control usage in terms of vehicle pitch rate was measured as $\sigma_{\dot{\theta}} = 0.045$ rad/sec based on $\sigma_{u_g} = 5.1$ ft/sec. Figure 25 shows that in order to maintain maximum damping level as provided by the SAS system $\delta_{SATN}/\dot{\theta} = 10$. The required saturation limit corresponding to $\sigma_{\dot{\theta}} = 0.045$ is therefore 0.158 rad/sec^2. From Fig. 26 this corresponds to a pilot rating of 3.0 which suggests that pilot opinion degradation will be negligible if the saturation limits are specified by $\sigma_{\ddot{\theta}}$ for a design gust of 5.1 ft/sec. To interpret this result in another way, if the saturation limits are such that less than 32 percent of all pitch rate amplitudes exceed the saturation limit, then pilot opinion degradation will be negligible. For higher probabilities of exceedance corresponding

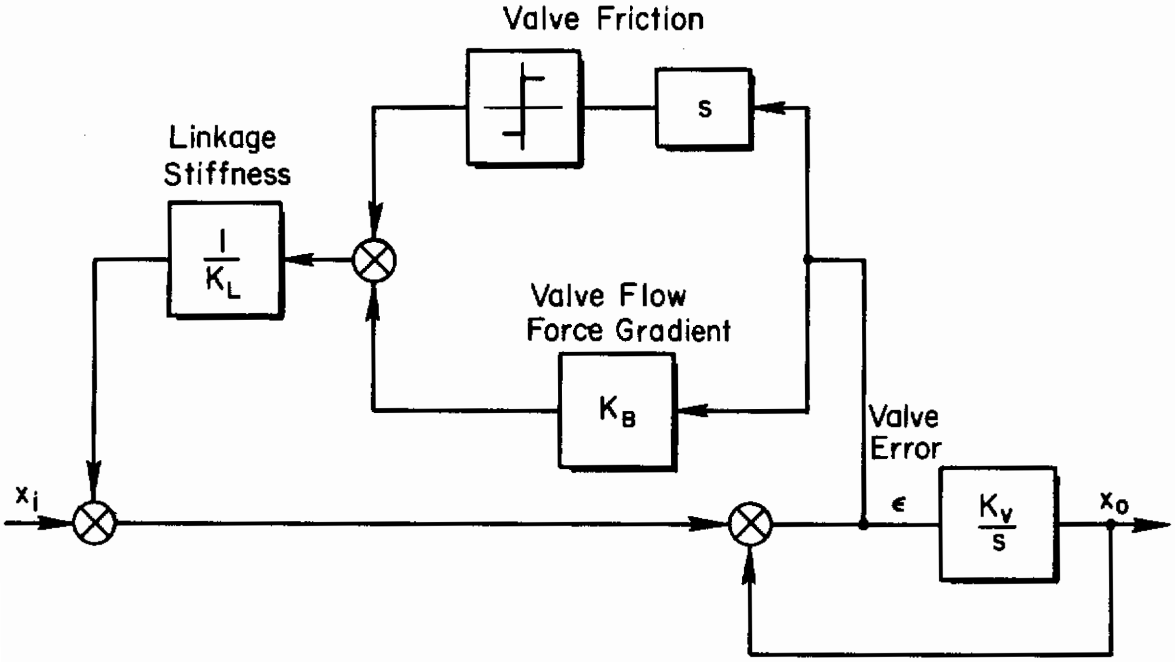
Valve Friction
s
Linkage Stiffness
$\frac{1}{K_L}$
Valve Flow Force Gradient
K_B
Valve Error
x_i
ϵ
$\frac{K_v}{s}$
x_o

≡ Effective Flow Force Diagram

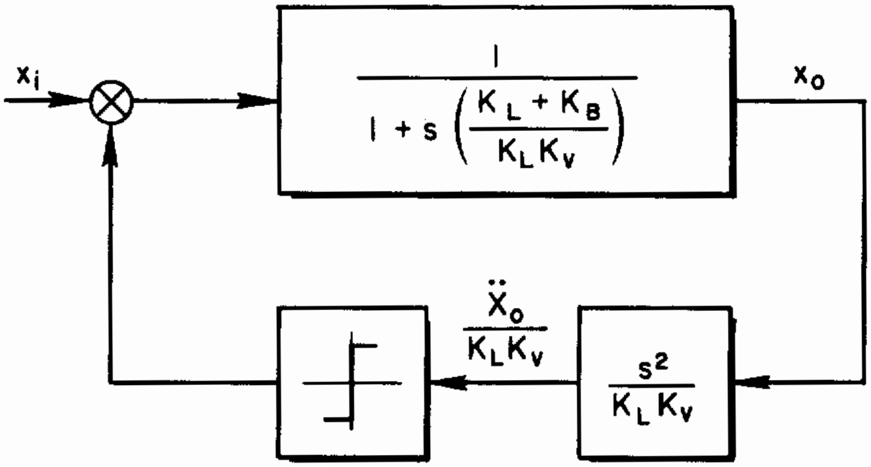
x_i
$\frac{1}{1 + s\left(\frac{K_L + K_B}{K_L K_v}\right)}$
x_o
$\frac{\ddot{X}_o}{K_L K_v}$
$\frac{s^2}{K_L K_v}$

K_L = Control Linkage Stiffness

K_B = Eqivalent Flow Force Spring Stiffness

K_v = Valve Flow Gain Constant

Figure 23. Effect of Valve Friction and Flow Forces on Effective Actuator Dynamics

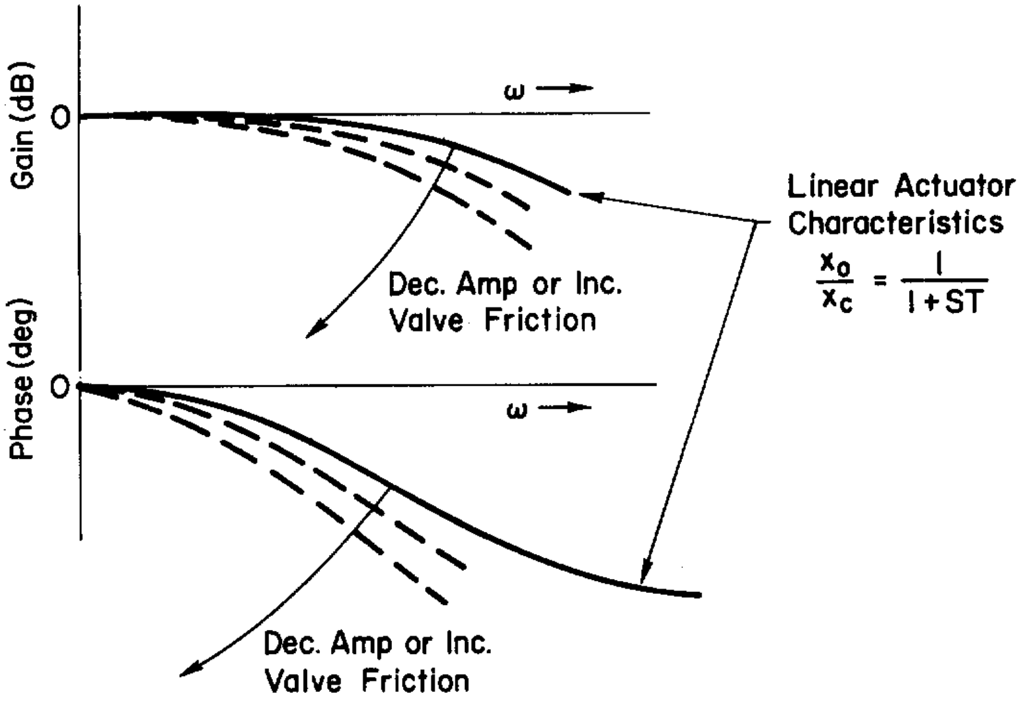

a) Effect of Valve Friction on Actuator Characteristics

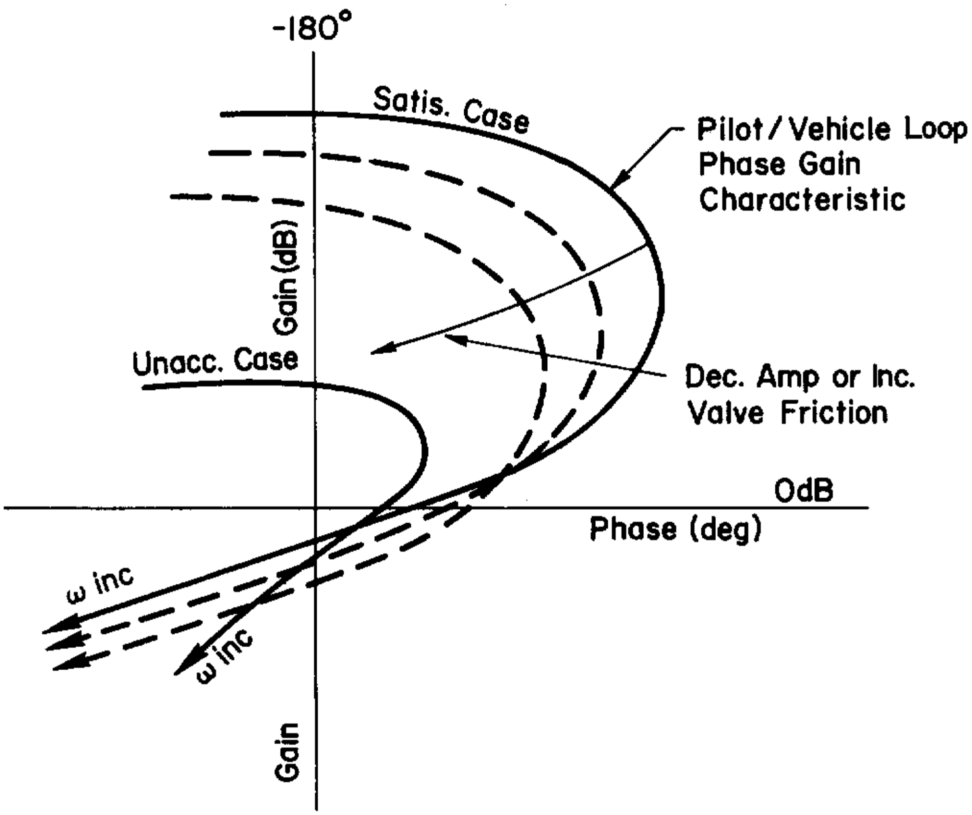

b) Effect of Valve Friction on Pilot/Vehicle Loop

Figure 24. Considerations of Valve Friction on Manual Control

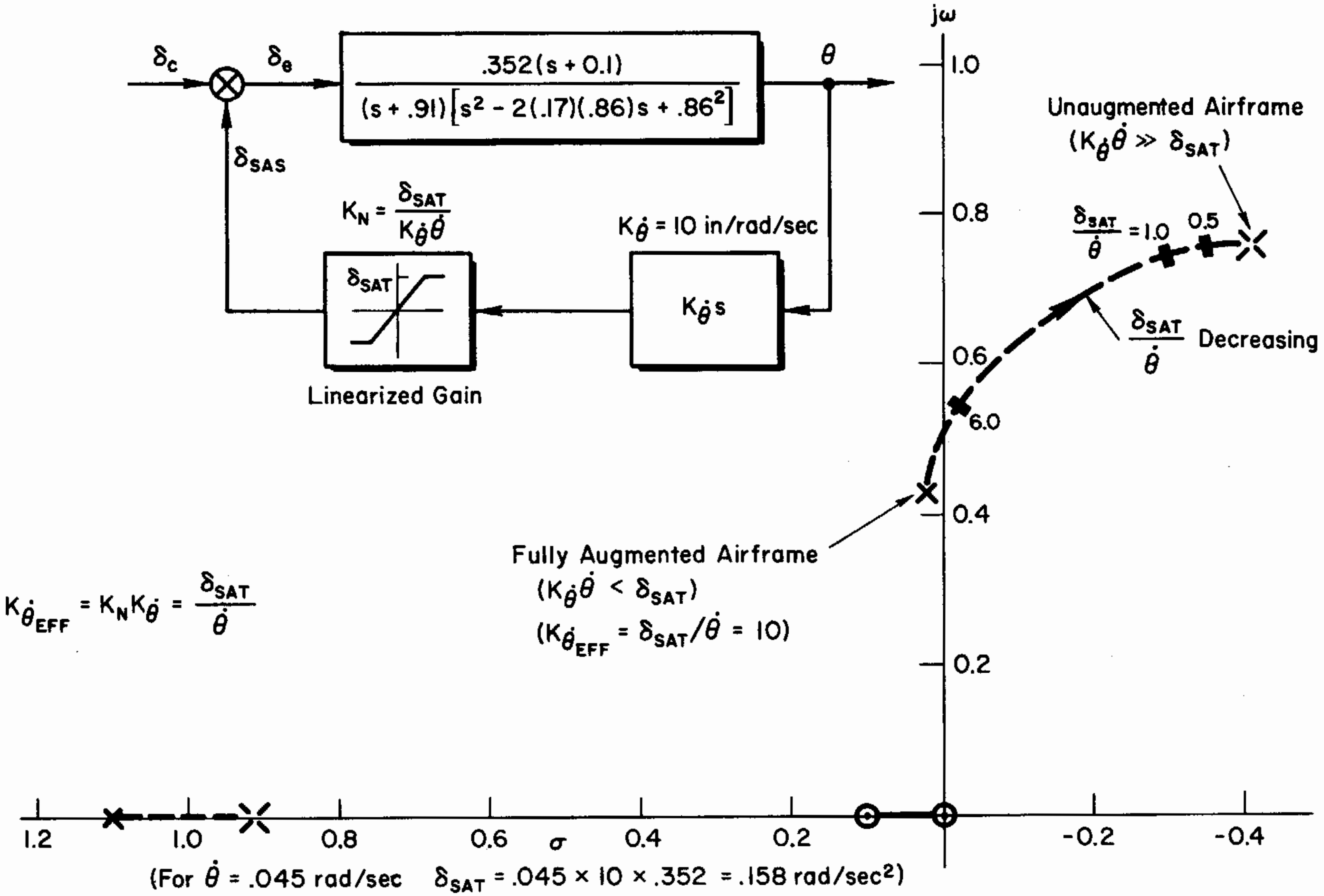
δ_c
δ_e
$\frac{.352(s+0.1)}{(s+.91)[s^2-2(.17)(.86)s+.86^2]}$
θ
δ_{SAS}
$K_N = \frac{\delta_{SAT}}{K_{\dot\theta}\dot\theta}$
δ_{SAT}
Linearized Gain
$K_{\dot\theta}$ = 10 in/rad/sec
$K_{\dot\theta}s$
$K_{\dot\theta_{EFF}} = K_N K_{\dot\theta} = \frac{\delta_{SAT}}{\dot\theta}$
jω
1.0
0.8
0.6
0.4
0.2
Unaugmented Airframe
$(K_{\dot\theta}\dot\theta \gg \delta_{SAT})$
$\frac{\delta_{SAT}}{\dot\theta}$ = 1.0
0.5
$\frac{\delta_{SAT}}{\dot\theta}$ Decreasing
6.0
Fully Augmented Airframe
$(K_{\dot\theta}\dot\theta < \delta_{SAT})$
$(K_{\dot\theta_{EFF}} = \delta_{SAT}/\dot\theta = 10)$
1.2
1.0
0.8
0.6
σ
0.4
0.2
-0.2
-0.4
(For $\dot\theta$ = .045 rad/sec δ_{SAT} = .045 × 10 × .352 = .158 rad/sec^2)

Figure 25. Effect of SAS Saturation on Vehicle Dynamics

$gM_u = 0.67$ $M_{\dot{\theta}} = -3$

$X_u = -0.1$ $\sigma_{u_g} = 5.1$

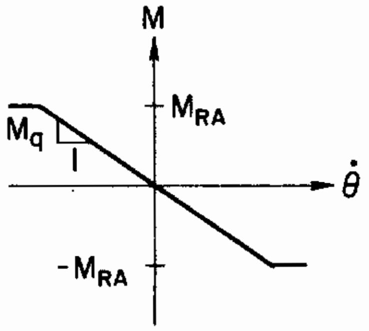

Measured Control Usage $\sigma_{\dot{\theta}} = 0.045$ rad/sec

Rate SAS Authority M_{RA}, rad/sec^2	M_{δ_e}/OPT	PR	Summary of Pilot Comments
Unlimited	0.441	3.0	Well damped. Predictable attitude response to control inputs.
0.15	0.432	3.0	Seems well damped. Several times noticed rather rapid response to large gust. Easy to control pitch.
0.1	0.352	4.0	Difficult to evaluate. Sometimes when maneuvering noticed rapid pitch motion. Frequently had overshoots in response to commands.
0.06	0.301	4.5	Pitch control requires attention. Must avoid abrupt control inputs. Needs damping.
0.03	0.253	5.5	Pitch quite difficult to control. Inadvertently develop large pitch angles when maneuvering. Gust quite annoying.
0	0.272	6.0	Very unstable, oscillatory. Difficult to select suitable control sensitivity. Probably could land it but mission accomplishment doubtful.

Figure 26. Experimental Effects of Pitch Rate Stabilization Authority on Handling Qualities

to smaller fractions of $\sigma_{\dot{\theta}}$, pilot opinion degradation occurs as shown in Fig. 27. This curve is based on the saturation values required to produce the probabilities of exceeding the limits in response to gust $\sigma_{u_g} = 5.1$ ft/sec.

8. Control System Breakout Forces

For this analysis the pilot is considered to produce stick force commands in response to vehicle motion cues while hovering in a gusty environment. For small amplitudes of control motion, increasing the breakout force decreases the effective controlled element gain (open-loop gain) by a factor of $K_F/(K_F + K_N)$, where K_F is the stick force gradient, and an approximation for K_N, utilizing analytic describing function properties (e.g., Ref. 36), is given by

$$K_N \doteq \frac{4}{\pi}\,\frac{F_b}{\sigma_{\delta_s}}$$

where K_N = gain contribution of the breakout force

F_b = breakout force

σ_{δ_s} = rms calculated control stick amplitude (based on gust inputs for $\sigma_{v_g} = 5$ ft/sec)

The effects of reduced controlled element gain on pilot opinion rating is shown in Fig. 28. The predicted combined breakout and stick gradient forces required to produce a degradation of four units (Cooper Scale) (gain reduced to 0.23 optimum) are shown in Fig. 29. This prediction is based on the notion that in the "mean operating range" ($\sigma_{\delta_s} \rightarrow 2\sigma_{\delta_s}$, 68% → 98% of probable stick motions) the effective gain is 0.23 times optimum and the corresponding decrement in pilot opinion rating is four units. In order to control the vehicle with small control motions, the pilot has to increase his gain due to the breakout force. This is the cause for his probable poor opinion rating and complaints of low stick sensitivity.

From a closed-loop view of the "unacceptable" case the reduction in open-loop gain that would result in a linear divergence is determined to be a factor of 1/5 (see Fig. 30, low frequency crossing of the $j\omega$ axis). The combination of breakout and stick gradient forces to effect this reduction of (force) gain is calculated similarly to the "acceptable" situation. In this case, there is the possibility, for small control motions, that a finite limit cycle may ensue. Figure 31 presents the combined breakout and stick gradient forces that could produce such a finite limit cycle. It is not conclusive, however, that the pilot will allow the vehicle to become uncontrollable, but would rather resort to large control motions to eliminate the limit cycling.

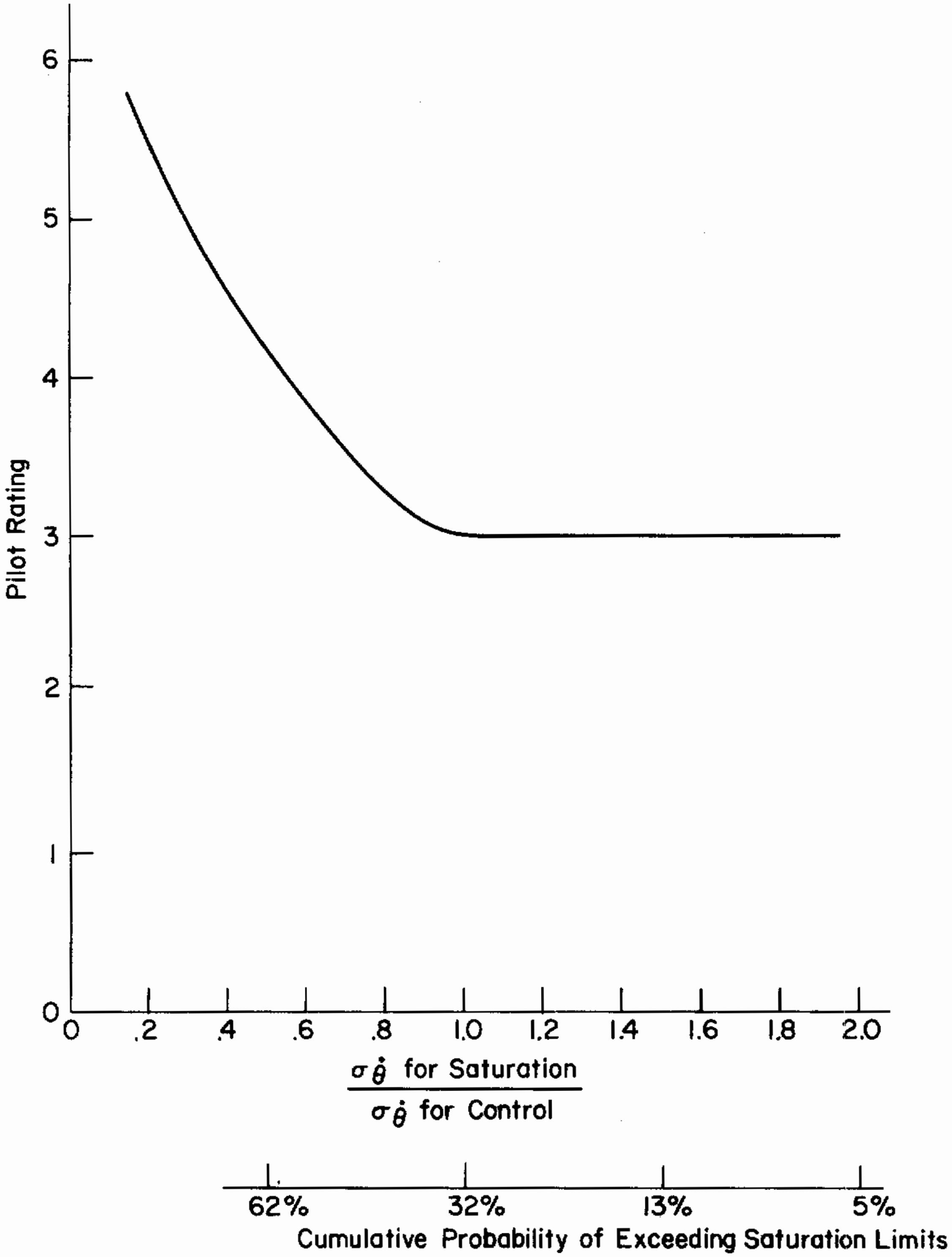

Figure 27. Effect of Stability Augmentation Authority Limits on Pilot Rating

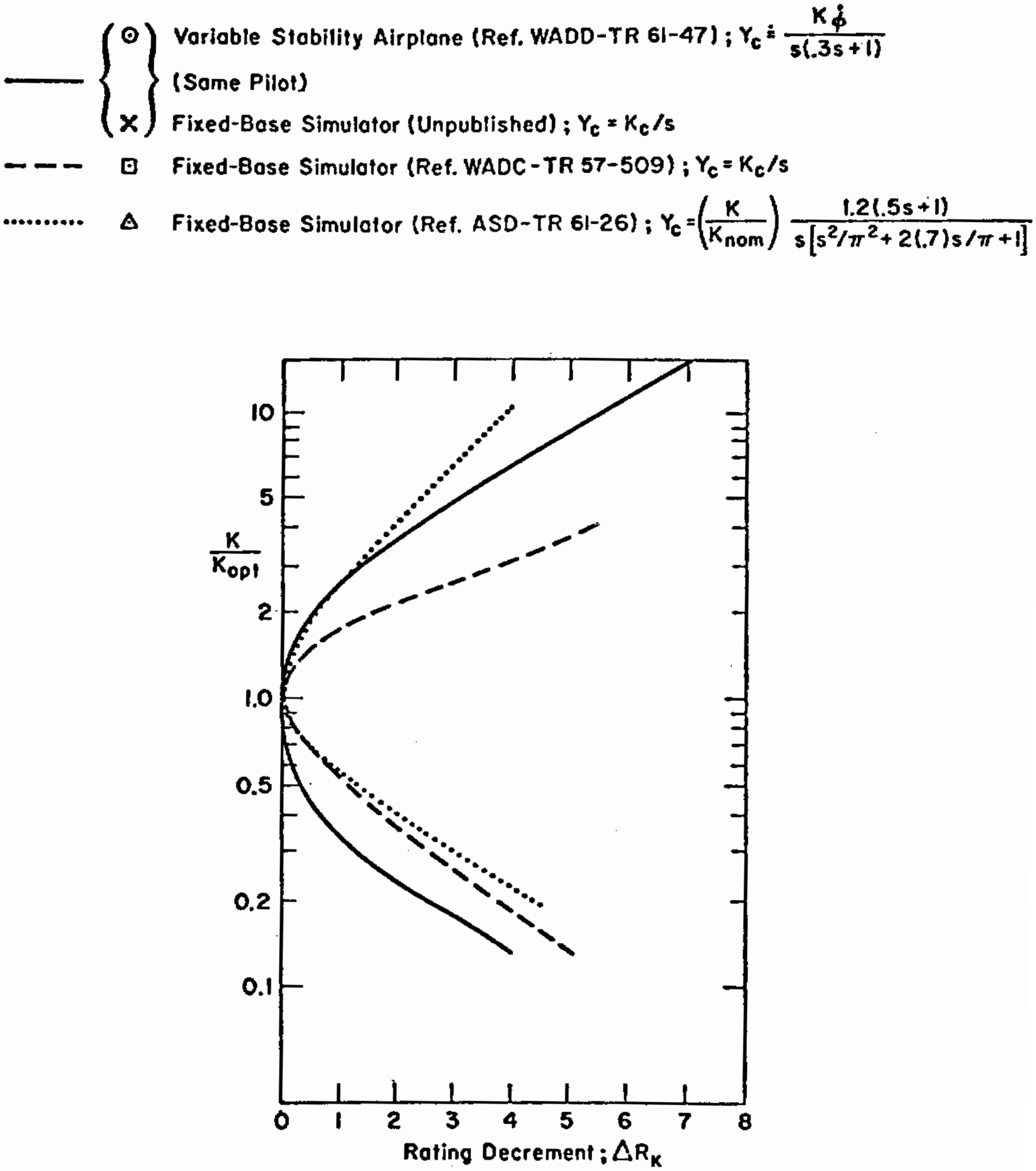

Figure 28. Pilot Ratings versus Controlled Element Gain

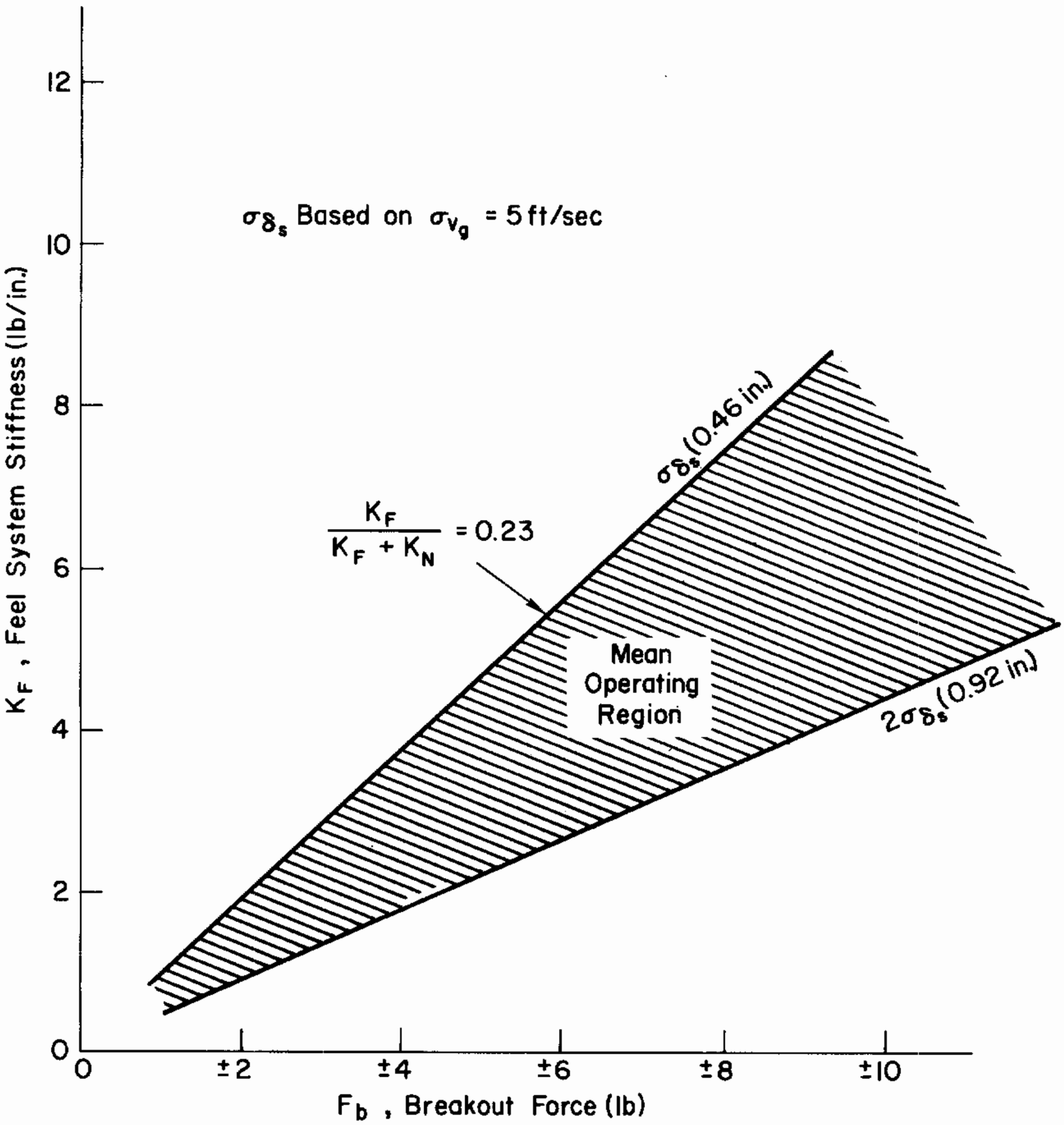

Figure 29. Predicted Breakout Force Required to Produce Pilot Opinion Degradation from PR = 2.5 to PR = 7.3 for Ref. 2 Satisfactory Data

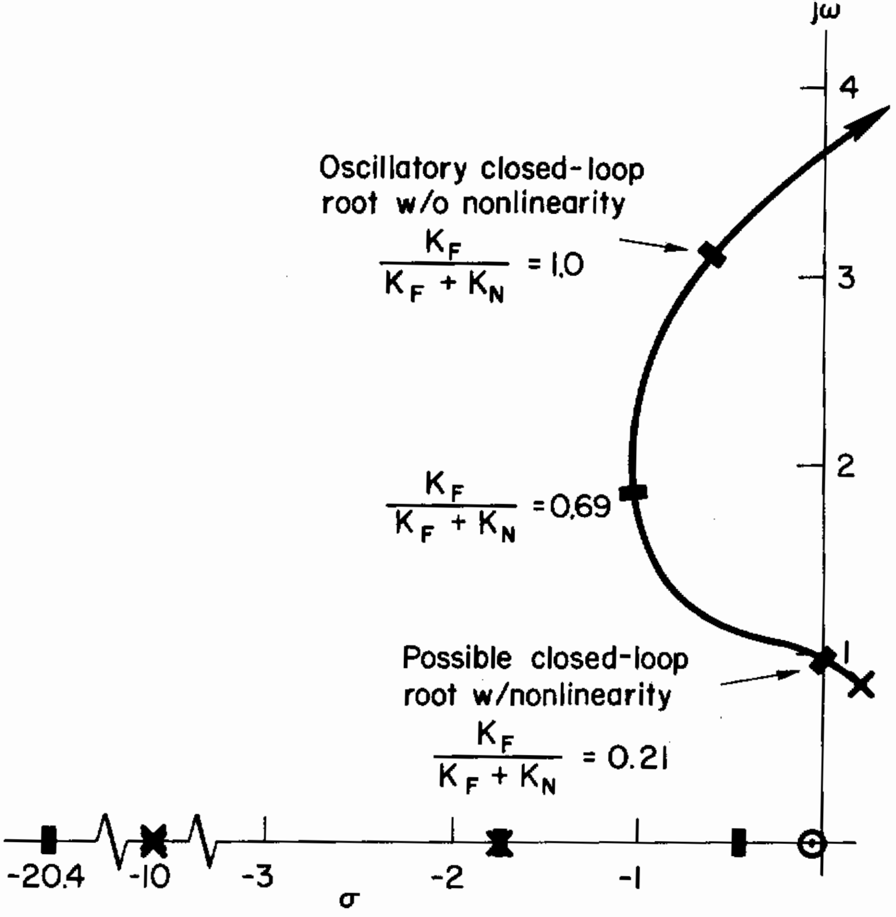

Figure 30. Breul Data — Unacceptable Case

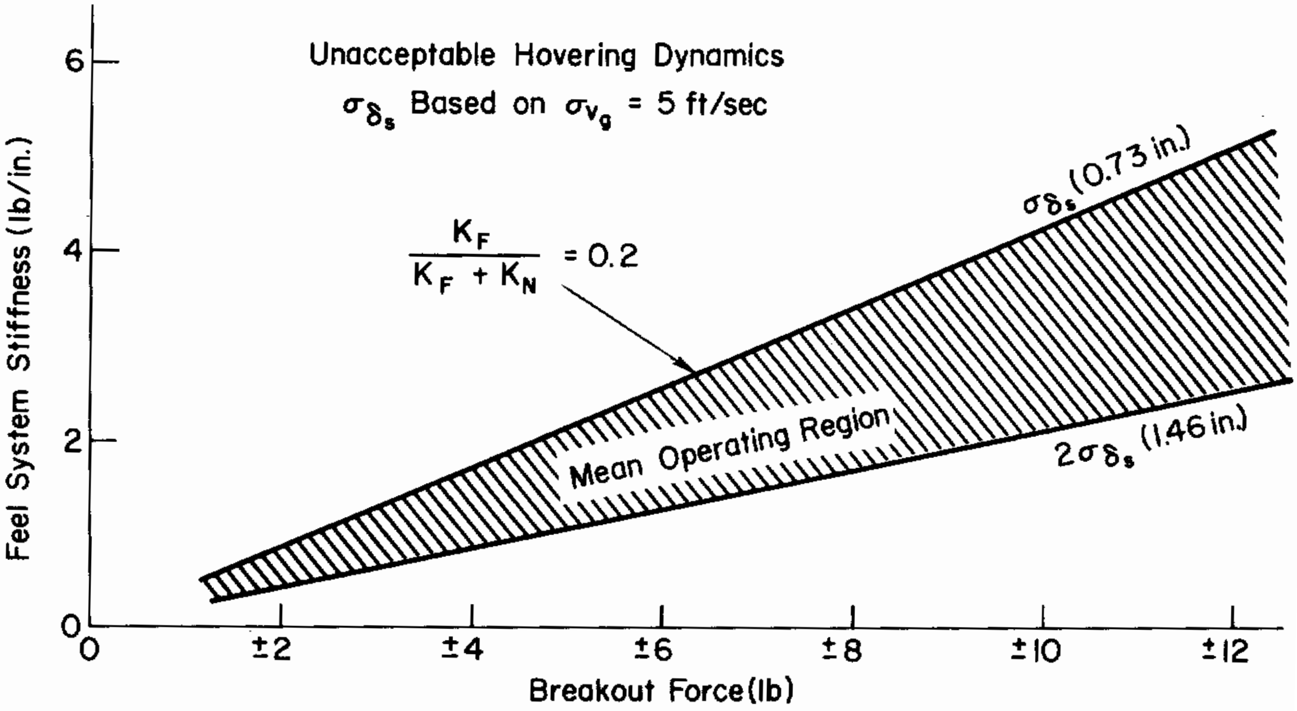

Figure 31. Breakout Force That May Produce Limit Cycling

In conclusion, the results of these analyses indicated that the effects of control system dynamics and nonlinearities are strongly related to inherent vehicle oscillatory mode dynamics. In the case of VTOL a stable vehicle is desired to minimize such control system properties. From a manual control viewpoint, nonlinear effects are reflected in a tendency for closed-loop limit cycle situations. Such limit cycle tendencies will be reflected as either position or attitude oscillations depending on the basic vehicle oscillatory mode.

SECTION IV

ASPECTS OF LATERAL/DIRECTIONAL CONTROL IN LOW SPEED AND TRANSITION FLIGHT

This section presents a study of the closed-loop piloting problems associated with the lateral/directional modes in the transition region from hover to low speed flight. The objective of this effort is an improved understanding of the pertinent handling quality problems for this flight region; and the study is an extension of the similar transition studies presented in Ref. 1. As in these previous studies, which explored longitudinal control, the basic approach here is to consider the piloting problems from the closed-loop viewpoint using appropriate quasi-linear pilot models. By so doing we hope to isolate the crucial vehicle parameters and factors which play a key role in establishing good and bad handling qualities.

In the first part of this section we will generically develop and appraise the closed-loop manual control techniques or tasks in transition. An example VTOL aircraft is used here to illustrate how the pilot control techniques are influenced by changes in the vehicle characteristics. The purpose of this part of the study is to follow step-by-step the interplay of pilot and vehicle characteristics through transition. In other words, we show how, in transition, the pilot may use the aileron and the rudder for control, the employment of either or both being directly related to the particular vehicle dynamic characteristics at the given point in transition. Such generic analyses serve to identify those derivatives which are most crucial in determining the control characteristics associated with transition flight.

In the final subsection we examine the results derived from available lateral/directional handling quality experiments. In many cases we are able to evoke the factors identified by the preceding generic studies to explain the root causes for the pilot rating trends or comments. Furthermore using these experimental results we are able to establish both good and bad levels of the key lateral parameters.

A. GENERIC ASPECTS OF CLOSED-LOOP MANUAL CONTROL IN TRANSITION

As a prelude to the detailed analyses of the available lateral/directional handling quality data, we will consider the types of tasks and maneuvers that the pilot will be required to perform in the transition flight regime. An adequate delineation of such piloting functions is necessary before evolving feasible control techniques and/or predicting handling quality requirements. However, we will not consider those aspects of transition which involve the time-varying effects (i.e., the continuous transition). Furthermore, since closed-loop control functions are a primary consideration in regard to the pilot assessment of handling qualities, we restrict our studies to control tasks and maneuvers which can be described by closed-loop situations.

1. **Types of Manual Closed-Loop Tasks**

Closed-loop control tasks in piloted flight encompass two basic functions:

a. Command maneuvers

b. Regulation tasks

The command maneuvers for the lateral/directional mode include:

a. Bank angle change, φ_c.

b. Heading change, ψ_c; this might include banked or flat turn, hover turns or decrab maneuvers.

c. Lateral displacement changes, y_c; this might include maneuvers such as lateral drift or sidestep.

In regulatory tasks we can expect that the pilot would maintain either attitude and/or ground position while subjected to self-induced or externally applied disturbances.

Each of the above functions implies that the pilot is active in performance of the closed-loop control task. Table V summarizes symbolically the appropriate loop structures and feedback functions that may be involved in accomplishing both the command and regulatory tasks. The breadth of coverage is adequate to span control situations from hover to forward flight.

TABLE V

CONTROL STRUCTURES AND FEEDBACK FUNCTION FOR CLOSED-LOOP TASKS

TASKS	COMMAND STRUCTURES		REGULATORY STRUCTURES	
	SINGLE LOOP	MULTILOOP	SINGLE LOOP	MULTILOOP
Bank Angle (φ)	$\varphi \rightarrow \delta_a$	$\varphi \rightarrow \delta_a$; $\beta \rightarrow \delta_r$	$\varphi \rightarrow \delta_a$	$\varphi \rightarrow \delta_a$; $\beta \rightarrow \delta_r$ $\varphi \rightarrow \delta_a$; $r \rightarrow \delta_r$
Heading (ψ)	$\psi \rightarrow \delta_a$	$\psi \rightarrow \delta_a$; $\varphi \rightarrow \delta_a$ $\psi \rightarrow \delta_a$; $\varphi \rightarrow \delta_a$ $\beta \rightarrow \delta_r$	$\psi \rightarrow \delta_r$	$\psi \rightarrow \delta_r$; $\varphi \rightarrow \delta_a$
Lateral Displacement (y)	$y \rightarrow \delta_a$	$y \rightarrow \delta_a$; $\varphi \rightarrow \delta_a$ $y \rightarrow \delta_a$; $\varphi \rightarrow \delta_a$ $\psi \rightarrow \delta_a$	$y \rightarrow \delta_a$	$y \rightarrow \delta_a$; $\varphi \rightarrow \delta_a$ $y \rightarrow \delta_a$; $\varphi \rightarrow \delta_a$ $\psi \rightarrow \delta_r$

2. Manual Closed-Loop Control Features of XC-142 in Transition

In this subsection we examine the closed-loop control features (for a typical VTOL airplane) at various points in transition. This exercise is used to:

a. Illustrate how we may evoke closed-loop performance and piloting merits as a means of predicting good and bad handling qualities.

b. Show how the vehicle's basic changes in stability characteristics influence the control structures (i.e., piloting technique) required to perform elementary regulatory and maneuver tasks.

A typical vehicle for consideration of the control structures described in Table V is the XC-142 whose derivatives and transfer functions are presented in Appendix D. The following represent the applicable control structures.

a. **Regulatory Control**

1) $\varphi \rightarrow \delta_a$ } Attitude

2) $\psi \rightarrow \delta_r \Big]_{\varphi} \rightarrow \delta_a$ } Attitude

3) $y \rightarrow \varphi \rightarrow \delta_a$ } Lateral Displacement

b. **Maneuvering Control**

1) Heading Control

$$\psi \rightarrow \varphi \rightarrow \delta_a$$

2) Coordination Control

$$\psi \rightarrow \varphi \rightarrow \delta_a \Big]_{\beta} \rightarrow \delta_r$$

The primary regulatory control loop $\varphi \rightarrow \delta_a$ is considered first, with and without pilot lead compensation since this loop is basic to all others. The regulatory and maneuvering loops are then evaluated to point our their deficiencies or advantages.

a. Regulatory Control

1) Bank angle regulation, $\varphi \rightarrow \delta_a$. Figures 32, 33, and 34 show the Bode and root locus representation of bank angle control for hover, mid-transition, and end transition, respectively. The open-loop pilot/vehicle bank angle transfer function is of the form:

$$Y_pY_c = \underbrace{K_{p_\varphi}T_{L_\varphi}\left(s+\frac{1}{T_{L_\varphi}}\right)e^{-\tau s}}_{\text{Pilot}}\;\underbrace{\frac{A_\varphi(s+1/T_{\varphi_1})(s+1/T_{\varphi_2})}{(s+1/T_R)(s+1/T_s)[s^2+2\zeta_{DR}\omega_{DR}s+\omega_{DR}^2]}}_{\text{Vehicle}}$$

This includes the pilot lead compensation required to form the K/s crossover region near 2-3 rad/sec. In mid-transition, lead is required just to obtain stability, and the lead requirements are moderately large ($T_{L_\varphi} \doteq 1$ sec) from hover through transition. The low dc gain at hover indicates very low steady state bank angle to command step aileron which will influence the maneuvering control aspects to be discussed later, and suggests that low frequency control of disturbance (e.g., gust) will be poor.

Bank angle control is considered marginal for conditions at and below the mid-transition point due to the fact that the basic vehicle is unstable and continuous pilot effort and concentration are necessary to generate the lead compensation required for stable closed-loop control. Further complicating the control problem is the overall intolerance of the closures to small changes in pilot compensation.

2) Heading regulation, $\psi \rightarrow \delta_r$
$\psi \rightarrow \delta_r\big]_\varphi \rightarrow \delta_a$

Rudder control of heading errors is normally employed in a closed-loop manner when tight control of the airplane is required (e.g., for regulation against lateral gusts). Where the airplane roll and yaw modes are coupled (e.g., in conventional flight), the pilot will be required to use the ailerons to keep the wings level, also. Thus, two control structures are envisioned in the transition region: the single-loop $\psi \rightarrow \delta_r$ control near hover and the multiloop situation where the $\varphi \rightarrow \delta_a$ inner loop is stabilized, depicted below.

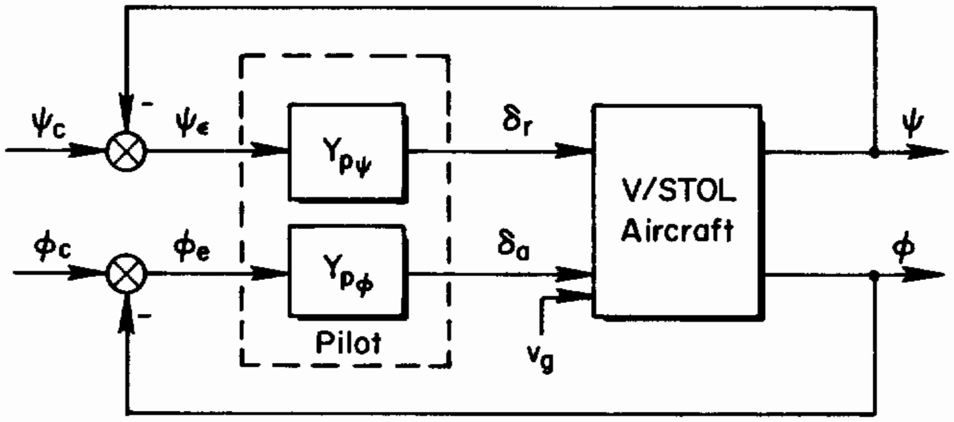

Heading and Bank Angle Regulation Using Aileron and Rudder,
$\psi \rightarrow \delta_r\big]_\varphi \rightarrow \delta_a$

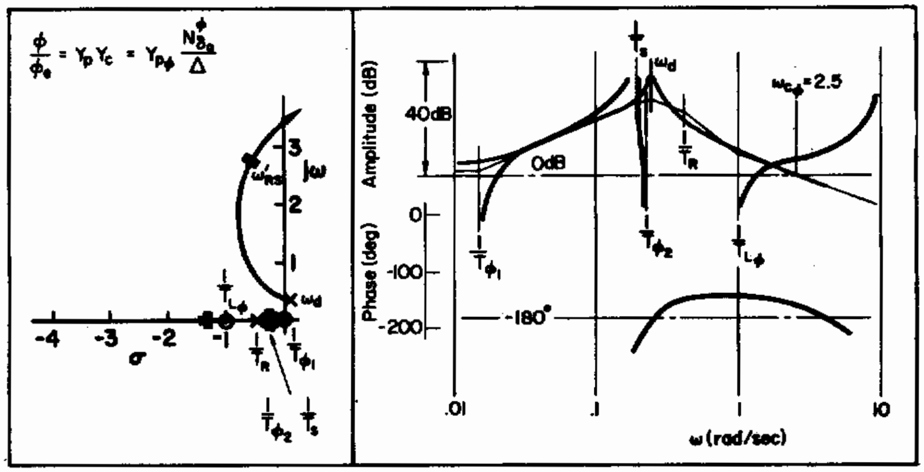

Figure 32. Manual Bank Angle Control in Initial Transition; XC-142A

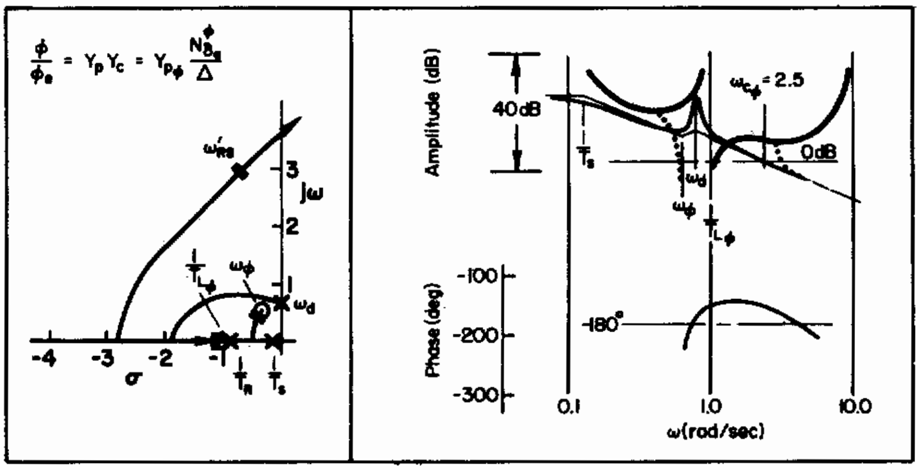

Figure 33. Manual Bank Angle Control in Midtransition; XC-142A

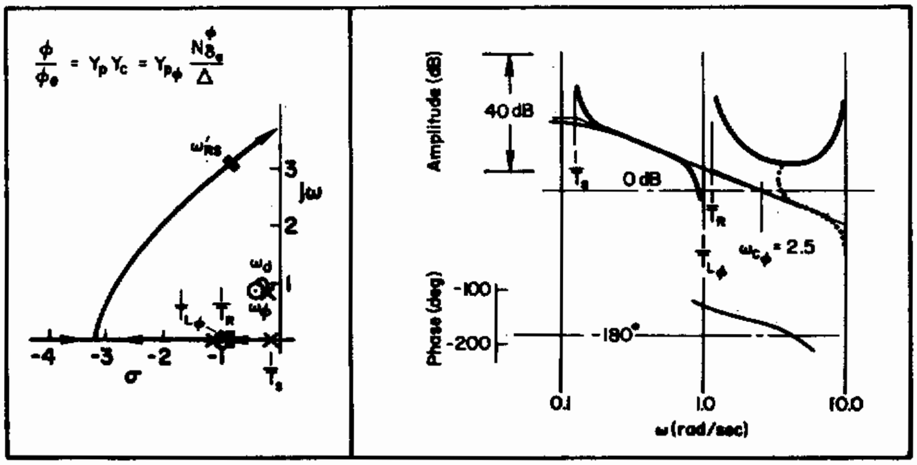

Figure 34. Manual Bank Angle Control in End Transition; XC-142A

Both control situations are shown for the three transition conditions in Figs. 35, 36, and 37 without pilot lead and with maximum (zero phase margin) gain. Comparison of the single- and multiloop plots illustrates how heading performance is improved by the roll closure as speed increases. For example, in the top (rudder only) diagrams of Figs. 36 and 37 the low Dutch roll mode (and associated numerator, ω_r) damping generally limits the attainable crossover frequency; and system performance is poor. In the lower plots, the roll closure has modified the ω_r zeros by combining them with the coupling numerator, $N^{\varphi\,\psi}_{\delta_a \delta_r}$, and has effectively cancelled them with the closed-loop roll-spiral mode (ω'_{RS}). Also, the Dutch roll damping has increased; and the combination of these effects permits higher crossover frequencies. These observations do not, however, apply to the hover case, Fig. 35, where there is no difference due to the inner loop because rudder activity does not generate bank angle and bank angle does not change heading, i.e., $L_\beta = 0$, and $rU_o = 0$.

The primary change in rudder-only control occurs as the airplane becomes more coupled (i.e., approaches end of transition) as shown by the location of the ω_r zeros of the numerator, $N^{\psi}_{\delta_r}$, in the right half plane (see Fig. 37). Such unstable zeros are traceable to the large lateral stability, L_v, and the positive L_{δ_r} (i.e., $-gL_v[1 - N_v L_{\delta_r}/N_{\delta_r}] > 0$) as established by the generic considerations (e.g., see Ref. 37). Because of these zeros the bandpass of the $\psi \rightarrow \delta_r$ closure is restricted to a relatively low value (i.e., $\omega_{c_\psi} \leq 0.3$ rad/sec) due to phase margin. Similar characteristics are apparent for mid-transition (Fig. 36) except that because the vehicle is directionally unstable ($\zeta_d < 0$) rudder control of heading is, at best, essentially neutrally stable. Furthermore, lead compensation makes this situation worse, the effect of additional lead being to keep the system unstable at the Dutch roll frequency, ω_d, as indicated by the (exaggerated) root locus sketch. Here the locus from the ω_d pole does not cross into the stable left half plane.

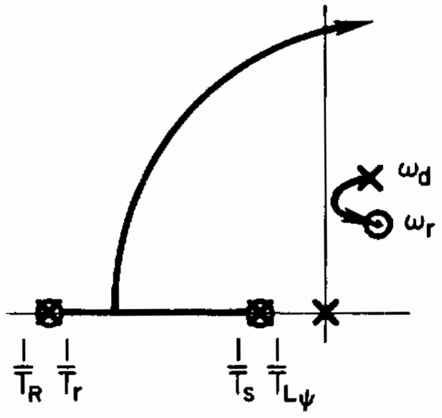

With the $\varphi \rightarrow \delta_a$ loop closed, the regulatory control of heading is significantly improved because both numerator and denominator are thereby stabilized, thus permitting the desired improvement in bandwidth.

Another regulatory control problem emerges as the directional stiffness gets larger (i.e., $\omega_d >> 0$). Basically this is a much more subtle effect and has to do with the ability of the pilot to reduce or adequately control the errors due to disturbances. Fundamentally, a broad K/s region in the open-loop controlled element ensures that the closed-loop system will have good closed-loop error control.* However, we note in Figs. 36b and 37b that, as the dynamics approach a conventional vehicle, the desired K/s features are not evident. In fact, over a relatively broad frequency range between the zero, $1/T'_r$ and the Dutch roll pole, ω'_d, the system has the K-like appearance normally associated with moderately damped second-order controlled elements. Because of this feature, good error

---

*The adjustment rules for pilot closures are based on the "crossover" model concept which requires a broad K/s region for valid application of the pilot model.

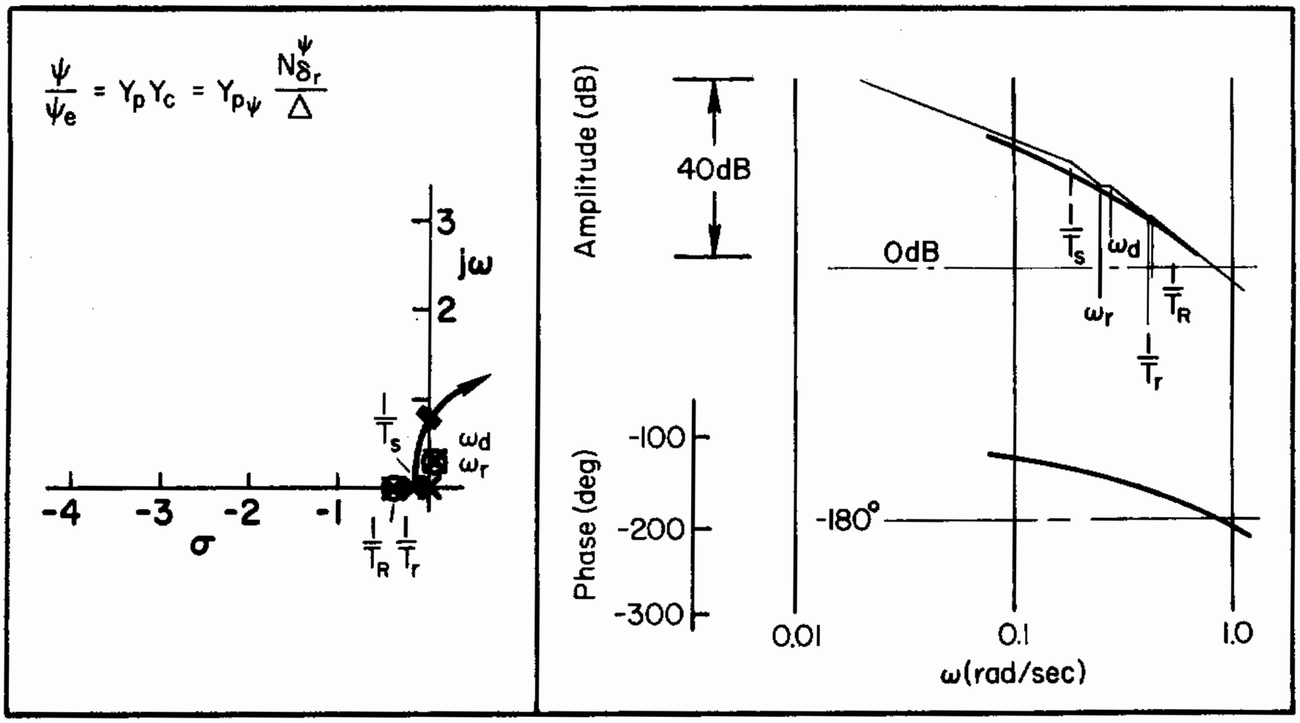

a) Rudder Only

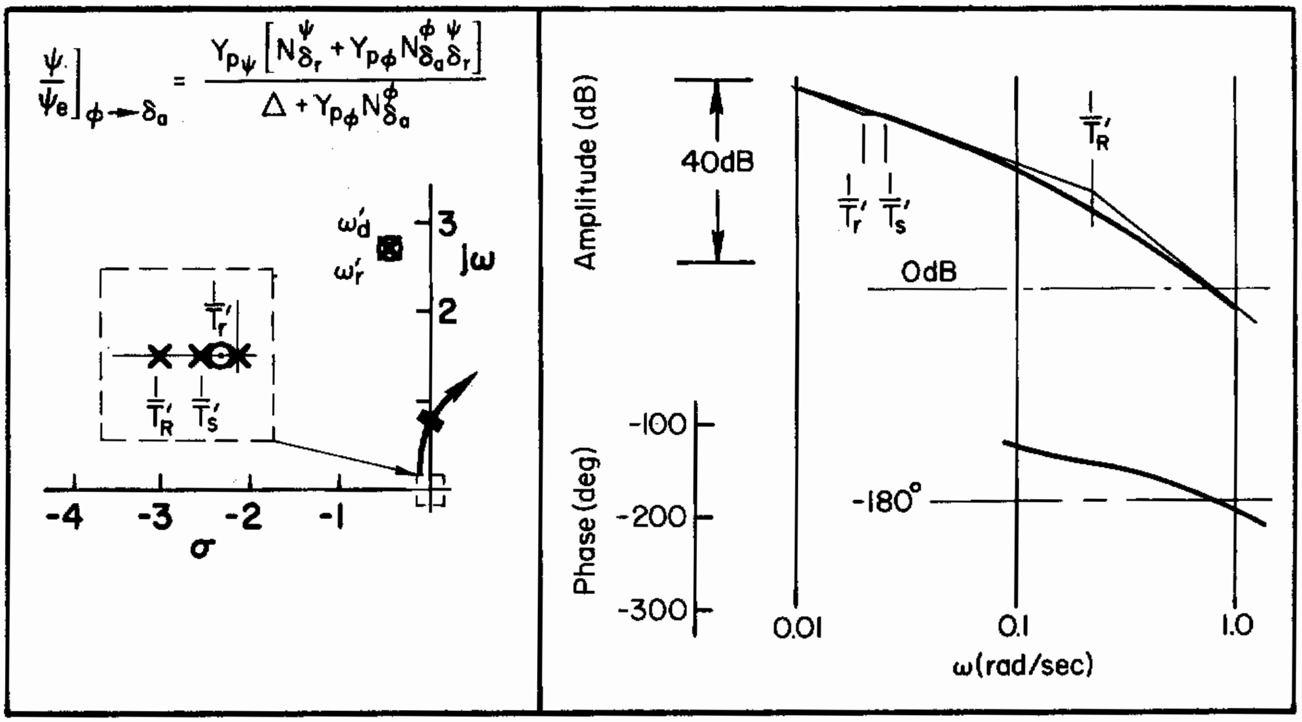

b) Rudder and Aileron

Figure 35. Heading Control During Initial Transition

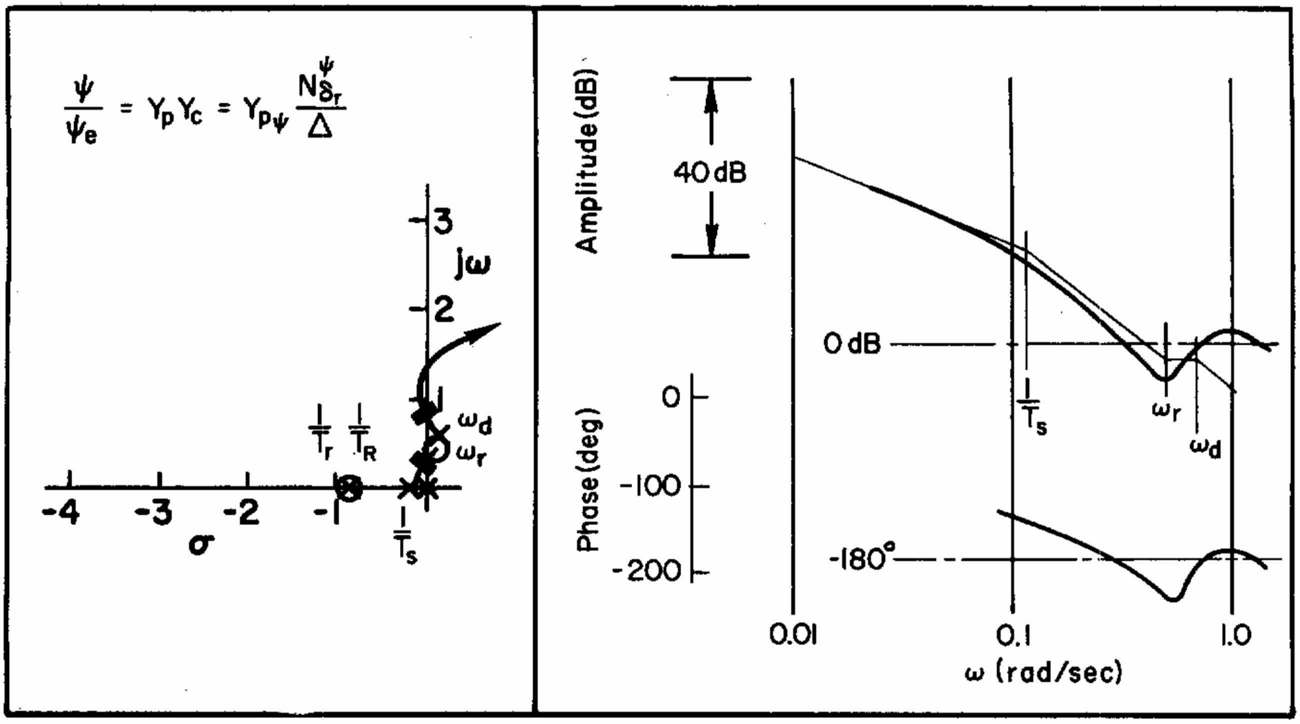

a) Rudder Only

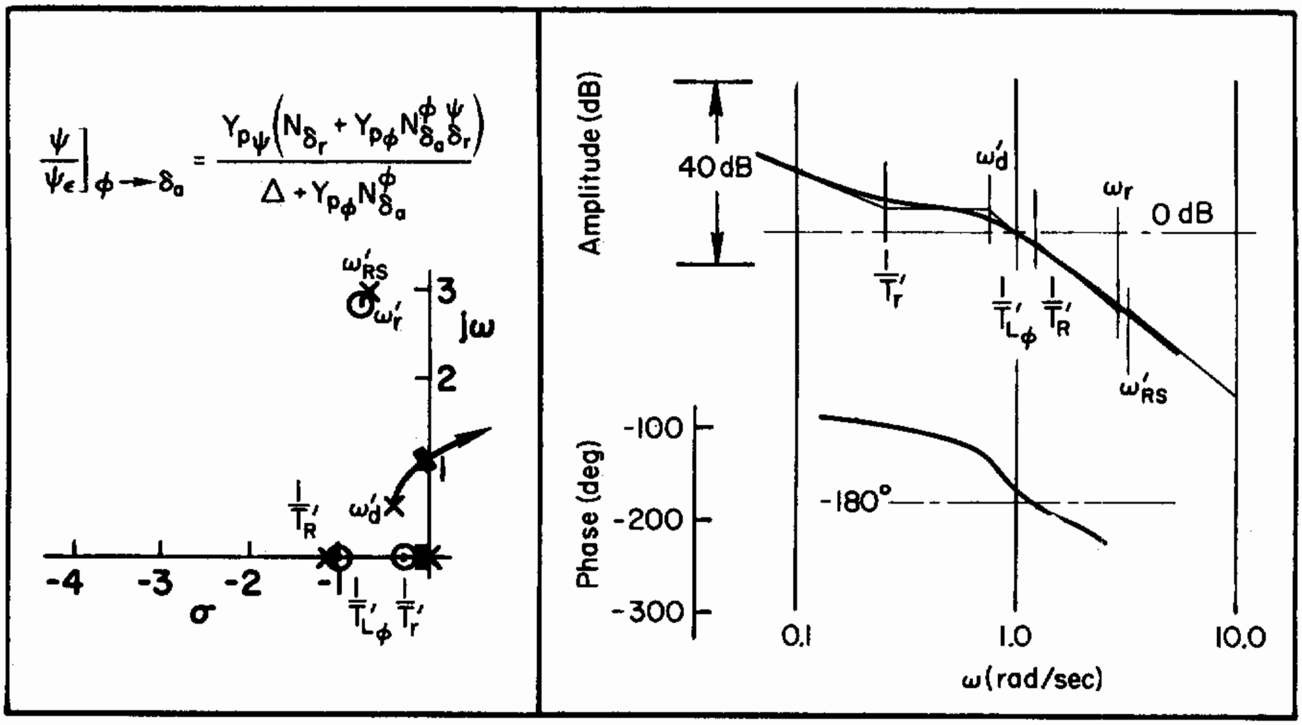

b) Rudder and Aileron

Figure 36. Heading Control During Midtransition

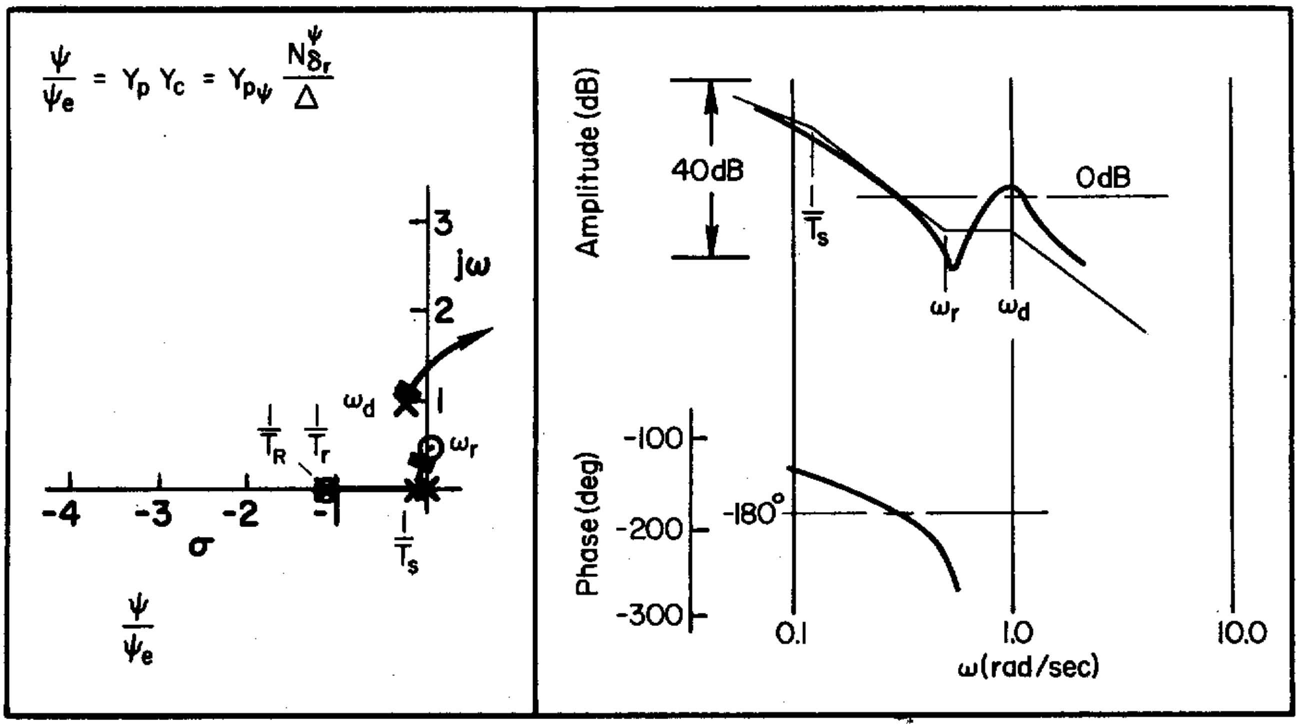

a) Rudder Only

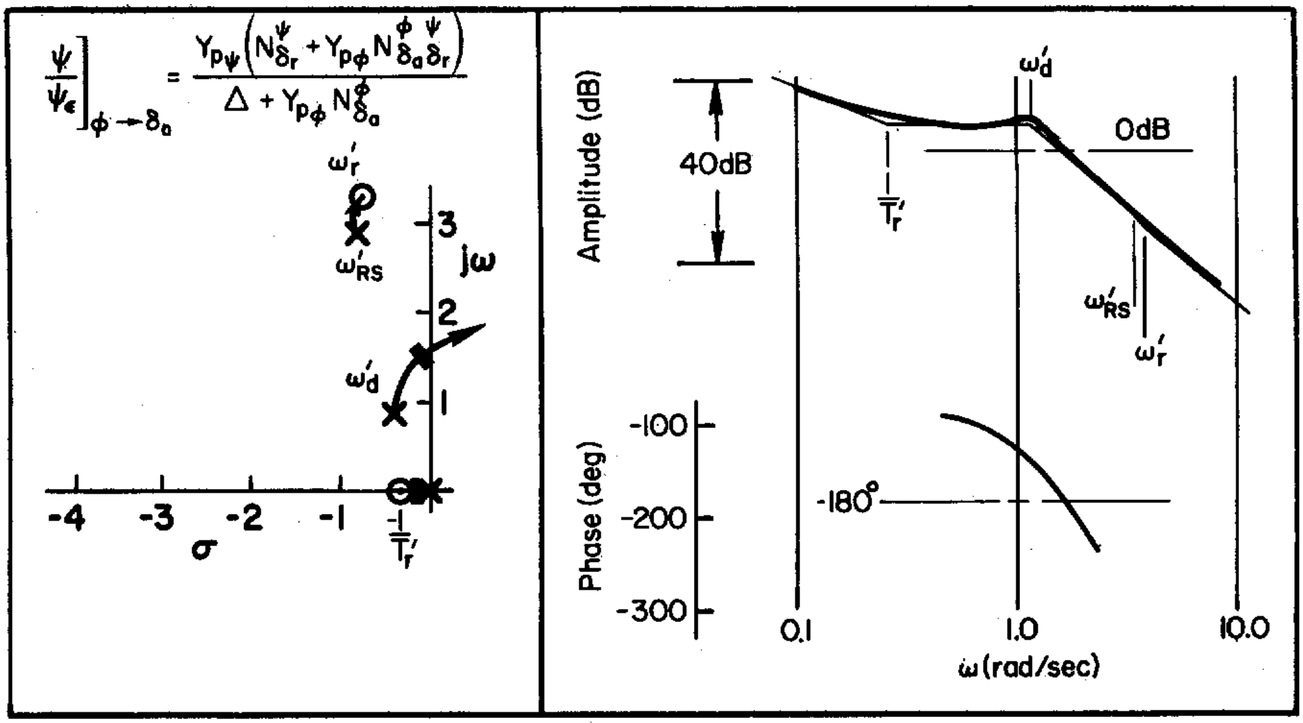

b) Rudder and Aileron

Figure 37. Heading Control During End Transition

control becomes largely a function of the bandwidth of the disturbance the pilot is attempting to control. Likewise, proper pilot equalization is largely dependent on the disturbance bandwidth. For example, if the disturbance bandwidth is less than $1/T_r'$, the pilot may use lag equalization (i.e., smooth control inputs) as shown in the sketch below. This produces a K/s region and allows a crossover frequency which is sufficiently greater than the input to obtain good error control. However, when the input bandwidth approaches ω_d' (the Dutch roll frequency) then obtaining a broad K/s region with the crossover frequency greater than the input frequency is much more difficult. This situation corresponds to that noted previously for low frequency second-order attitude control systems in hover. The pilot is now forced to introduce lead compensation near ω_d' as sketched below to obtain the desired K/s region.

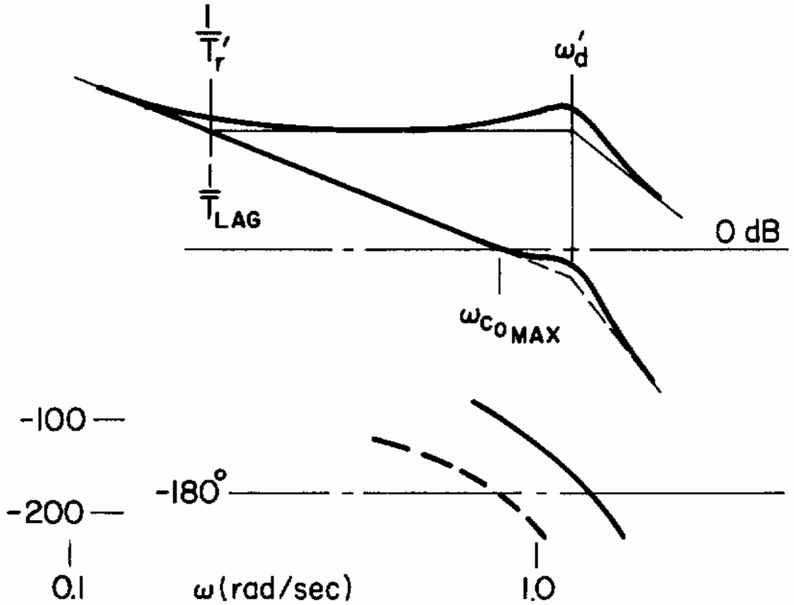

Use of Lag Equalization $1/T_r'$

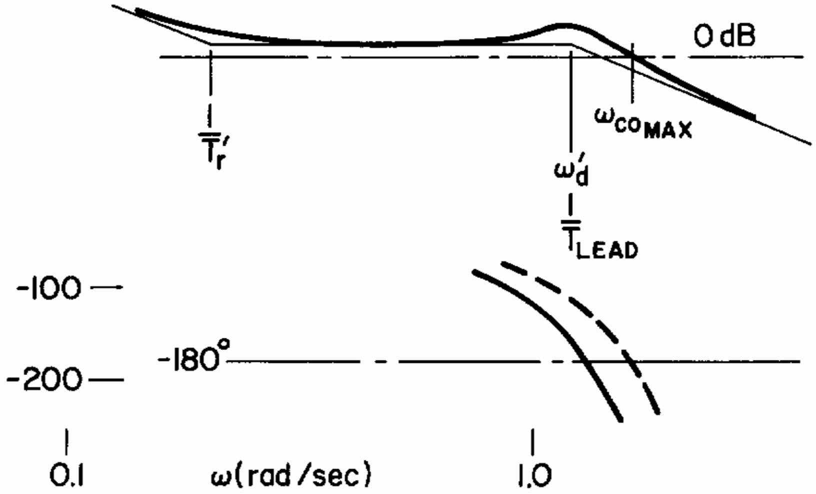

Use of Lead Equalization at ω_d'

Unfortunately, the addition of lead does not, however, yield much improvement in error reduction although the crossover frequency is now near 2 rad/sec. This is graphically illustrated by the sketches below which show the increase in closed-loop (dotted line) mid-frequency

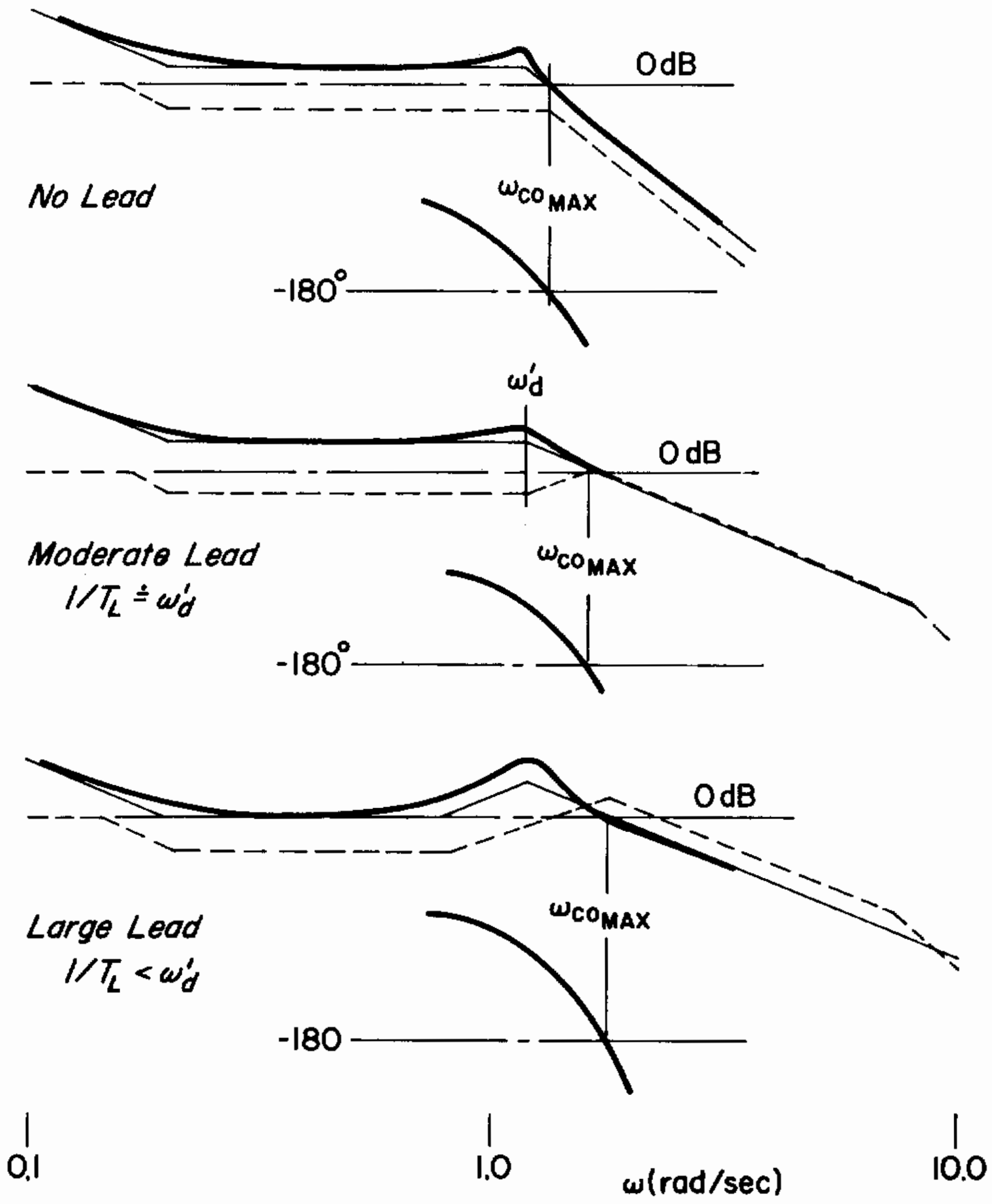

0dB
No Lead
ωco MAX
-180°
ω'd
0 dB
Moderate Lead
1/T_L ≐ ω'd
ωco MAX
-180°
0 dB
Large Lead
1/T_L < ω'd
ωco MAX
-180
0.1
1.0
ω(rad/sec)
10.0

End of Transition Example

"droop" associated with increasing lead. The pilot appears to be approaching a point of diminishing returns for his additional lead generating effort. In effect he becomes "boxed in" because:

a) Decreasing T_L reduces the potential crossover frequency and eliminates any stable K/s regions greater than the input bandwidth.

b) Increasing T_L and maintaining a given phase margin (i.e., increasing crossover frequency) will not reduce the errors.

3) Lateral displacement regulation, $y \rightarrow \varphi \rightarrow \delta_a$. The loop structure for lateral displacement control with inner-loop bank angle closure is shown below. The outer loop characteristics for three speeds in transition are shown in Fig. 38. The hover condition is the only case where a stable region exists without outer-loop lead compensation, because of the pilot lead, T_{L_φ}, used in the inner, attitude loop. As the speed increases there is only a very small stable region for a simple outer-loop gain closure and no K/s region. Therefore, lateral displacement cannot be closed on directly unless outer-loop lead is generated. Since $\dot{y} = U_0\psi + v$, it is generally more practical for the pilot to provide anticipation or lead by closing two inner aileron loops, bank angle and heading. Under these circumstances the intermediate heading control loop sets the bandwidth of the lateral deviation closure. That is, as shown in Ref. 20, if the airplane has good heading control in forward flight the lateral deviation control will be good.

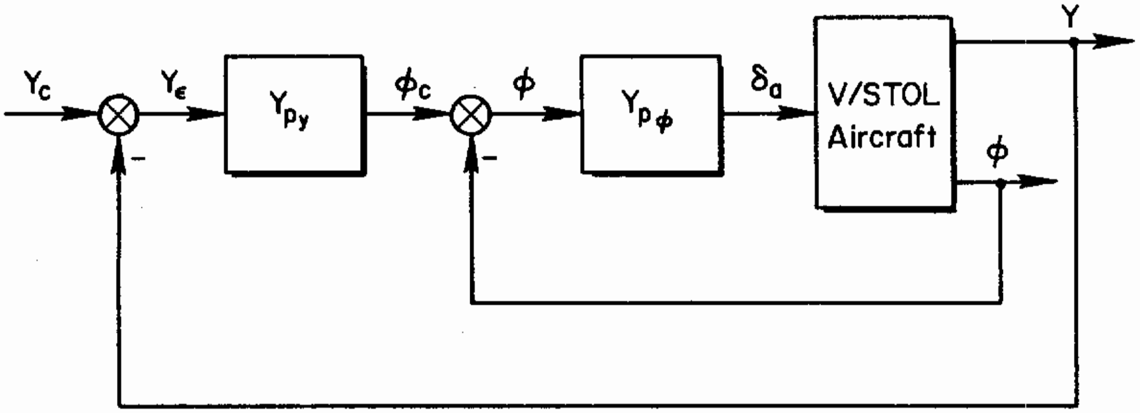

Lateral Displacement Control Through Aileron with
Bank Angle Inner Loop, $y \rightarrow \delta_a\big]_{\varphi} \rightarrow \delta_a$

a) Hover $\left.\frac{y}{y_\epsilon}\right]_{\phi\to\delta_a} = \frac{Y_{p\phi}Y_{py}gN^{\phi}_{\delta_a}}{s^2\left(\Delta+Y_{p\phi}N^{\phi}_{\delta_a}\right)}$

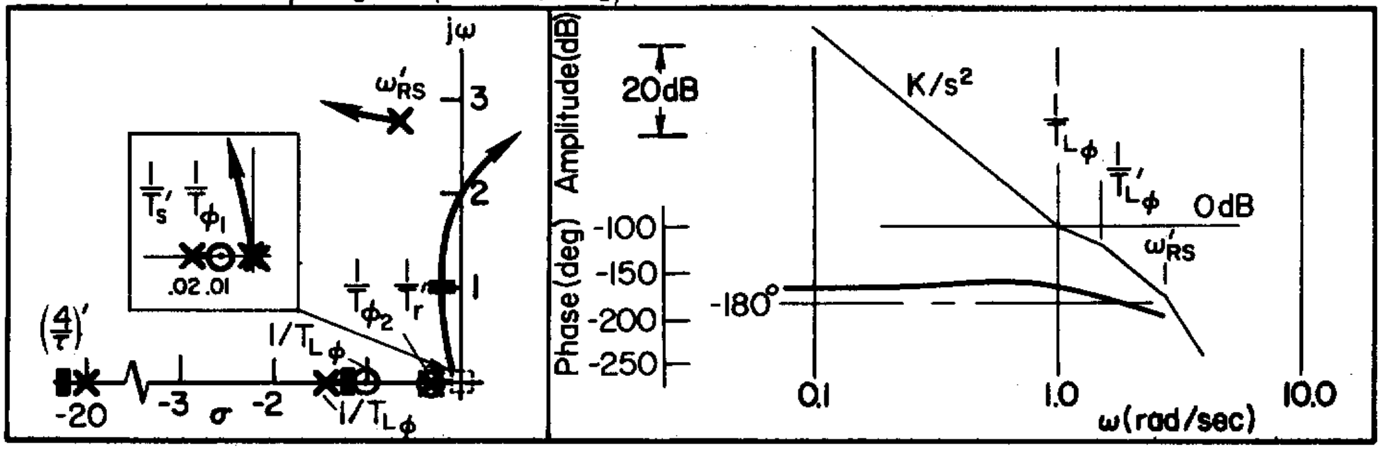

b) Mid-Transition $\left.\frac{y}{y_\epsilon}\right]_{\phi\to\delta_a} = \frac{Y_{py}N^{y}_{\delta_a}Y_{p\phi}}{\Delta+Y_{p\phi}N^{\phi}_{\delta_a}}$

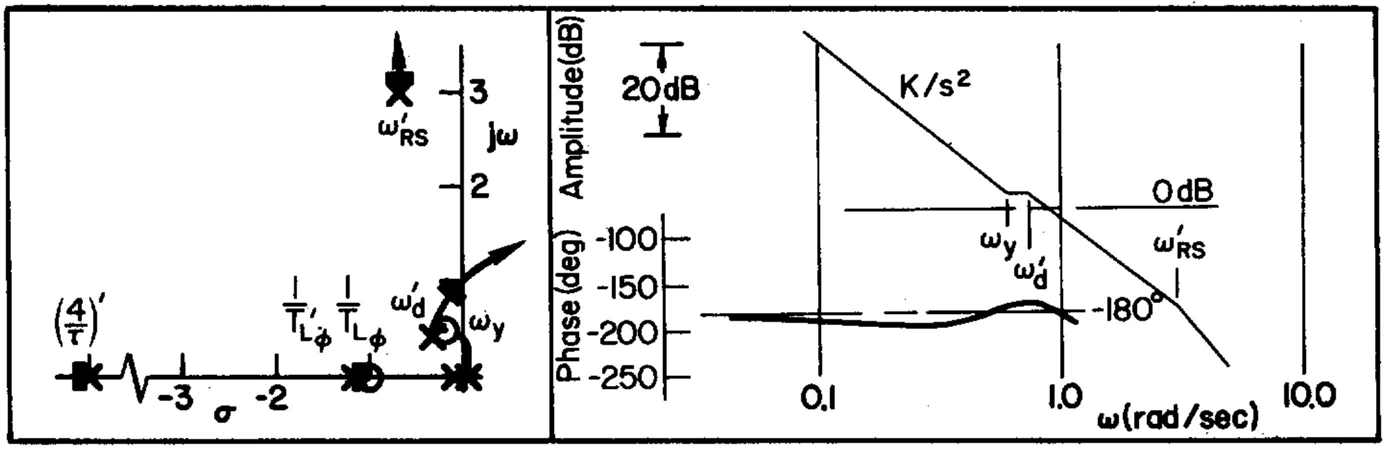

c) End Transition $\left.\frac{y}{y_\epsilon}\right]_{\phi\to\delta_a} = \frac{Y_{py}N^{y}_{\delta_a}Y_{p\phi}}{\Delta+Y_{p\phi}N^{\phi}_{\delta_a}}$

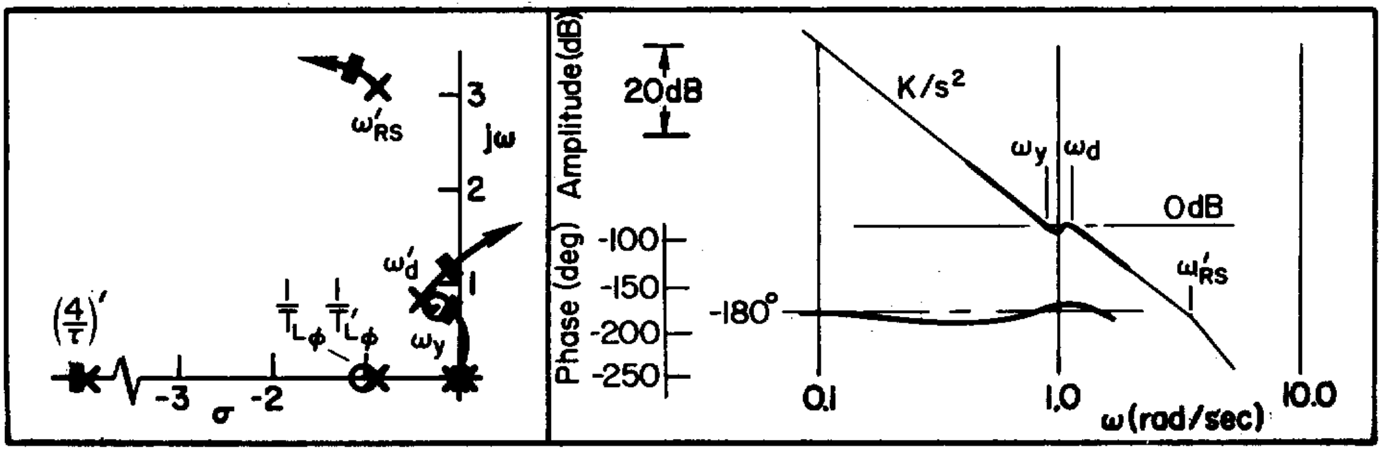

Figure 38. Multiloop Lateral Displacement Control with Ailerons

b. Maneuvering Control

1) Heading control, $\psi \rightarrow \varphi \rightarrow \delta_a$. Figures 39, 40, and 41 present the heading to aileron transfer function characteristics, with and without inner-loop bank angle control, from hover through transitions. The associated block diagram is shown below. The outer loops are shown closed without lead to permit simple comparisons. Pilot closure of the roll inner loop is necessary to stabilize and/or damp the lateral oscillatory mode as well as to improve the outer-loop bandpass for the heading closure. At hover the vehicle does not possess directional stiffness* and therefore cannot be turned with the ailerons. This is evident from the fact that the $\psi \rightarrow \delta_a$ closures with or without $\varphi \rightarrow \delta_a$ are unstable. As the speed and directional stiffness increase, turning becomes possible with the ailerons if the bank angle inner loop is also closed. At the end of transition, Fig. 41, bank angle needn't be closed, but the heading bandwidth is relatively low ($\omega_{c_\psi} < 0.3$ rad/sec) and the closed-loop control depicted is, in fact, very poor. This is due to the location of the numerator factors in the right half plane, as a consequence of the combination of yawing moment due to aileron, N_{δ_a}, lateral

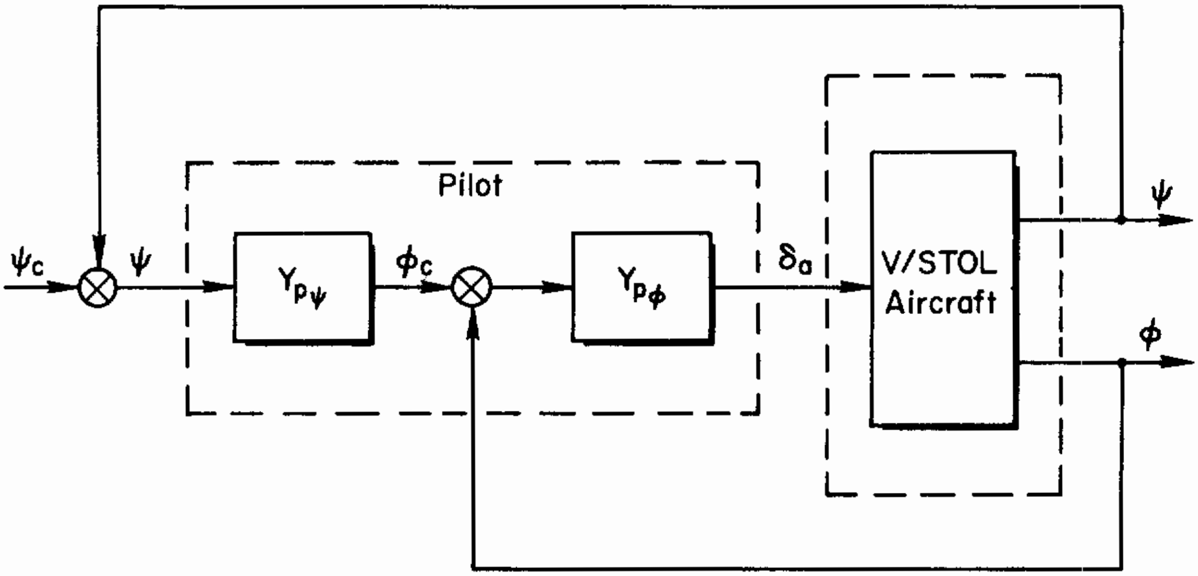

Heading Control Through Aileron
with Bank Angle Inner Loop, φ, $\psi \rightarrow \delta_a$

---

*The reader is reminded that in the hover condition the lateral oscillatory mode, ω_d, is defined by the lateral stability term, L_v, not N_v.

stability, L_v, and directional stiffness, N_v, which results in a positive value of $g(L'_{\delta_a}/N'_{\delta_a})N'_v[1 - N'_{\delta_a}L'_v/L'_{\delta_a}N'_v]$. As a result, there is a large effective time delay in the heading response to aileron commands, as shown, for example, in the following sketch.

A point to be reiterated here is that good heading control depends on favorable locations for the numerator zeros of the φ/δ_a and ψ/δ_a transfer functions (i.e., in left half plane). These zeros change drastically with relatively small changes in the control derivative, N'_{δ_a}.

2) Coordination Control. A final pilot control function which may be desirable or important is the act of coordinating turn or heading maneuvers, i.e., using the rudder to keep the body-oriented lateral acceleration acting on the airplane zero. This acceleration is defined by $a_y = \dot{v} - g\varphi + rU_o \doteq Y_v v$ at the vehicle c.g. In forward flight $\dot{v}$ is usually small so keeping the lateral acceleration, a_y, or sideslip, v, near zero by proper use of rudder provides a coordinated turn rate equal to $g\varphi/U_o$. However, as speed decreases, rU_o becomes negligible and the initial response in v to a bank angle is also small. Therefore, to begin with, bank angle maneuvers are automatically coordinated so that $a_y = v = 0$ and $\dot{v} = g\varphi$; but this cannot be maintained since as the vehicle increases side velocity $\dot{v}$ diminishes to zero as a first order washout given by

$$\frac{\dot{v}}{\varphi} = \frac{-gs}{s - Y_v}$$

The end result is a constant speed lateral drift with the component of gravitational acceleration along the y body axis (i.e., $g\varphi$) balanced by aerodynamic reaction $Y_v v$.

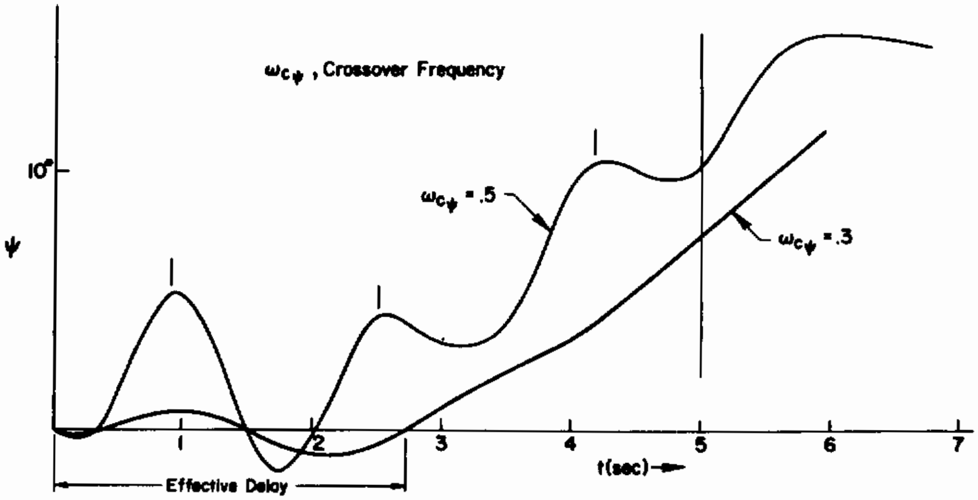

Heading Response Delay Characteristics to ψ Command at End of Transition (ψ, $\varphi \rightarrow \delta_a$ Heading Closure)

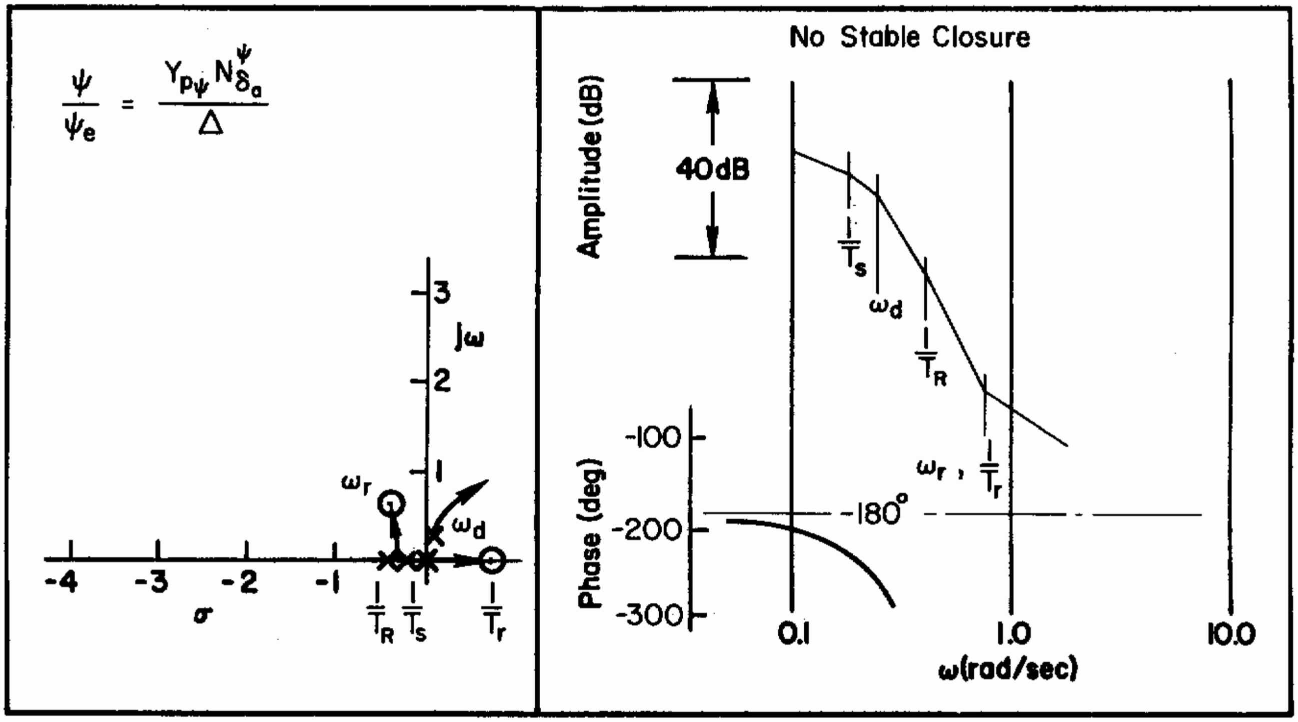

a) Single Loop Heading Control With Ailerons

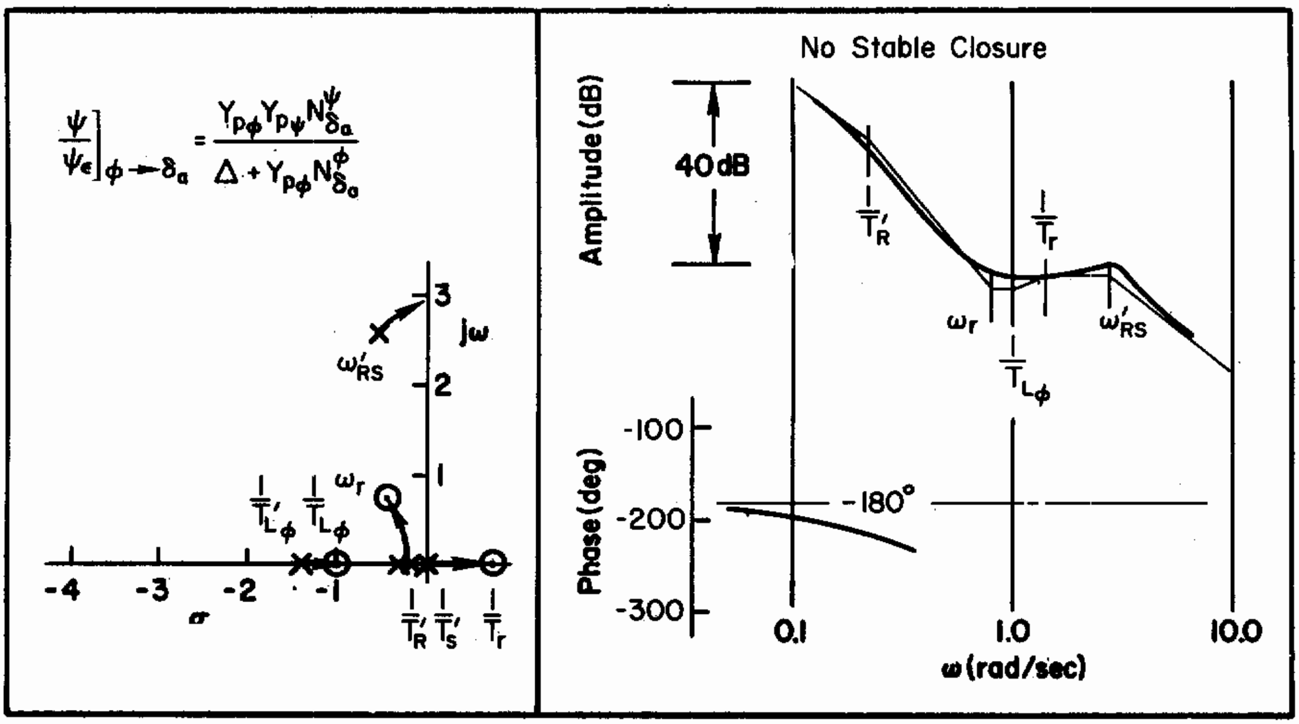

b) Heading Control Using Ailerons and Bank Angle

Figure 39. Heading Control During Initial Transition

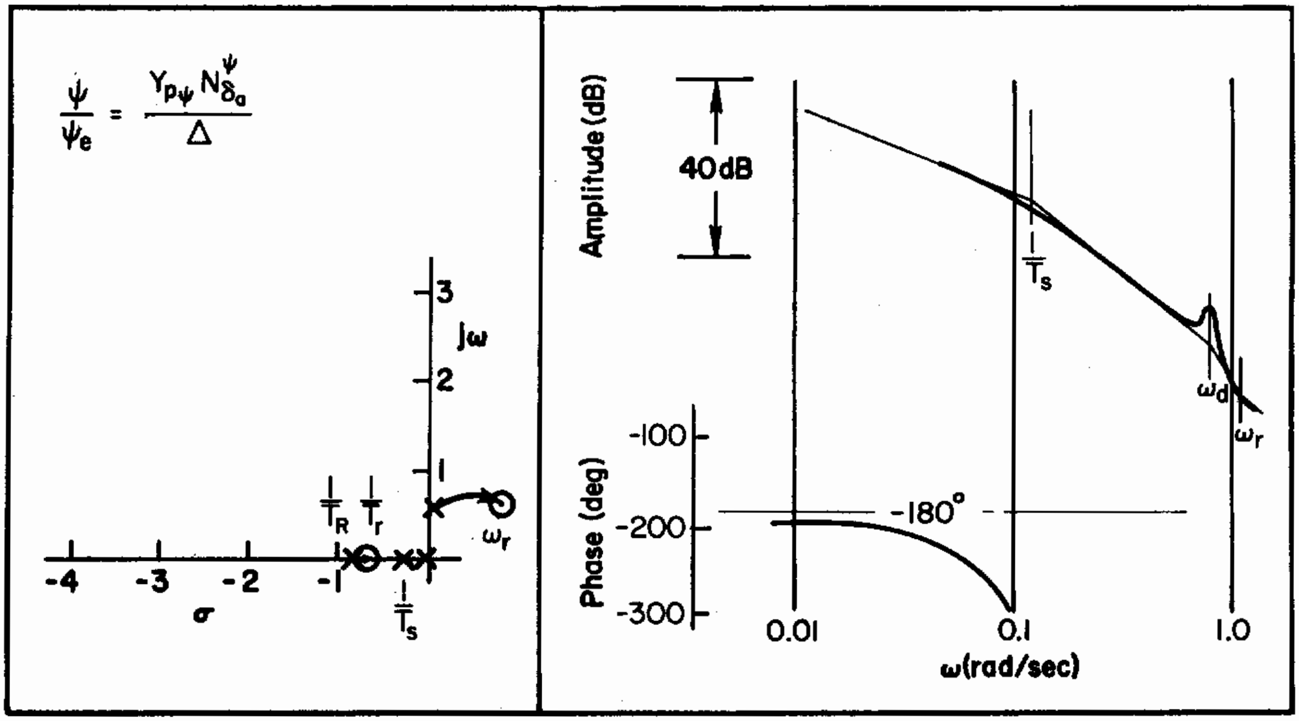

a) Single Loop Heading Control With Ailerons

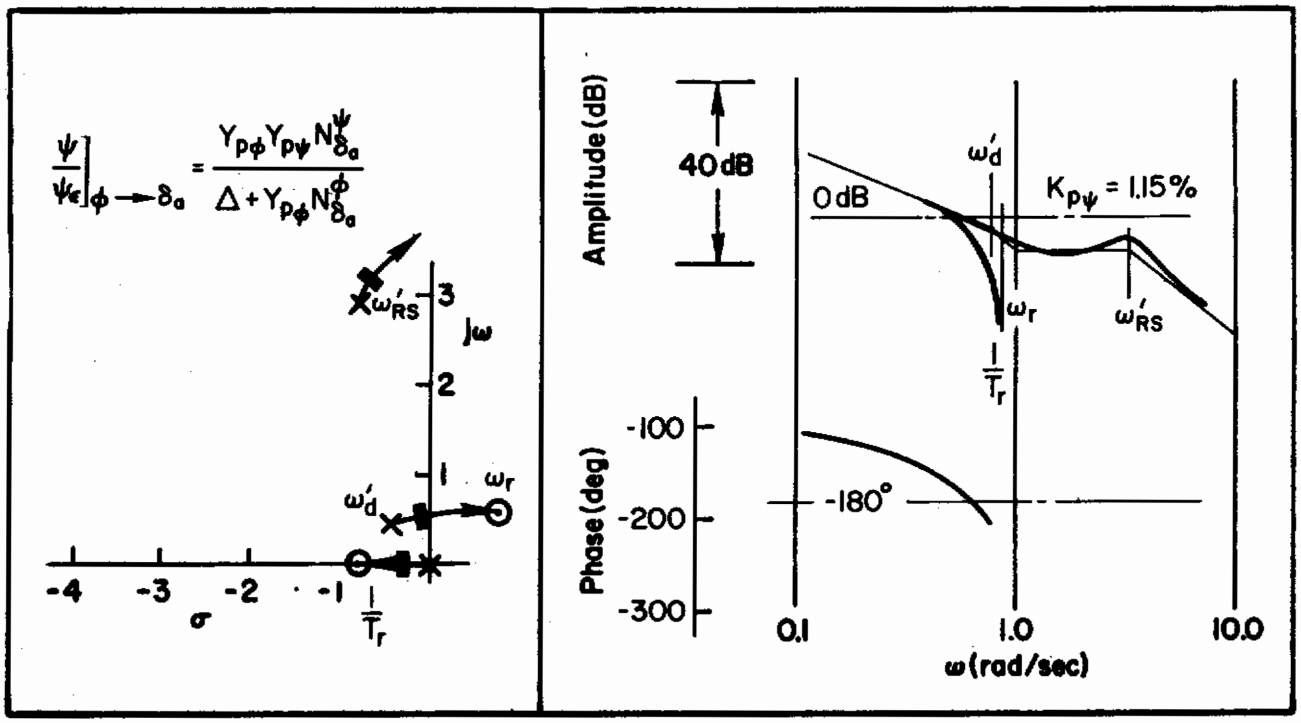

b) Heading Control With Ailerons and Bank Angle

Figure 40. Heading Control During Midtransition

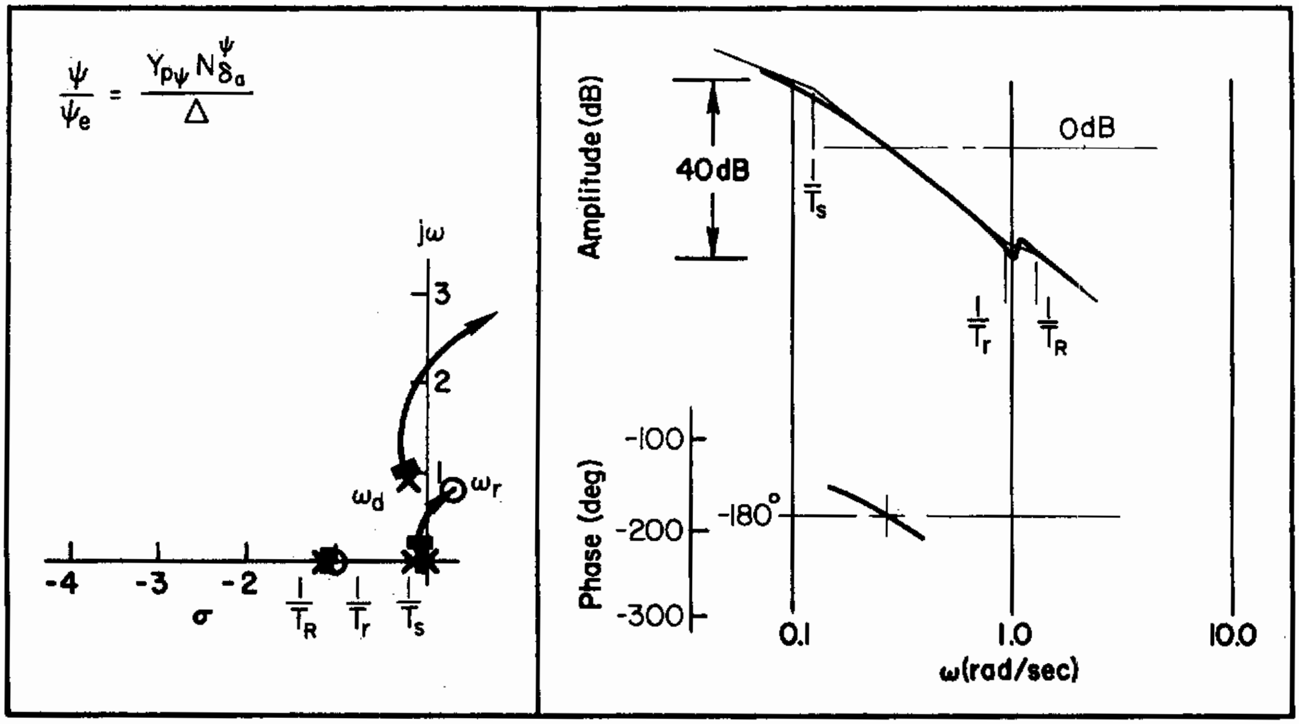

a) Single Loop Heading Control With Ailerons

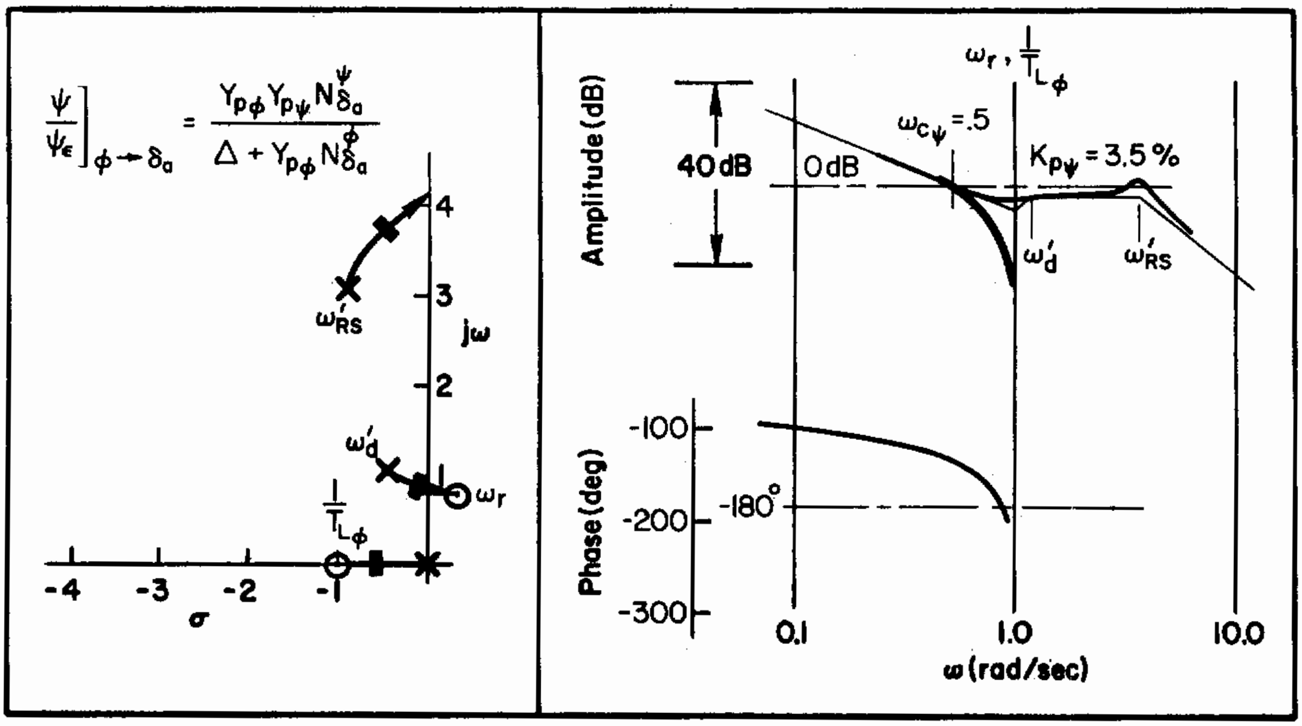

b) Heading Control With Ailerons and Bank Angle

Figure 41. Heading Control During End Transition

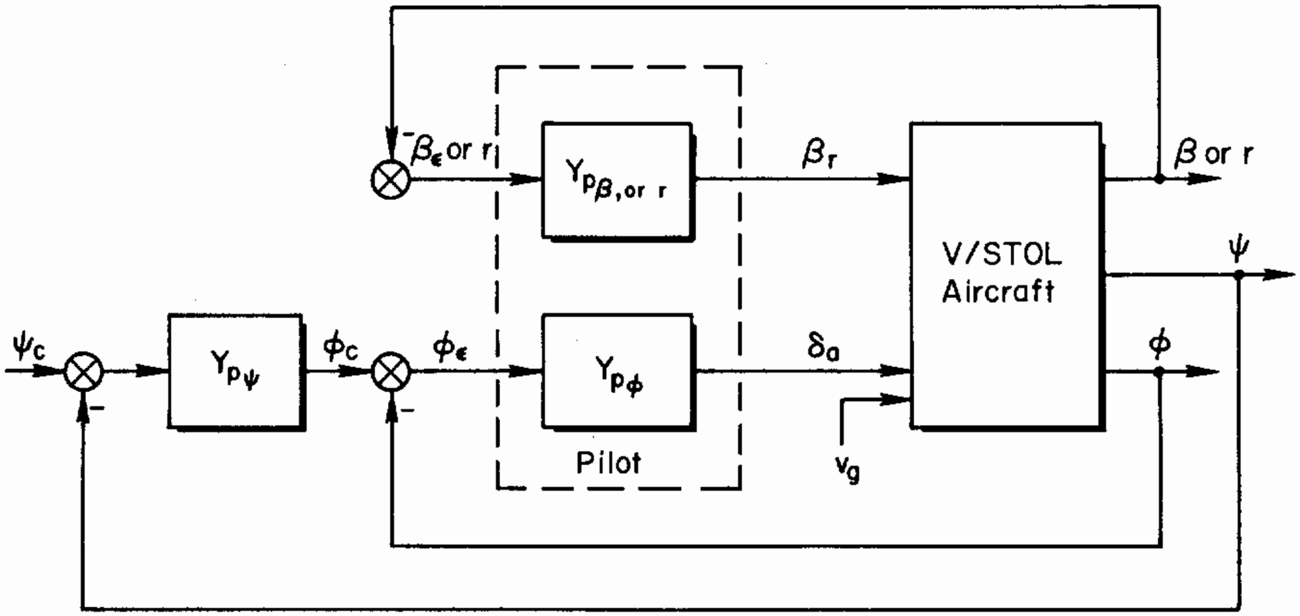

Heading Control Through Bank Angle
With Sideslip or Yaw Rate Stabilization

$$\psi \rightarrow \delta_a \left| \begin{array}{l} \varphi \rightarrow \delta_a \\ \beta \text{ or } r \rightarrow \delta_r \end{array} \right.$$

Figures 42, 43, and 44 show the $\psi \rightarrow \varphi \rightarrow \delta_a|_{\beta \rightarrow \delta_r}$ control structure. Closing the β loop has moved the Dutch roll root, ω_d', to a higher frequency (compare to previous figure of $\psi \rightarrow \varphi \rightarrow \delta_a$ alone) and this stiffens the airplane. Unfortunately, the uncompensated $\beta \rightarrow \delta_r$ closures used here to provide simple comparisons tend to reduce the damping of the Dutch roll mode, $\zeta_d'\omega_d'$, and the $\varphi \rightarrow \delta_a$ numerator factor, $\zeta_\varphi'\omega_\varphi'$. As a result, no overall improvement is achieved in the heading closures. In fact, the reduced damping tends to restrict the heading bandpass due to the peaking of the closed-loop Dutch roll mode (e.g., see Fig. 43). The restriction of the heading bandwidth because of the numerator factor, $\zeta_\varphi\omega_\varphi$, was explored in Ref. 20; and the results of this study are considered later in this section. Basically, it is sufficient to note here that the tightness of the heading closure depends on this numerator damping term $\zeta_\varphi'\omega_\varphi'$.

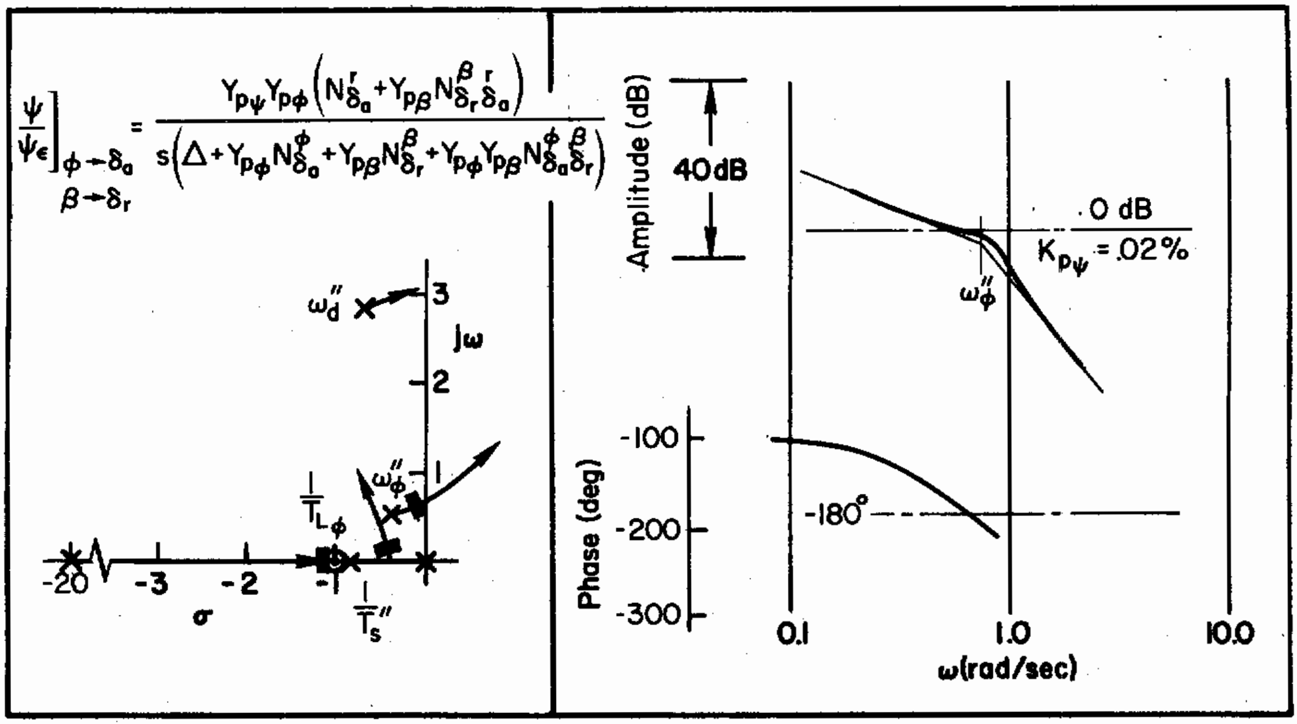

Figure 42. Heading Control with Aileron Using Rudder Coordination; ψ, $\varphi \to \delta_a$, $\beta \to \delta_r$; Initial Transition (Hover)

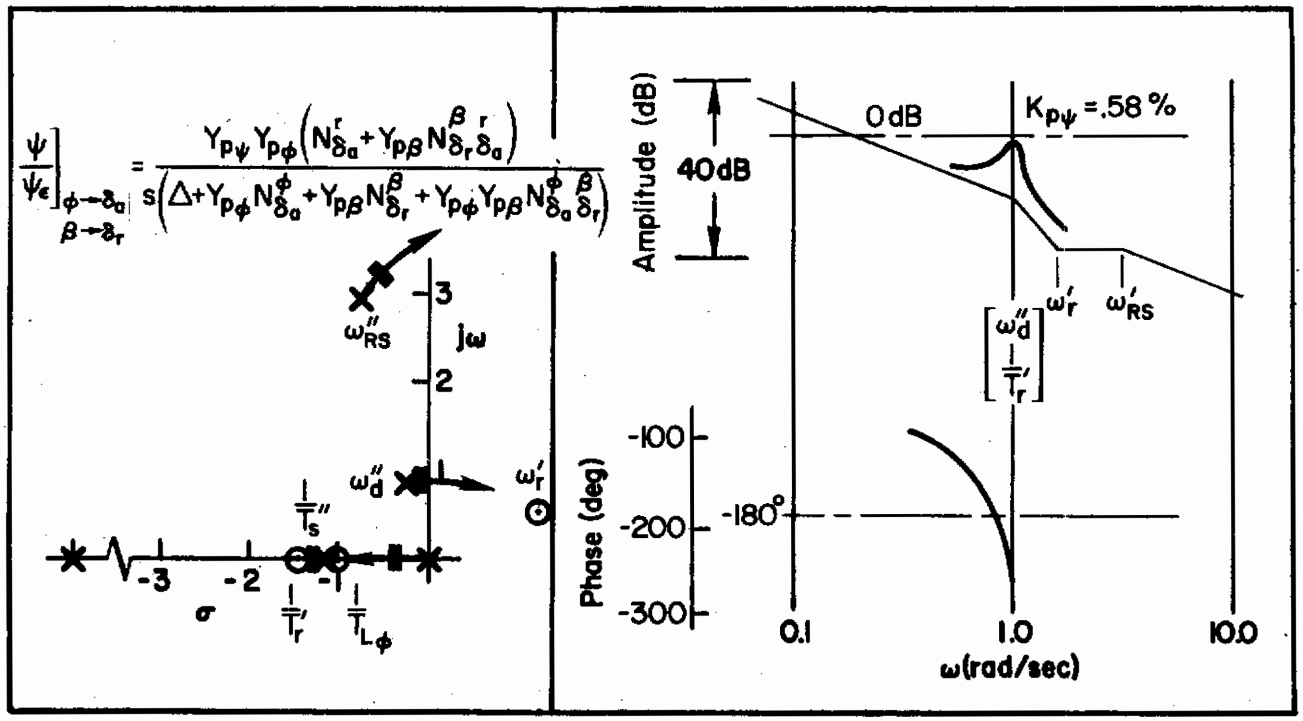

Figure 43. Heading Control with Aileron Using Rudder Coordination; ψ, $\varphi \to \delta_a$, $\beta \to \delta_r$; Midtransition

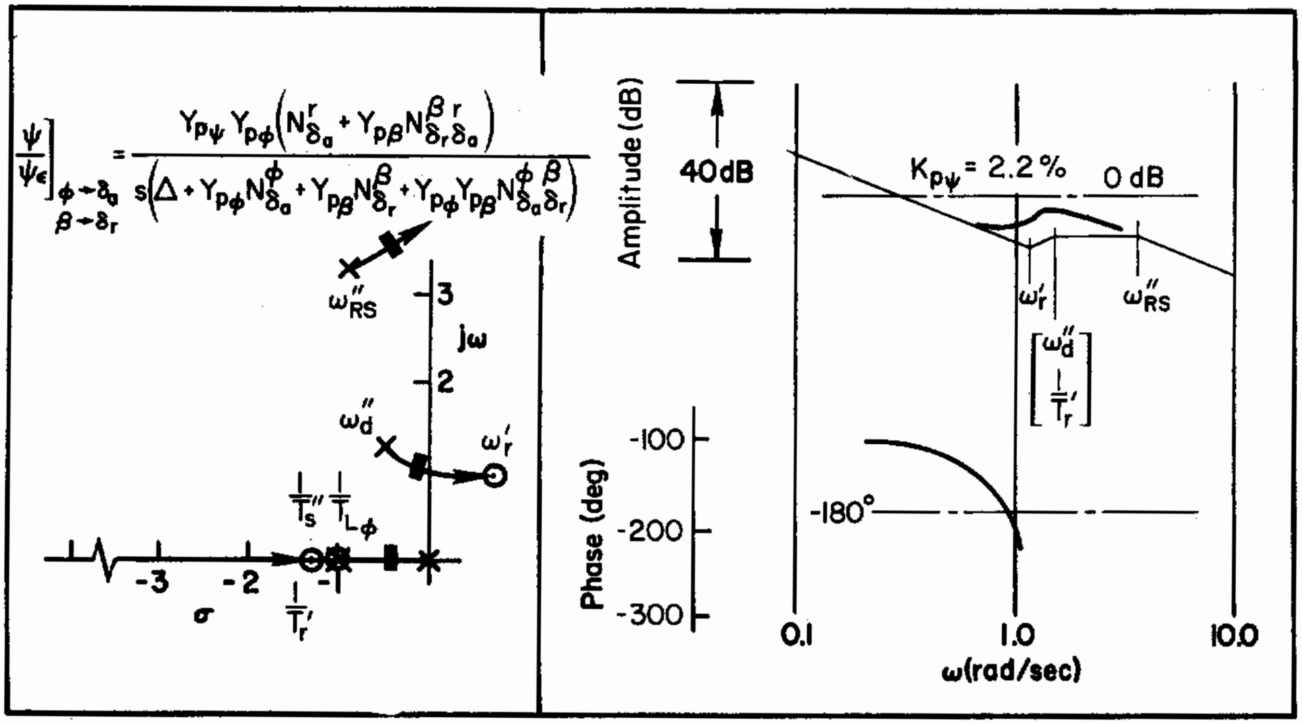

Figure 44. Heading Control with Aileron Using Rudder Coordination; ψ, $\varphi \rightarrow \delta_a$, $\beta \rightarrow \delta_r$; End Transition

B. CONSIDERATION OF EXPERIMENTAL RESULTS

The results of several experimental programs covering lateral/directional control at low-speed conditions will be considered in the following subsections. The understanding gained from the foregoing generalized considerations of pilot/vehicle control are applied to the case situations examined experimentally in Refs. 18, 19, 22, and 25.

This is done by detailed closed-loop analyses for selective flight tested configurations. The majority of these dynamic configurations were tested for several different piloting control situations and tasks which included ILS tracking, hovering turns, and general low-speed flight with and without synthetic lateral turbulence. Only an overall pilot rating was given after completion of the test series, and no weighting was assigned by the pilot to the various tasks. As a result, in these analyses we consider piloting techniques and closed-loop control structures covering both regulatory and maneuver control situations to find a cause for the given rating. Note, also, that conclusions as to the probable cause will often be directed at a single closed-loop deficiency. Thus, in this discourse, we are suggesting that in many cases a single adverse factor accounts for the rating, and, in the pilot's eyes, overshadows all other desirable features. Where possible, pilot comments are used to support such conclusions, but in general the evidence consists primarily of the anlytical review of the data.

1. Directional Damping, N_r, and Stability, N_v

The in-flight model-following simulator experiments of Refs. 18 and 19 studied the lateral/directional handling qualities of tandem and single rotor helicopter configurations respectively. The two experiments were designed to determine the requirements on directional stability, N_v, and damping, N_r. In the NASA tests (Ref. 18) the pilot task was to null the localizer and glide slope indicators on an ILS approach, while in the NRCC tests (Ref. 19) the pilot maintained a ground track and glide slope through visual alignment of a ground-fixed indicator. A closed-loop analysis of the two experiments was performed in Ref. 20, the results of which are discussed briefly in the following paragraphs because of their overall pertinence to the present study and for general reference.

Since the basic ILS task was maneuvering the airplane to zero the deviations from the localizer beam the minimum control technique would be $\psi \rightarrow \varphi \rightarrow \delta_a$. Lateral displacement control is not considered because, as was pointed out in the previous section, it is always nearly $g\varphi/s^2$ and therefore has a very low bandwidth.

The important conclusion derived from the ILS tracking task was the influence of the numerator damping term $\zeta_\varphi\omega_\varphi$ or $1/T_{\varphi_1}$ on the heading loop crossover frequency.

More specifically, the extent to which the heading gain and crossover frequency can be increased depends on the value of $\zeta_d'\omega_d'$, which in turn is most strongly influenced by the basic value of $\zeta_d\omega_d$ and the roll/aileron numerator damping $\zeta_\varphi\omega_\varphi$. In effect, the heading loop crossover frequency (or bandwidth or dominant response frequency) is determined by the value of $\zeta_\varphi\omega_\varphi$, which in turn is approximately given by

$$\zeta_\varphi\omega_\varphi \doteq \frac{-Y_v - N_r}{2}$$

The other terms associated with this approximation (such as L_r, L_{δ_r}, and N_{δ_a}) are either negligible or were not present in the simulator.

A similar dependence of the achievable heading response speed (or crossover) is found when the φ/δ_a numerator is nonoscillatory, i.e., when $4N_\beta < (Y_v - N_r)^2$ which occurs for low directional stability, N_β. In this case the most critical parameter in the heading closure is the closed-loop pole of the roll closure, which becomes almost equal to $1/T_{\varphi_1}$. The approximate factor for this zero, for the above condition on N_β, is

$$\frac{1}{T_{\varphi_1}} \doteq -Y_v + \frac{N_\beta}{Y_v - N_r}$$

Figure 45 shows the correlation obtained in Ref. 20 using the above basic φ-numerator characteristics as metrics. In this figure all the NASA data of Ref. 18 and the three low N_v NRCC cases of Ref. 19 were plotted to establish a boundary value of $\zeta_\varphi\omega_\varphi$ (or $1/T_{\varphi_1}$) $\doteq 0.4$/sec associated with the 3-1/2 rating. The low N_v cases were chosen to minimize pilot rating changes due to gust effects. This value for $\zeta_\varphi\omega_\varphi$ (or $1/T_{\varphi_1}$), which, as explained above, is to be taken as a measure of the heading response, converts to a heading-loop crossover frequency between about 0.25 to 0.3 rad/sec. For crossovers less than 0.25 to 0.3 rad/sec, the pilot will begin to complain that the aircraft will not follow into a turn using "aileron" control. These results are in good agreement with the conclusions reached in Ref. 21 where the supersonic transport configurations studied are very much different in size and approach speed. In fact, the two in-flight simulators of Refs. 18 and 19 are themselves much different in size and weight, but the pilot ratings of similar dynamic situations in the two aircraft gave surprisingly good agreement, as indicated in Fig. 45.

The $\psi \rightarrow \varphi \rightarrow \delta_a$ control structure therefore requires $\zeta_\varphi\omega_\varphi$ or $1/T_{\varphi_1} \geq 0.4$. When this requirement is not met rudder control of heading (rather than with ailerons), i.e., $\psi \rightarrow \delta_r$ may be attempted; but this is directly influenced by the level of N_v. In the maneuvers discussed above, the influence of gust disturbances was slight since, generally, $N_v \leq 0.01$. Since increasing values of N_v will change the disturbance level directly, Ref. 19 also concerned itself with a regulatory pilot task of maintaining heading in the presence of gust induced heading disturbances. Because the gust disturbances were only directional in nature (i.e., L_v was zero) and the vehicle's roll characteristics were suppressed (high $-L_p$), the pilot was assumed to be interested primarily in the single-loop regulation of heading with pedals. This is similar to the hover dynamics case where the inner-loop bank angle closure does not affect the $\psi \rightarrow \delta_r$ closures. The pilot's ratings in these tests were a strong function of the directional damping, N_r, the directional stability, N_v, and rudder effectiveness, N_{δ_r}. The important analytical results of Ref. 20 were:

a. The pilot's rating shows a strong correlation with rms heading response, σ_ψ, and with rms control deflection, σ_{δ_r}.

b. The directional damping, N_r, requirements are a strong function of N_v and the gust level, σ_{v_g}, as reflected in the value of σ_ψ.

2. Lateral Stability, L_v, and Directional Damping, N_r

The experiment of Ref. 22 is essentially a continuation of the variable stability measurements made in Ref. 19 for $L_v = 0$ and discussed above. In the Ref. 22 experiment various levels of dihedral, accompanied by changes in directional damping and control sensitivity, were tested. The effects of lateral dynamics were supposedly suppressed by keeping the roll damping and roll control sensitivity at a high but constant value. However, note that a large value of roll damping can be a significant factor in defining

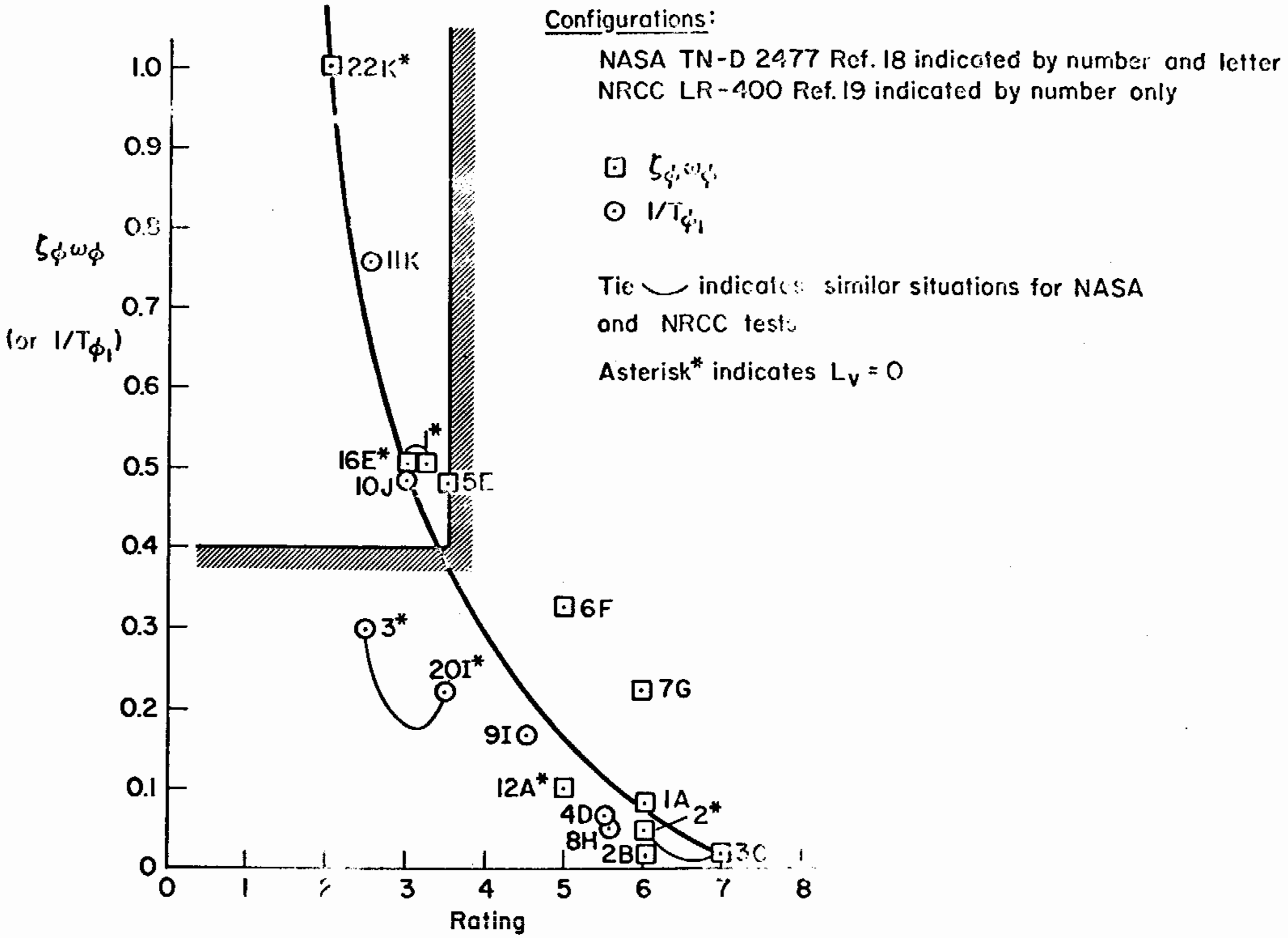

Figure 45. Correlation of Lateral Numerator Damping Factor, $\zeta_\varphi \omega_\varphi$ (or $1/T_{\varphi_1}$), with Pilot Rating, taken from Ref. 20

the airplane oscillatory mode response for low N_β conditions (i.e., the oscillatory mode can become equal to $\sqrt{gL_v/L_p}$ instead of $\sqrt{N_\beta}$). The aerodynamic coupling derivatives N_p and L_r were considered negligible and Y_p and Y_r were shown to have an insignificant effect on the dynamic characteristics. The visual flight task performed by the pilot during the evaluation included hovering turns and a complete circuit terminated by a low-speed (30 kt), steep angle (11°), VFR approach to touchdown. Both a simulated steady wind and synthetic lateral turbulence were introduced into the simulation.

The results of the experiment for the circuit flying task are shown in Fig. 46. The results for the hovering task are very similar, as expected, since the hovering was done into a simulated 15 kt headwind. The line connecting the points of minimum directional damping on Fig. 46 represents the variation in optimum control sensitivity; i.e., increasing or decreasing N_{δ_r} about these points degrades the pilot rating. Analyzing points along this line tends to eliminate the contribution of sensitivity to the pilot ratings as the dynamic properties of the vehicle itself change. The stability derivatives for the optimum control sensitivity conditions of Fig. 46 as well as the aileron and rudder transfer functions are presented in Appendix D.

Since the major complaint of the pilots participating in these experiments centered on the ability to control the disturbance caused by the turbulence, only the gust regulation piloting functions are given detailed consideration. Basically, aileron control as related to the turning ability of the vehicle was not effectively tested in this experiment, and we would not expect the ratings to be influenced by the heading to aileron control technique. That is, the r/δ_a numerators are identical in all cases and $1/T_{\varphi_1}$ or $\zeta_\varphi\omega_\varphi$ are approximately equal to 0.3 except for the satisfactory case at $L_v = -0.05$ where $1/T_{\varphi_1} = 0.2$. Consequently, we will exclude the $\psi, \varphi \rightarrow \delta_a$ closure from the discussion.

Turning directly to the gust regulation task we see, from the tabulated data in Appendix D, that all the 3-1/2 rating cases have $\omega_d < 0.5$ with the spiral mode canceling the $1/T_{\varphi_2}$ zero, or in more familiar terms, hover dynamics. The multiloop control technique in this case would be $\psi \rightarrow \delta_r\big]_{\varphi \rightarrow \delta_a}$. The reason why the inner roll loop has to be closed is that for positive dihedral ($L_v \neq 0$), the side gust feeds through the aerodynamics (i.e., L_v) to produce roll disturbances as well as heading disturbances. The added roll disturbances not only require the use of ailerons to suppress them directly, but can also complicate the heading response to further degrade the performance for the heading control task.

A typical heading closure for a 3-1/2 pilot rating case and moderate dihedral ($-L_v = 0.02$) is given in Fig. 47. In the attitude roll closure (considered the inner loop) the Dutch roll (ω_d) and the corresponding rudder numerator second order (ω_r) are both easily modified (to ω_d' and ω_r') so as to improve the outer loop characteristics. Inner-loop crossover frequencies near 2.5 rad/sec with phase margins of 30° to 40° and 4 to 6 dB of gain margin require only pilot's gain adaptation (i.e., no lead). The resulting outer rudder control loop has a large K/s region which extends

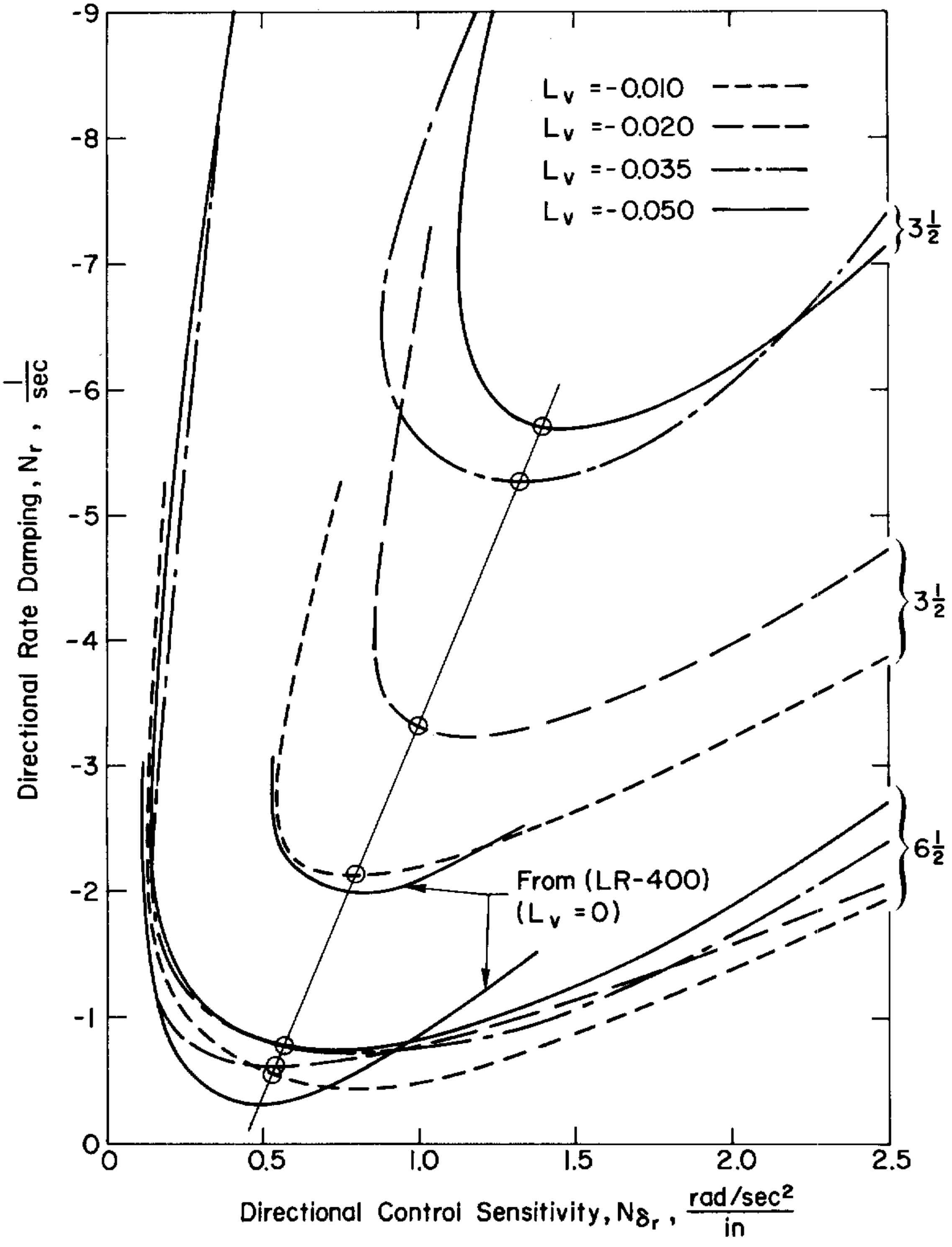

Figure 46. Comparison of Handling Qualities Boundaries for Various Values of Dihedral Effect, Circuit Flying Task; from Ref. 22

Inner Loop $\dfrac{\phi}{\phi_e} = \dfrac{L_{\delta_a}(s+.36)}{(s+10)\left[s^2+2(.71)(.27)s+(.27)^2\right]} = \dfrac{K_{p\phi}(s-13)^2}{(s+13)^2}$

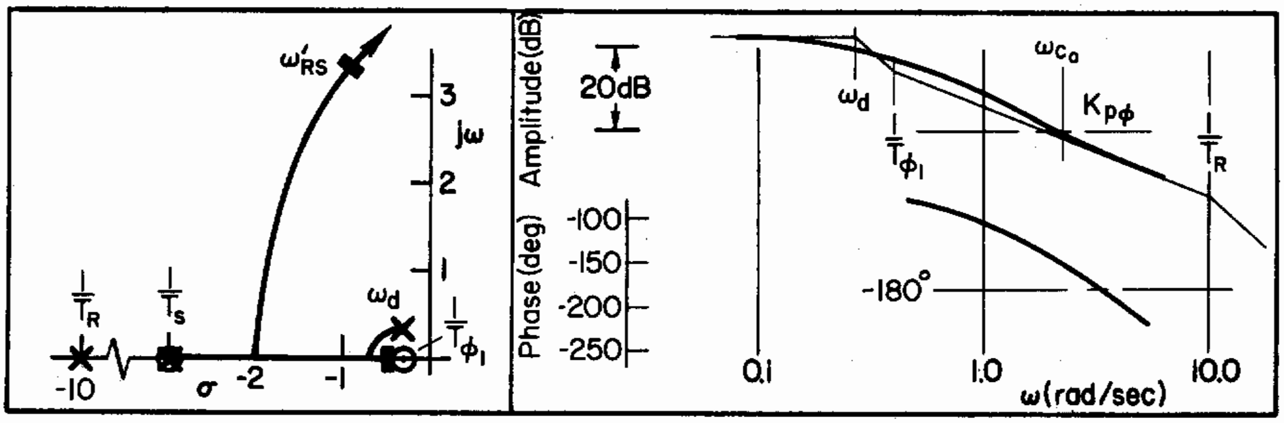

Coupling Numerator $\dfrac{Y_{p\phi}N^{\phi\ r}_{\delta_a\delta_r}}{N^{r}_{\delta_r}} = \dfrac{K_{p\phi}(s-13)^2A_{\phi_r}s}{(s+13)^2A_r(s+10)\left[s^2+2(.039)(.25)s+(.25)^2\right]}$

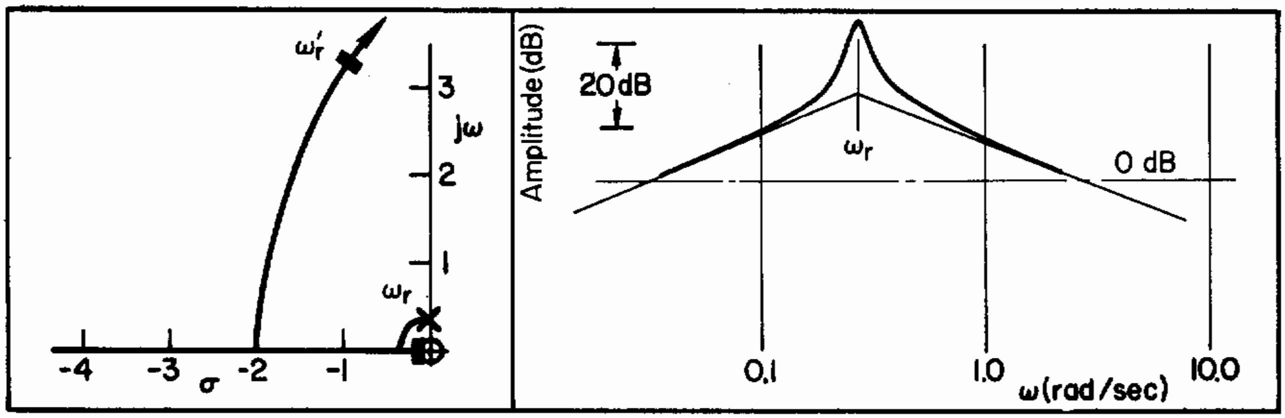

Outer Loop $\dfrac{\psi}{\psi_e}\Big|_{\phi\rightarrow\delta_a} = \dfrac{A_r(s+.025)}{s(s+.39)(s+2.96)} = \dfrac{Y_{p\psi}(s+13)^2}{(s+13)^2}$ (High frequency roots are shown)

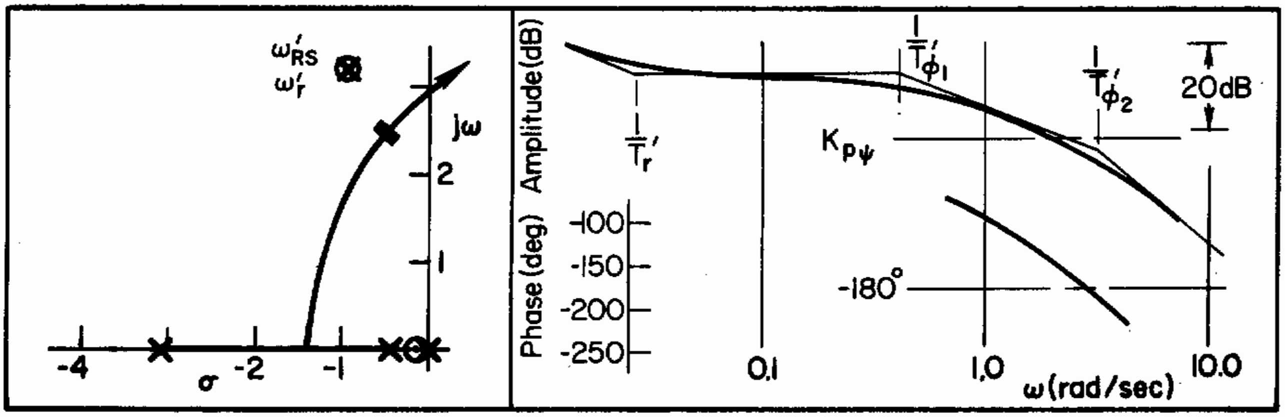

Figure 47. Multiloop Heading Closure with Rudder for Moderate Dihedral (L_v = −0.02) and Pilot Rating of 3-1/2

from approximately $1/T'_{\varphi_1}$ to $1/T'_{\varphi_2}$. The larger the yaw damping, N_r, in this case, the longer will be the K/s region since

$$-N_r \doteq \frac{1}{T_{\varphi_2}}$$

$$\frac{N_\beta}{-N_r} \doteq \frac{1}{T_{\varphi_1}} \quad \text{for small } Y_v$$

Actually a good multiloop situation is one where a simple inner-loop closure will provide a good control structure in the outer loop, i.e., minimal or no pilot compensation with a K/s characteristic in the region of crossover. In this case, Fig. 47, the outer-loop crossover is about 2.0 rad/sec in a K/s region with approximately the same gain and phase margins as for the inner loop and without any need for pilot's lead. The conditions for satisfactory L_v can therefore be derived from these results and interpreted in terms of Dutch roll frequency; that is, $\omega_d^2 \doteq gL_v/L_p \leq 0.25$, where $N_r^2 > 4N_\beta$. This is identical to the hover requirement shown in Fig. 2 for Category I systems.

For the 6-1/2 rating cases, $N_r^2 < 4N_\beta$ and the vehicle resembles a conventional airplane since the roll numerator is complex and in the vicinity of the Dutch roll mode. The traditional handling qualities rules regarding ω_φ, ω_d, ζ_φ, and ζ_d now apply.

The closures typical for any of the 6-1/2 cases (i.e., $-L_v = 0.02$) are shown in Fig. 48. In this case the inner-loop closure ($\varphi \rightarrow \delta_a$) cannot modify the Dutch roll (ω_d) characteristic, although it does modify the corresponding rudder numerator (ω_r). The net effect on the outer loop is small, so it is essentially independent of the inner-loop closure. The dominant airplane gust response motion with both loops closed, not obvious from Fig. 48, consists of the more conventional coupled roll and yaw disturbances due to the aerodynamic terms, L_v and N_v.

Since it is evident from Fig. 48 that the roll attitude control features exhibit good gust regulatory characteristics (e.g., a broadband K/s region with simple gain compensation for the closure), we turn to the heading control characteristics for the cause of the 6-1/2 rating. Here the evidence pointing to poor heading control with the rudder is the relatively low frequency second-order character of the ψ/ψ_ϵ Bode with the φ-loop closed. It will be remembered from the discussion relative to Fig. 37 that such features pose a compensation dilemma to the pilot. In essence, because the dominant oscillatory mode frequency, ω_d, is near 1 rad/sec the effective gust bandpass is likewise nearly the same, the pilot cannot obtain the desired high-gain, broadband K/s region for crossover with either lead or lag compensation. In fact, the lead compensation needed to obtain a K/s region reduces the low frequency gain and consequently the gust regulatory performance σ_ψ as shown in the plot below. This

a) Inner Loop $\frac{\phi}{\phi_\epsilon} = \frac{L_{\delta_a}}{(s+.042)(s+10)} = \frac{K_{p\phi}(s-13)^2}{(s+13)^2}$ (High frequency roots not shown)

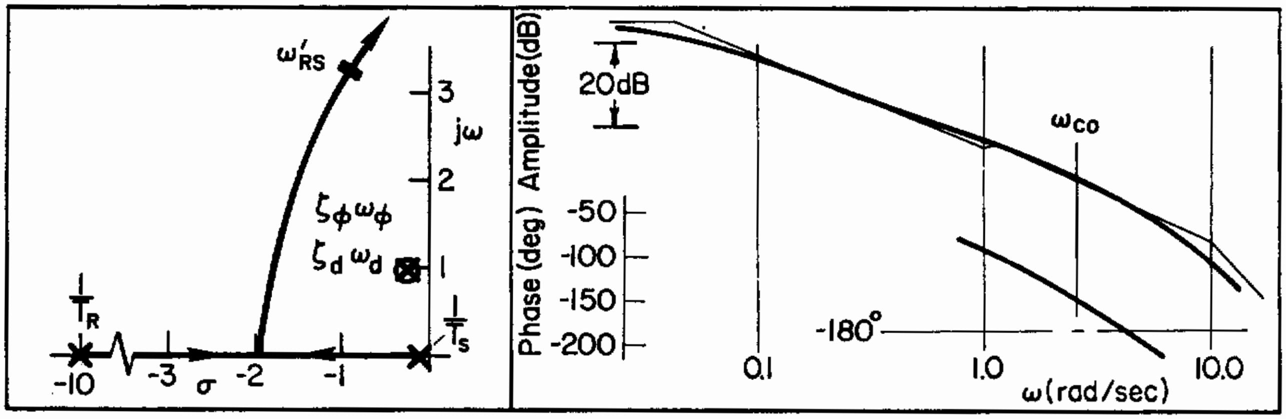

b) Coupling Numerator $Y_{p\psi}\frac{N^{\phi\ r}_{\delta_a\delta_r}}{N^{r}_{\delta_r}} = \frac{K_{p\phi}(s-13)^2 A_{\phi_r}\, s}{(s+13)^2 A_r (s+10)\left[s^2+2(.039)(.25)s+(.25)^2\right]}$

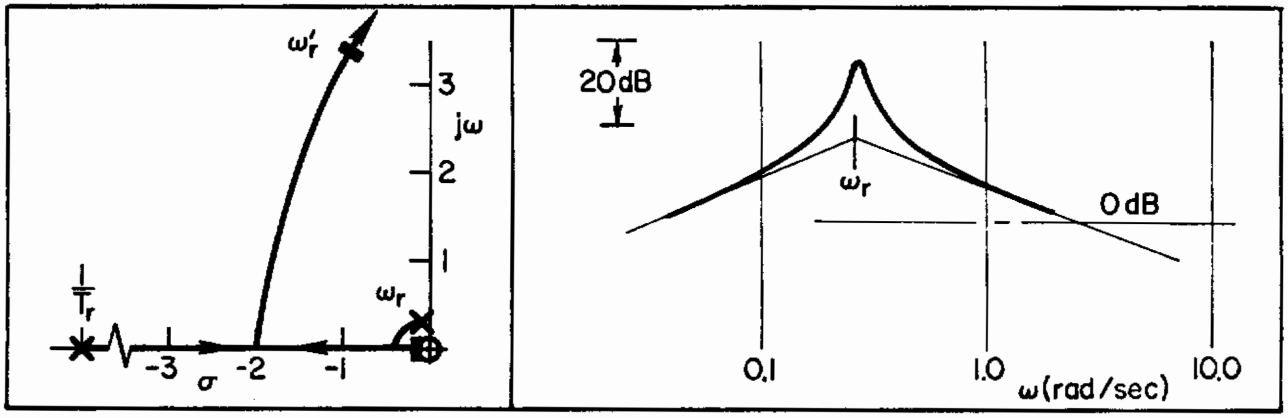

c) Outer Loop $\left.\frac{\psi}{\psi_\epsilon}\right]_{\phi\rightarrow\delta_a} = \frac{A_r(s+.025)}{s\left[s^2+2(.37)(1.02)s+(1.02)^2\right]} = K_{p\psi}(s+2.5)\frac{(s-13)^2}{(s+13)^2}$

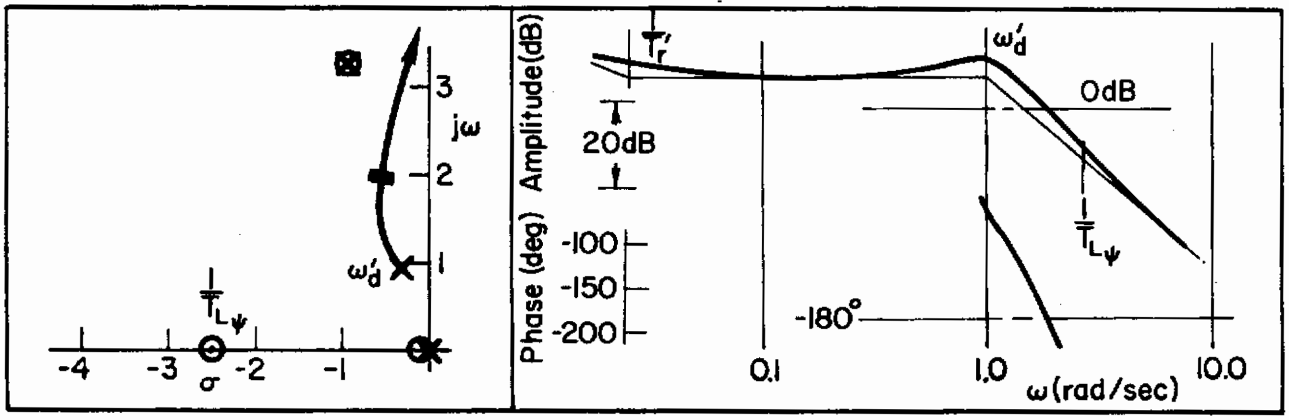

Figure 48. Regulatory Control of Heading; Multiloop; $\psi \rightarrow \delta_r$, $\varphi \rightarrow \delta_a$

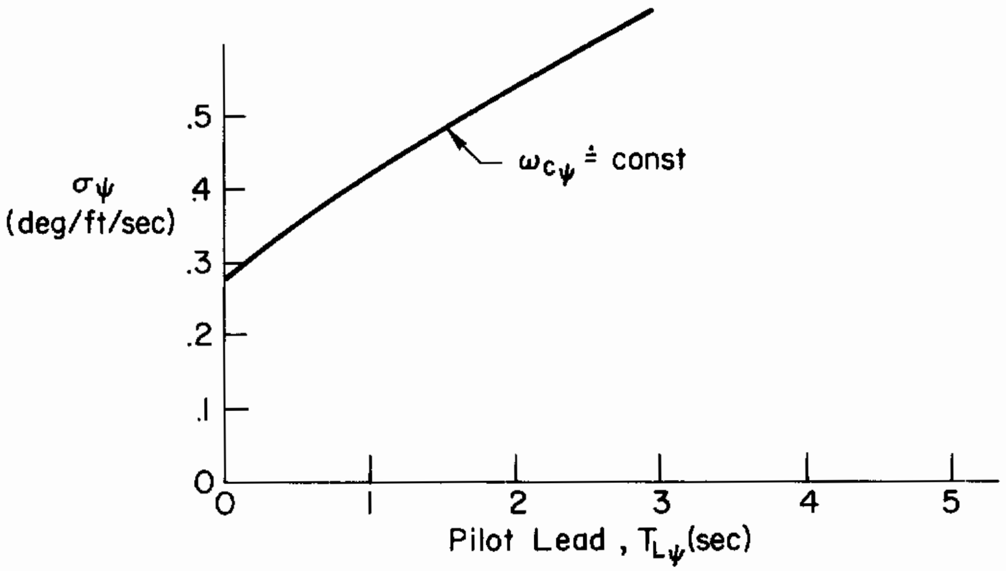

Effect of Pilot Lead Compensation on Heading Error
for Constant, Closed-Loop Bandwidth (i.e., $\omega_{c_\psi} \doteq$ constant)

plot was computed in a manner similar to that outlined in Appendix E for the determination of the rms values of ψ, φ, $N_{\delta_r}\delta_r$, and $L_{\delta_a}\delta_a$ without lead. The results of the latter computations are shown in Table VI, below. In this table, the ψ-excursion provides a measure of the pilot's success in

TABLE VI

SUMMARY OF RMS RESPONSES FOR σ_{v_g} = 1.0 FT/SEC

	CASE		σ_ψ	$N_{\delta_r}\sigma_{\delta_r}$	σ_{δ_r}	σ_φ	$L_{\delta_a}\sigma_{\delta_a}$	σ_{δ_a}
$-N_r$	$-L_v$	PR	(deg)	(deg/sec^2)	(in.)	(deg)	(deg/sec^2)	(in.)
2.2	0.01	3-1/2	0.23	1.23	0.027	0.022	0.115	0.0012
3.3	0.02	3-1/2	0.157	1.14	0.020	0.048	0.35	0.0036
5.7	0.05	3-1/2	0.091	1.09	0.014	0.108	1.38	0.014
0.7	0.01	6-1/2	0.354	1.01	0.030	0.021	0.071	0.00072
0.7	0.02	6-1/2	0.350	1.01	0.029	0.041	0.141	0.0014
0.7	0.05	6-1/2	0.340	0.994	0.025	0.101	0.35	0.0036

the principal task of maintaining heading. The φ-response describes the roll attitude deviations of the vehicle from a "wings level" condition. Finally, $N_{\delta_r}\delta_r$; δ_r and $L_{\delta_a}\delta_a$; δ_a provide a measure of both the required rms control power and the rms control deflection exercised by the pilot.

Although the rms gust velocity was 8.9 ft/sec (an extreme value) in the tests, Table VI summarizes the computed values of the rms responses for a unit rms gust input. The six cases were chosen to represent low, medium, and high dihedral ($-L_v$ = 0.01, 0.02, and 0.05) at the 3-1/2 and 6-1/2 pilot rating boundaries. When the analytical results of Table VI are compared with the observed pilot ratings, there is a reasonable correlation with heading performance, σ_ψ, and the given ratings. This correlation is verified by pilot commentary (of low N_r cases) as reported in Ref. 22: "...at low damping, the pilots mainly objected to the disturbances caused by the turbulence, and they insisted on dampings high enough to keep these motions small."

The effects of lateral stability, L_β or L_v, have not been mentioned here because of the "good" φ-loop features. That is, the pilot is capable of maintaining good bank angle control with only moderate effort. In addition, the cases selected from Ref. 24 correspond to the lower L_v conditions where $N_r^2 < 4N_\beta$.

Coming back to the effects of lead as shown in the preceding sketch the pilot's general reaction to this control situation has been observed, also, in the Princeton variable-stability Navion experiments reported in Refs. 23 and 24. Although tested for higher directional stability levels, the ψ-loop Bode diagram sketched below for these Princeton tests has a very

$$\left.\frac{\psi}{\psi_\epsilon}\right|_{\phi \to \delta_a} = \frac{N_{\delta_r}(s + 1/T_r)}{s\left[s^2 + 2\zeta_d'\omega_d's + \omega_d^{2\prime}\right]} \quad K_{p_\psi} e^{-\tau s}$$

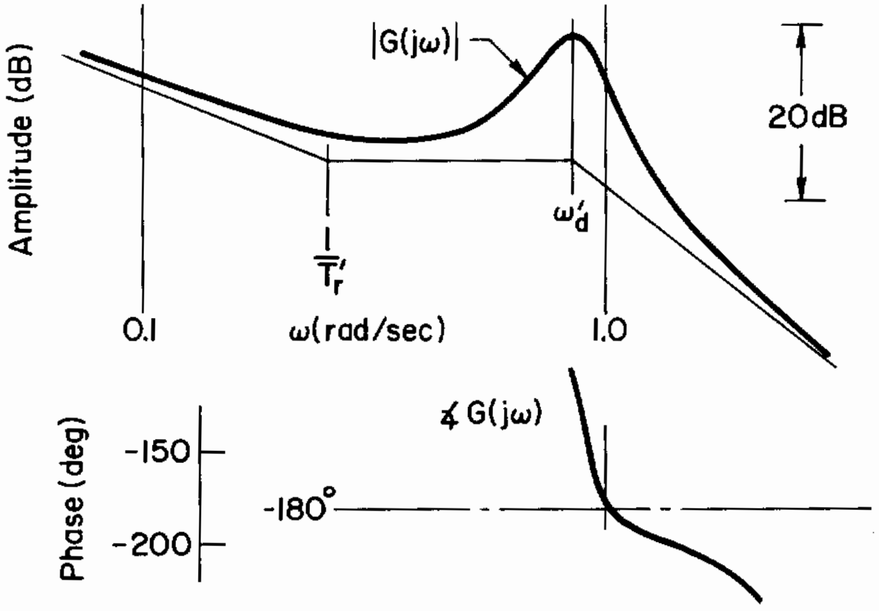

Heading Closures from Ref. 24

similar appearance to that of Fig. 48c. In the present case, the deterioration of pilot opinion was specifically attributed to excessive turbulence sensitivity in yaw and to the predominant yawing motion in the airplane's response which could not be precisely controlled with rudders. An increase in N_r for these configurations permitted the pilot to make an acceptable "feet-off" approach.

In terms of our initial findings from the Ref. 22 experiments, when $N_r^2 \leq 4N_\beta$ and the pilot's desire the $\psi \rightarrow \varphi \rightarrow \delta_a$ control structure, N_r should be determined such that $\zeta_\varphi \omega_\varphi > 0.4$ (i.e., $N_r > 0.8$). This is approximately the level of directional damping deemed necessary in Ref. 24 to provide satisfactory control. Furthermore, with N_r below this level, a rudder to heading control is forced on the pilot due to the predominance of yawing motions, but this is a futile exercise and leaves the pilots, as reported in Ref. 24, "...with undesirable heading excursions they are forced to live with." From the control technique standpoint, these results may be summarized in the following way:

> Heading control with the rudders can be satisfactory when $N_r^2 \geq 4N_\beta$, in which case the pilot rating is directly proportional to σ_ψ. When N_r^2 becomes less than $4N_\beta$ the rudder technique is no longer acceptable and the pilot transitions to an aileron control of heading. In this case the ratings are directly proportional to N_r, with 0.8 being the minimum acceptable.

3. Aileron-Rudder Control Cross-Coupling Effects, N_{δ_a} and L_{δ_r}

The data analyzed here were obtained from the Ref. 25 variable-stability, single-rotor helicopter study in which the control coupling terms N_{δ_a} and L_{δ_r} were varied. The piloting task in this experiment consisted of hovering turns out of simulated wind, transitions to forward flight, a constant speed-constant angle steep approach, and a decelerating transition with landing. The results of Ref. 25 (Fig. 49) are presented in the form of contours of constant pilot opinion separating the "normal operation," "emergency operation," and "no operation" regions (3-1/2 and 6-1/2 boundaries) as assessed by three pilots while performing the visual flight tasks in the presence of a simulated turbulence.

The stability axes derivatives used in the basic vehicle were set at values which produced a "good" vehicle before the control coupling terms were added. The derivatives were obtained from Ref. 25 and are presented in Appendix D.

Since the task of performing turns out of wind is notably a difficult maneuver some mention as to the method of simulation mechanization is pertinent. In this experiment, side velocity due to wind was simulated by displacing the ailerons and rudder in proportion to $U_o \sin\psi$, where U_o was the simulated wind speed of 15 kt. As the helicopter rotated out of the wind (i.e., changed heading) aileron and rudder were therefore required to control the rolling and yawing moments due to $L_v (U_o \sin\psi)$ and $N_v (U_o \sin\psi)$

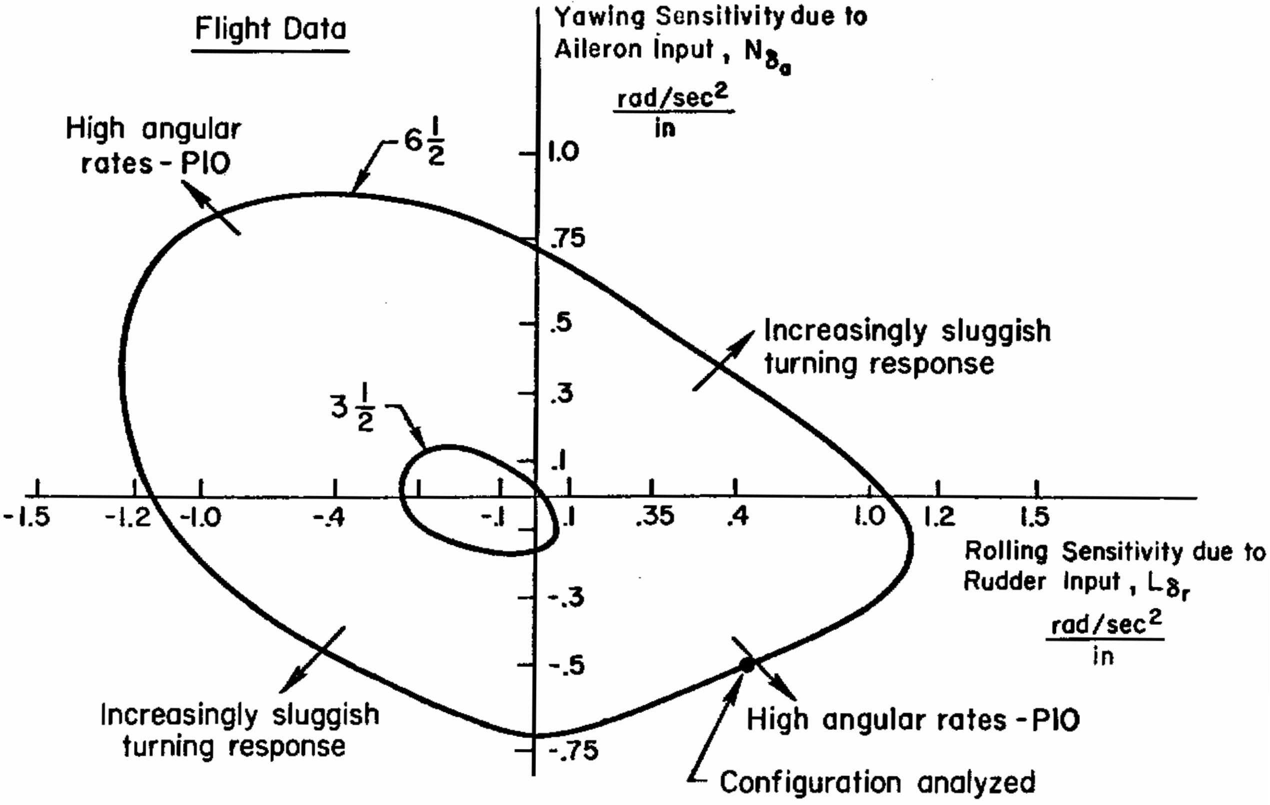

Figure 49. Lateral/Directional Control Cross-Coupling Handling Qualities Boundaries (Reproduced from Ref. 25)

respectively. With the proper control displacement ratio the helicopter could be hovered at $90^{\circ}\psi$ without any side translation and without any bank angle. In a true wind this would be impossible unless the side force derivatives were zero. Also, since the simulated wind was not actually a moving air mass, the ground translation was directly attributable to sideslip. In a true wind, the vehicle may be translating with respect to the ground but may be stationary (i.e., $\beta = 0$) with respect to a moving air mass. In any case, the task is one in which aileron and rudder control coordination during the maneuvering phase is required. Again the many different tasks performed by the pilot may be divided into the two basic closed-loop categories; maneuvering tasks where attitude (φ and/or ψ) is changing, and regulatory tasks where it is desired that attitudes remain fixed.

Analysis of both the regulatory and maneuvering tasks provides the basis for our appraisal of the results of the Ref. 25 control cross-coupling experiment. Regulatory tasks (i.e., maintaining bank angle, $\varphi \rightarrow \delta_a$, and heading, $\psi \rightarrow \delta_r$) under gust conditions are considered first; and favorable and adverse aileron and rudder coupling terms are covered. Next we consider maneuvering with conventional aileron heading control, $\psi, \varphi \rightarrow \delta_a$, for various combinations of N_{δ_a} and L_{δ_r}. Finally, because of the extreme levels of the coupling terms we also consider the need for rudder coordination during the heading maneuver. Accordingly we add a parallel $\beta \rightarrow \delta_r$ loop to supplement the basic $\psi \rightarrow \varphi \rightarrow \delta_a$ heading maneuver structure.

a. Regulatory Control

1) N_{δ_a} variable, $L_{\delta_r} = 0$. For analysis of the regulatory tasks we selected cases where the effect of one variable could be studied independently of the other. Appendix D presents the selected cases with their corresponding vehicle characteristics and pilot ratings. The closures for four levels of aileron yawing moment are presented in Figs. 50-53. These closures show the φ/δ_a loop and the ψ/δ_r loop with $\varphi \rightarrow \delta_a$ closed. The closure details show a combination of problem areas but none appear sufficient to consistently or adequately account for the change in pilot rating and the pilots' general objections. For the high proverse yawing moment cases (Fig. 50), heading regulatory control is considered only fair because of the relatively poor low frequency ψ-loop gain (i.e., less than 6 dB). In the case of high adverse yaw (Fig. 53) the regulatory control problem appears in the φ-loop and is reflected by the poor dc gain features of this closure.

For all cases, the closures can be made with very little pilot lead ($T_{L\varphi} \leq 0.1$ sec) in the inner (φ) loop and no lead required for the outer (ψ) loop. All crossovers are attainable in the desired frequency regions at −20 dB per decade slope with adequate phase and gain margins. In summary, the roll and heading closures show little differences for all N_{δ_a} cases, and good closure can be achieved except for the low dc gain problem in the two extreme N_{δ_a} cases.

Using these closures and the corresponding gust-numerators, the calculated error performance to side gusts given below does reflect the rating changes. This "correlation" is consistent with previous analyses

SUMMARY OF RESULTS ON N_{δ_a} EFFECTS

N_{δ_a} $\frac{\text{rad/sec}^2}{\text{in.}}$	$N_{\delta_a}/L_{\delta_a}$	σ_ψ/σ_{v_g} RUDDER CONTROL $\frac{\text{deg}}{\text{ft/sec}}$	PR
0.75	1.13	0.32	6-1/2
0	0	0.15	3-1/2
−0.2	−0.3	0.12	3-1/2
−0.75	−1.13	0.26	6-1/2

(e.g., Ref. 20) where degraded error performance, σ_ψ, was indicative of the poorer ratings. However, in the present instance this is but one facet of the total piloting problems revealed by the totality of analyses conducted.

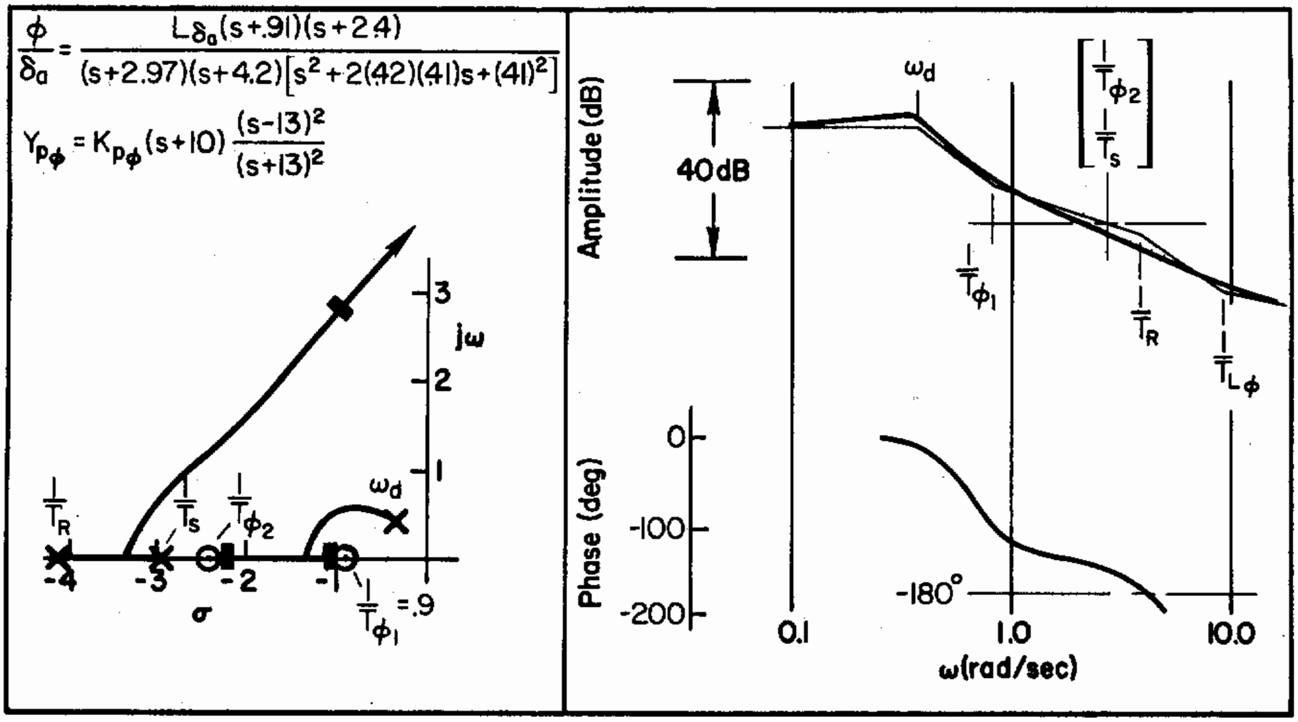

$$\frac{\phi}{\delta_a} = \frac{L_{\delta_a}(s+.91)(s+2.4)}{(s+2.97)(s+4.2)\left[s^2+2(.42)(.41)s+(41)^2\right]}$$

$$Y_{p_\phi} = K_{p_\phi}(s+10)\frac{(s-13)^2}{(s+13)^2}$$

3
jω
2
1
$\frac{1}{T_R}$
$\frac{1}{T_s}$
$\frac{1}{T_{\phi_2}}$
ω_d
-4
-3
-2
-1
σ
$\frac{1}{T_{\phi_1}}=.9$
Amplitude (dB)
40dB
ω_d
$\left[\frac{1}{T_{\phi_2}} \frac{1}{T_s}\right]$
$\frac{1}{T_{\phi_1}}$
$\frac{1}{T_R}$
$\frac{1}{T_{L_\phi}}$
Phase (deg)
0
-100
-200
-180°
0.1
1.0
10.0
ω(rad/sec)

$$\left.\frac{\psi}{\psi_\epsilon}\right|_{\phi \to \delta_a} = \frac{A_\psi(s+.036)\left[s^2+2(.28)(3.1)s+(3.1)^2\right]}{s(s+1.44)(s+1.92)\left[s^2+2(.3)(2.8)s+(2.8)^2\right]}$$

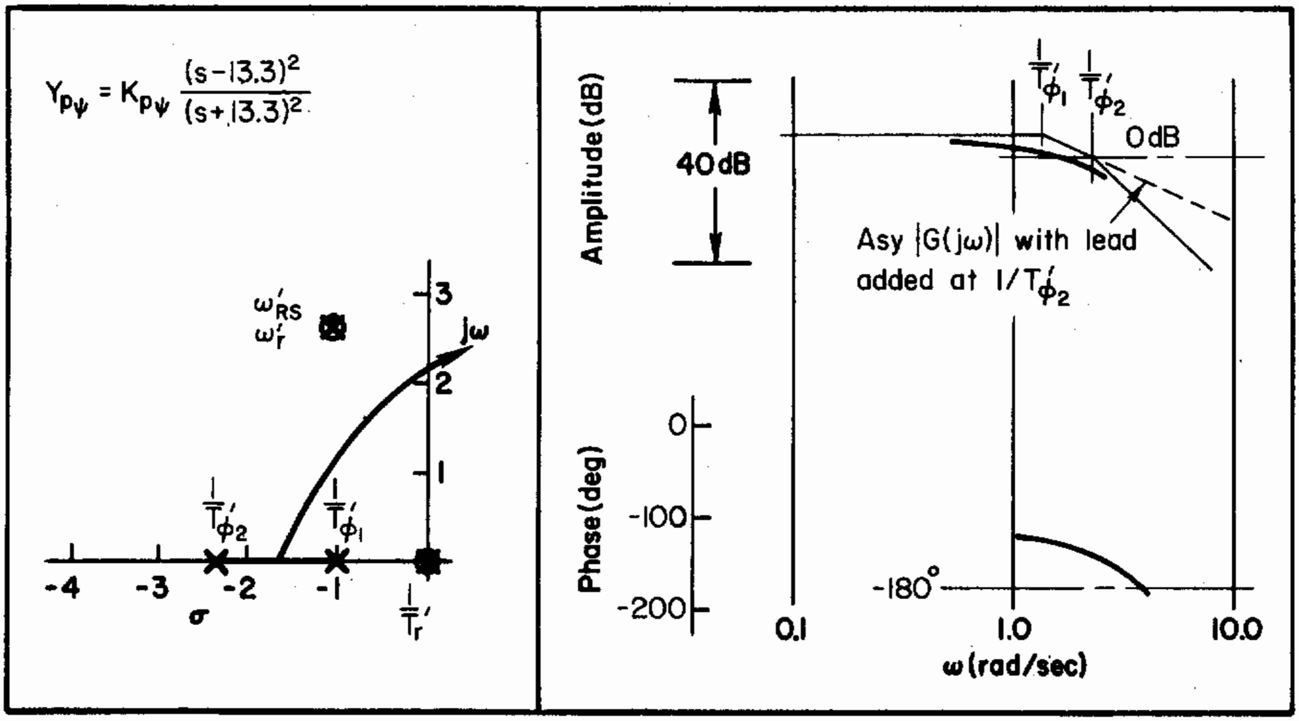

$$Y_{p_\psi} = K_{p_\psi}\frac{(s-13.3)^2}{(s+13.3)^2}$$

ω'_{RS}
ω'_r
3
jω
2
1
$\frac{1}{T'_{\phi_2}}$
$\frac{1}{T'_{\phi_1}}$
-4
-3
-2
-1
σ
$\frac{1}{T'_r}$
Amplitude (dB)
40dB
$\frac{1}{T'_{\phi_1}}$
$\frac{1}{T'_{\phi_2}}$
0dB
Asy $|G(j\omega)|$ with lead added at $1/T'_{\phi_2}$
Phase (deg)
0
-100
-200
-180°
0.1
1.0
10.0
ω (rad/sec)

Figure 50. Attitude Regulatory Closure with Rudder for High Proverse Yaw and Pilot Rating of 6-1/2

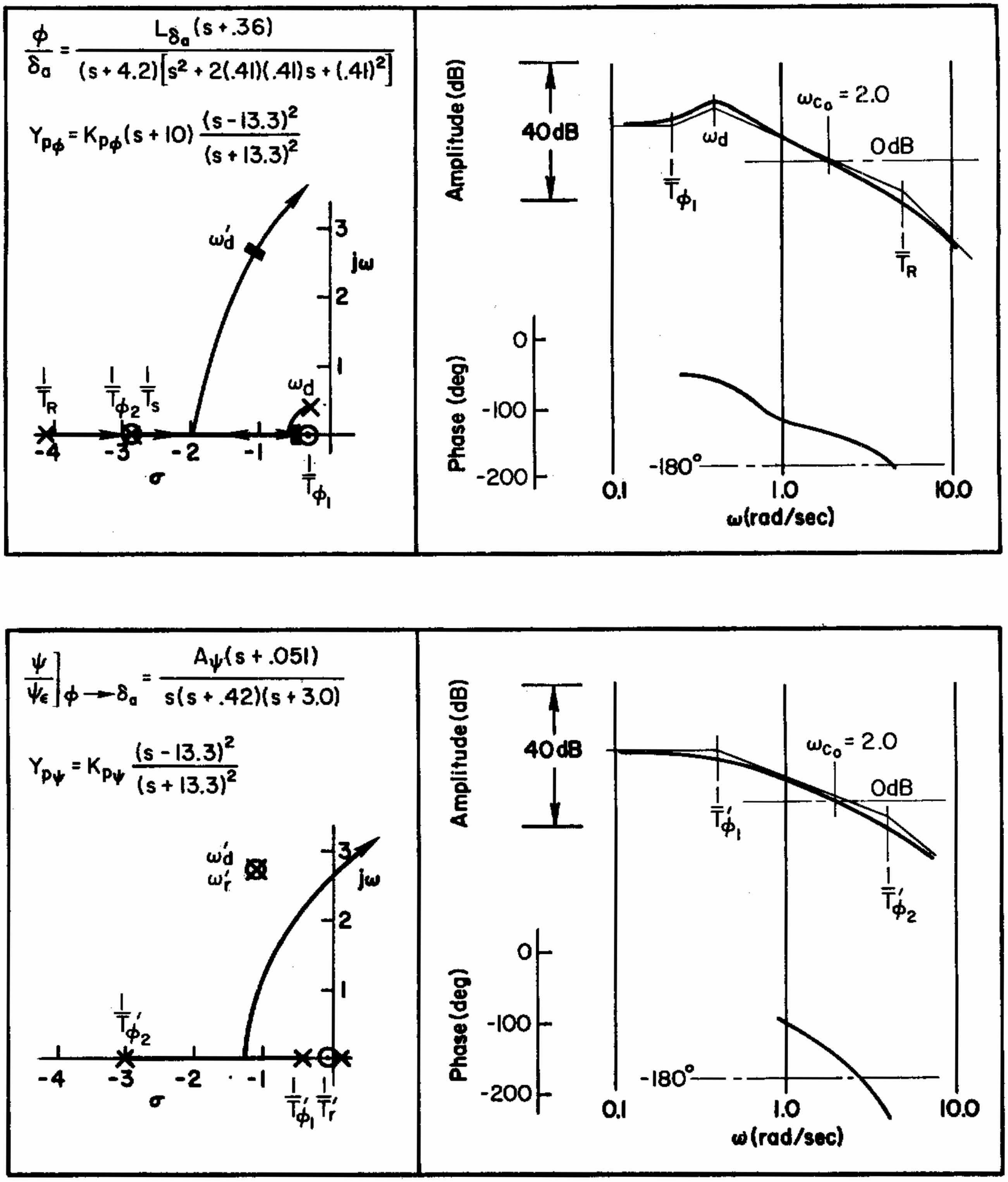

Figure 51. Heading Closure with Rudder for $N_{\delta_a} = 0$ and Pilot Rating of 3-1/2

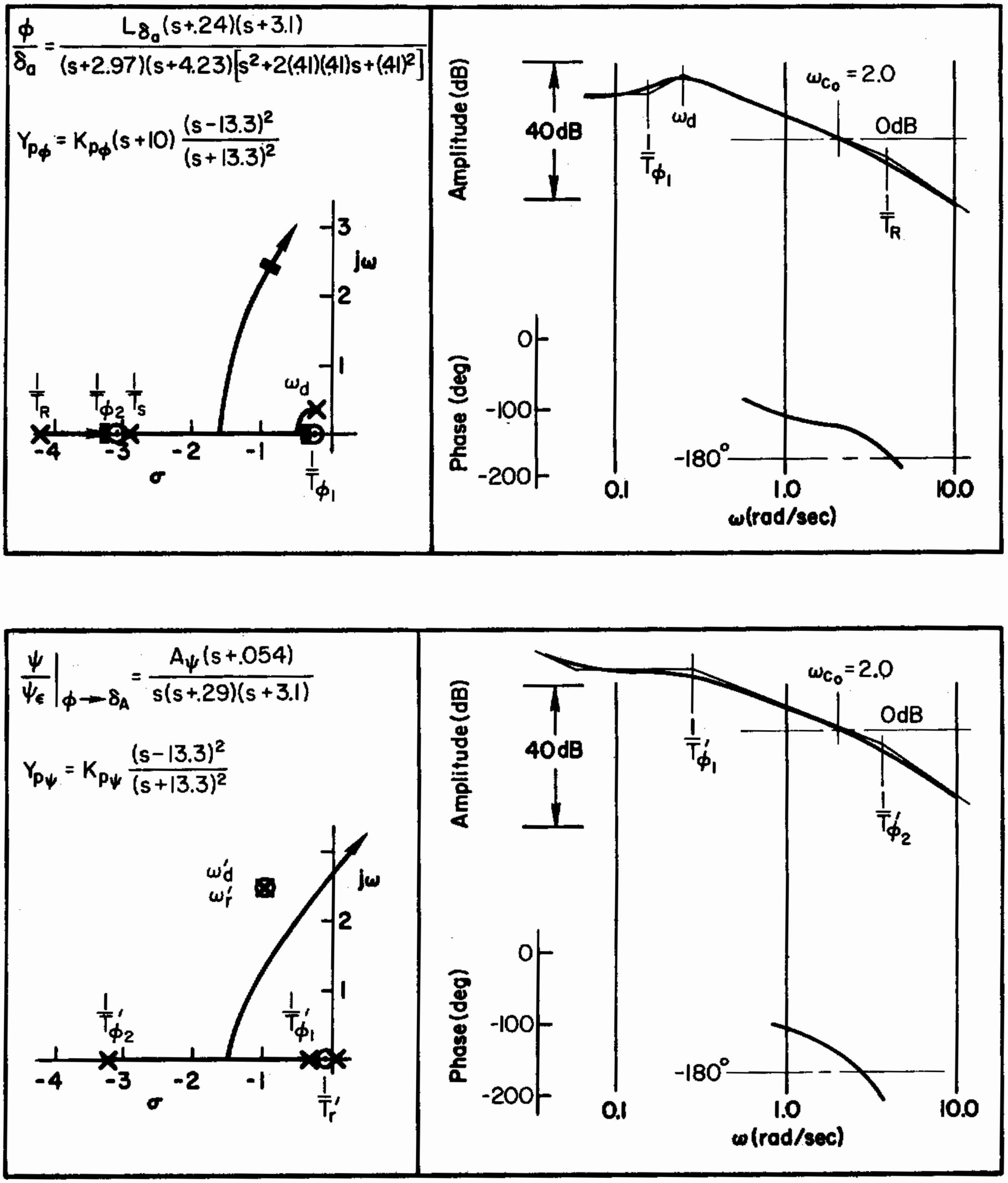

Figure 52. Heading Closure with Rudder for Low Adverse Yaw and Pilot Rating of 3-1/2

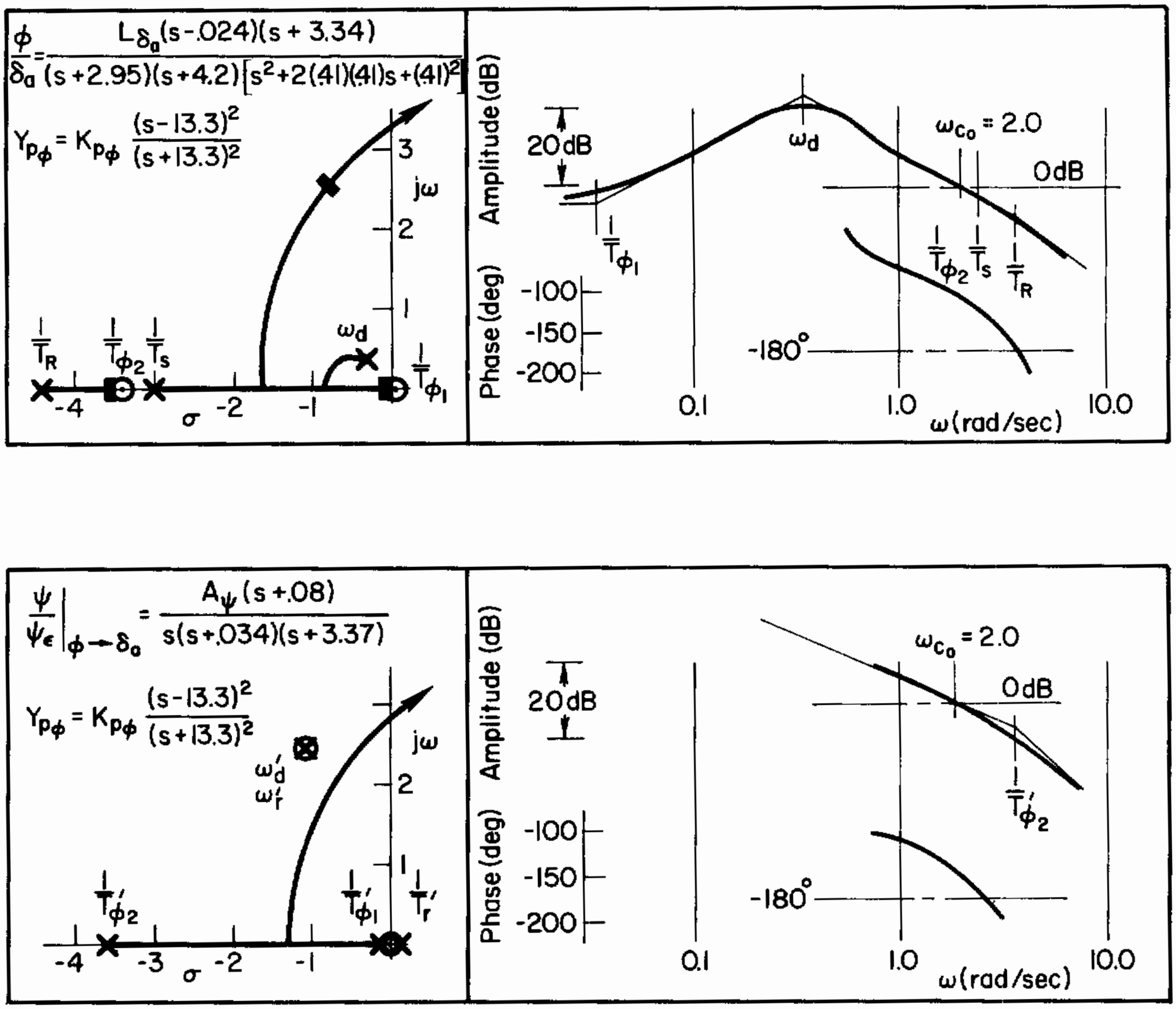

Figure 53. Heading Closure with Rudder for
High Adverse Yaw and Pilot Rating of 6-1/2

2) $N_{\delta_a} = 0$, L_{δ_r} variable. For the cases of $N_{\delta_a} = 0$ and L_{δ_r} variable the resulting closures were found to be identical to Fig. 51 for all cases, i.e., the effects of L_{δ_r} on the closures were negligible (see Appendix F). For example, closure of the inner aileron loop easily brings the adverse $N^{r}_{\delta_r}$ zeros in the right-half plane into the left-half (stable plane) through the favorable low-frequency lead provided by the coupling numerator. The closures are therefore essentially the same as those presented in Fig. 51 where $N_{\delta_a} = L_{\delta_r} = 0$. Also the gust performance $(\sigma_\psi/\sigma_{v_g})$ for rudder control does not change with L_{δ_r} and the associated rating change. In short there is no noticeable effect of L_{δ_r} on the gust regulation problem. The rating degradation is possibly due to maneuvering problems which are considered next.

b. Maneuver Control

The maneuver control aspects considered in the following are specifically related to heading control. Heading control problems are traceable, in part, to basic changes in the vehicle dynamics as speed is reduced; i.e., the effective decoupling of the lateral/directional axis due to loss in directional stiffness, N_v. This of course implies the inherent destruction of aileron heading control unless the pilot uses the rudder either to augment the directional stiffness or to provide equivalent coordination. Rudder and aileron cross-coupling effects complicate such control situations. The results of Ref. 25 are analyzed here to provide a detailed understanding of the piloting problems involved.

1) **Aileron Only.** If the pilot does not utilize a coordination structure and attempts turning or heading changes using the ailerons only in the manner of the sketch below the outer loop heading control has a restricted bandpass due to aileron yaw. This bandpass (i.e., crossover frequency) restriction is due to the effect of negative N_{δ_a} (adverse yaw) on the $N^{\varphi}_{\delta_a}$ numerator factor, $1/T_{\varphi_1}$, when $N_v \doteq 0$ or $\zeta_\varphi \omega_\varphi$

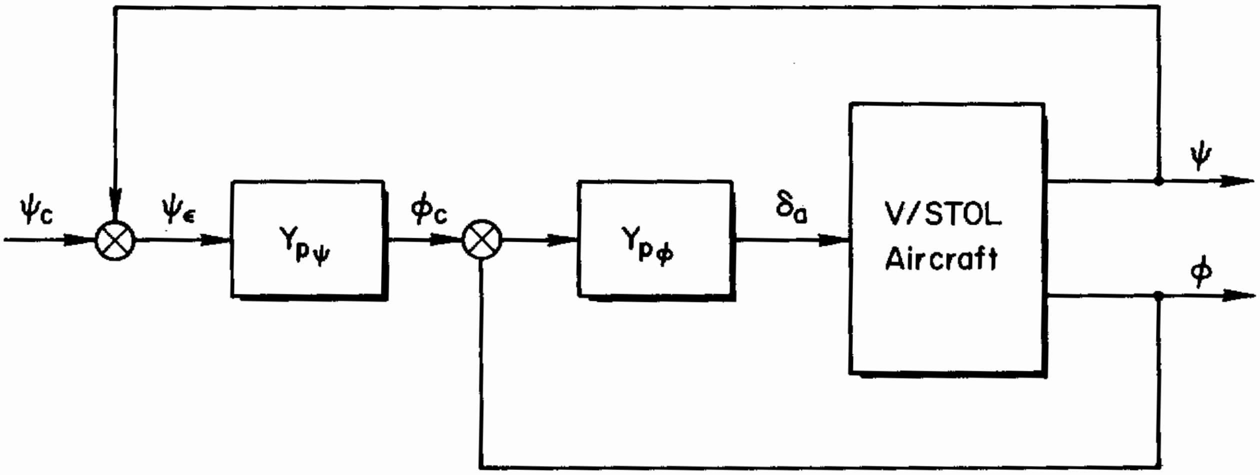

Heading control through aileron $\phi, \psi \rightarrow \delta_a$

when $N_v > 0$, i.e., $1/T_{\varphi_1}\ \zeta_\varphi\omega_\varphi$ decreases with increasing negative N_{δ_a}. Table VII, the results of detailed analyses, shows the bandpass restrictions as a function of negative N_{δ_a}. The large adverse yaw case (i.e., $N_{\delta_a} = -0.75$) produces a complex pair in the r/δ_a numerator;

TABLE VII

EFFECT OF AILERON COUPLING ON HEADING PERFORMANCE

AILERON YAW N_{δ_a} rad/sec^2/in.	PREDICTED HEADING BANDPASS ω_{c_ψ} rad/sec	PILOT RATING
0	0.40	3-1/2
−0.2	0.30	3-1/2
−0.5	0.1	6-1/2 (PIO)
−0.75	Unstable (Reversal in heading)	> 6-1/2 (Uncontrollable)

and the heading loop can no longer be closed by moving the stick in the direction of intended turn, i.e., K_{p_ψ} = positive. The root locus gain being negative (N_{δ_a}) consequently results in the aperiodic instability shown in the sketch below. We may presume that the restricted bandpass and unstable control attending aileron-only usage will force the pilot to use the rudders to improve the heading response.

$$\frac{\psi}{\psi_\epsilon} = \frac{K_{p_\psi} A_r/\delta_a [s^2 + 2\zeta_r'\omega_r' s + \omega_r'^2](s + 1/T_r')}{[s^2 + 2\zeta_d'\omega_d' s + \omega_d'^2](s + 1/T_R')(s + 1/T_s')}$$

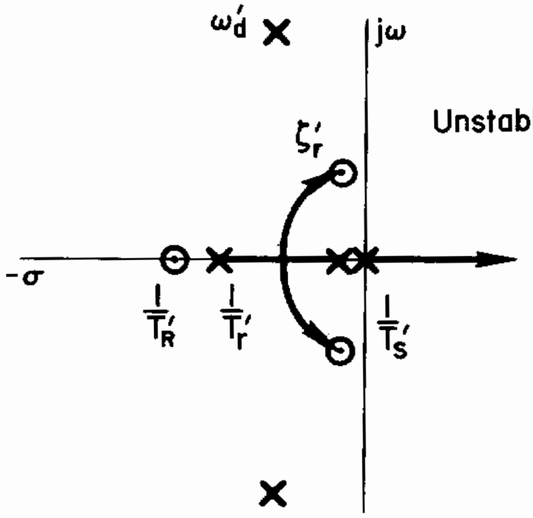

2) Aileron with Rudder Coordination. For these analyses it is most informative to consider cases involving both N_{δ_a} and L_{δ_r} since pilot comments describing the vehicle behavior indicate PIO conditions when both coupling terms become large (e.g., Fig. 49). Due to the symmetry of Fig. 49, it is not necessary to explore all combinations of N_{δ_a} and L_{δ_r}. This is true also because, and is a reflection of the fact that, N_{δ_a} and L_{δ_r} appear as a product in the coupling numerators and in the rudder required for coordination. Although both signs of L_{δ_r} are used in the analyses to follow, $L_{\delta_r} > 0$ presents a more difficult task in turns out of wind than $L_{\delta_r} < 0$. For example note that from the generic root locus plot for the numerator, $N^{\beta}_{\delta_r}$, sketched below, that the zeros are in the right half plane for $L_{\delta_r} > 0$. An attempt to coordinate the vehicle with rudders under such circumstances may lead to a destabilizing condition regardless of what N_{δ_a} is because the $\beta \rightarrow \delta_r$ closure drives toward this zero. Another reason $L_{\delta_r} < 0$ was not as difficult as $L_{\delta_r} > 0$ was due to the wind simulation previously discussed. Because the mechanization of wind was independent of the vehicle's side velocity, the rolling moment generated due to L_v (i.e., $U_o \sin \psi$) when the pilot puts in a rudder deflection cancelled the rolling moment due to $L_{\delta_r}\delta_r$ and resulted in no ground translation. Without any movement over the ground the pilot naturally assumed there was no sideslip and therefore did not need to move the ailerons. In a true wind this would not be the case since some bank angle would be required to produce the slip necessary to overcome the side force due to the wind.

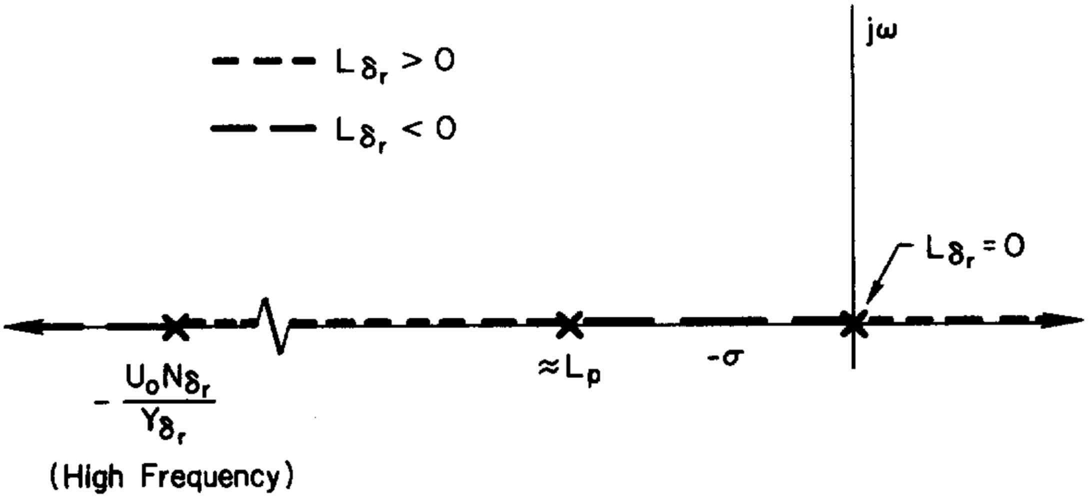

Sketch of the Zero Locus for

$$N^{\beta}_{\delta_r} = 1 + \frac{-gL_{\delta_r}N_r/Y_{\delta_r}}{s(s-L_p)(s-N_{\delta_r}U_o/Y_{\delta_r})}$$

damped roll spiral mode, ω_{RS}, from the bank angle closure.

The consequence of the large control coupling terms (i.e., N_{δ_a} and/or L_{δ_r}) can be vividly illustrated by considering the ability to coordinate the vehicle in the given situation (e.g., in the wind or during a turn maneuver). The turn maneuver coordination task is illustrated in the block diagram below as a closed-loop situation, in which sideslip, β, is maintained zero with the rudder and the desired heading, ψ, is controlled with the ailerons through a series bank angle command structure.

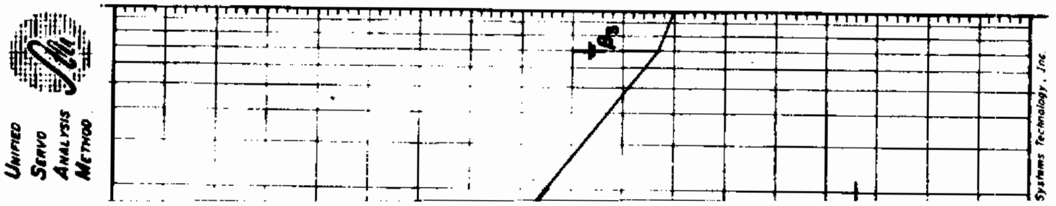

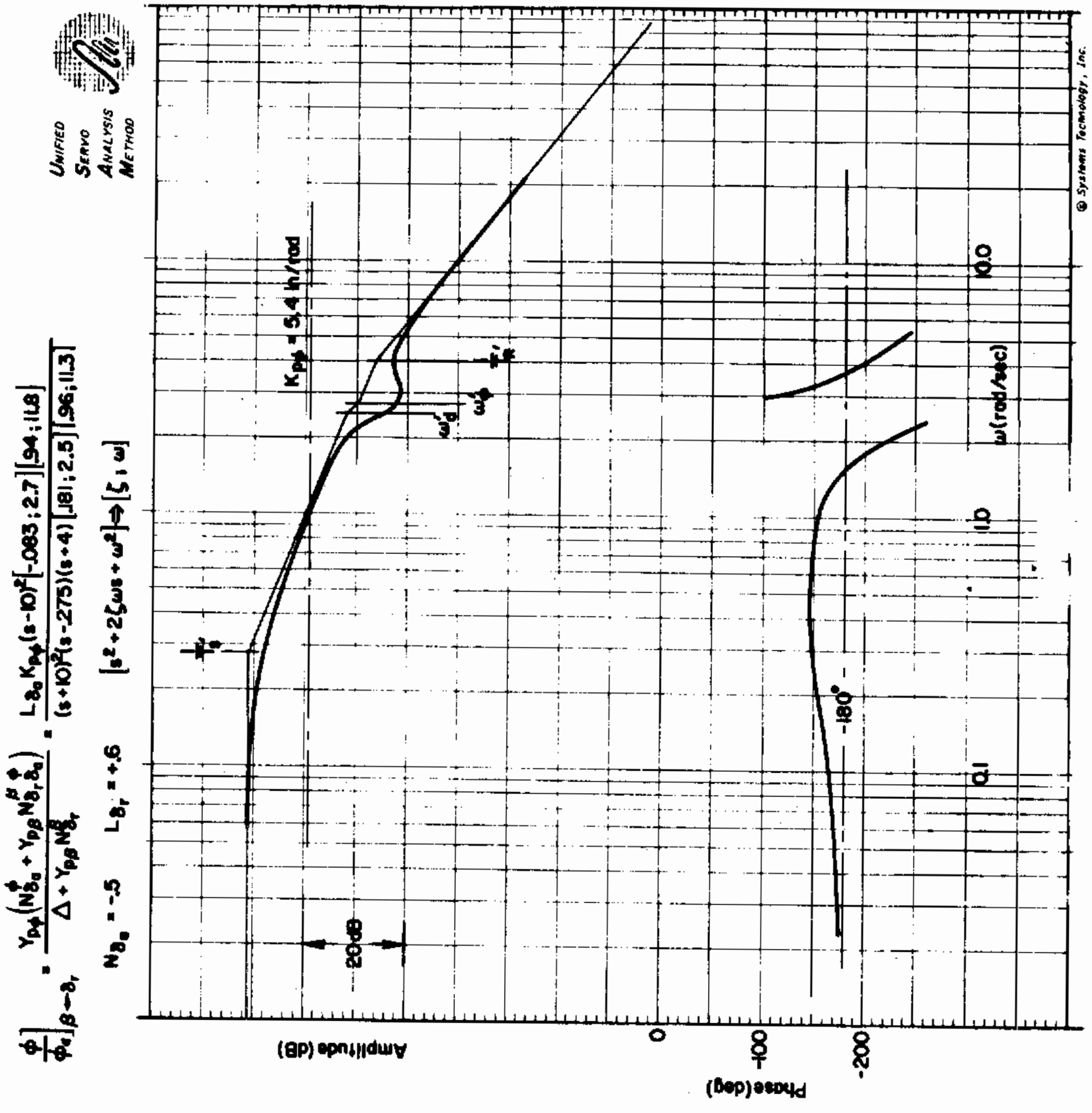

ank Angle Control with Rudder Coordination, $\varphi \to \delta_a$, $\beta \to \delta_r$

β
Φ
jω
6
4
ω_d'
$1/T_s$

$$N_{\delta_a} = -.5 \text{ rad/sec}^2\text{/inch}$$

$$L_{\delta_r} = +.6 \text{ rad/sec}^2\text{/inch}$$

Coupling Numerator

$$N^{r}_{\delta_a} + Y_{p\beta} N^{\beta\ r}_{\delta_r \delta_a}$$

$$N' = \frac{Y_{p\beta} N^{\beta\ r}_{\delta_r \delta_a}}{N^{r}_{\delta_a}} = \frac{K_{p\beta}(s-10)^2}{(s+10)^2} \quad \frac{-.02\ \left[s^2+2(-.35)(7.5)s+(7.5)^2\right]}{(-.5)(s+4)(s-.22)(s+.24)}$$

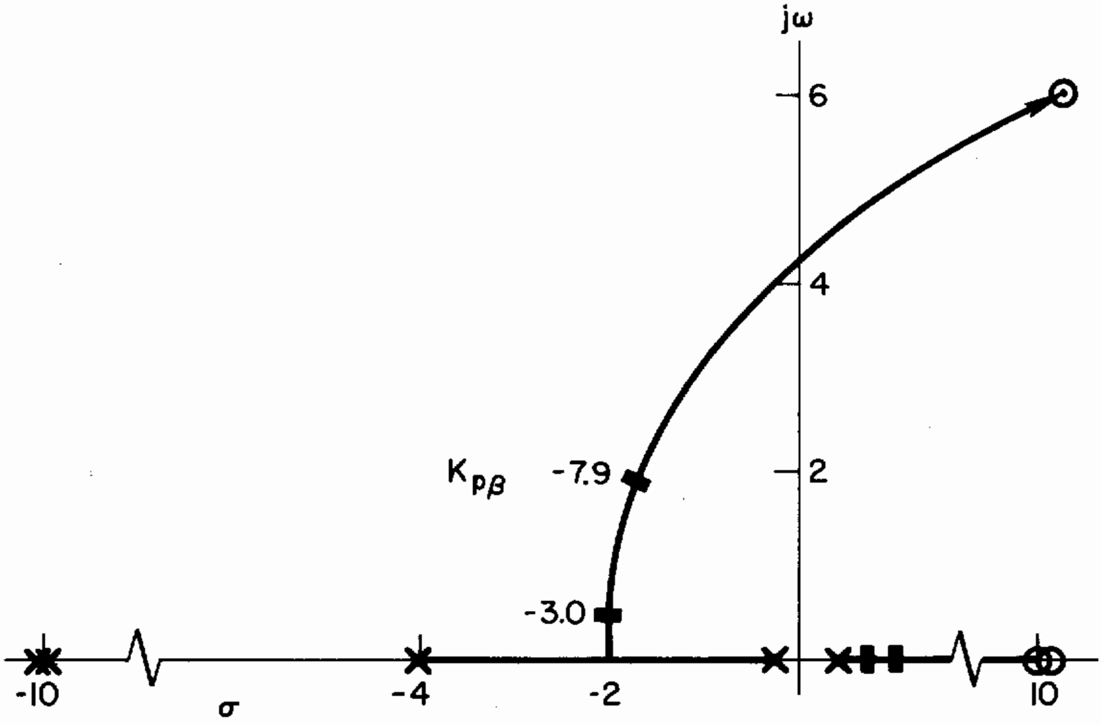

Figure 57. Effect of Sideslip Closure on Yaw Rate Numerator

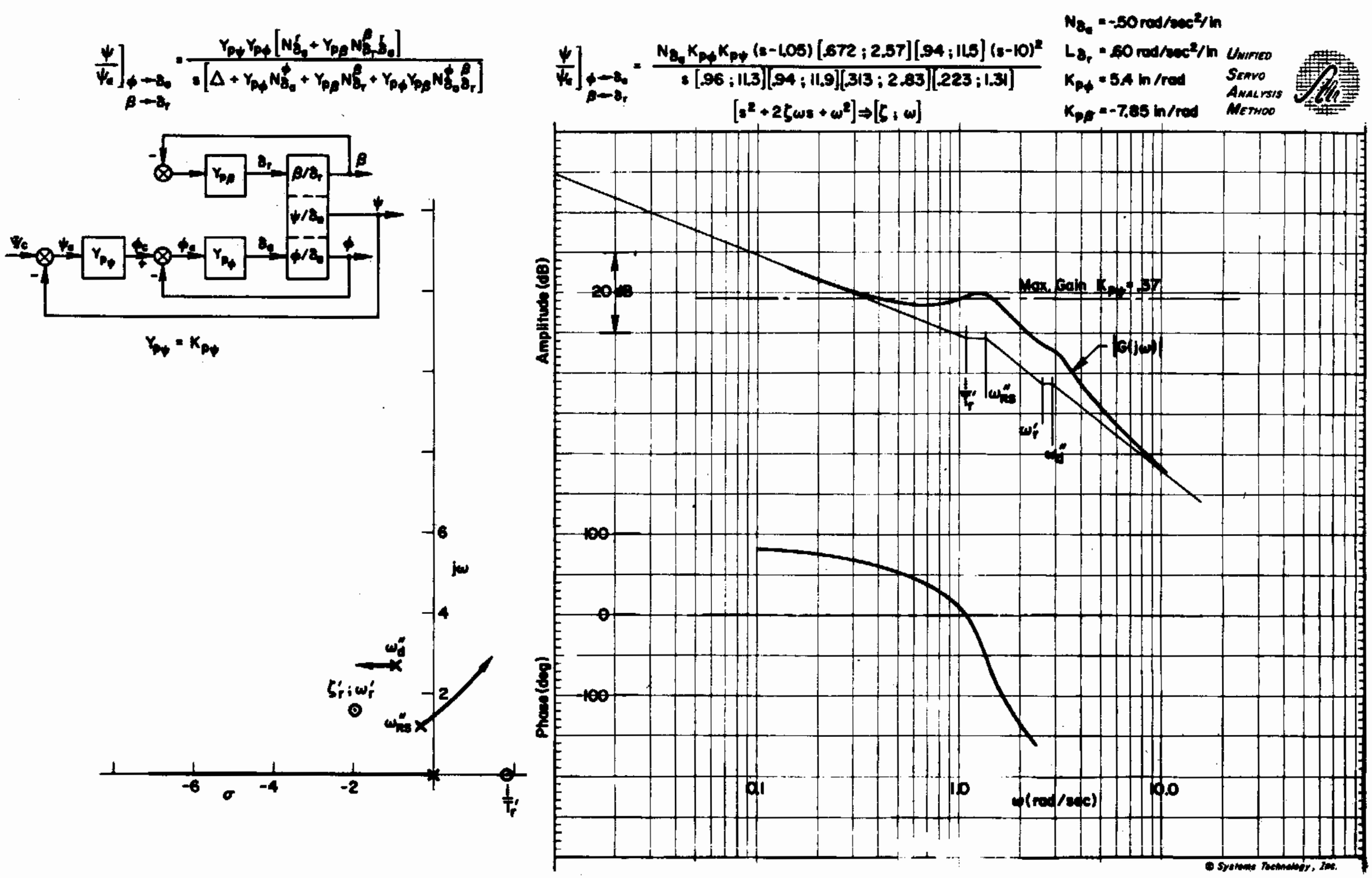

Figure 58. Coordination Control with Large Adverse Control Cross Coupling Terms, N_{δ_a} and L_{δ_r}

Furthermore, this closed-loop structure exhibits the familiar PIO syndrome. That is, introducing a small lag in the heading loop (e.g., smoothing the control inputs), the pilot may increase his gain, which correspondingly increases the heading bandpass (see sketch below). With this lagged control technique (dashed lines), the system is stable at the higher gain. However, if this lag is removed while retaining the higher gain setting, the ψ-loop is violently unstable. Thus, while the relatively modest performance at the gain levels shown would warrant an increase in gain, the system is susceptible to a PIO if the pilot tries to tighten up control of any of the loops.

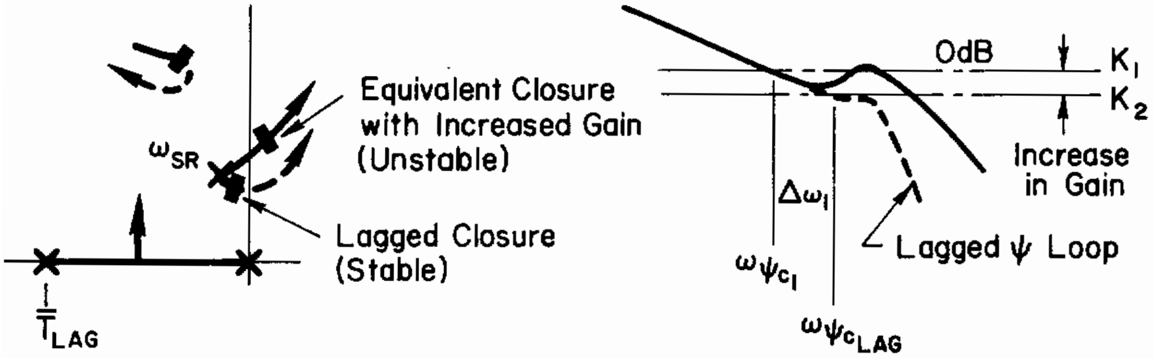
ω_{SR}
Equivalent Closure with Increased Gain (Unstable)
Lagged Closure (Stable)
$\frac{1}{T_{LAG}}$
0dB
K_1
K_2
Increase in Gain
$\Delta\omega_1$
Lagged ψ Loop
$\omega_{\psi_{c_1}}$
$\omega_{\psi_{c_{LAG}}}$

b) Positive N_{δ_a} (Favorable) and Negative L_{δ_r} (Adverse). With favorable aileron yaw, the PIO tendency is very apparent in the φ-loop if the β-loop is closed (see Fig. 59). Increasing the β-loop gain drives Dutch roll poles and zeros into the right half plane. To have a stable φ-closure, β must therefore be kept loose.

Without the L_{δ_r} coupling term, this PIO condition would probably not exist. The main effect of L_{δ_r} is to modify the gain of the coupling numerator, $N^{\varphi\ \beta}_{\delta_a \delta_r}$. With $L_{\delta_r} = 0$, the poles in the sketch (zeros of $\varphi/\delta_a]_{\beta \rightarrow \delta_r}$) do not become complex and therefore do not produce the destabilizing ω_φ/ω_d "effect" in the bank angle closure that is responsible for the PIO tendency.

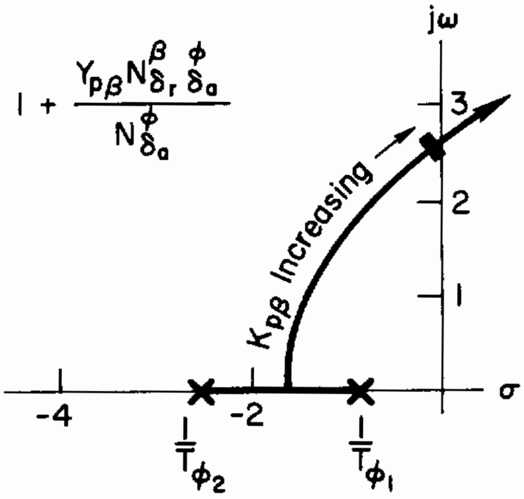
$1 + \frac{Y_{p\beta} N^{\beta\ \phi}_{\delta_r \delta_a}}{N^{\phi}_{\delta_a}}$
$j\omega$
3
2
1
σ
-4
-2
$K_{p\beta}$ Increasing
$\frac{1}{T_{\phi_2}}$
$\frac{1}{T_{\phi_1}}$

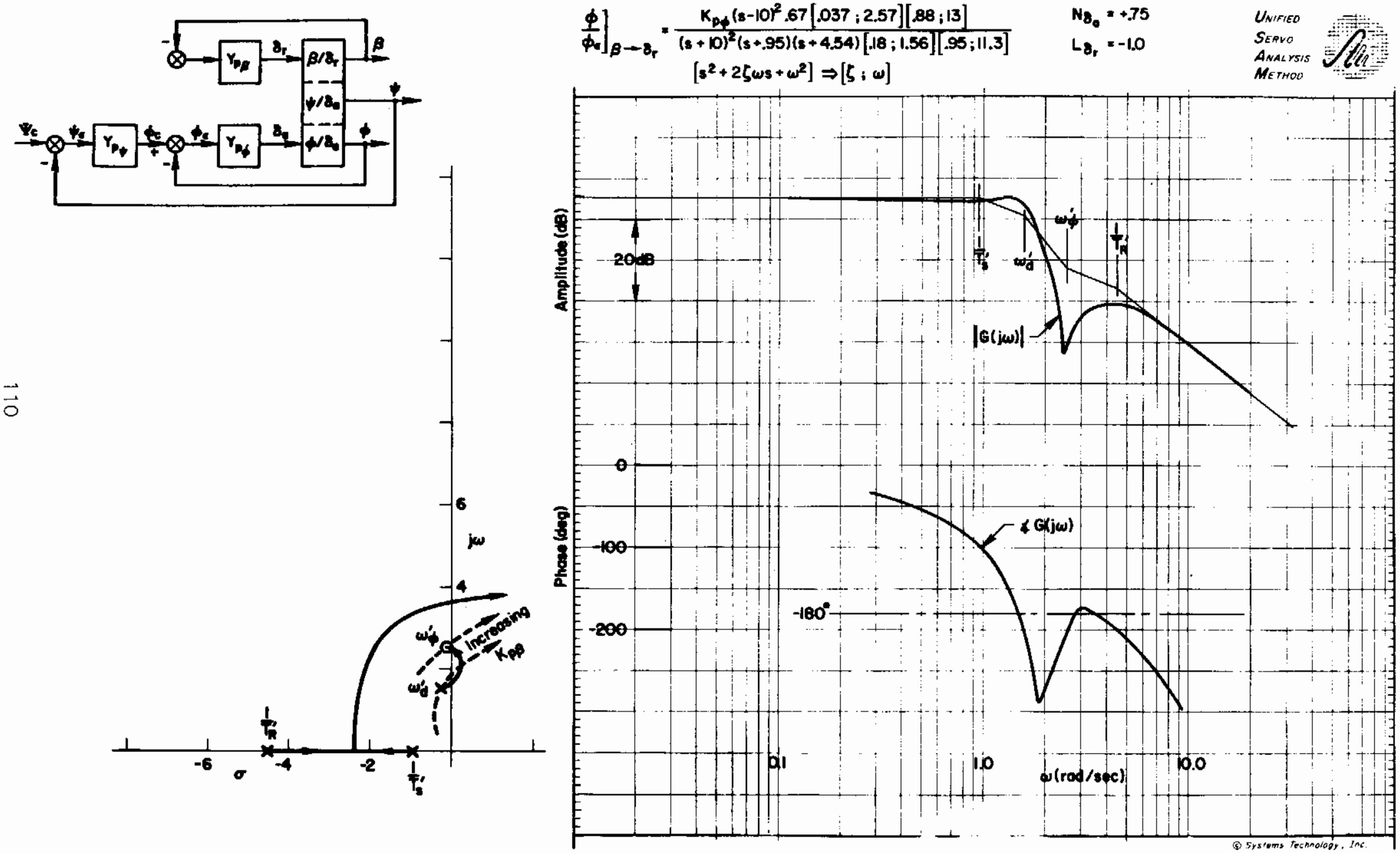

Figure 59. Bank Angle Control with Large Proverse Control Coupling Terms

c) Positive N_{δ_a} and L_{δ_r}. For the final case, where both N_{δ_a} and L_{δ_r} are positive, the problem is a sluggish turning response. In order to turn, it is necessary to establish a bank angle; unless, of course, the vehicle is at hover with no wind where a pure rotation may be called a turn.

Since the response to a rudder input will have a large roll component due to L_{δ_r} the pilot must crossfeed rudder to aileron to get a relatively "pure" yawing response. That is, to make the net rolling moment identically zero, the ratio of aileron to rudder must be $\delta_a/\delta_r = -L_{\delta_r}/L_{\delta_a}$. For the extreme values of L_{δ_r} tested, this ratio is greater than one, numerically, which imposes severe coordination problems on the pilot's open-loop use of the rudder. Furthermore, the net "pure" yawing moment, assuming perfect cross control (i.e., zero roll as above) is given by $N_{\delta_r}\delta_r(1 - L_{\delta_r}N_{\delta_a}/L_{\delta_a}N_{\delta_r})$; similarly, the net "pure" rolling moment with perfect yaw cancellation is given by $L_{\delta_a}\delta_a(1 - L_{\delta_r}N_{\delta_a}/L_{\delta_a}N_{\delta_r})$. The cross products, $L_{\delta_r}N_{\delta_a}$ and $L_{\delta_a}N_{\delta_r}$ thus figure heavily in the net "pure" control power available about each axis; and positive values (upper right and lower left quadrants in Fig. 49) can drastically reduce the control power to where response is considered "too sluggish."

In summary, both regulatory and command tasks employing aileron and rudder control show the consequence of changes in the various stability and/or control derivatives. Regulatory control tasks are extremely sensitive to such key derivatives as N_β and N_r; and pilot ratings appear to correlate reasonably well with error performance merits (i.e., σ_ψ, σ_φ, σ_δ, etc.) for simple dynamic situations. However, for complex dynamics (e.g., complex, nonminimum phase zeros) such correlations may not be as conclusive. In these cases careful inspection of the experimental conditions and pilot comments lead to the additional consideration of control structures more appropriate to maneuvering control.

Several of the primary piloting difficulties stem from the derivatives N_β and L_β as they affect the level of oscillatory mode frequency, ω_d. These difficulties which imply increased pilot workload (i.e., in terms of compensation needs) and rudder control usage are cited below:

a. With low directional stiffness (i.e., $N_\beta \rightarrow 0$) the lateral oscillatory mode defined by L_β and the pilot must use the rudder to coordinate turn maneuvers.

b. Large directional stiffness ($N_\beta >> 0$) increases the gust sensitivity of the vehicle and tends to compromise the effectiveness of the rudder control as a means for suppressing the resulting heading disturbance.

c. Where large aileron and rudder cross-coupling terms of opposite sign are present, there is a strong tendency for pilot-induced oscillations (PIO). For N_{δ_a} and L_{δ_r} of the same sign, increasing magnitudes produce increasing sluggishness of control due to the effective cancellation of available control power.

SECTION V

CONCLUDING REMARKS

The results of the studies in this report suggest that the predominant effects of VTOL stability and control characteristics on handling qualities are, in general, closely related to the closed-loop aspects of the pilot/vehicle system. This overall conclusion is clearly reflected by the following more detailed conclusions drawn from the data and analyses presented in the text.

A. PRELIMINARY LATERAL HOVER DYNAMICS REQUIREMENTS

The fundamental dynamic requirements for lateral hover control are essentially the same as those for the longitudinal mode. These requirements were derived from the correlations and study of available experiments, and confirmed by the predicted closed-loop pilot control functions and desires. These generally applicable (i.e., for conventional vehicles, too) closed-loop desires are not summarized here (see Ref. 1) but they do provide a fundamental basis for expressing the requirements in terms of the open-loop airframe dynamic factors, as summarized below.

1. Basic Dynamic Requirements

Basic dynamic requirements for satisfactory manual control in hover which cover conventional VTOL characteristics plus angular rate or position feedbacks are:

a. Lateral oscillatory mode $\omega_d \leq 0.5$ rad/sec

   1) Oscillatory mode damping; $\zeta_d \geq 0$, or
   2) Roll subsidence mode; $1/T_R \geq 1.25 \text{ sec}^{-1}$

b. Lateral oscillatory mode; $\omega_d > 0.5$ rad/sec

   1) Oscillatory mode damping; $\zeta_d > 0.3$

Note that the above form of specification does not include the detailed effects of some combinations of gust sensitive aerodynamic derivatives or control system dynamics, as partially covered below.

2. Control System Aspects

The effects of translational control coupling terms (e.g., X_δ or Y_δ) were found to be generally detrimental to manual attitude control. However, a potential improvement in hover control can be achieved with proper tailoring of the vehicle's angular and translational damping (i.e., M_q and X_u terms). This is a consequence of the migration of hover numerator terms, $1/T_{\varphi_1}$ or $1/T_{\theta_1}$, into the right half plane (i.e., nonminimum phase zero) caused by the relation between the control translation term, X_δ or Y_δ, and the speed stability terms, M_u or L_v.

The "effective" system lags due to physical limitations in the flight control system tend to degrade manual control if the ratio of the lag break frequency to the Dutch roll frequency is less than 10:1 (i.e., $1/\omega_d T_c > 10$). For other nonlinearities such as control system backlash, threshold, or actuator velocity saturation, the basic vehicle dynamics should be stable to avoid divergent pilot/vehicle limit cycles.

B. LATERAL/DIRECTIONAL CONTROL IN TRANSITION AND LOW SPEED FLIGHT

The lateral control problem in transition is analogous to the longitudinal problem in that the multiloop aspects of manual pilot control are dominant. Control of bank angle with the aileron as an inner loop is usually essential for heading control; and one of the primary uses of the rudder is to coordinate aileron turn maneuvers (i.e., $\psi, \varphi \rightarrow \delta_a$) when the directional stiffness is low or the level of aileron adverse yaw is high. A secondary task for rudder control is the regulation of heading disturbances. Here quantitative, generally applicable, requirements are not too clear-cut. The basic consideration as indicated by the analyses presented is the achievement of reasonably good gust suppression (σ_ψ/σ_{v_g} low) with moderate pilot effort ($\sigma_\delta/\sigma_{v_g}$ low). Use of the rudder by the pilot either as a means of coordinating the vehicle during turn maneuvers or to suppress yaw disturbances is strongly affected by the relation between yaw damping, N_r, and directional stiffness, N_v or N_β. The basic requirement for good heading control is that the outer heading loop crossover frequency, ω_c (without pilot lead), be greater than about 0.3 rad/sec (e.g., Refs. 20, 21). For simple, uncomplicated dynamics (e.g., minimal roll-yaw coupling terms) this requirement reduces (see Ref. 20) to $\zeta_\varphi\omega_\varphi$ or $1/T_{\varphi_1} > 0.40$. For control-coupled cases, i.e., large aileron yaw and rudder roll, it may be impossible to achieve $\omega_c \doteq 0.3$ without exciting PIO. In any event the above simple criterion on $\zeta_\varphi\omega_\varphi$, $1/T_{\varphi_1}$ is no longer applicable and more detailed study of the situation is required.

C. CONSIDERATION OF FUTURE EXPERIMENTAL PROGRAMS

Because of the evidence gained from the analyses of this report and those of Ref. 1, it now appears that the control problems underlying handling qualities ratings can be recognized by pre-experimental closed-loop analyses. Basically, the feasibility of such an approach is due to the fact that a compatible set of closure rules have now been evolved which encompass both longitudinal and lateral control problems. Thus, it is possible to search for crucial situations and cite the probable reasons for the expected piloting problem. From an experimental design viewpoint, it is obvious that such a procedure can minimize the number of experimental points and configurations necessary for a pilot evaluation.

REFERENCES

1. Craig, Samuel J., and Anthony Campbell, Analysis of VTOL Handling Qualities Requirements. Part I. Longitudinal Hover and Transition, AFFDL-TR-67-179, Part I, Oct. 1968.

2. Miller, David P., and Edward W. Vinje, Fixed-Base Flight Simulator Studies of VTOL Aircraft Handling Qualities in Hovering and Low-Speed Flight, AFFDL-TR-67-152, Jan. 1968.

3. Progress Report and Project Briefing at AFFDL, Northrop Corp., Norair Div., June 1968.

4. Breul, H. T., A Simulator Study of Low Speed VTOL Handling Qualities in Turbulence, Grumman Aircraft Engineering Corp., Research Rept. RE-238, Feb. 1966.

5. Faye, Alan E., Jr., Attitude Control Requirements for Hovering Determined Through the Use of a Piloted Flight Simulator, NASA TN D-792, Apr. 1961.

6. Salmirs, Seymour, and Robert J. Tapscott, The Effects of Various Combinations of Damping and Control Power on Helicopter Handling Qualities During Both Instrument and Visual Flight, NASA TN D-58, Oct. 1959.

7. A'Harrah, R. C., and S. F. Kwiatkowski, "A New Look at V/STOL Flying Qualities," Aero. Eng., Vol. 20, No. 7, July 1961, pp. 22-23, 86-92.

8. Perry, D. H., and H. W. Chinn, A Preliminary Flight Simulation Study of Jet-Borne VTOL Aircraft Handling Qualities, Aeronautical Research Council, C. P. No. 902, 1967.

9. Development of VTOL Handling Qualities Design Criteria, Boeing Co., Airplane Div., Briefing presented to V/STOL Handling Qualities Committee, 24 Oct. 1966.

10. Lollar, Thomas E., and Gerhard K. L. Kriechbaum, "VTOL Handling Qualities Criteria and Control Requirements," J. AHS, Vol. 13, No. 3, July 1968, pp. 20-30.

11. McDonnell, John D., Pilot Rating Techniques for the Estimation and Evaluation of Handling Qualities, AFFDL-TR-68-76, Dec. 1968.

12. McRuer, Duane, Dunstan Graham, Ezra Krendel, and William Reisener, Jr., Human Pilot Dynamics in Compensatory Systems — Theory, Models, and Experiments with Controlled Element and Forcing Function Variations, AFFDL-TR-65-15, July 1965.

13. McDonnell, J. D., and H. R. Jex, A "Critical" Tracking Task for Man-Machine Research Related to the Operator's Effective Delay Time; Part II. Experimental Effects of System Input Spectra, Control Stick Stiffness, and Controlled Element Order, NASA CR-674, Jan. 1967.

14. Graham, D., Research on the Effect of Nonlinearities on Tracking Performance, AMRL TR-67-9, July 1967.

15. McRuer, D. T., and H. R. Jex, "Effects of Task Variables on Pilot Models for Manually Controlled Vehicles," AGARD, Flight Mechanics Panel Specialists' Meeting on Stability and Control, Cambridge, England, 20-26 Sept. 1966.

16. Gallagher, J. T., and F. B. O'Donnell, "Investigation of the Application of Direct Translational Control to VTOL Aircraft," J. Aircraft, Vol. 2, No. 6, Nov.-Dec. 1965, pp. 538-545.

17. Breul, H. T., A Simulator Study of Tilt-Wing Handling Qualities, Grumman Aircraft Engineering Corp., Research Rept. RE-162, Mar. 1963.

18. Garren, John F., Jr., James R. Kelly, and John P. Reeder, Effects of Gross Changes in Static Directional Stability on V/STOL Handling Characteristics Based on a Flight Investigation, NASA TN D-2477, Oct. 1964.

19. Daw, D. F., D. G. Gould, and D. M. McGregor, A Flight Investigation of the Effects of Weathercock Stability on V/STOL Aircraft Directional Handling Qualities, National Research Council of Canada Rept. LR-400, May 1964.

20. Walton, R. P., and I. L. Ashkenas, Analytical Review of Military Helicopter Flying Qualities, Systems Technology, Inc., TR-143-1, Nov. 1965.

21. Stapleford, Robert L., Donald E. Johnston, Gary L. Teper, and David H. Weir, Development of Satisfactory Lateral-Directional Handling Qualities in the Landing Approach, NASA CR-239, July 1965.

22. McGregor, D. M., A Flight Investigation of the Influence of Various Levels of Dihedral Effect on V/STOL Aircraft Directional Handling Qualities, National Research Council of Canada Rept. LR-412, Nov. 1964.

23. Seckel, E., G. E. Miller, and W. B. Nixon, Lateral-Directional Flying Qualities for Power Approach, Princeton University Rept. No. 727, Sept. 1966.

24. Franklin, James A., Lateral-Directional Flying Qualities for Power Approach — Influence of Dutch Roll Frequency, Princeton University Rept. No. 797, Sept. 1967.

25. McGregor, D. M., An Investigation of the Effects of Lateral-Directional Control Cross-Coupling on Flying Qualities Using a V/STOL Airborne Simulator, National Research Council of Canada Rept. LR-390, Dec. 1963.

26. Greif, Richard K., Emmett B. Fry, Terrence D. Gossett, and Ronald M. Gerdes, "Simulator Investigations of Various Control Systems for VTOL Aircraft," Conference on V/STOL and STOL Aircraft, NASA SP-116, Apr. 4-5, 1966, pp. 249-267.

27. Salmirs, Seymour, and Robert J. Tapscott, Instrument Trials with a Helicopter Stabilized in Attitude about Each Axis Individually, NACA TN 3947, Jan. 1957.

28. Ashkenas, I. L., A Study of Conventional Airplane Handling Qualities Requirements. Part II, Lateral-Directional Oscillatory Handling Qualities, AFFDL-TR-65-138, Part II, Oct. 1965.

29. Vinje, Edward W., and David P. Miller, Analytical and Flight Simulator Studies to Develop Design Criteria for VTOL Aircraft Control Systems, United Aircraft Res. Labs. Rept. H910482-23, Feb. 1969.

30. McRuer, D. T., and H. R. Jex, "A Review of Quasi-Linear Pilot Models," IEEE Trans., Vol. HFE-8, No. 3, Sept. 1967, pp. 231-249.

31. Ashkenas, Irving L., Henry R. Jex, and Duane T. McRuer, Pilot Induced Oscillations: Their Cause and Analysis, Systems Technology, Inc., Tech. Rept. 239-2, 20 June 1964.

32. Stapleford, R. L., J. Wolkovitch, R. E. Magdaleno, et al., An Analytical Study of V/STOL Handling Qualities in Hover and Transition, AFFDL-TR-65-73, Oct. 1965.

33. Taylor, I. E., XC-142A Flight Control System Simulator Summary Report, LTV Vought Aeronautics Div., Rept. No. 2-53310/5R-984, May 1965.

34. Ashkenas, I. L., and D. T. McRuer, The Determination of Lateral Handling Quality Requirements from Airframe-Human Pilot System Studies, WADC-TR-59-135, June 1959.

35. Magdaleno, R. E., H. R. Jex, and W. A. Johnson, Tracking Quasi-Predictable Displays, paper pres. at 5th Annual NASA-University Conf. on Manual Control, Cambridge, Mass., Mar. 1969.

36. Graham, Dunstan, and Duane McRuer, Analysis of Nonlinear Control Systems, John Wiley, 1961.

37. Wolkovitch, J. and R. P. Walton, VTOL and Helicopter Approximate Transfer Functions and Closed-Loop Handling Qualities, Systems Technology, Inc., Tech. Rept. 128-1, Jan. 1965.

38. Stapleford, Robert L., Samuel J. Craig, and Jean A. Tennant, Measurement of Pilot Describing Functions in Single-Controller Multiloop Tasks, NASA CR-1238, Jan. 1969.

APPENDIX A

PILOT/VEHICLE ANALYSES FOR LATERAL HOVER

INTRODUCTION

The basic lateral mode dynamic requirements presented in Section II have been substantiated from pilot/vehicle analyses. This appendix summarizes these closed-loop analyses and the VTOL dynamic characteristics reviewed in developing the requirements. The major portion of these dynamics were assembled from the documented experiments in Refs. 2-10.

Approximately 30 detailed pilot/vehicle closed-loop analyses and more than 50 closed-loop survey sketches were made during the studies. These closures considered the multiloop-attitude/lateral-position hover task for a broad range of aerodynamic properties and transfer functions which include both satisfactory and unacceptable handling qualities levels. A complete listing of these dynamics, transfer function factors, and pilot ratings are included for reference. However, it is neither worthwhile nor practical to include each detailed closure analysis. Therefore, we include here selected case studies which exhibit the analytical details of the closed-loop treatment and substantiate key handling quality aspects and dynamic requirements of Section II.

The appendix starts with a brief review of the available open-loop VTOL dynamic characteristics culled from the references. These characteristics are separated into three controlled element forms encompassing conventional helicopter dynamics plus various levels of attitude and translational augmentation. The pilot/vehicle closure aspects are discussed next with the detailed system surveys (i.e., root locus and Bode frequency response diagrams) shown for the example cases. The pilot's describing function used in these studies is described as a prelude to the latter.

OPEN-LOOP AIRFRAME DYNAMICS

The lateral hover mode dynamics selected for the closed-loop analyses are shown in Tables A-I, A-II, A-III, A-IV, and A-V. The selection of these configurations is based on the identification of the boundaries for satisfactory and unacceptable dynamics characteristics shown in Table I of Section II. The characteristics in the tables encompass a range of attitude dynamic characteristics, $N_{\delta}^{\varphi}/\Delta$, which represent three types of augmentation systems:

1. Conventional and simple attitude rate feedback — L_p augmentation — Tables A-I, A-II, and A-III ($1/T_E \leq 1/T_R$).
2. Attitude position feedback — L_φ augmentation — Table A-IV ($1/T_E > 1/T_R$).

3. Translational or lateral position rate feedback — Y_v augmentation — Table A-V ($Y_v >> L_p$ and $1/T_R \doteq Y_v$).

The remaining data used in this study are listed in Tables A-VI, A-VII, and A-VIII. These dynamic characteristics were used to isolate the important aerodynamic parameters and to identify the boundaries for satisfactory ($3 < PR < 4$) and unacceptable ($6 < PR < 7$) handling qualities levels.

TABLE A-I

OPEN-LOOP PARAMETERS FOR SELECTED CASES

(Ref. 4)

CONFIG.	AERODYNAMIC CHARACTERISTICS			DYNAMIC* CHARACTERISTICS				PR
	Y_v	L_v	L_p	$1/T_{\varphi_1}$	$1/T_R$	ζ_d	ω_d	
1	−0.037	−0.01	−2.5	0.037	2.55	−0.018	0.36	2.7
2	−0.037	−0.01	−1.25	0.037	1.42	−0.134	0.5	3.7
3	−0.037	−0.03	−3.75	0.037	3.82	−0.029	0.5	5.5
4	−0.037	−0.04	−2.5	0.037	2.68	−0.104	0.69	6.5
5	−0.037	−0.04	−1.25	0.037	1.7	−0.239	0.87	7.3

SATISFACTORY CASES

UNACCEPTABLE CASES ↓

*Denotes form

$$\frac{N_\delta^\varphi}{\Delta} = \frac{(s + 1/T_{\varphi_1})}{(s + 1/T_R)[s^2 + 2(\zeta_d)(\omega_d)s + \omega_d^2]}$$

TABLE A-II

OPEN-LOOP PROPERTIES FOR VTOL CONFIGURATION WITH ATTITUDE RATE AUGMENTATION ($1/T_E \leq 1/T_R$)

(Ref. 7)

CONFIG. NO.	AERODYNAMIC			DYNAMIC CHARACTERISTICS*				PILOT RATING	
	Y_v	L_v	L_p	$1/T_{\varphi_1}$	$1/T_R$	ζ_d	ω_d		
1	−0.93	−0.16	−4.93	0.93	5.2	0.35	1.0	3.0	SATISFACTORY CASES
2	−0.87	−0.16	−3.06	0.87	3.6	0.14	1.2	3.8 → 4.0	
3	−0.63	−0.16	−1.66	0.63	2.6	−0.12	1.4	5.8	
4	−0.075	−0.16	−1.875	0.075	2.6	−0.25	1.4	7.0	UNACCEPTABLE CASES
5	−0.24	−0.08	−0.86	0.24	1.8	−0.29	1.2	7.0	

*Denotes form $\dfrac{N_\delta^\varphi}{\Delta} = \dfrac{(s + 1/T_{\varphi_1})}{(s + 1/T_R)[s^2 + 2(\zeta_d)(\omega_d)s + (\omega_d)^2]}$

TABLE A-III

CATEGORY I ($1/T_E \leq 1/T_R$) ATTITUDE RATE AUGMENTATION SYSTEM (Ref. 2)

$gM_u = 0.667$, $X_u = -0.1$, $M_q = -3.0$, $M_{\delta_p} = 0.431$, $\sigma_{u_g} = 1.28$, $\sigma_{v_g} = 5.14$, $N_v = 0.002$, $N_r = -1.0$, $N_{\delta_r} = 0.2$

PILOT	gL_v	Y_v	L_p	L_φ	REAL ROOTS RR (1)	RR (2)	RR (3)	COMPLEX ROOTS	OPTIMUM CONTROL SENSITIVITY	PR
A	−0.333	−0.05	−1	0	−1.230			+0.0898 ± j 0.513	0.254	4.0
	↓	↓	↓	−1	−0.494			−0.2780 ± j 0.835	0.268	3.0
A	−0.33	−0.05	−3	0	−3.037			−0.0067 ± j 0.331	0.366	2.5
	↓	↓	↓	−1	−2.673			−0.1883 ± j 0.328	0.383	2.5
				−2	−2.140	−0.524	−0.386		0.392	2.25
A	−1.0	−0.05	−2	0	−2.210			−0.0798 ± j 0.668	0.433	4.5
	↓	↓	↓	−1	−1.764			−0.1431 ± j 0.758	0.448	4.0
				−2	−1.048			−0.5011 ± j 0.894	0.468	3.0
A	−1.0	−0.05	−5	0	−5.040			−0.0051 ± j 0.445	0.533	2.75
	↓	↓	↓	−2	−4.614			−0.2180 ± j 0.437	0.555	2.5
				−4	−4.081			−0.4847 ± j 0.243	0.570	2.0
B	−0.333	−0.2	−1	0	−1.252			−0.0263 ± j 0.515	0.275	5.0
	↓	↓	↓	−1	−0.634			−0.2832 ± j 0.872	0.264	3.5
B	−0.333	−0.2	−4	0	−4.022			−0.0892 ± j 0.274	0.392	3.5
	↓	↓	↓	−1	−3.759			−0.2206 ± j 0.305	0.423	3.0
				−3	−3.057	−0.425	−0.719		0.424	3.0
B	−1.0	−0.2	−2	0	−2.222			−0.0112 ± j 0.671	0.352	6.0
	↓	↓	↓	−1	−1.792			−0.2038 ± j 0.792	0.398	5.0
				−2	−1.171			−0.5143 ± j 0.965	0.419	4.0
B	−1.0	−0.2	−5	0	−5.041			−0.0795 ± j 0.438	0.552	3.5
	↓	↓	↓	−1	−4.838			−0.1811 ± j 0.464	0.613	3.0
				−3	−4.368			−0.4159 ± j 0.440	0.590	3.0

Note: Category I ($1/T_E \leq 1/T_R$) is assumed on the basis that $1/T_R = \sqrt[3]{gL_v}$ and $1/T_E = L_\varphi/L_p$.

TABLE A-IV

CATEGORY II ($1/T_E > 1/T_R$) ATTITUDE AUGMENTATION SYSTEMS
(Ref. 2)

$gM_u = 0.667$, $X_u = -0.1$, $M_q = -3.0$, $M_{\delta_p} = 0.431$, $\sigma_{u_g} = 1.28$, $\sigma_{v_g} = 5.14$, $N_v = 0.002$, $N_r = -1.0$, $N_{\delta_r} = 0.2$

PILOT	gL_v	Y_v	L_p	L_φ	REAL ROOTS			COMPLEX ROOTS	OPTIMUM CONTROL SENSITIVITY	PR
					RR (1)	RR (2)	RR (3)			
B	−0.33	−0.05	−1	−2	−0.233			−0.4086 ± j 1.301	0.264	3.5
	↓	↓	↓	−4	−0.136			−0.4571 ± j 1.928	0.302	4.0
	−0.33	−0.05	−3	−4	−0.143			−1.4537 ± j 1.274	0.403	2.0
	−0.333	−0.20	−4	−5	−0.284			−1.958 ± j 0.924	0.413	3.0
	↓	↓	−1	−2	−0.389			−0.4055 ± j 1.312	0.283	4.0
	−0.33	−0.20	−1	−4	−0.288			−0.4561 ± j 1.931	0.281	4.5
	−1	−0.05	−2	−4	−0.341			−0.8544 ± j 1.669	0.465	3.25
	−1	−0.05	−5	−6	−1.540	−0.260	−3.250		0.592	2.0
	−1.0	−0.2	−2	−4	−0.508			−0.8458 ± j 1.681	0.377	4.5
	−1.0	−0.2	−5	−6	−0.454	−3.260	−1.486		0.613	3.0

Note: Category II ($1/T_E > 1/T_R$) is assumed on the basis that $1/T_R \doteq \sqrt[3]{gL_v}$ and $1/T_E = L_\varphi/L_p$.

TABLE A-V

OPEN-LOOP PROPERTIES FOR VTOL CONFIGURATION WITH TRANSLATIONAL AUGMENTATION ($Y_v > L_p$)

(Ref. 7)

CONFIG. NO.	AERODYNAMICS			DYNAMIC CHARACTERISTICS*				PILOT RATING
	Y_v	L_v	L_p	$1/T_{\varphi_1}$	$1/T_R$	ζ_d	ω_d	
1	−4.93	−0.16	−0.93	4.93	5.2	0.35	1.0	3.0
2	−3.06	−0.16	−0.87	3.06	3.6	0.14	1.2	3.8 → 4.0
3	−1.66	−0.16	−0.63	1.66	2.6	−0.12	1.4	5.8
4	−1.875	−0.16	−0.075	1.875	2.6	−0.25	1.4	7.0
5	−0.86	−0.08	−0.24	0.86	1.8	−0.29	1.2	7.0

*Denotes form $\frac{N_\delta^\varphi}{\Delta} = \frac{(s + 1/T_{\varphi_1})}{(s + 1/T_R)[s^2 + 2(\zeta_d)(\omega_d)s + (\omega_d)^2]}$

TABLE A-VI

CONVENTIONAL LATERAL DYNAMIC CONFIGURATIONS

Source: A'Harrah and Kwiatkowski, Ref. 7

CONFIG. OR TEST COND. NO.	AERODYNAMIC DIMENSIONAL DERIVATIVES			CONTROL FEATURES		VEHICLE DYNAMICS FUNCTIONS LITERAL FORMS				BEST PILOT RATING	REMARKS
				SENSITIVITY	POWER	CHARACTERISTIC EQUATION; $\Delta = (s + 1/T_R)(s^2 + 2\zeta_d\omega_d s + \omega_d^2)$			ATTITUDE $N_{\varphi\delta_a} = L_{\delta_a}(s + 1/T_{\varphi_1})$		
	L_p* or Y_v	L_v	Y_v* or L_p	L_δ rad/sec/in.	$L(\delta)$ rad/sec^2	$1/T_R$	ζ_d	ω_d	$1/T_{\varphi_1} = Y_v$		
1	−2.5	−0.02	−0.10	0.70	Not applicable	2.6	0	0.5	2.5	4.5	$\sigma_{u_g} \doteq 5$ fps
2	↓	↓	−0.28	0.70	↓	↓	0.173	↓	↓	4.3	
3	↓	↓	−0.46	0.35 < 0.70	↓	↓	0.350	↓	↓	3.5	
4	↓	↓	−0.82	0.35	↓	↓	0.700	↓	↓	3.0	
5	−5.1	−0.04	−0.06	0.70	↓	5.2	0	↓	5.1	4.5	
6	↓	↓	−0.225	0.35 < 0.70	↓	↓	0.173	↓	↓	3.8 < 4.3	
7	↓	↓	−0.400	0.35 < 0.70	↓	↓	0.350	↓	↓	3.0 < 4.0	
8	↓	↓	−0.750	0.35	↓	↓	0.700	↓	↓	3	
9	−1.65	↓	−0.172	0.70	↓	2.02	−0.11	0.8	1.65	4.8 < 5.2	
10	−1.60	↓	−0.40	0.70	↓	↓	0	↓	1.60	4.5	
11	−1.50	↓	−0.65	0.70	↓	↓	0.11	↓	1.50	4.3	
12	−1.40	↓	−0.95	0.70	↓	↓	0.21	↓	1.40	3.0 < 4.0	
13	−3.90	−0.08	−0.16	0.70	↓	4.04	0	↓	3.90	4.5	
14	↓	↓	−0.35	0.70	↓	↓	0.11	↓	↓	4.3	
15	↓	↓	−0.53	0.70	↓	↓	0.21	↓	↓	3.0 < 4.0	
16	↓	↓	−0.87	0.35	↓	↓	0.44	↓	↓	3.0	
17	−2.2	↓	−0.05	0.096	↓	2.6	−0.17	1.0	2.20	5.5	
18	−2.15	↓	−0.26	0.70	↓	↓	−0.087	↓	2.15	5.0	
19	−2.10	↓	−0.47	0.70	↓	↓	0	↓	2.10	4.5	
20	−2.05	↓	−0.70	0.70	↓	↓	0.087	↓	2.05	3.8 < 4.3	
21	−2.0	↓	−0.95	0.70	↓	↓	0.173	↓	2.0	3.0 < 4.0	

*Note: An interchange of the Y_v for the L_p derivative in the characteristic equation, $s(s + Y_v)(s + L_p) + gL_v = 0$, changes the controlled element form to the effective translational augmentation.

TABLE A-VI (Concluded)

CONFIG. OR TEST COND. NO.	AERODYNAMIC DIMENSIONAL DERIVATIVES			CONTROL FEATURES		VEHICLE DYNAMICS FUNCTIONS LITERAL FORMS				BEST PILOT RATING	REMARKS
				SENSITIVITY	POWER	CHARACTERISTIC EQUATION; $\Delta = (s + 1/T_R)(s^2 + 2\zeta_d\omega_d s + \omega_d^2)$			ATTITUDE $N_{\varphi\delta_a} = L_{\delta_a}(s + 1/T_{\varphi_1})$		
	Y_v^* or L_p	L_v	L_p^* or Y_v	L_δ rad/sec/in.	$L(\delta)$ rad/sec^2	$1/T_R$	ζ_d	ω_d	$1/T_{\varphi_1} = Y_v$		
22	−0.86	−0.08	−0.24	N/A	N/A	1.8	−0.29	1.2	0.86	7.0	
23	−3.18	−0.16	−0.06	↓	↓	3.6	−0.144	1.2	3.18	5.5	
24	−3.16	↓	−0.26	↓	↓	↓	−0.072	↓	3.16	5.0	
25	−3.14	↓	−0.45	↓	↓	↓	0	↓	3.14	4.5	
26	−3.09	↓	−0.67	↓	↓	↓	0.072	↓	3.09	4.3	
27	−3.06	↓	−0.87	↓	↓	↓	0.144	↓	3.06	3 < 4	
28	−2.95	↓	−1.33	↓	↓	↓	0.29	↓	2.95	3	
29	−1.875	↓	−0.075	↓	↓	2.6	−0.25	1.4	1.875	7.0	
30	−1.66	↓	−0.63	↓	↓	↓	−0.12	↓	1.66	5.5	
31	−1.48	↓	−0.985	70	↓	↓	−0.06	↓	1.48	5.0	
32	−4.97	↓	−0.021	70	↓	5.2	−0.087	1.0	4.97	5.0	
33	−4.96	↓	−0.202	N/A	↓	↓	0	↓	4.96	4.5	
34	−4.95	↓	−0.382	↓	↓	↓	0.087	↓	4.95	4.3	
35	−4.94	↓	−0.563	↓	↓	↓	0.173	↓	4.94	3 < 4	
36	−4.93	↓	−0.926	↓	↓	↓	0.35	↓	4.93	3	

TABLE A-VII

CONVENTIONAL LATERAL DYNAMIC CONFIGURATIONS

Source: Breul, Ref. 4

CONFIG. NO. (TEST COND. NO.)	AERODYNAMIC DIMENSIONAL DERIVATIVES			CONTROL FUNCTIONS		VEHICLE DYNAMIC LITERAL FACTORED FORMS				BEST PILOT RATING	REMARKS
				SENSITIVITY	POWER	CHARACTERISTIC EQUATION; $\Delta = (s + 1/T_R)(s^2 + 2\zeta_d\omega_d s + \omega_d^2)$			ATTITUDE $N_{\varphi\delta_a} = (s + 1/T_{\varphi_1})$		
	Y_v	L_v	L_p	L_δ rad/sec^2/in.	$L(\delta)$ rad/sec^2	$1/T_R$	ζ_d $(1/T_{d_1})$	ω_d $(1/T_{d_2})$	$1/T_{\varphi_1}$		
1	−0.0370	0	0	Not applicable	0.850	0	(0)	(0)	0.037	4.3	Constant gust level $\sigma_{u_g} = 6$ fps
2	↓	↓	−1.25	↓	0.500	1.25	(−0.0370)	↓	↓	1.8	
3			−2.50		0.850	2.50	↓			1.5	
4			−3.75		↓	3.75				2.0	
5			−5.00			5.00				2.2	
6		−0.01	0		0.500	0.697	−0.486	0.679		5.2	
7		↓	−1.25		0.500	1.415	−0.134	0.477		3.3	
8			−2.50		0.675	2.55	−0.018	0.355		2.6	
9			−3.75		↓	3.772	0.024	0.292		2.8	
10			−5.00			5.012	0.047	0.253		2.4	
11		−0.02	0		0.850	0.876	−0.489	0.857		7.7	
12		↓	−1.25		0.500	1.531	−0.188	0.648		5.2	
13			−2.50		0.675	2.596	−0.06	0.497		4.0	
14			−3.75		0.850	3.795	−0.009	0.411		3.5	
15			−5.00		↓	5.025	0.015	0.357		2.3	
16		−0.03	0			1.001	−0.49	0.982		6.5	
17		↓	−1.25			1.624	−0.218	0.771		6.4	
18			−2.50			2.64	−0.085	0.604		4.5	
19			−3.75		0.675	3.817	−0.029	0.503		5.2	
20			−5.00		0.850	5.038	−0.001	0.437		4.1	
21		−0.04	0		0.850	1.1	−0.491	1.081		8.7	
22		↓	−1.25		0.675	1.703	−0.239	0.869		6.8	
23			−2.50		0.675	2.681	−0.104	0.693		6.5	
24			−3.75		0.850	3.838	−0.044	0.579		6.5*	
25			−5.00		0.675	5.05	−0.013	0.504		6.7*	
26		−0.06	0		0.850	1.257	−0.492	1.239		8.0	
27		−0.06	−5.00		0.850	5.075	−0.031	0.616		5.7*	

*Control saturation due to gust level (i.e., $M_u\sigma_u \geq M_\delta\sigma_\delta$)

TABLE A-VIII

LATERAL DYNAMIC CONFIGURATIONS

Source: Miller, Ref. 2

CONFIG. NO. (TEST COND. NO.)	AERODYNAMIC DIMENSIONAL DERIVATIVES			CONTROL FUNCTIONS		VEHICLE DYNAMIC LITERAL FACTORED FORMS				BEST PILOT RATING	BEST PILOT RATING
				SENSITIVITY	POWER	CHARACTERISTIC EQUATION; $\Delta = (s + 1/T_R)(s^2 + 2\zeta_d\omega_d s + \omega_d^2)$			ATTITUDE $N_{\varphi_{\delta_a}} = (s + 1/T_{\varphi_1})$	$\sigma = 0$	$\sigma = 5$
	Y_v	L_v	L_p	L_δ rad/sec^2/in.	$L(\delta)$ rad/sec^2	$1/T_R$	ζ_d $(1/T_{d_1})$	ω_d $(1/T_{d_2})$	$1/T_{\varphi_1}$		
1	−0.25	−0.01	−1.0	0.277	Not applicable	1.255	−0.005	0.506	0.25	4.5	5.5
2			−2.0	0.323		2.08	0.21	0.393	0.25	2.7	4.2
3			−3.0	0.370		3.04	0.33	0.33	0.25	2.0	3.2
4			−4.0	0.417		4.02	0.404	0.28	0.25	2.0	3.0
5		−0.031	−1.0	0.317		1.52	−0.165	0.811	0.25	4.0	5.0
6			−2.0	0.363		2.23	0.017	0.67	0.25	2.0	4.0
7			−3.0	0.410		3.11	0.121	0.57	0.25	2.0	4.0
8			−4.0	0.456		4.06	0.186	0.496	0.25	2.0	3.5
9	−0.05	−0.01	−1.0	0.247		1.22	−0.169	0.512	0.05	4.2	4.5
10			−2.0	0.293		2.08	−0.033	0.393	0.05	2.7	3.0
11			−3.0	0.340		3.04	0.022	0.325	0.05	2.0	2.7
12			−4.0	0.386		4.02	0.052	0.283	0.05	2.0	2.4
13		−0.031	−1.0	0.282		1.475	−0.258	0.823	0.05	5.0	5.5
14			−2.0	0.328		2.209	−0.118	0.672	0.05	3.0	4.5
15			−3.0	0.375		3.11	−0.048	0.567	0.05	2.5	3.5
16			−4.0	0.421		4.061	−0.011	0.495	0.05	2.5	3.0

Before considering the closed-loop aspects, a few additional comments on the open-loop dynamics and the source of the data in the tables are worthwhile.

Conventional and Simple Rate Augmentation Systems

The conventional low Y_v dynamic cases of Table A-I are normally associated with VTOL or helicopter aircraft and were considered an example of conventional helicopter characteristics. The satisfactory cases exhibit a lower Dutch roll frequency and a smaller value of negative damping ratio compared to the unacceptable case. This is because L_v is smaller and the damping is greater, i.e., $\omega_d \doteq \sqrt{gL_v/L_p}$, $\zeta_d \doteq Y_v/2\omega_d$.

The reason for selecting the configurations of Table A-II from Ref. 7 was the level of the static lateral stability term, L_v. Here L_v is 0.16 rad/sec^2/fps for all configurations. This L_v is the highest level tested of all the experiments reviewed. By using this extreme L_v value, we are able to explore conditions which:

1. Have the highest level of L_v rated as satisfactory from any source.

2. Provide a basis for comparing the effectiveness of attitude and translational damping augmentation schemes for large lateral speed stability levels.

Configurations in Table A-II are classified as having conventional helicopter dynamic characteristics plus L_p augmentation simply because the attitude damping term, L_p, is much greater than the corresponding translation term, Y_v. However, this translational term, Y_v, which is approximately 1 for both satisfactory configurations, is somewhat larger than would be expected for a helicopter or VTOL. As a result, the numerator term $1/T_{\varphi_1}$ and ω_d are almost equal. This relation causes φ/δ response not only to be stable, but also to exhibit a moderate degree of attitude stiffness. These features are indicated respectively by the gain and phase characteristics shown in the φ/δ Bode diagram of Fig. A-1. It will be shown later that the above dynamic features tend to reduce the required pilot compensation, but adversely affect the closed-loop attitude, φ, response to gust.

Attitude Stabilization Systems

Block diagrams representing the vehicle with attitude and rate feedback are shown in Fig. A-2. Based on the relation of $1/T_E$ to $1/T_R$, the augmented vehicle exhibits either the increased stiffness associated with an "attitude" system or basically a rate output for a step stick command (see Fig. A-3). When related to the frequency domain, or Bode diagram, these definitions are clearly shown. Where the mid-frequency open-loop Bode feature is a K/s region, the system is defined as a rate system, although it may contain

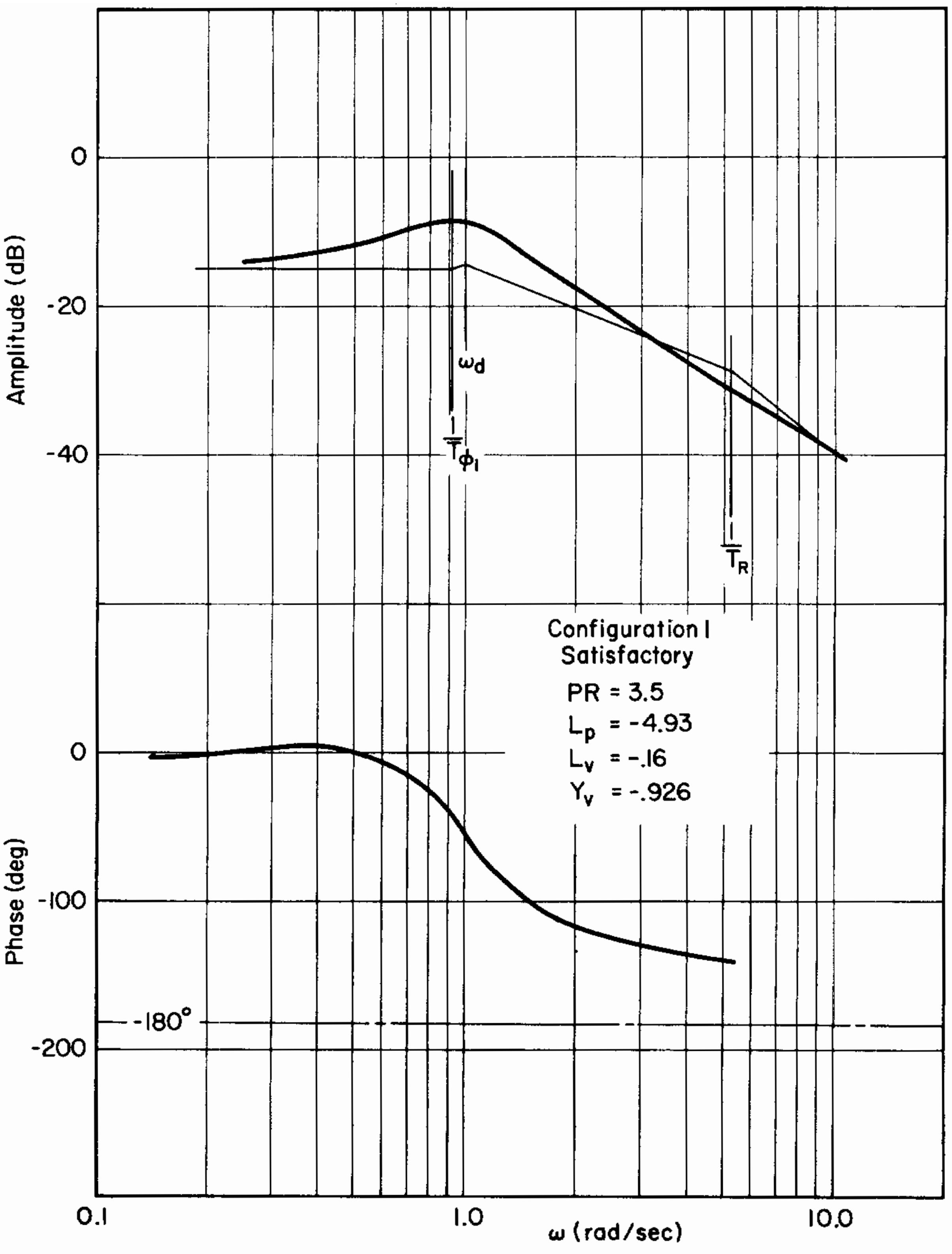

Figure A-1. Large Y_v, Attitude Rate Augmentation, φ/δ_a

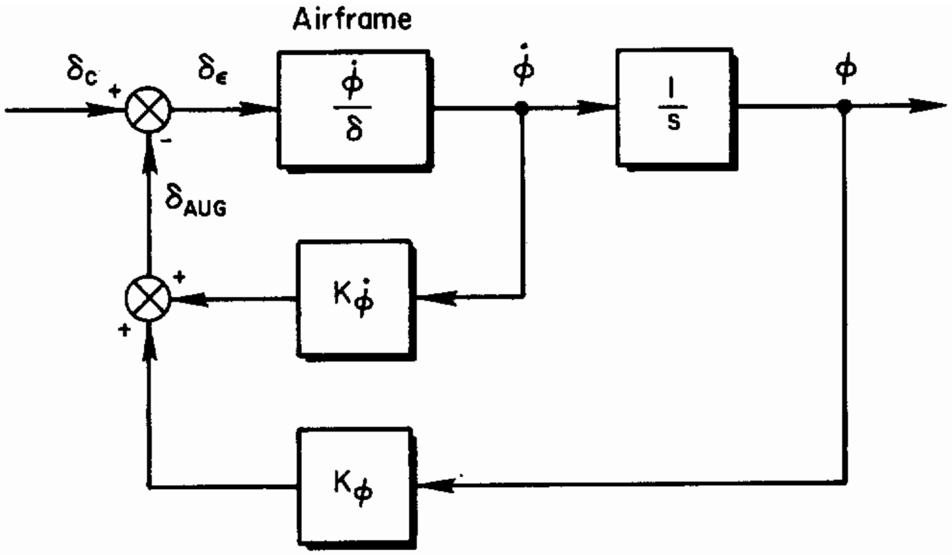
Airframe
δ_c
+
δ_ϵ
$\frac{\dot\phi}{\delta}$
$\dot\phi$
$\frac{1}{s}$
ϕ
-
δ_{AUG}
+
$K_{\dot\phi}$
+
K_ϕ

EQIVALENT SYSTEM

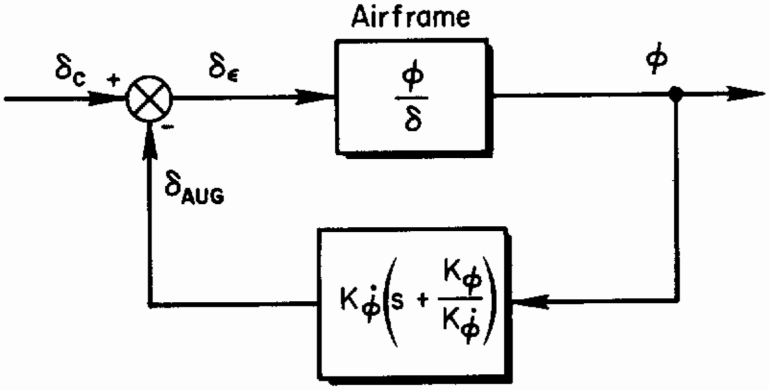
Airframe
δ_c
+
δ_ϵ
$\frac{\phi}{\delta}$
ϕ
-
δ_{AUG}
$K_{\dot\phi}\left(s+\frac{K_\phi}{K_{\dot\phi}}\right)$

Define: $\frac{1}{T_E} = \frac{K_\phi}{K_{\dot\phi}}$

$$\frac{\phi}{\delta_e} = \frac{L_\delta\left(s+\frac{1}{T_{\phi_1}}\right)}{\left(s+\frac{1}{T_R}\right)\left[s^2+2\zeta_d\omega_d s+\omega_d^2\right]}$$

Figure A-2. Attitude Augmentation Block Diagram

	ATTITUDE CONTROL; φ/δ	ROOT LOCUS; φ/φ_ϵ	AUGMENTED OPEN-LOOP BODE FEATURES	EFFECTIVE AUGMENTATION
Category I: $\frac{1}{T_E} \le \frac{1}{T_R}$ $(\omega_d' < \omega_d)$	$\frac{L_\delta(s+1/T_{\varphi_1})}{(s+1/T_R')[s^2+2\zeta_d'\omega_d's+\omega_d'^2]}$	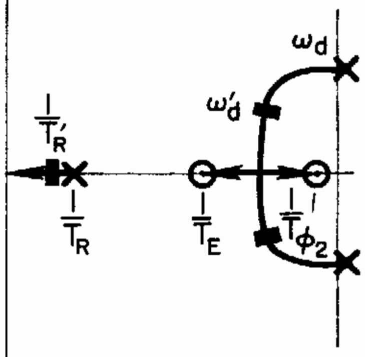 ω_d ω_d' $\frac{1}{T_R'}$ $\frac{1}{T_R}$ $\frac{1}{T_E}$ $\frac{1}{T_{\phi_2}'}$	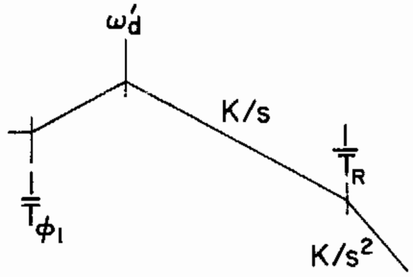 ω_d' K/s $\frac{1}{T_R}$ $\frac{1}{T_{\phi_1}}$ K/s^2	RATE
Category II: $\frac{1}{T_E} > \frac{1}{T_R}$ $\left(\frac{1}{T_{\varphi_1}} \doteq \frac{1}{T_R'}\right)$	$\frac{L_\delta}{[s^2+2\zeta_d'\omega_d's+\omega_d'^2]}$	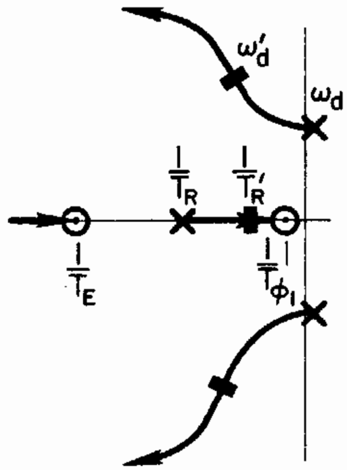 ω_d' ω_d $\frac{1}{T_R}$ $\frac{1}{T_R'}$ $\frac{1}{T_E}$ $\frac{1}{T_{\phi_1}}$	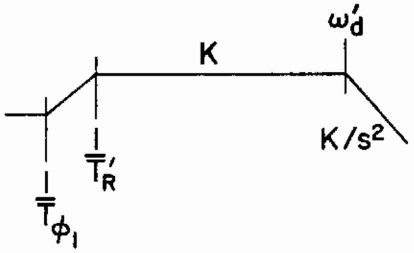 K ω_d' K/s^2 $\frac{1}{T_{\phi_1}}$ $\frac{1}{T_R'}$	ATTITUDE

Figure A-3. Classification Scheme for Attitude Augmentation System attitude feedback compensation. An attitude system, on the other hand, has a flat region in the Bode form. This system may also contain rate feedback. Figure A-3 shows the Bode features. The ratio of attitude to attitude rate feedback gains ($K_\varphi/K_{\dot\varphi}$) (i.e., $1/T_E = K_\varphi/K_{\dot\varphi}$) determines which category a given attitude augmentation level fits.

UARL Lateral Attitude Stabilization Study (Ref. 2). The UARL augmentation did not contain $K_{\dot\varphi}$, only an increased L_p value. If this L_p is assumed to be $K_{\dot\varphi}$, then a value for $1/T_r$ based on a realistic basic value of L_p must be sought for purposes of classifying the systems. From the approximate factors of Ref. 37 we note that

$$\frac{1}{T_r} \doteq \sqrt[3]{gL_v} + \frac{-L_p - Y_v}{4}$$

when $$\left|\frac{gL_v}{L_p^3}\right| > 1$$

For the magnitudes of gL_v used (e.g., 0.333 and 1.0)

$$\frac{1}{T_r} \doteq \sqrt[3]{gL_v}$$

(since Y_v and L_p are usually small, we can neglect the Y_v component and assume L_p is zero). Using this "basic" value of $1/T_r$, the relationship between $1/T_E$ and $1/T_{r_{BASIC}}$ is then determined.

The UARL attitude stabilization studies covered the range of attitude and rate augmentations as shown in Tables A-III and A-IV, when divided into the two categories of $1/T_E < 1/T_{r_{BASIC}}$ (i.e., $1/T_{r_{BASIC}} \doteq \sqrt[3]{gL_v}$) and $1/T_E > 1/T_{r_{BASIC}}$.

Category II Systems, $1/T_E > 1/T_R$ (Refs. 9 and 26). With no aerodynamic derivatives the vehicles tested in the Boeing and NASA reports (Refs. 9 and 26) reduced to inertial bodies where $\varphi/\delta \doteq K/s^2$. Rate and attitude feedbacks were then used to provide stabilization. The characteristic equation is given by

$$\frac{\varphi}{\delta} = \frac{L_\delta}{s^2 + \underbrace{K_{\dot\varphi}L_\delta s}_{-L_{\dot\varphi}} + \underbrace{K_\varphi L_\delta}_{\omega_n^2}}$$

Hence

$$\zeta = \frac{K_{\dot{\varphi}}}{2}\sqrt{\frac{L_\delta}{K_\varphi}}$$

$$\omega_n = \sqrt{L_\delta K_\varphi}$$

Since $1/T_R = 0$, obviously $1/T_E > 1/T_R$. These are therefore true attitude or Category II systems as indicated in the Bode plots of Fig. A-4.

For the low stiffness conditions where ω_n is small, attitude feedback (K_φ) is small, there is a high amount of bank angle for a given stick input and the dominant response approaches that of a K/s^2 or inertial body system in the desired region of crossover.

Salmirs, Ref. 27. In a flight test experiment on a single rotor helicopter performed by Salmirs (Ref. 27), an attitude stabilization system was evaluated while flying low-speed instrument landing approaches. The helicopter configuration used for comparison supposedly possessed good basic flying qualities. The attitude-to-rate feedback ratio ($1/T_E$) was quite small and therefore did not greatly improve the overall system. Figure A-5 is the open-loop Bode plot for the basic and estimated augmented vehicle. The exact augmentation was not derivable since the ratio of stick angle to stick displacement was not given. The estimated values were assumed based on an effective stick gain.

The value of L_p was given, but the other aerodynamic derivatives were taken from Ref. 37 for the H-24, a similar vehicle.

The pilots reported a significant decrease in concentration required, although only a small general improvement in the roll axis. As can be seen from the figure, the basic system was made stable by the attitude feedback ($1/T_E < 1/T_R$), but the frequencies were only slightly changed.

Translational Augmentation Systems

The large Y_v data from the fixed-base experiments conducted by A'Harrah (Ref. 7) is considered representative of effective translational augmentation. In this case the lateral dynamics are defined approximately as

$$1/T_R = -Y_v \quad \text{and} \quad 1/T_{\varphi_1} = 1/T_R$$

$$\omega_d \doteq \sqrt{\frac{gL_v}{Y_v}}$$

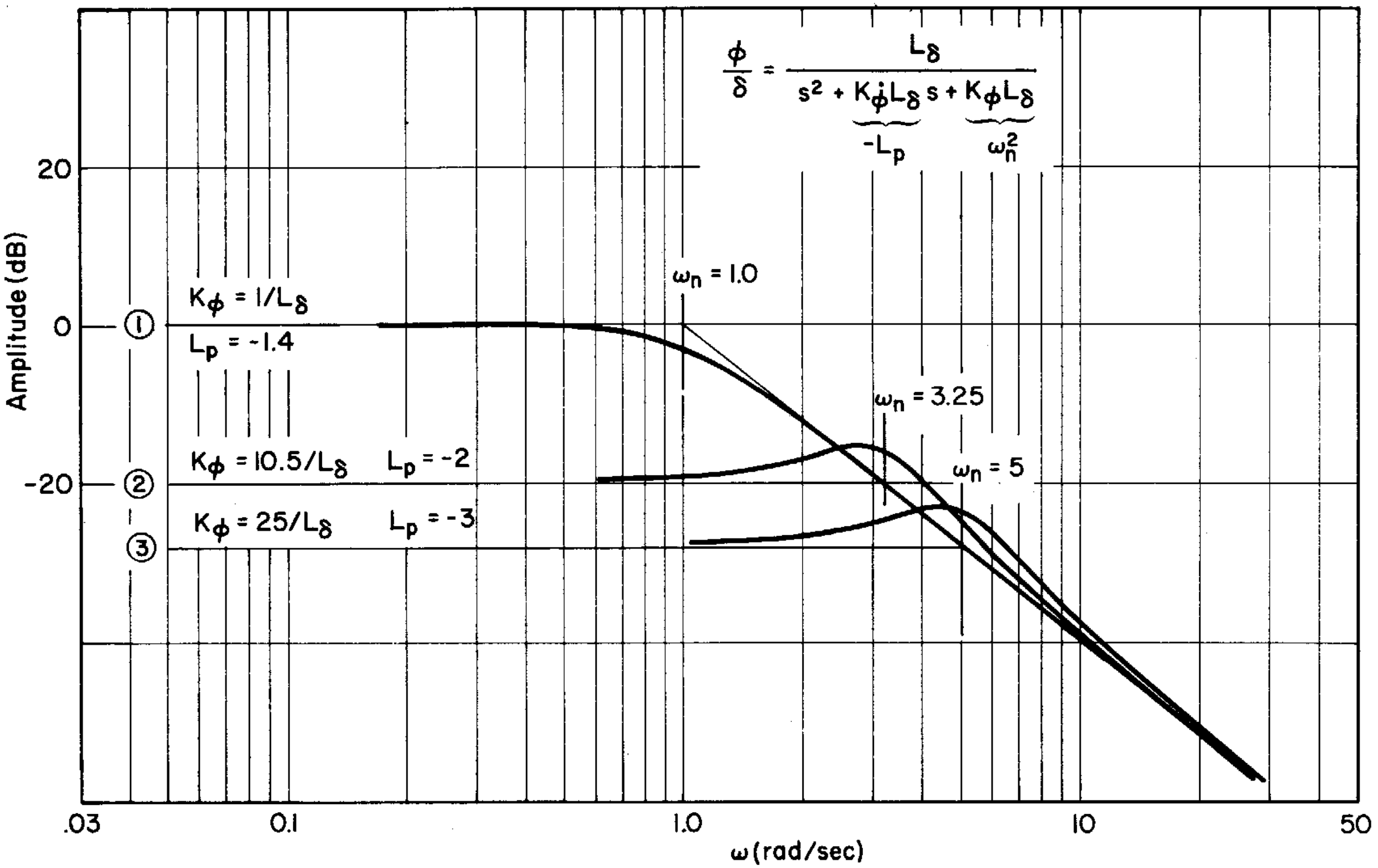

Figure A-4. Attitude Response Features for Category II ($1/T_E > 1/T_R$) Systems

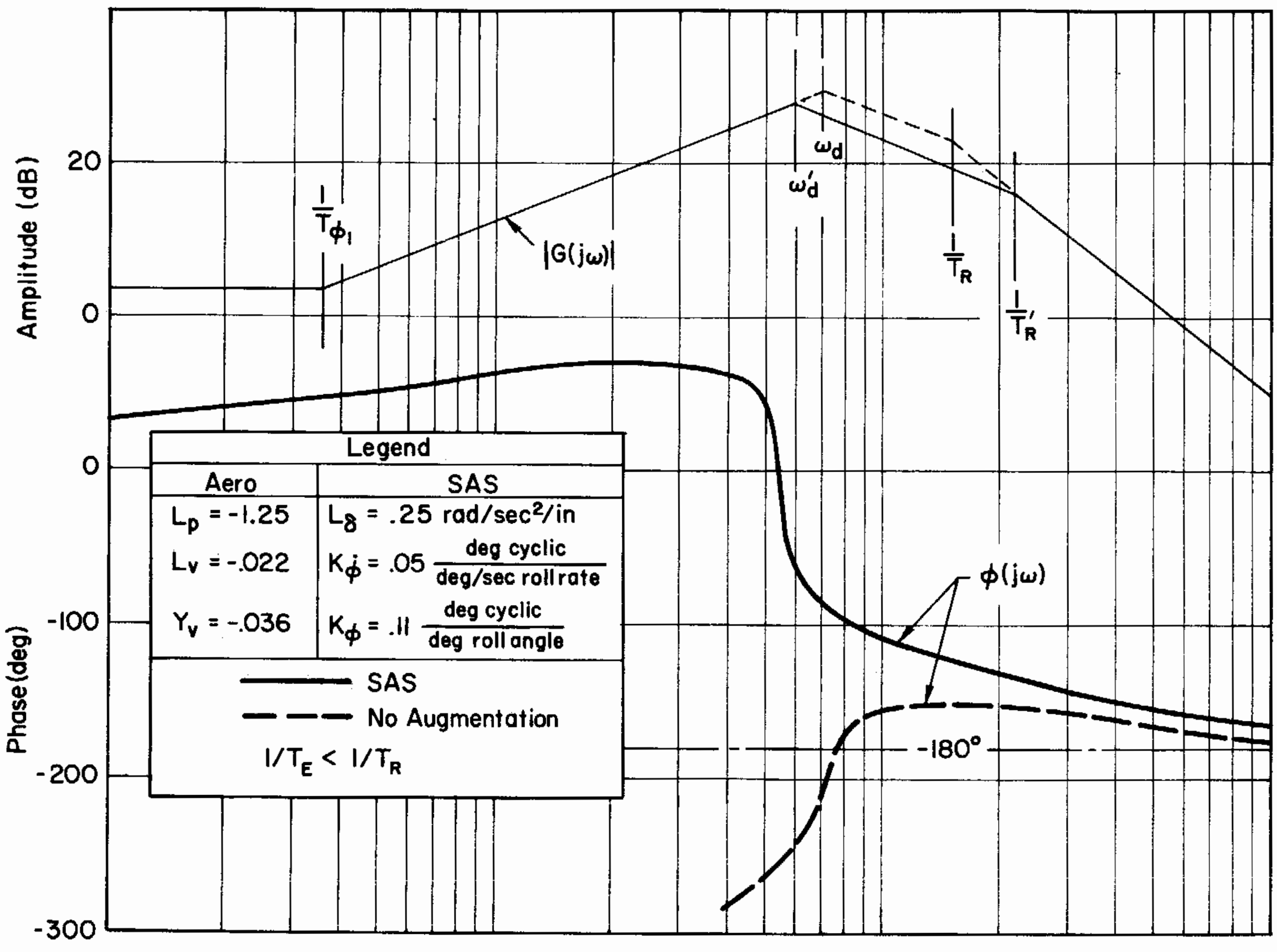

Figure A-5. Comparison of Helicopter Attitude Loop Dynamics with and without Attitude Stabilization (Ref. 27); $\varphi \rightarrow \delta_a$

The φ/δ dynamic characteristics for a satisfactory handling quality level are given in Fig. A-6. Again, since the attitude numerator zero $1/T_{\varphi_1}$ and the aperiodic mode $1/T_R$ are approximately equal to Y_v, these terms cancel in the φ/δ response and the Bode diagram has the appearance of a low frequency attitude system.

PILOT/VEHICLE CLOSED-LOOP CONSIDERATIONS

The basic closed-loop control envisioned for the lateral hover mode will not differ from that assumed for the longitudinal analyses in Ref. 1, primarily because the effective controlled elements involved are the same. Therefore the brief review of the pilot model and control structure, which is presented here for continuity, is governed by those concepts previously noted for the longitudinal analyses.

Pilot Model

The primary task in the hover mode is to control lateral deviations from a point on the ground or along a path. As shown below, this task is normally accomplished by controlling roll attitude, φ, and lateral deviation from the path, y, with the control stick, δ. Implied by this control structure is a multiloop control technique in which the pilot functions in series. Thus the pilot is concerned with both the inner attitude loop dynamics as well as the outer position loop features.

The closed-loop system represented by a series closure is therefore one in which the pilot directs translation by reference to and commands of attitude. The block diagram below shows the series closure and definitive symbols which will be used throughout this study. The underlying reason for this more complex technique is the fact that the direct closed-loop control of $y \rightarrow \delta$ is unacceptable (i.e., unstable) and this deficiency can be corrected by the additional control of the inner loop.

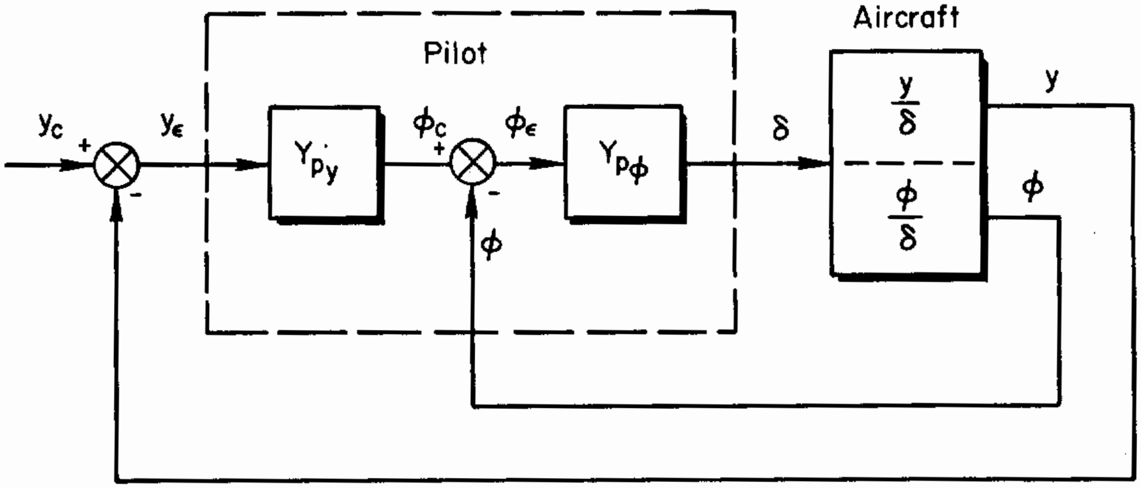

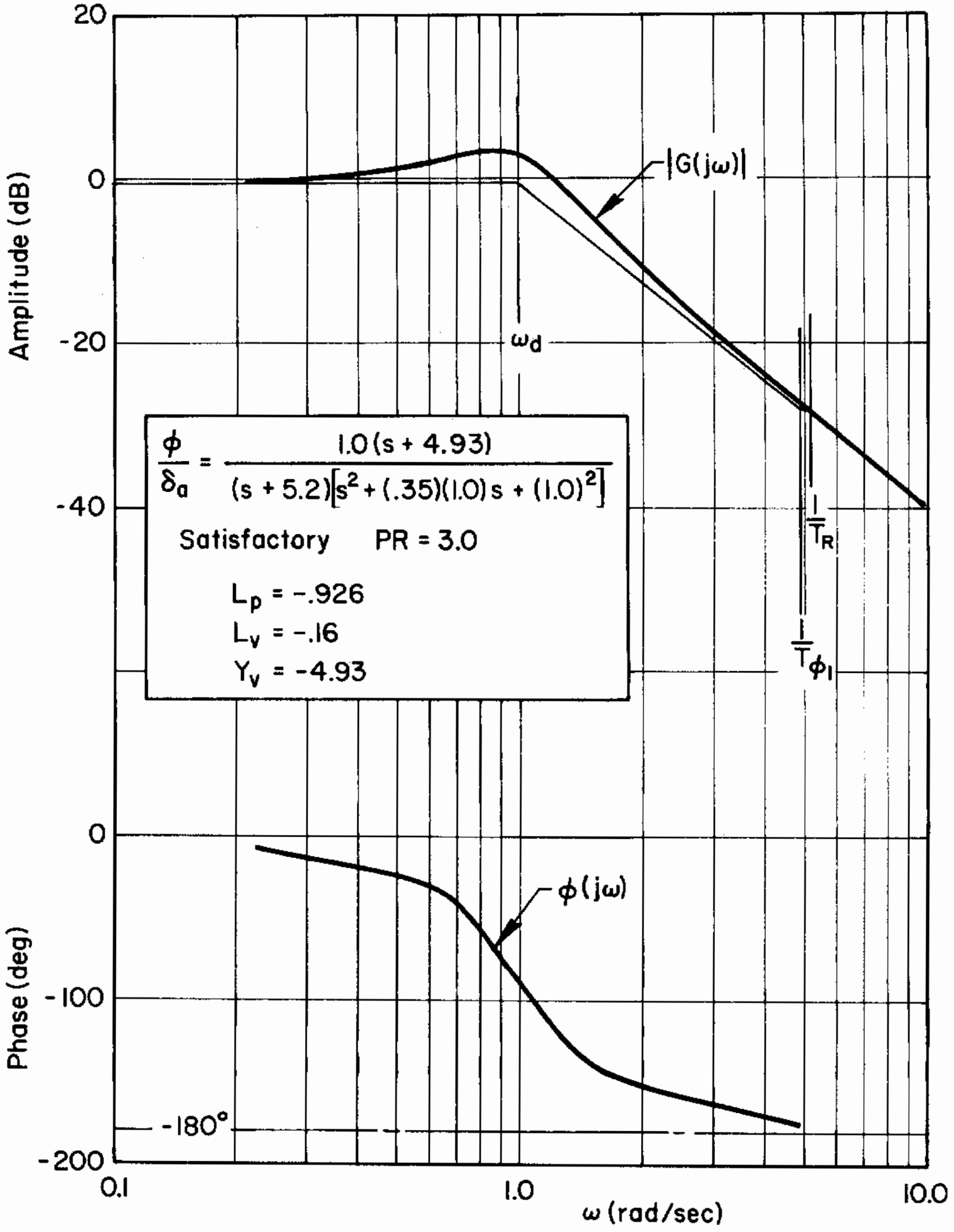

Figure A-6. Effective Translation Augmentation, $Y_v >> L_p$ and $1/T_R \doteq 1/T_\varphi \doteq Y_v$

The basic closure aspects which have governed the present analyses are specifically: (1) the pilot model, (2) the pertinent multiloop control structure, and (3) the adjustment rules for the pilot compensation requirement in the inner and outer loop (see Ref. 1). The pilot compensation requirements which will be discussed here are those associated with the quasi-linear describing function form of the crossover model which represents the overall average or long-term piloting control characteristics as explained in Ref. 12. Adaptation by the pilot is assumed to take place as necessary during precision hover to compensate for the aircraft dynamic deficiencies and to achieve acceptable closed-loop error performance. The basic pilot ratings are affected both by the extremes of such adaptation and the resulting performance.

The form of the pilot describing function adopted for these analyses is based on the crossover model concept described in Ref. 12 for single-loop control. This concept is extended to include the multiloop control situations in Ref. 38. The pilot describing function contains only lead equalization and a time delay, i.e.,

$$Y_p = K_p e^{-\tau_e s}(s + \frac{1}{T_L})$$

By using a second-order Padé approximation for the delay term, τ_e, this expression becomes

$$Y_p = \frac{K_p(s - 4/\tau_e)^2(s + 1/T_L)}{(s + 4/\tau_e)^2}$$

A nominal level of -0.4 sec is used to τ_e to approximate the effects of the neuromuscular lag and to account for the fact that the pilot is acting in a multiloop task.

The adjustment rules governing the pilot selection of equalization depend on the closed-loop control structure. Basically, in the present multiloop situation the minimal compensation for the inner loop (attitude) is lead equalization to cancel the adverse phase contribution due to the aircraft roll subsidence root, $1/T_R$. However, the underlying rules used for selecting the inner-loop equalization are:

1. To achieve an inner-loop crossover frequency, $\omega_{c_\varphi} > 2$ rad/sec.
2. To have equalization which results in improved outer-loop features (i.e., ω_{c_y}, K_M, and φ_M or σ_{y_ϵ}).

Loop Characteristics — Position Loop. In the final multiloop closure $(y, \varphi \to \delta_a)$, compensation requirements of the position loop must be considered also. Assuming that the inner attitude loop is closed, the effective position loop may be expressed generically by an effective single-loop transfer function

$$\left(\frac{y}{\delta_a}\right)_{\varphi \to \delta_a} = \frac{-gL_\delta}{s\left(s + \frac{1}{T_R'}\right)\left(s^2 + 2\zeta_d'\omega_d's + \omega_d'^2\right)} \cdot \frac{\left(s - \frac{4}{\tau_e'}\right)^2}{\left(s + \frac{4}{\tau_e'}\right)}^{*} \qquad (A\text{-}1)$$

where typically the closed-loop roots are

$$\frac{1}{T_R'} \doteq \frac{1}{T_{\varphi_1}} \doteq -Y_v$$

$$\omega_d' \doteq 3 \text{ rad/sec}$$

Lateral position-loop closure characteristics with and without pilot position lead (i.e., $\dot{y}$ feedback) in the outer loop are shown in Figs. A-11 and A-12 for the satisfactory and unacceptable dynamics, respectively.

In the satisfactory case, the potential closure crossover frequencies are relatively low for the no-lead case, being near $1/T_R'$ (see Eq. A-1). The location of the basic vehicle real zero, $1/T_{\varphi_1}$, near the origin in the attitude loop is the reason for the low crossover frequency in the y-loop and the low value of Y_v accounts for this location of the vehicle real zero. When the attitude loop is closed with a gain sufficient to achieve a satisfactory crossover frequency, a closed-loop pole is generated close to the real zero. This low frequency pole, together with the pole at the origin, produces a low frequency complex pole pair when the outer loop is closed. This low frequency complex pole pair limits the outer-loop crossover frequency.

The crossover frequency is slightly higher for the unacceptable case than for the satisfactory case, indicating that the crossover of the position loop improves as the attitude loop deteriorates. This is because the real closed-loop pole from the attitude loop is located further from the origin in the unacceptable cases. This is a consequence of the higher values of L_v and reduced values of L_p in the unacceptable cases which result in a higher frequency (e.g., $\omega_d \doteq \sqrt{L_v g/L_p}$).

---

*The expression $(s - 4/\tau_e')^2/(s + 4/\tau_e')$ is the second-order Padé approximation for the pilot's effective delay, τ_e, after the closure.

The introduction of lead compensation (i.e., position rate) in the outer position loop has two primary effects:

1. Basic pilot adjustment rules outlined in Ref. 1 are fulfilled (e.g., crossover is achieved in a K/s region).
2. The closure features are altered and the attitude closure, in lieu of the position loop, becomes the factor limiting control.

A relatively small amount of pilot lead improves the outer-loop performance substantially. A crossover frequency of approximately 1 rad/sec can be achieved with $T_L = 1$ sec for the satisfactory case, and $T_L = 0.4$ sec for the unacceptable case.

The fact that moderate lead improves the outer-loop crossover frequency emphasizes the importance of the inner-loop closure. Basically, lead in the position loop is generated by biasing or overdriving of the attitude near the low frequency crossover, ω_{c_y} (i.e., φ lead y since $y/\varphi \doteq -g/s^2$). Thus, to enable the pilot to lead position, one may envision that the attitude control functions must be well separated from the desired low frequency position control (i.e., $\omega_{c_\varphi} >> \omega_{c_x}$). Likewise, the φ-loop must be reasonably well damped, $\zeta' >> 0$, or otherwise these two control operations will conflict. Of course, the above analogy describes the piloting functions in the multiloop situation as more or less separate operations which occur simultaneously, but at different frequencies.

From a more analytic viewpoint, the preceding conclusion may be illustrated by the sketch on the following page of the open-loop position Bode with the φ-loop closed. Notice that the y-loop bandpass is reduced by the lightly damped lateral oscillatory mode of the attitude closure. The tradeoff implied by this tie between inner- and outer-loop control plays a key role in pilot opinion. That is, as the pilot needs an increased outer-loop bandwidth and gain for tighter position control (e.g., for control under lateral gust conditions), the requirements for inner-loop bandwidth and/or damping become more critical. In any case, the restricting factors may be expressed as a function of closed-loop damping of the attitude loop, since ω_{c_y} lies between $2\zeta_d'\omega_d'$ (for $1/T_R'$ or $1/T_{L_y}$ close to ω_{c_y}) and $\sqrt{2\zeta_d'\omega_d'}$ (for $1/T_R' \to 0$). This means that the requirements for attitude-loop damping will be partly based on the outer bandwidth requirement. We note also that the position bandwidth needs will depend on the gust sensitive lateral side force parameter, Y_v. The effects of the side force parameter on gust regulatory control is explored later in this appendix.

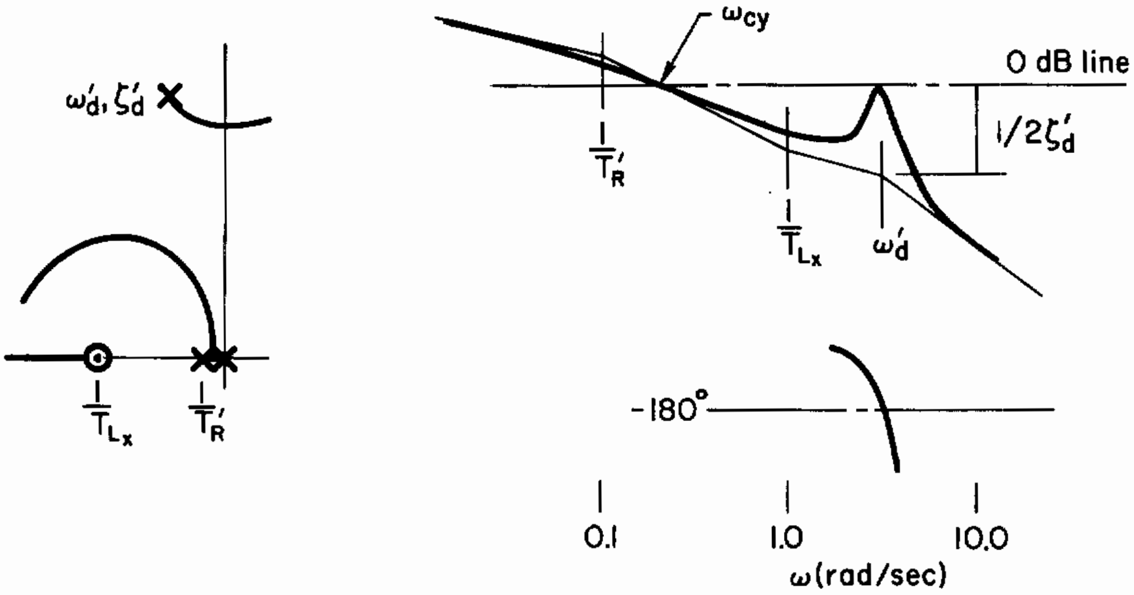

Open-Loop Position Control, $y/y_\epsilon|_{\varphi \rightarrow \delta_a}$

Conventional Lateral Dynamics — Lateral Side Force Large ($Y_v >> 0$). The dynamic characteristics from the A'Harrah experiments, Table A-II, which were considered "conventional" have relatively large Y_v levels. For the present, these data offer the best clue to the inferred airframe damping required to maintain an acceptable outer-loop to inner-loop bandwidth (i.e., $\omega_{c_y}/\omega_{c_\varphi}$). Basically, these results suggest that the damping ratio, $\zeta_d \doteq 0.30$, is necessary for satisfactory ratings when the lateral oscillatory mode, ω_d, is greater than 0.50 rad/sec.

The multiloop control structure with attitude, φ, as the inner loop is essential in these satisfactory cases even though the basic vehicle is stable. For the inner-loop closure, the minimal compensation required is a lead approximately equal to the roll subsidence mode, $1/T_R$. Figure A-13 shows the attitude-loop closure with the lead compensation ($1/T_L = 1/T_R$) as well as a closure without lead. It is evident that a low bandpass ($\omega_{c_\varphi} < 2$ rad/sec) occurs if the adverse phase contribution from the roll subsidence mode is not cancelled by introducing lead.

Figure A-14 shows the position-loop closure for the preceding attitude closure. Note that a phase margin requirement in the inner loop is not necessary because the final outer-loop closure tends to stabilize the Dutch roll mode, ω_d'. In addition, no outer-loop lead compensation is necessary because a broad K/s crossover region has resulted from the attitude-loop closure with the moderately large $1/T_{\varphi_1}$ zero.

In summary, for these marginally satisfactory dynamic properties, the pilot compensation requirements are not excessive, even though a multiloop control structure is necessary to obtain the desired outer-loop bandpass ($\omega_{c_x} \doteq 1$ rad/sec). Primary restrictions on the closed-loop control are:

- Low attitude regulatory control to low dc gain of attitude closure.
- Lead compensation in the outer loop destabilizes the closed-loop Dutch roll mode, ω_d', and lowers the position-loop bandpass (e.g., $\omega_{c_y} \doteq 2\zeta_d'\omega_d'$).

Attitude Augmented Dynamics. In extending the pilot/vehicle closed-loop considerations to the attitude augmentation systems, we are concerned with the closure details of both Category I and II systems. Primary discussion is directed at Category II system (i.e., $1/T_E > 1/T_R$) because Category I (i.e., $1/T_E < 1/T_R$) and conventional VTOL dynamics are similar from a closed-loop viewpoint.

Category I Systems ($1/T_E \le 1/T_R$). The closure characteristics for an unsatisfactory (i.e., PR $\doteq$ 5.0) Category I system from Table A-III are considered first. The dynamics shown in Fig. A-15 are clearly in the "in-between" area and were selected because they represent the transition region between Category I and II systems. The associated closed-loop piloting difficulties for the attitude-loop closure details are illustrated by the system survey in Fig. A-15. In this rate system the level of $1/T_R$ determines the moderate lead required (i.e., $1/T_{L_\varphi} = 1/T_R = 1.79$) to achieve the attitude-loop bandpass near 3 rad/sec. Without lead there is a restricted bandwidth (i.e., $\omega_c < 3.0$ rad/sec) and closed-loop damping, ζ', would be less than open-loop damping (see solid root locus trace on the figure). When lead is added to cancel out $1/T_R$, then the closed-loop characteristics are significantly improved, although the closed-loop situation is obviously quite sensitive to small changes in the lead. In addition, we note that only a relatively small improvement in the dc or "broadband gain" level is possible with increased lead compensation. This infers that attitude errors under gusty conditions may be somewhat large. To envision this latter point, note from the sketch that even if the lead is increased in Fig. A-15 such that $1/T_{L_\varphi} \doteq \omega_d$, the dc and effective broadband gain region is relatively unchanged, thus the low frequency attitude errors are not reduced.

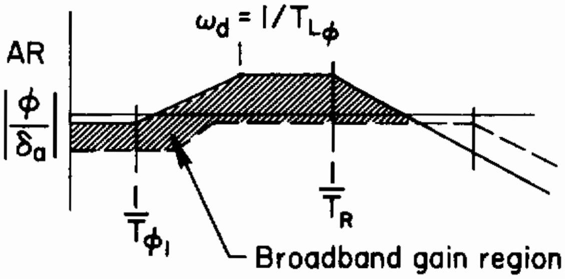
$\omega_d = 1/T_{L_\phi}$
AR
$\left|\frac{\phi}{\delta_a}\right|$
$\frac{1}{T_{\phi_1}}$
$\frac{1}{T_R}$
Broadband gain region

In the position loop, a minimum lead of 1 sec must be provided to ensure a K/s-like crossover region and positive stability near 1 rad/sec (see Fig. A-16). The damping of the attitude closed-loop oscillatory mode tends to restrict the outer-loop bandpass unless this damping for the inner-loop exceeds about 0.2. In fact, the gain margin for this position closure is set by the inner-loop damping. This closed-loop damping level is closely tied to the basic augmented airframe feedback, $K_{\dot\varphi}$, since the level of rate damping establishes the needed pilot lead compensation (i.e., to cancel the adverse phase contribution of $1/T_R$) for good attitude bandpass.* Thus a subtle tie between inner- and outer-loop bandwidths is inferred. This aspect will be more clearly illustrated in the following discussion of Category II systems.

---

*The damping of the bare airframe lateral oscillatory mode ω_d is primarily due to the feedback term $K_{\dot\varphi}$ since L_p is assumed small.

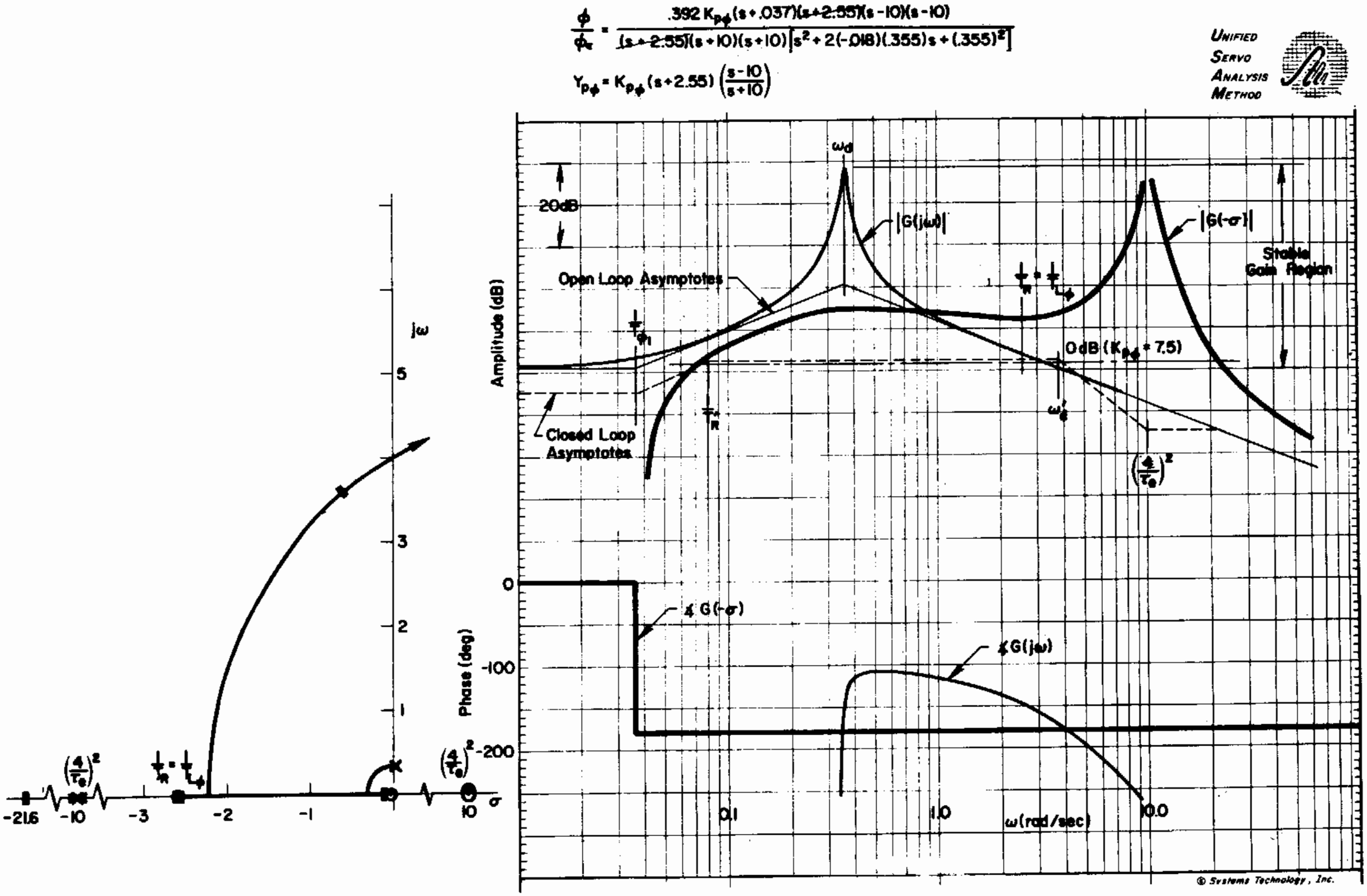

$$\frac{\phi}{\phi_c} = \frac{.392\,K_{p_\phi}(s+.037)\cancel{(s+2.55)}(s-10)(s-10)}{\cancel{(s+2.55)}(s+10)(s+10)\left[s^2+2(-.018)(.355)s+(.355)^2\right]}$$

$$Y_{p_\phi} = K_{p_\phi}(s+2.55)\left(\frac{s-10}{s+10}\right)$$

Figure A-7. Roll Attitude Loop Closure for Satisfactory Dynamics (PR = 2.7); φ → δ_a

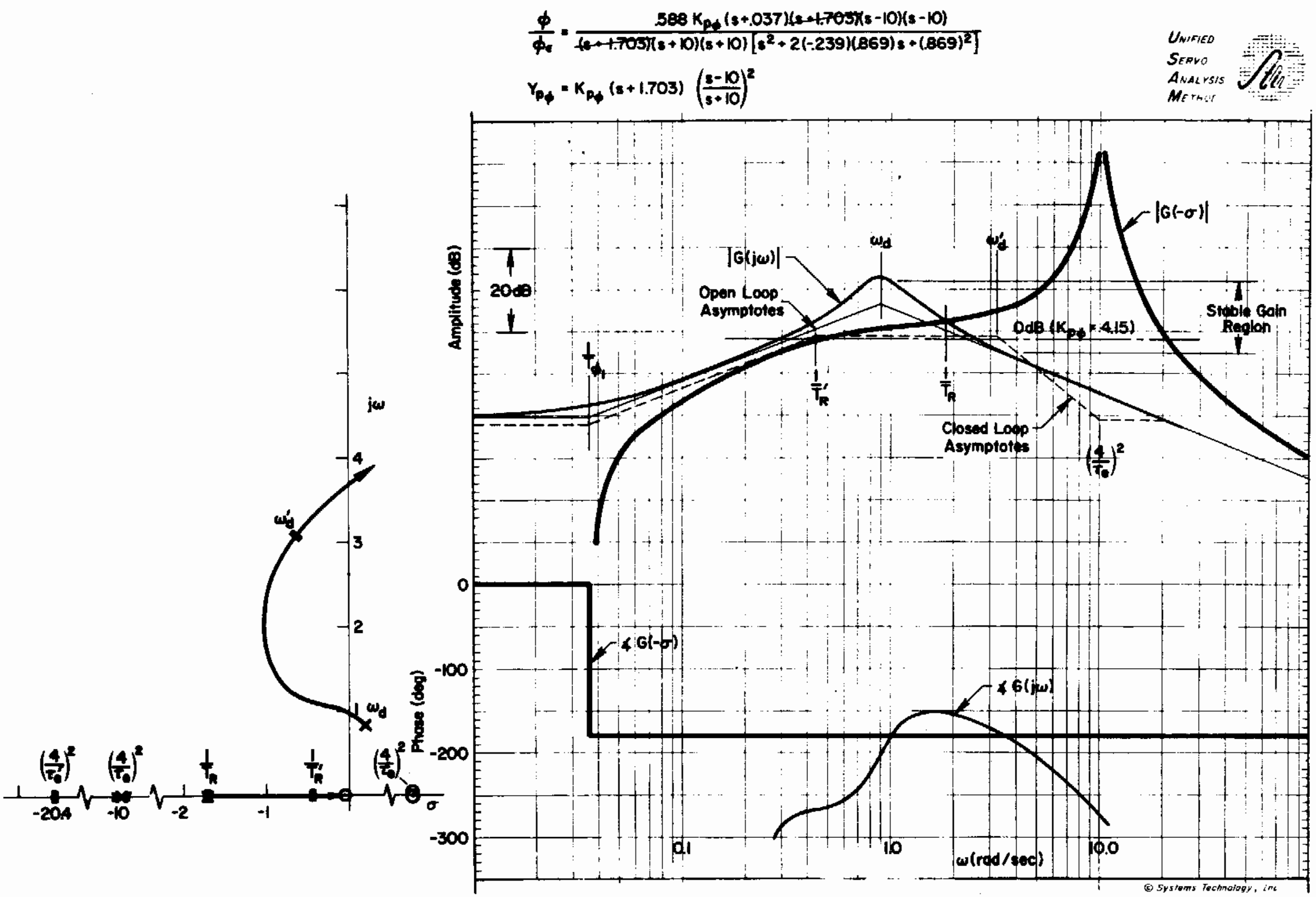

Figure A-8. Roll Attitude Loop Closure for Unacceptable Dynamics (PR = 7.3); $\varphi \longrightarrow \delta_a$

$$\frac{\phi}{\phi_\epsilon} = \frac{.154\,K_{p\phi}T_{L\phi}(s+.037)(s-10)(s-10)(s+1/T_{L\phi})}{(s+2.55)(s+10)(s+10)\left[s^2+2(-.018)(.355)s+(.355)^2\right]}$$

UNIFIED
SERVO
ANALYSIS
METHOD

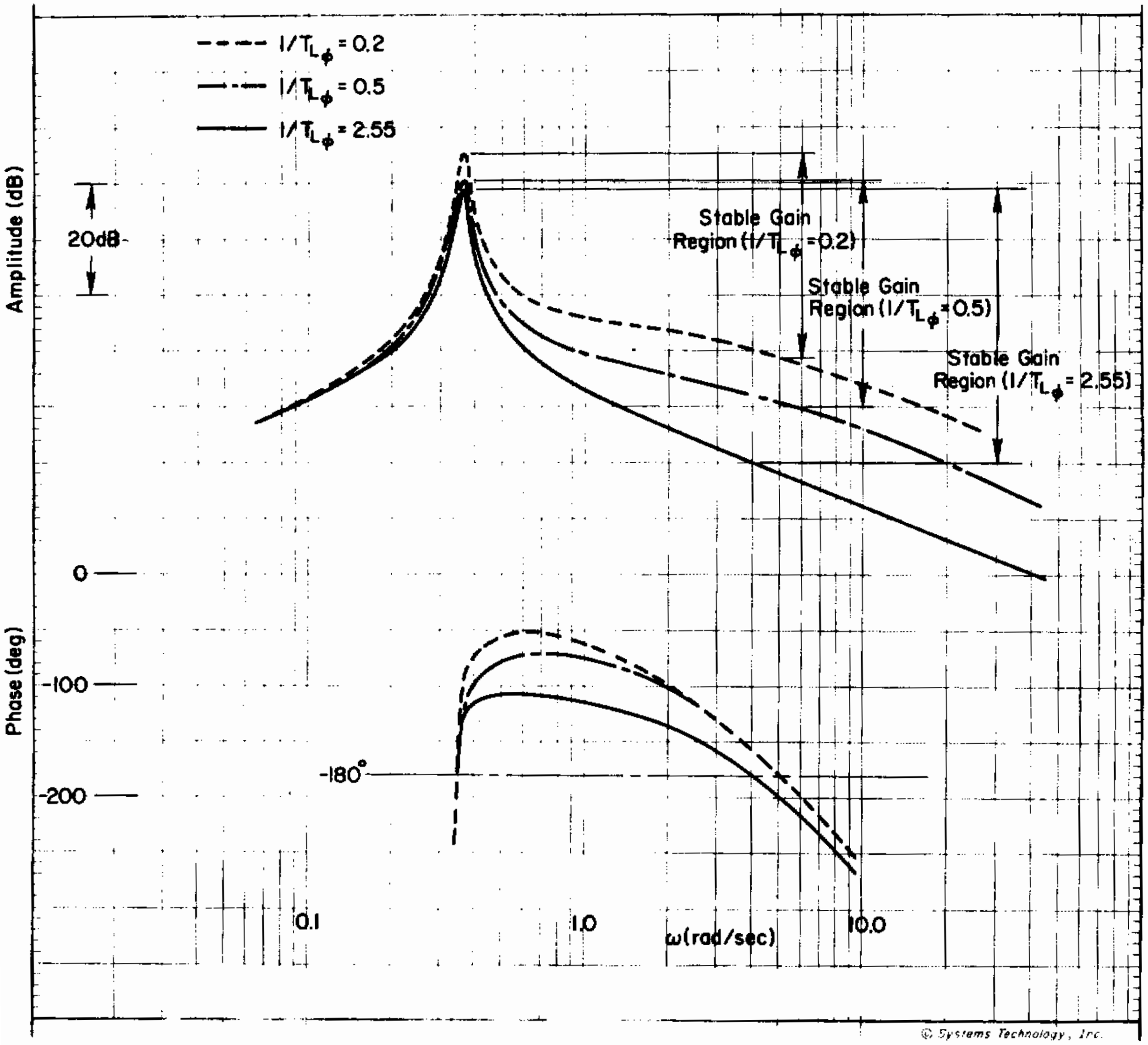

© Systems Technology, Inc.

Figure A-9. Effect of Increased Attitude Loop Lead — Satisfactory Case; $\psi \rightarrow \delta_a$

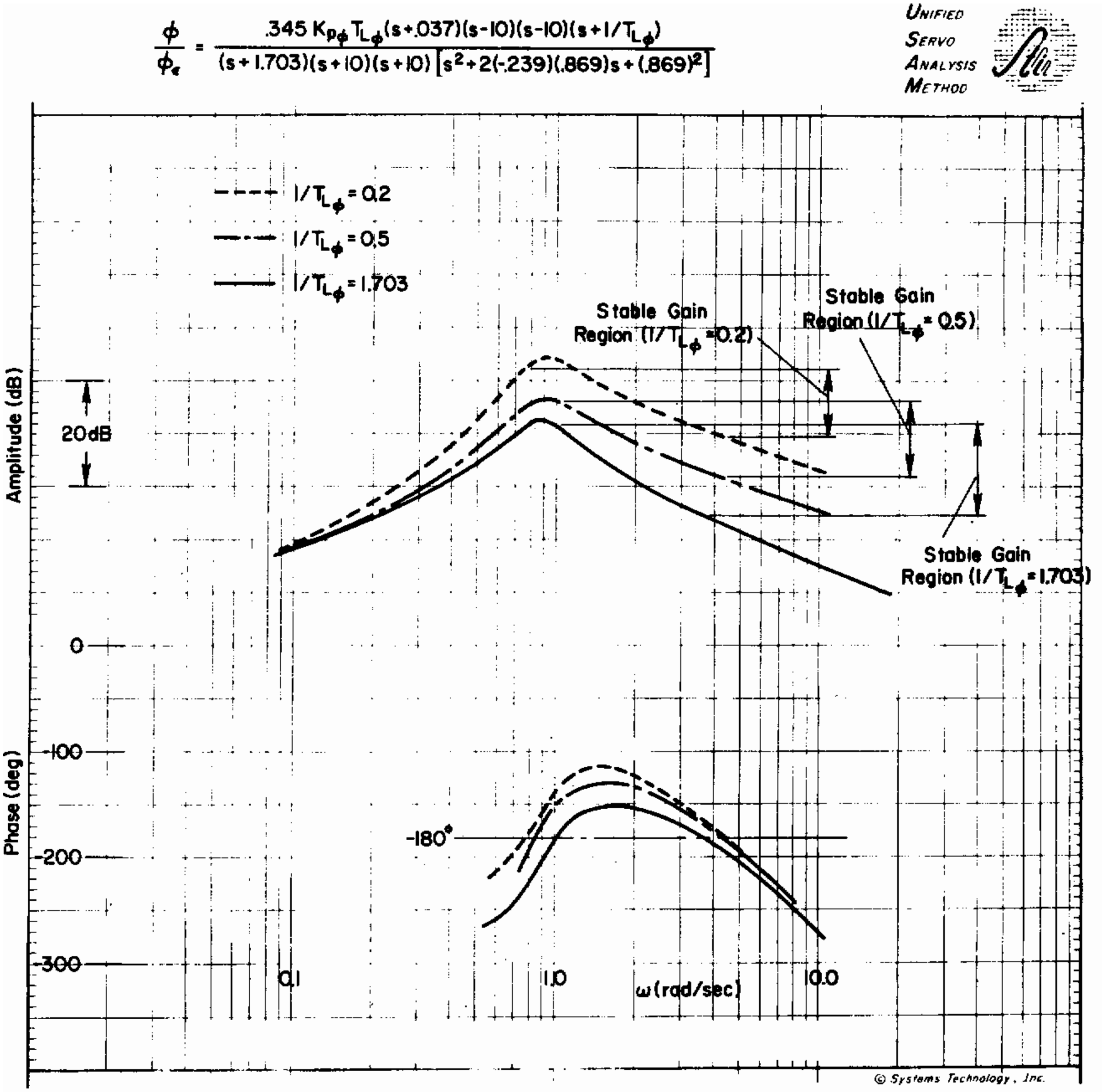

Figure A-10. Effect of Increasing Attitude Loop Lead — Unacceptable Case

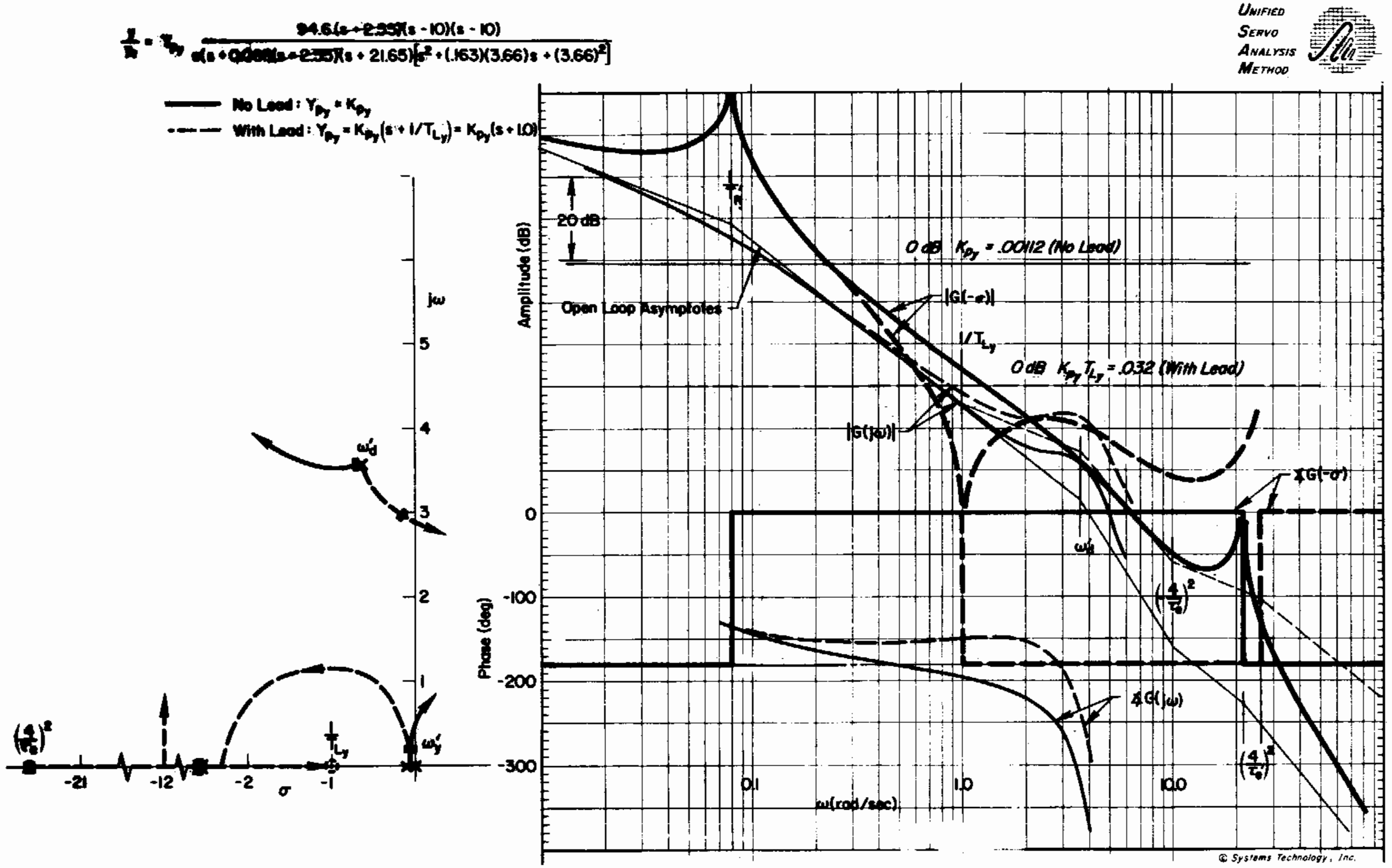

Figure A-11. Lateral Position Loop Closure, Satisfactory Dynamics, y, φ ⟶ δ_a (with and without Pilot Lead)

$$\frac{y}{y_c} = Y_{p_y}\frac{78.5(s-10)(s-10)\cancel{(s+1.703)}}{s(s+0.420)\cancel{(s+1.703)}(s+20.4)\left[s^2+(.193)(3.14)s+(3.14)^2\right]}$$

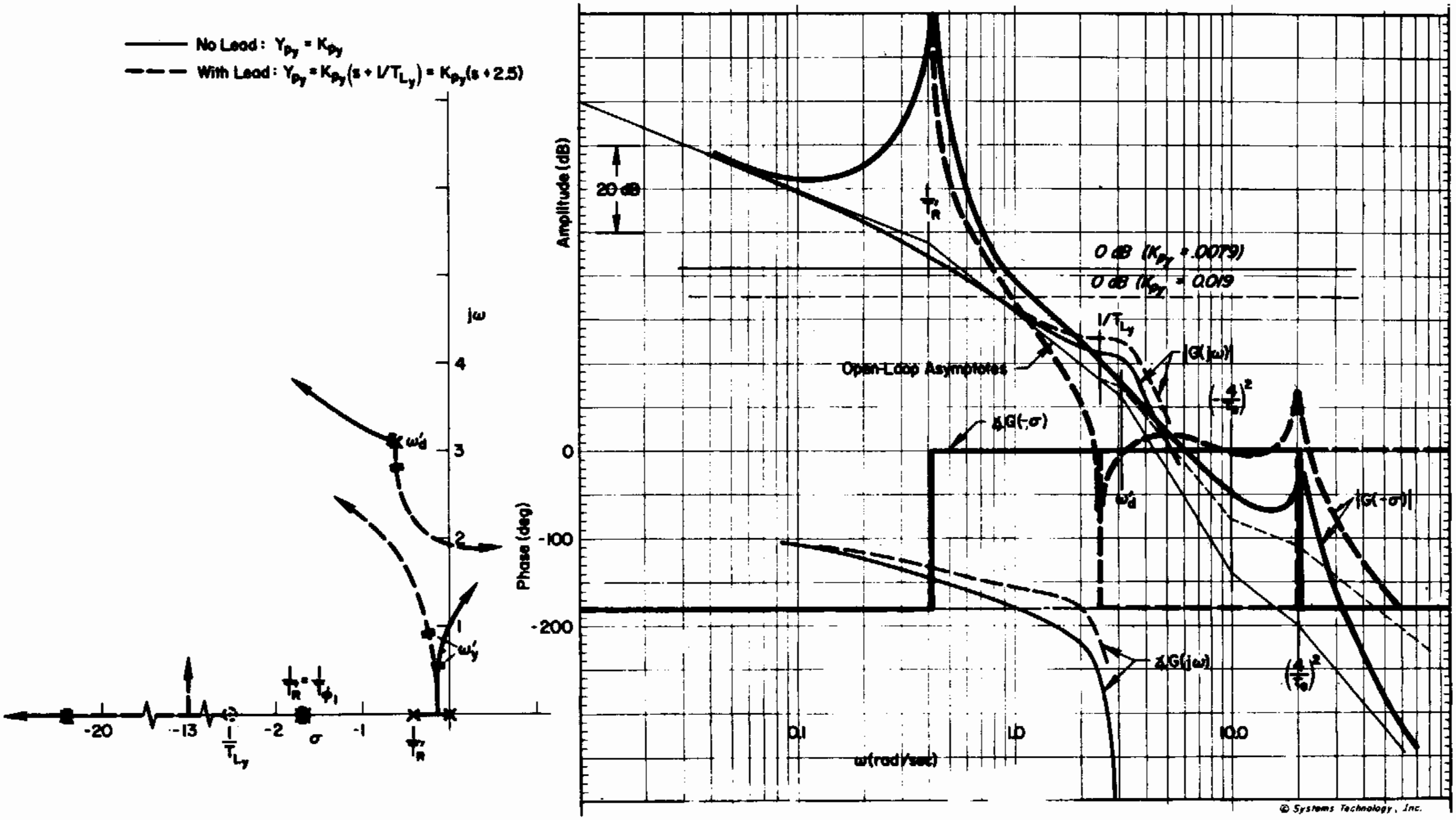

Figure A-12. Lateral Position Loop Closure, Unacceptable Dynamics, y, φ → δ_a (with and without Pilot Lead)

$$\frac{\phi}{\phi_c} = \frac{L_{\delta_a} K_{p_\phi} T_{L_\phi}(s+.87)(s+1/T_{L_\phi})(s-10)^2}{(s+3.6)(s+10^2)\left[s^2+2(.144)(1.2)s+(1.2)^2\right]}$$

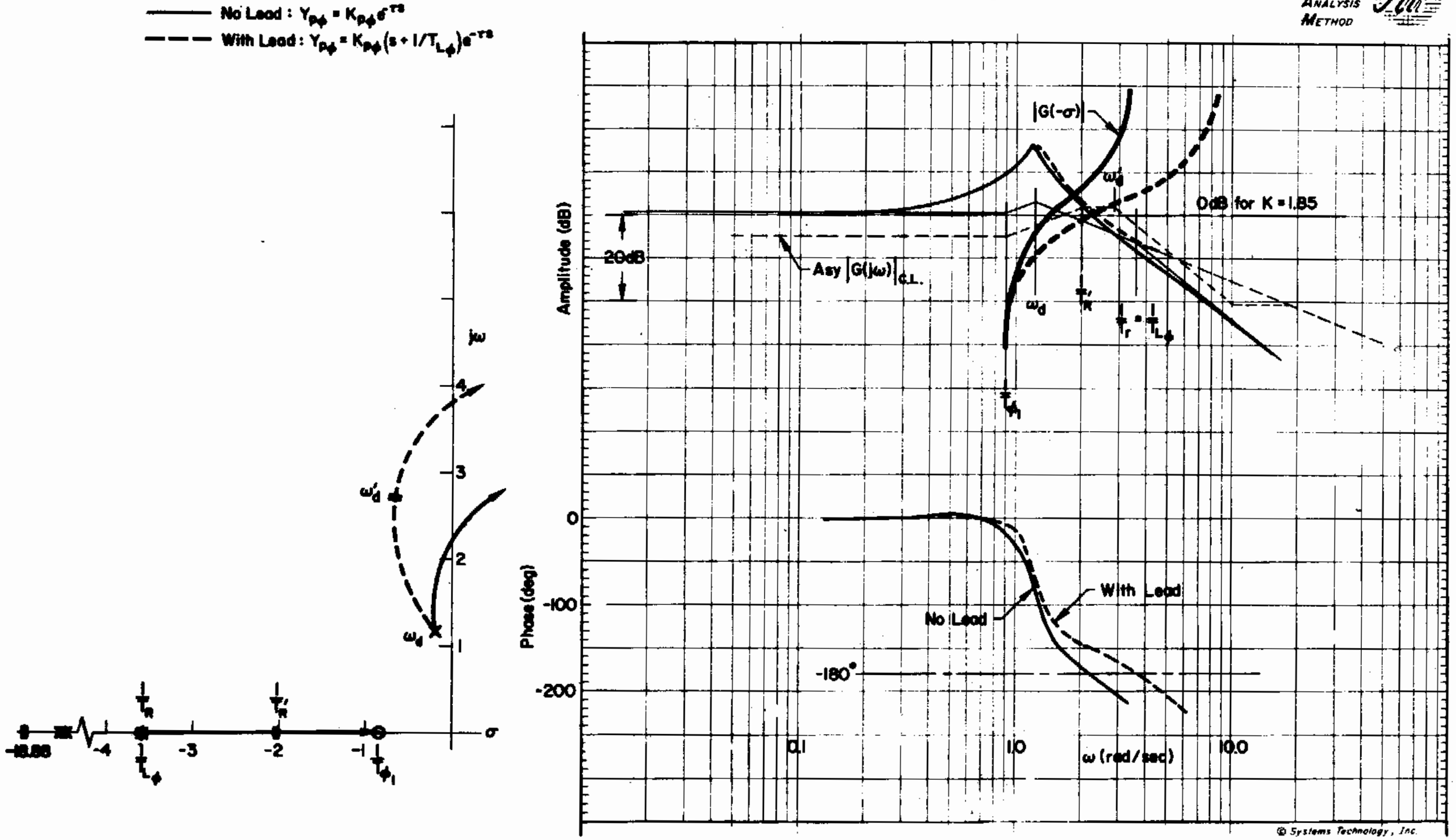

Figure A-13. Roll Attitude Loop Closure for Large Lateral Side Force ($Y_v >> 0$), $\varphi \rightarrow \delta_a$

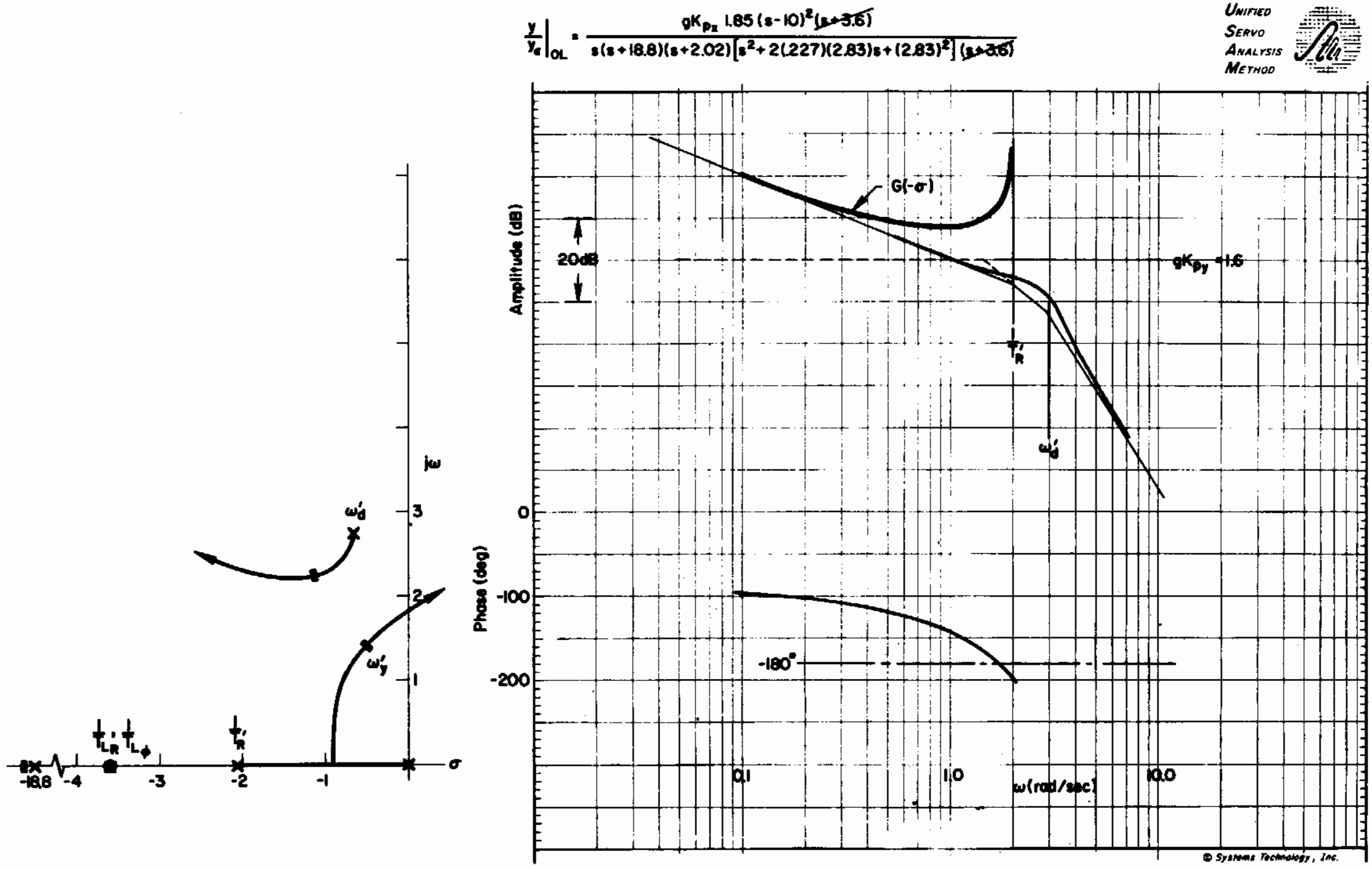

Figure A-14. Position Loop Closure with Large Lateral Side Force ($Y_v >> 0$), y, φ → δ_a

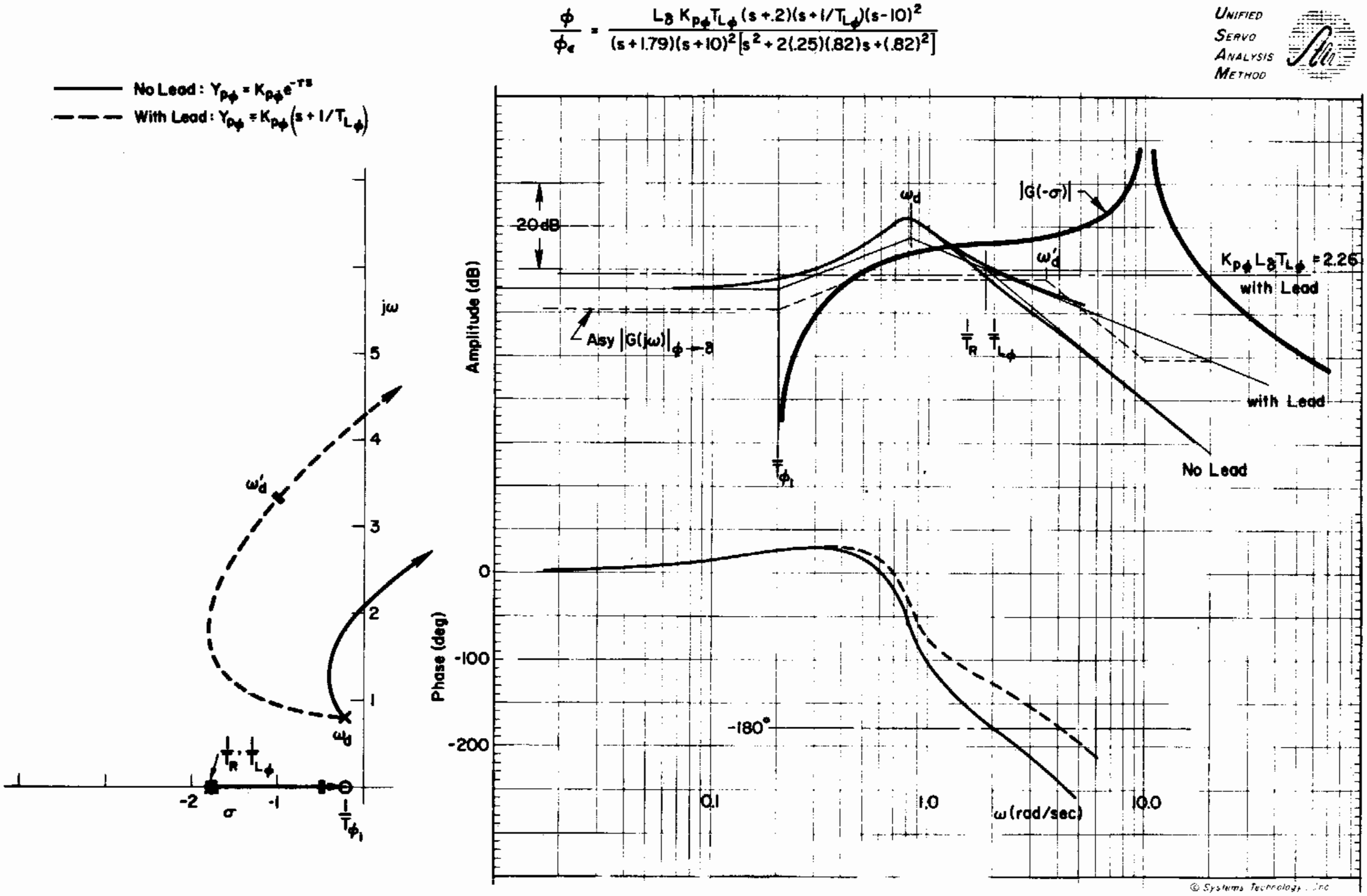

$$\frac{\phi}{\phi_e} = \frac{L_\delta K_{p_\phi} T_{L_\phi}(s+.2)(s+1/T_{L_\phi})(s-10)^2}{(s+1.79)(s+10)^2\left[s^2+2(.25)(.82)s+(.82)^2\right]}$$

Figure A-15. Roll Attitude Closure for Category I System, $1/T_E < 1/T_R$, $\varphi \longrightarrow \delta_a$

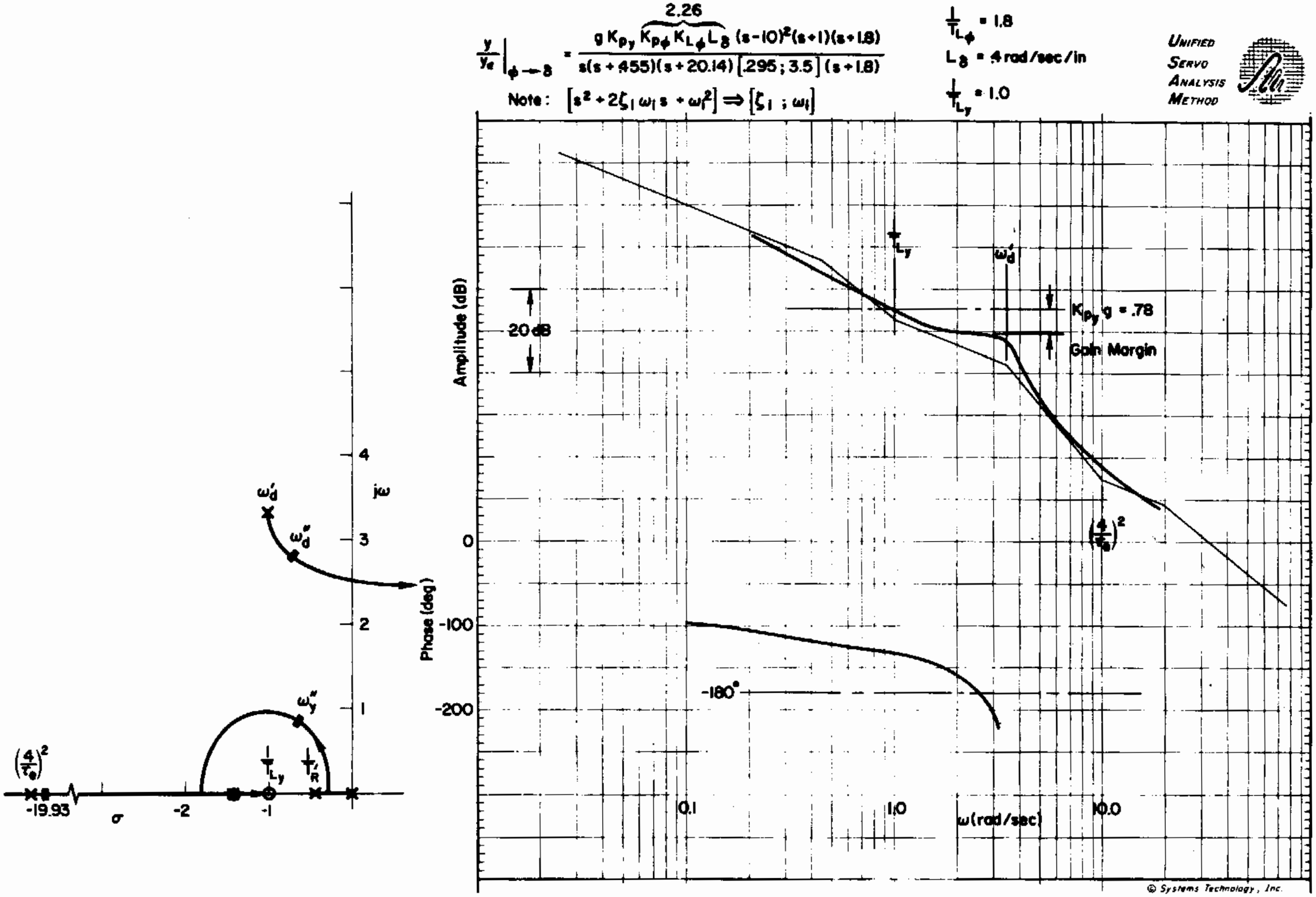

Figure A-16. Position Loop Closure for Category I System, $1/T_E < 1/T_R$; $y, \phi \rightarrow \delta_a$

Category II Systems ($1/T_E > 1/T_R$). The key closure features associated with Category II systems are those required to achieve adequate attitude and position bandwidths and the level of broadband gain (i.e., gain characteristics below the augmented airframe frequency, ω_N) in the attitude loop. A typical situation illustrating these closure difficulties is shown in Figs. A-17 and A-18.* This example from Table A-IV was tested in Ref. 2 and was given a marginal pilot rating (i.e., PR $\doteq$ 4). Note that the lead required is moderately high ($1/T_{L_\varphi} = 1.37$) and equal to the oscillatory mode, ω_d (i.e., $1/T_{L_\varphi} = \omega_d$). This lead partially cancels the adverse phase characteristics of the ω_d mode, and provides a K/s-like crossover region. Thus the basis for the pilot lead compensation in a Category II system differs from that previously implied for Category I system where $1/T_{L_\varphi} \doteq 1/T_R$. This is an important distinction because it infers that insofar as attitude control is concerned, the pilot's effort (effort here infers lead generation and overall concentration) for Category I and II systems do not differ significantly, although the basis for his compensation does differ.

Note also we may infer from Fig. A-17 that lead compensation in excess of that required to cancel the adverse effects of the airframe oscillatory mode (i.e., $1/T_{L_\varphi} = \omega_d$) is not necessarily beneficial. Such was the case for the Category I system of Fig. A-15 where error regulation was not improved with increases in lead beyond $1/T_{L_\varphi} = 1/T_R$. For example, if we envision a low frequency lead much less than ω_d (e.g., $1/T_{L_\varphi} = 1/T_R$), the attitude Bode features are:

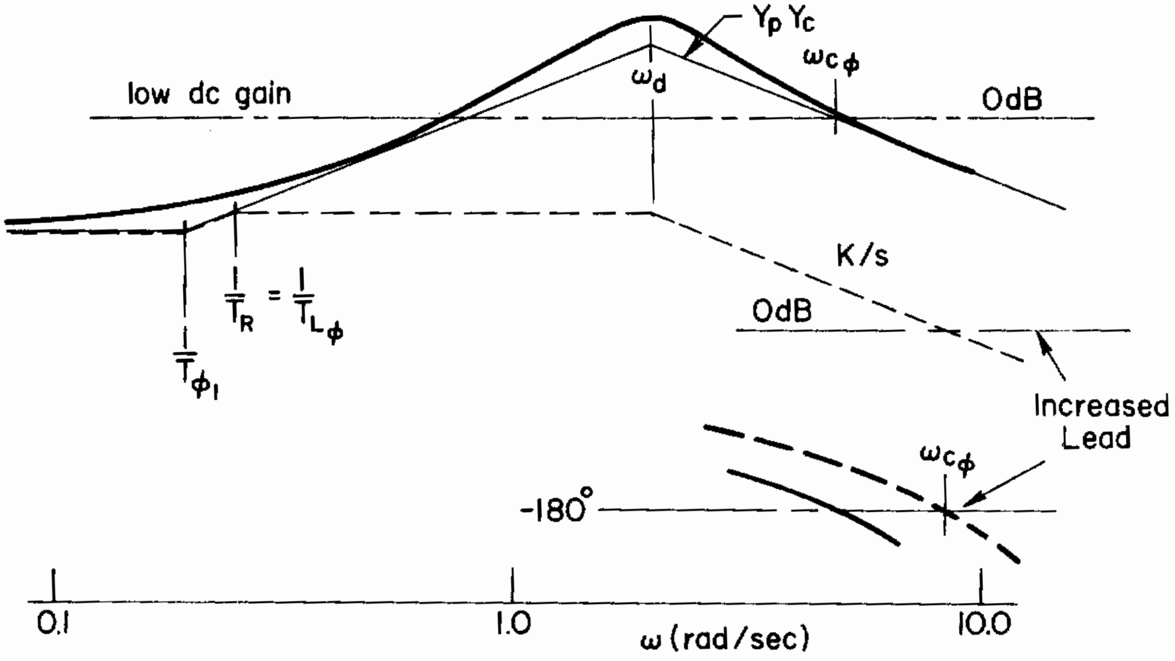

Bode Features of Attitude Closure
with Large Pilot Lead ($1/T_{L_\varphi} = 1/T_R$)

Here, even though the crossover frequency ω_{c_φ} is obviously increased beyond that shown in Fig. A-17, the resultant dc gain and broadband gain level characteristics are not significantly greater. These features suggest then that the pilot would not see an improvement in his error regulatory capability even with the increased effort involved in generating a low frequency lead. However, the increases in attitude lead tend to increase the closed-loop damping of the root ω_d' which can be important to the outer- or position-loop closure.

---

*Figures A-17 through A-26 are placed following page A-41.

The position-loop closure shown in Fig. A-18 also suggests some control problems because the position-loop bandpass is restricted due to the low gain margin. The low gain margin is due to the combination of the pilot's attitude- and position-loop leads and the damping of the closed-loop root, ω_d'. Since the damping of this root is a function of the inner-loop lead (i.e., a lower frequency lead increases the damping), the pilot can not improve the outer-loop bandwidth beyond that shown because of the tie between inner- and outer-loop leads. In effect, whether he induces more inner- or outer-loop lead is immaterial, for the net closed-loop situation remains essentially unchanged. Thus the pilot is faced with a "boxed-in" situation and is unable to improve the closure if the need arises (e.g., an increased gust disturbance level). Note also that without the ability to improve the attitude damping, he is highly dependent on the inherent vehicle damping level. If the vehicle damping is less than about 0.3, then the piloting control situation deteriorates.

To further explore the above point, we will consider potential closures for the low frequency attitude system from Ref. 9 which are shown in Figs. A-19 and A-20. Here three inner-loop closure situations (i.e., attitude loop) are explored, including a lead closure and closures with lead equal to or greater than the effective time constant of the lateral oscillatory mode (i.e., $1/\omega_d$). With a gain closure the inner loop is restricted to a crossover ≤ 2 rad/sec and closed-loop damping, $\zeta_d' < 0.25$. With this closure, outer-loop lead is mandatory as indicated in Fig. A-20 to provide a stable closure. Note also that the inner loop $\zeta_d \doteq 0.25$ restricts the usable outer-loop lead.

By adding inner-loop lead, the control situation is improved for the attitude loop. These improvements are summarized below.

1. Increases ω_d' and extends the K/s region in the position loop.
2. Improves damping so that there is no decrease in ω_{c_x} if more outer-loop lead is added $(d|G(j\omega)|/d\omega \leq 0)$.

Increasing the inner-loop lead beyond $1/\omega_d$ (i.e., to $1/T_{L_\varphi} = 0.5$) does not help particularly for the following reasons:

1. Closed-loop damping is not improved.
2. No significant increase in ω_{c_φ} due to the fact that the inner-loop lead is nearly cancelled by the pilot's $e^{-\tau s}$ pole.

3. Outer-loop lead of 0.7 → 1.0 is still necessary because of large K/s^2 region.

4. The very low dc gain results in poor error control.

As a final consideration for the attitude feedback systems (Category II), we note that as attitude feedback gain K_φ is increased to bring the oscillatory mode frequency ω_d to values greater than 2 rad/sec, the pilot may close only the position loop. Thus the piloting task is reduced to a single-loop position control function. Typical position closure for this situation is shown in Figs. A-21 and A-22 when ω_d is 3.25 and 5 rad/sec, respectively. In each case moderate lateral position lead near 1 rad/sec is needed to provide a stable crossover near 1 rad/sec. Leads greater than this (i.e., lower frequency) expand the K/s-like region and increase the phase margin and potential crossover frequencies. With the stabilized aircraft, a damping equal to or greater than 0.3 keeps the ω_d peak from reducing the outer-loop gain margin (i.e., $d|G(j\omega)|/d\omega < 0$) and allows the pilot to use leads greater than 1 rad/sec in the position-loop closure.

In summary, for attitude system, Category II, we find that:

1. Lead compensation greater than $1/\omega_d$ (i.e., $1/T_{L\varphi} < \omega_d$) does not significantly improve the pilot's performance in terms of regulatory control of disturbances. Thus the lead reversal characteristic exhibited in the unacceptable closures of conventional VTOL dynamics is somewhat apparent for the low frequency attitude systems since the broadband gain region is reduced as lead in increased beyond $\omega_d = 1/T_{L\varphi}$.

2. Closed-loop damping of the attitude loop must be greater than 0.3 to prevent outer-loop limitation. This is primarily due to the fact that the damping of the closed-loop pilot/vehicle system is generally less than that of the basic airframe (see sketch).

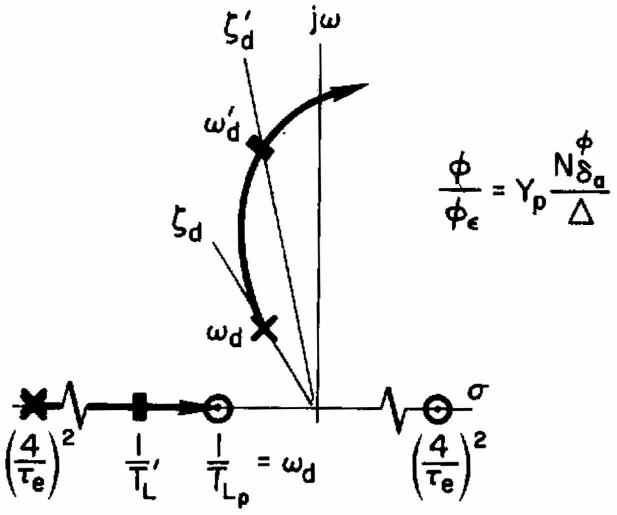
ζ_d'
$j\omega$
ω_d'
ζ_d
ω_d
σ
$\frac{\phi}{\phi_\epsilon} = Y_p \frac{N^{\phi}_{\delta_a}}{\Delta}$
$\left(\frac{4}{\tau_e}\right)^2$
$\frac{1}{T_L'}$
$\frac{1}{T_{L_p}} = \omega_d$
$\left(\frac{4}{\tau_e}\right)^2$

Translational Rate Augmented Dynamics. The typical closures with the translational rate augmented dynamics are shown in Figs. A-23 through A-26. The closures considered include both satisfactory and unacceptable dynamics.

Satisfactory Conditions. The closure for the configuration noted as satisfactory ($3 \leq PR \leq 4$) is shown in Figs. A-23 and A-24. Basically the vehicle open-loop features are distinguished by the stable, oscillatory mode. The attitude closure in Fig. A-23 illustrates the need for moderate pilot lead compensation to insure an inner-loop crossover frequency greater than 2 rad/sec. Since the dynamics resemble low frequency attitude systems (i.e., $1/T_{\varphi_1} \doteq 1/T_R$), this lead compensation by the pilot tends to partially cancel the adverse low frequency phase contribution of the lateral oscillatory mode, ω_d (i.e., $1/T_{L_\varphi} \doteq \omega_d$). Thus, insofar as attitude compensation is concerned, it appears that the pilot can follow the same stratagem for control as normally used with conventional VTOL or helicopter characteristics. Except for the low broadband gain region (below ω_{c_φ}) the attitude closures are nominally good from the pilot compensation viewpoint. The low gain features result in poor attitude performance under gust conditions. Likewise, in the position loop the closure is again gain margin limited due to peaking of ω_d' in the region of 2 rad/sec (see Fig. 24).

Unacceptable Closures. The unacceptable closures of Figs. A-25 and A-26 exhibit the same unacceptable characteristics as have been noted for the conventional VTOL dynamics. However, these closures are included for reference so that a complete cross section of closure situations could be illustrated. Note that in the position-loop closure (e.g., see Fig. A-26) the bandpass is severely limited by the closed-loop lateral oscillatory mode damping. In fact, the deterioration in pilot rating clearly follows the reduction in crossover frequency, ω_{c_x}, which in turn is closely related to the effective closed-loop damping, $\zeta'\omega'$, of the lateral oscillatory mode.

GUST REGULATORY CONTROL

One of the main factors affecting the precision of pilot control in hover is the level of airframe gust sensitivity. The two aerodynamic stability derivatives of importance are the lateral stability, L_v, and the side force parameter, Y_v. The extreme values of these parameters tested by A'Harrah (Ref. 7) in combination with the conventional dynamic range tested by Breul* (Ref. 4) provide a broad range of examples from which to illustrate the complex effects of these parameters on pilot compensation and closed-loop performance. The consequences of various levels of these derivatives are illustrated in the following by their effect on the closed-loop rms (i.e., root mean square) error, σ_φ, σ_y, and σ_δ.

---

*Note the parameter ranges tested by Vinje and Miller in Ref. 2 are essentially equivalent to Ref. 4 data. Thus we infer the same parameter coverage by citing the Ref. 4 results.

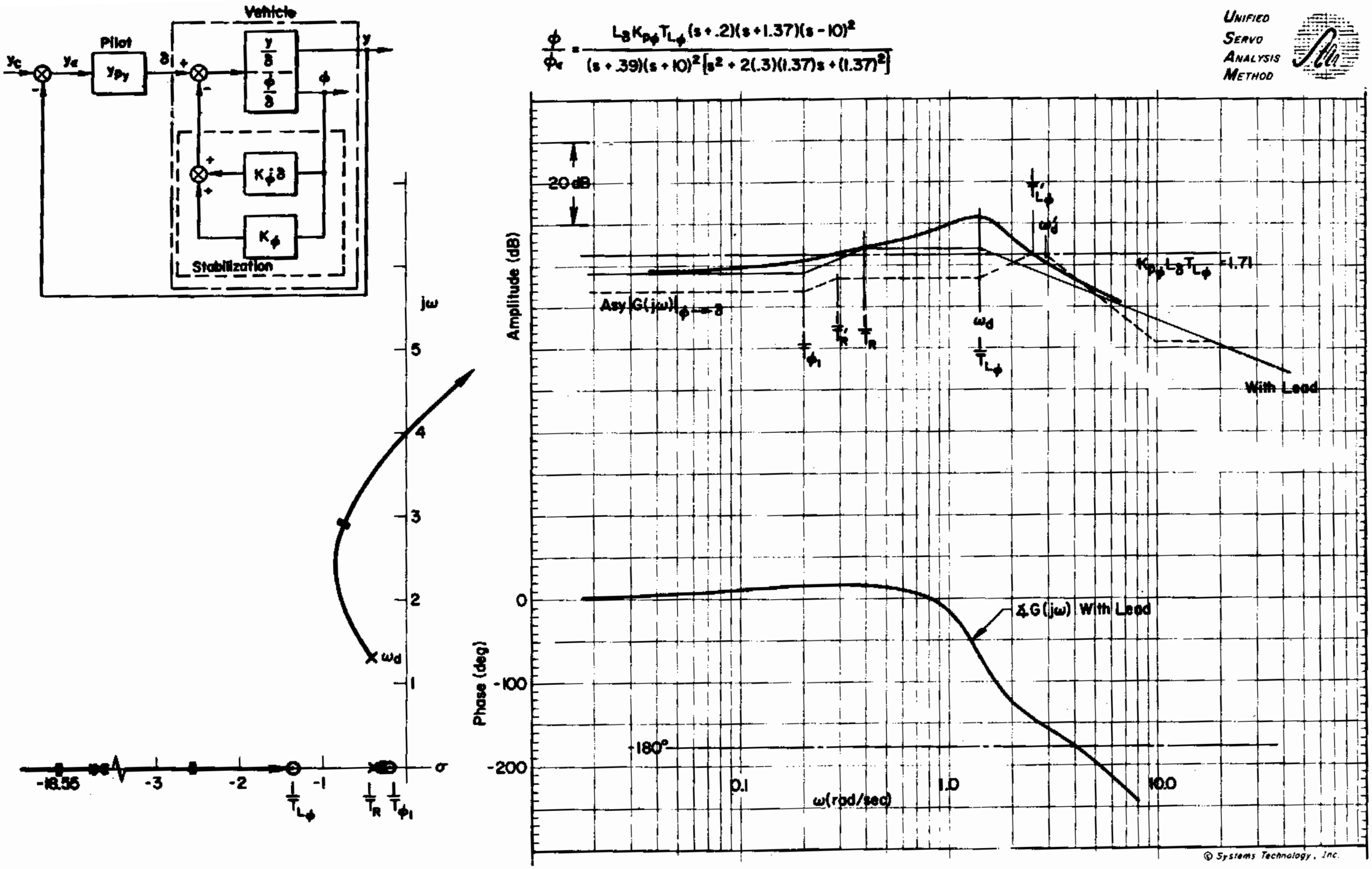

Figure A-17. Roll Attitude Control for Category II System, $1/T_E < 1/T_R$; $\phi \rightarrow \delta_a$

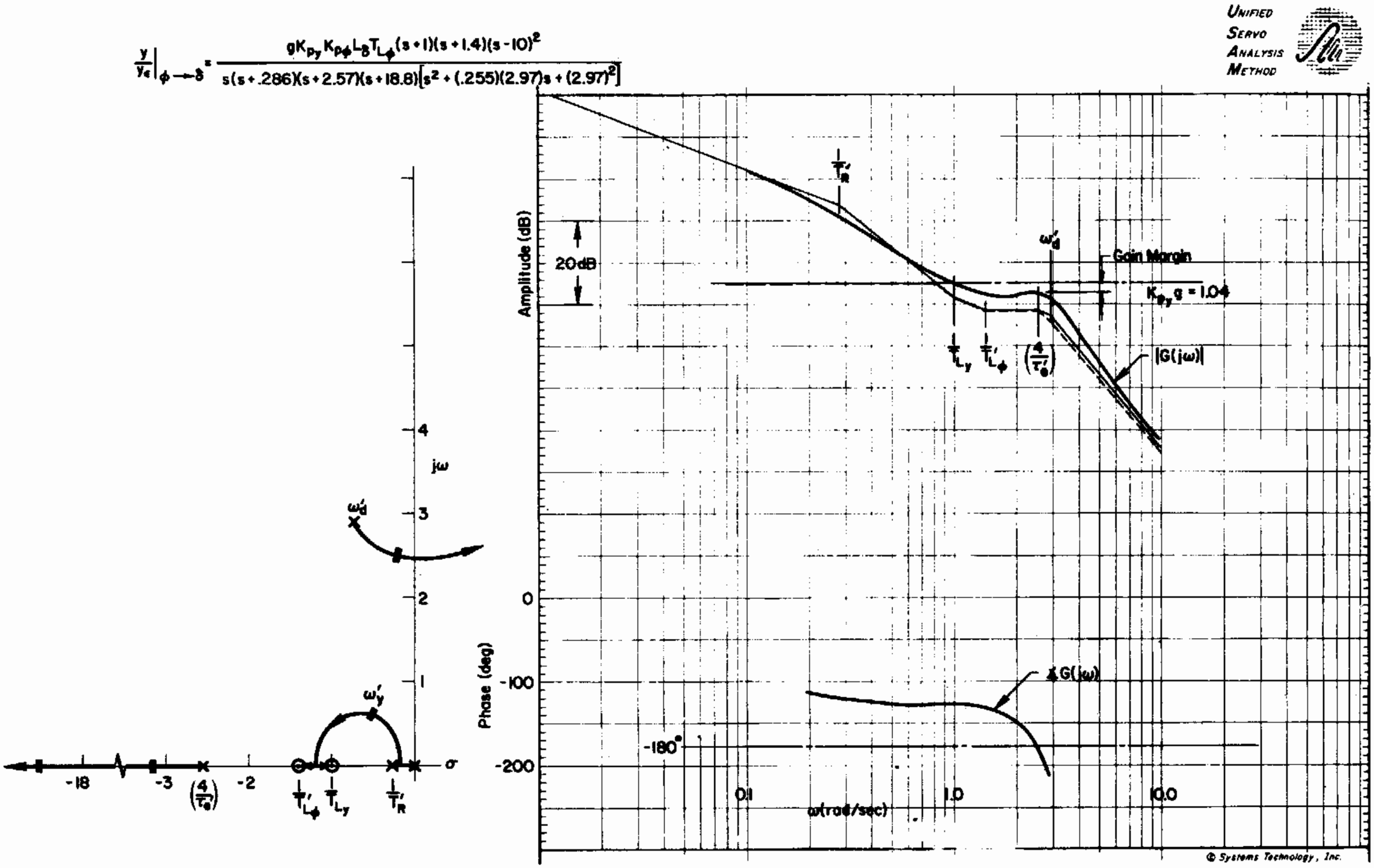

$$\left.\frac{y}{y_\epsilon}\right|_{\phi \to \delta} = \frac{gK_{p_y}K_{p_\phi}L_\delta T_{L_\phi}(s+1)(s+1.4)(s-10)^2}{s(s+.286)(s+2.57)(s+18.8)\left[s^2+(.255)(2.97)s+(2.97)^2\right]}$$

Figure A-18. Lateral Position Control for Category II System, $1/T_E > 1/T_R$; y, $\varphi \longrightarrow \delta_a$

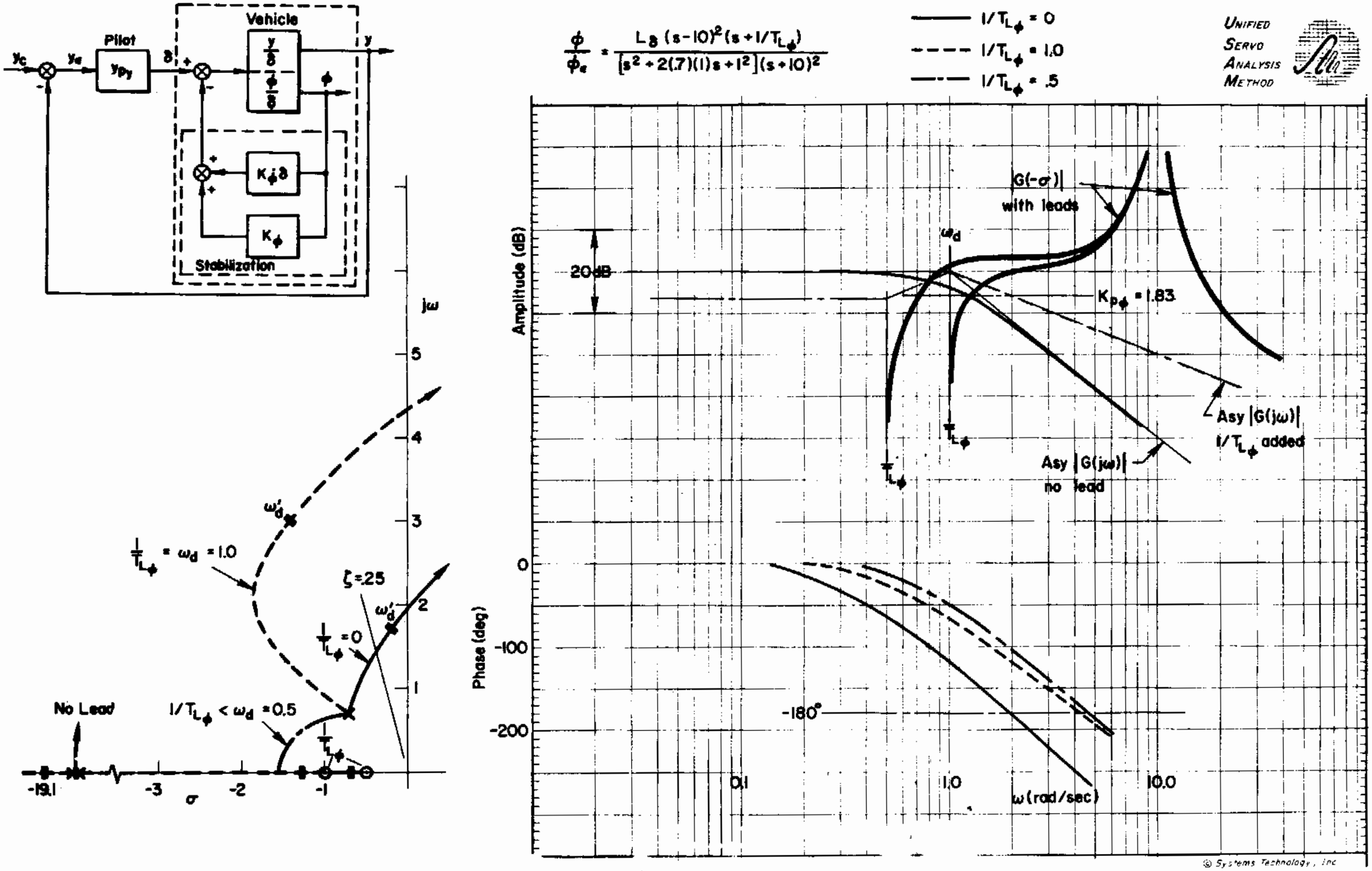

Figure A-19. Roll Attitude Control of Category II System for Various Pilot Compensation Levels

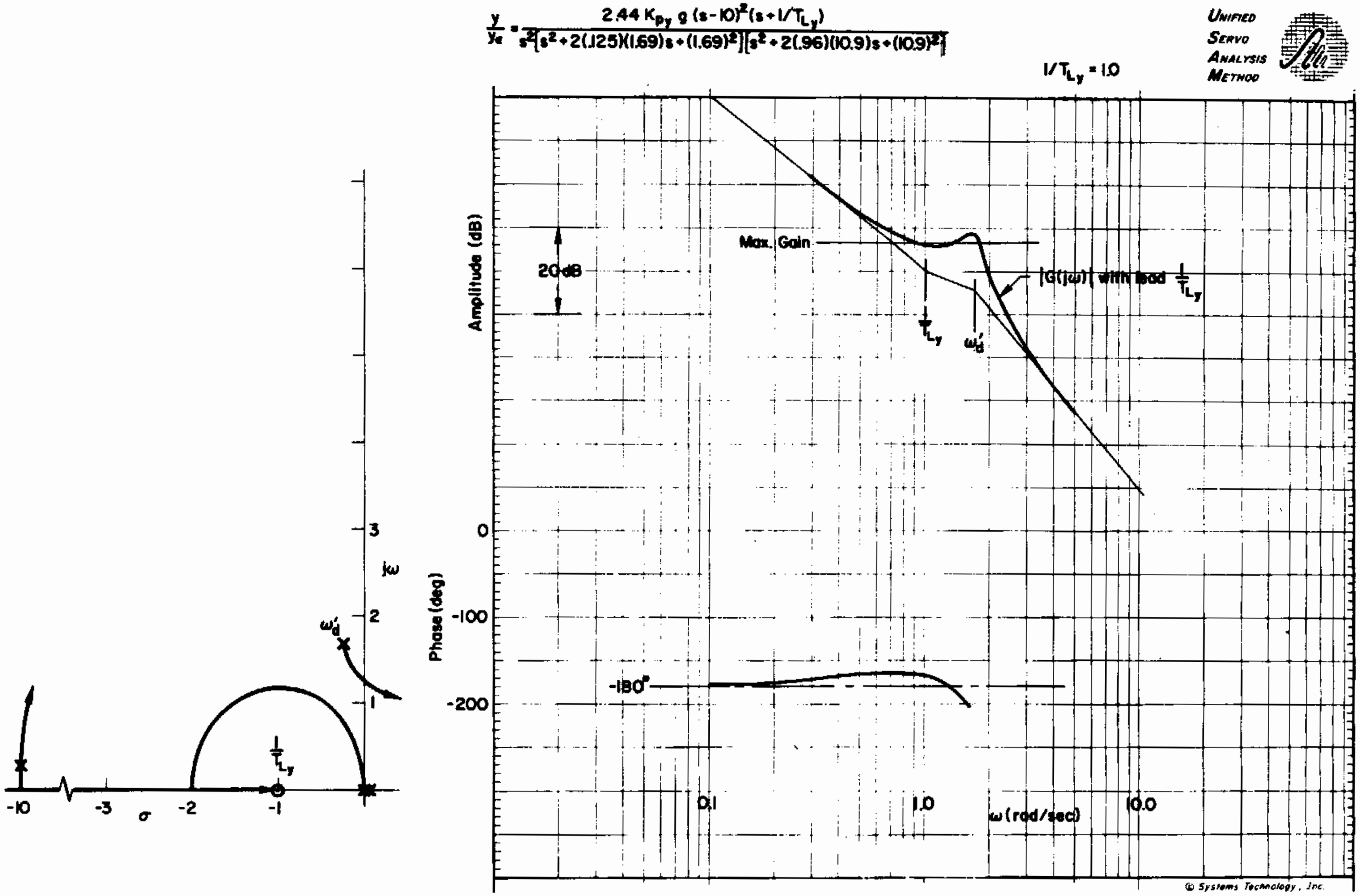

Figure A-20. Lateral Position Loop Closure for Category II System; $y, \varphi \longrightarrow \delta_a$

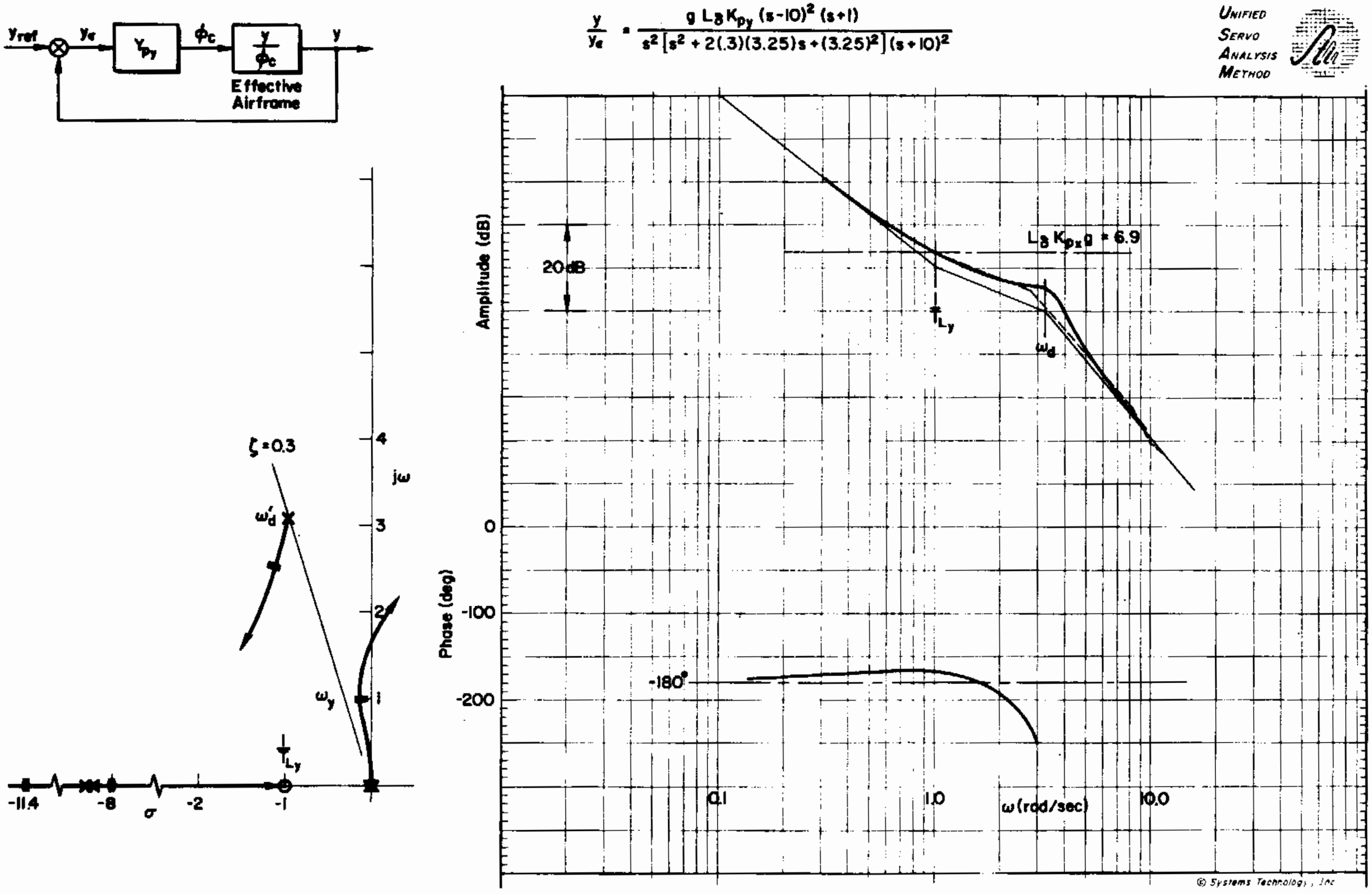

Figure A-21. Position Closure with Attitude Augmentation System, $1/T_E > 1/T_R$, $\omega_d \geq 2.0$ rad/sec, $y \longrightarrow \varphi_c$

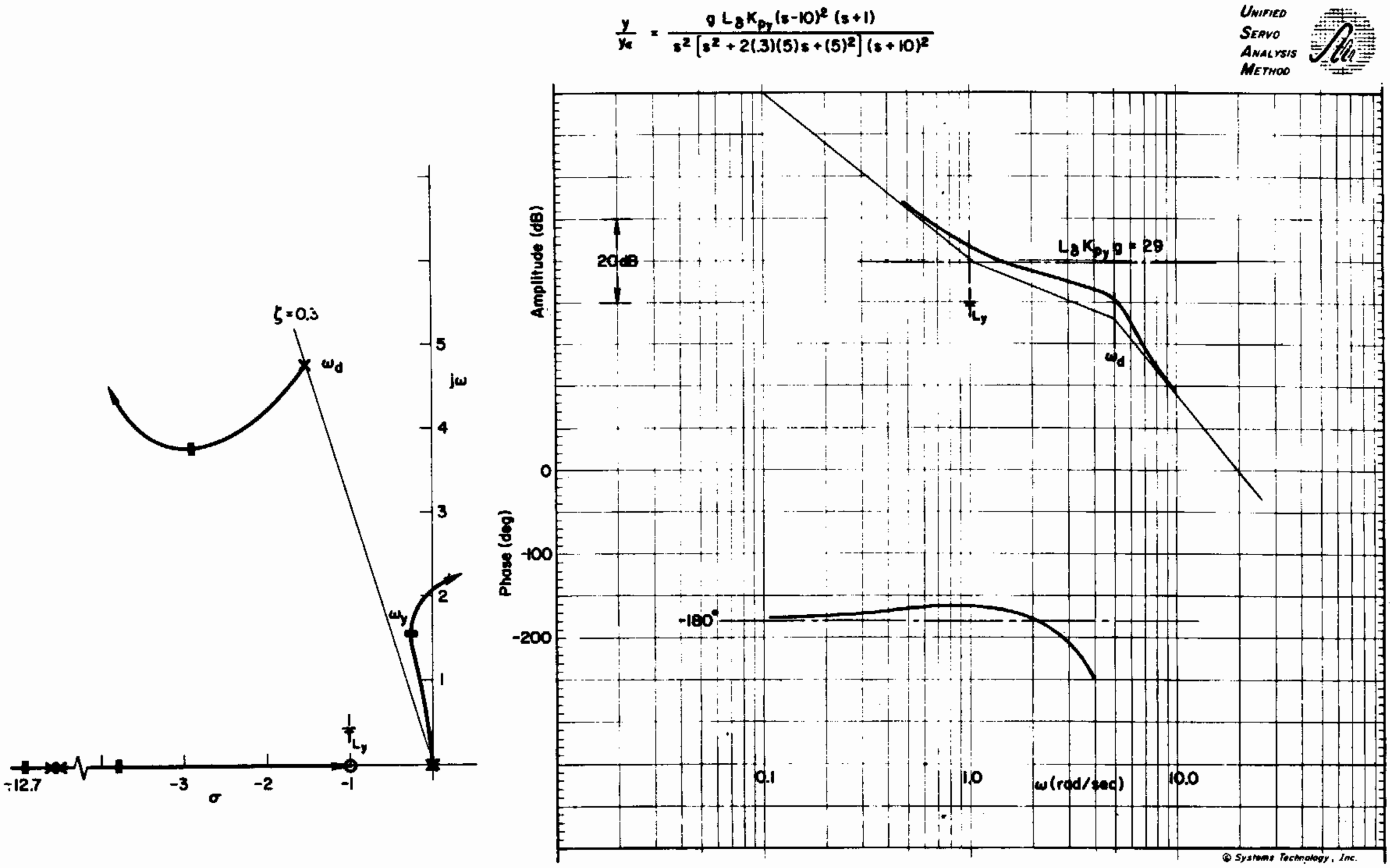

Figure A-22. Position Closure with Attitude Augmentation, $1/T_E > 1/T_R$, $\omega_d \geq 2.0$ rad/sec, $y \rightarrow \delta_a$

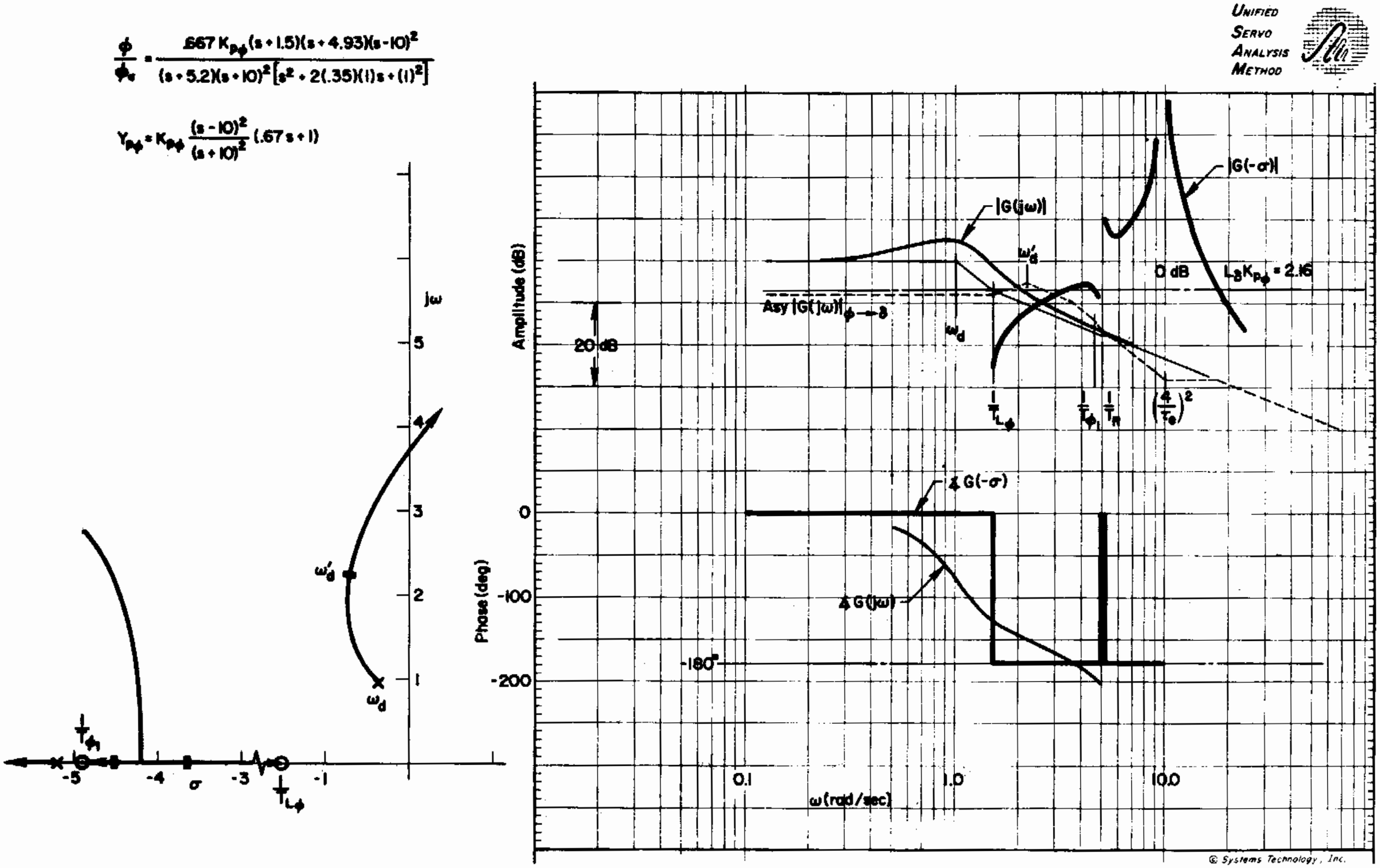

$$\frac{\phi}{\phi_c} = \frac{.667\,K_{p_\phi}(s+1.5)(s+4.93)(s-10)^2}{(s+5.2)(s+10)^2\left[s^2+2(.35)(1)s+(1)^2\right]}$$

$$Y_{p_\phi} = K_{p_\phi}\frac{(s-10)^2}{(s+10)^2}(.67s+1)$$

Figure A-23. Roll Attitude Control, Translational Augmentation; Satisfactory Dynamics, $\varphi \to \delta_a$

$$\frac{y}{y_e} = \frac{.667 K_{p_\phi} K_{p_y} (s+1.5)(s-10)^2 g}{(s)(s+3.62)(s+4.54)(s+17.79)\left[s^2+2(.297)(2.328)s+2.328^2\right]}$$

$$Y_{p_\phi} Y_{p_y} = K_{p_y} K_{p_\phi} (.667s+1) \frac{(s-10)^2}{(s+10)^2}$$

UNIFIED SERVO ANALYSIS METHOD

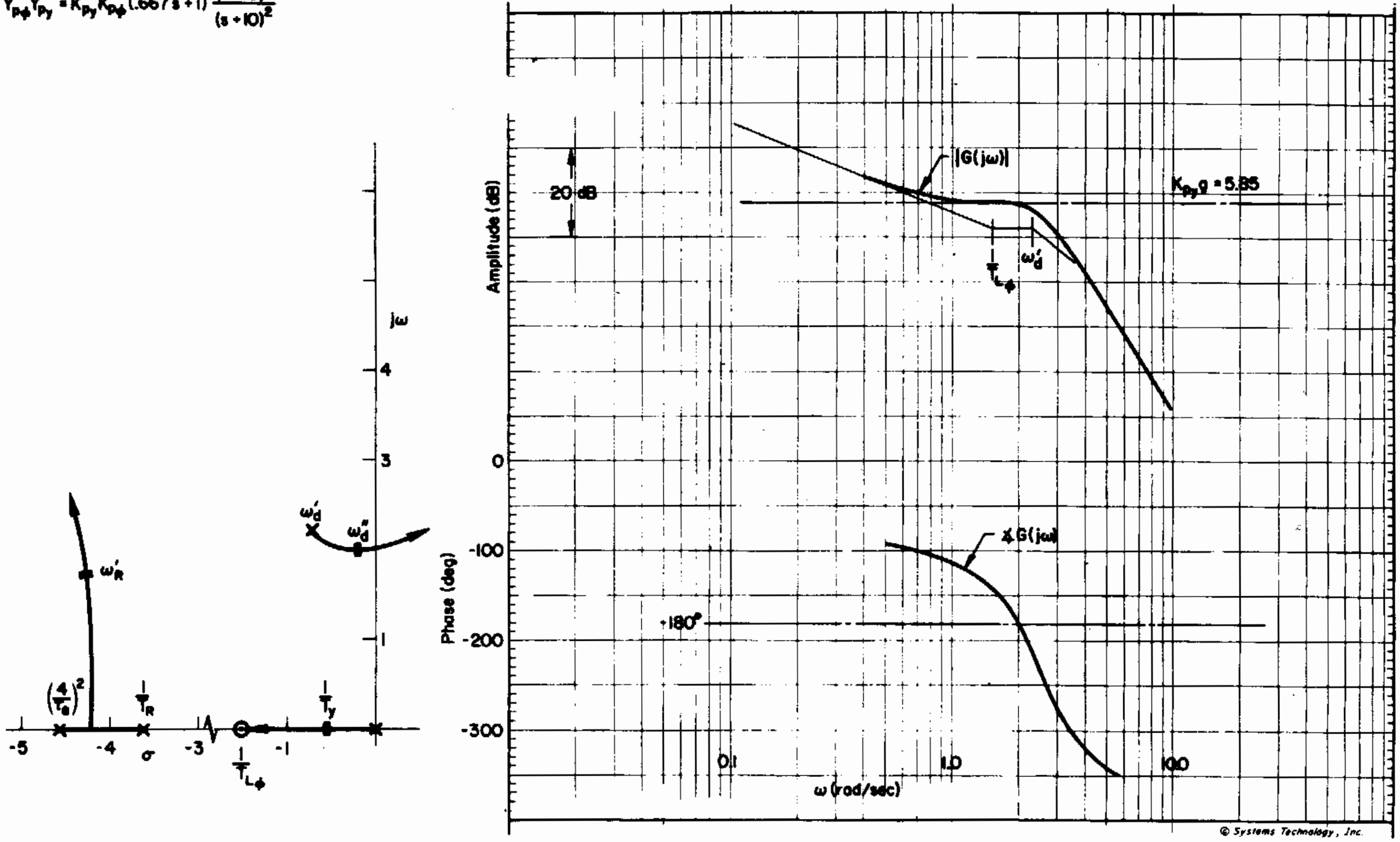

Figure A-24. Lateral Position Control, Translational Augmentation, Satisfactory Dynamics, y, Φ → δ_a

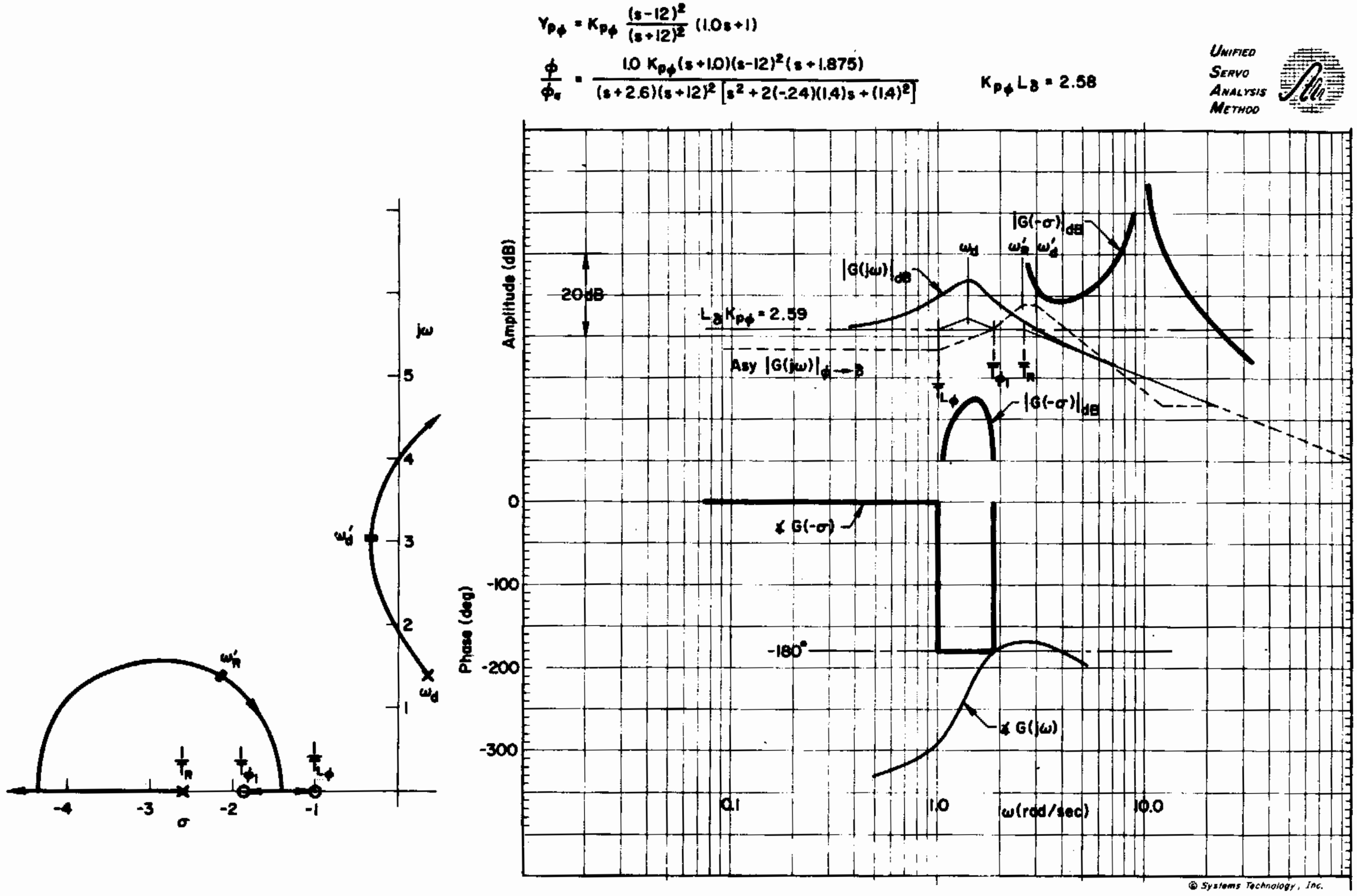

$$Y_{p_\phi} = K_{p_\phi} \frac{(s-12)^2}{(s+12)^2}(1.0s+1)$$

$$\frac{\phi}{\phi_e} = \frac{1.0\,K_{p_\phi}(s+1.0)(s-12)^2(s+1.875)}{(s+2.6)(s+12)^2\left[s^2+2(-.24)(1.4)s+(1.4)^2\right]}$$

$K_{p_\phi} L_\delta = 2.58$

Figure A-25. Roll Attitude Control Translational Augmentation, Unacceptable Dynamics, $\varphi \rightarrow \delta_a$

Loop closed with $1/T_{I_y} = 1.0$ 7

$$\frac{y}{y_c}\bigg|_{\phi \to \delta} = \frac{(3.23)(2.59)(s+1)(s-12)^2}{(s+1)(s+2.61)(s+23.5)[.21\,;3.1][.32\,;1.45]}$$

$$\left[s^2 + 2\zeta_i \omega_i s + \omega_i^2\right] \Rightarrow \left[\zeta_i\,;\omega_i\right]$$

$$\frac{y}{y_a} = K_{p_\phi} K_{p_y} (1.0s+1) \frac{(s-12)^2}{(s+12)^2}$$

$$Y_c' Y_{p_y} = \frac{1.0\, K_{p_\phi} K_{p_y} (s+1)(s-12)^2 g}{(s)(s+23.56)\left[s^2 + 2(.83)(2.54)s + (2.54)^2\right]\left[s^2 + 2(.11)(3.06)s + (3.06)^2\right]}$$

UNIFIED
SERVO
ANALYSIS
METHOD

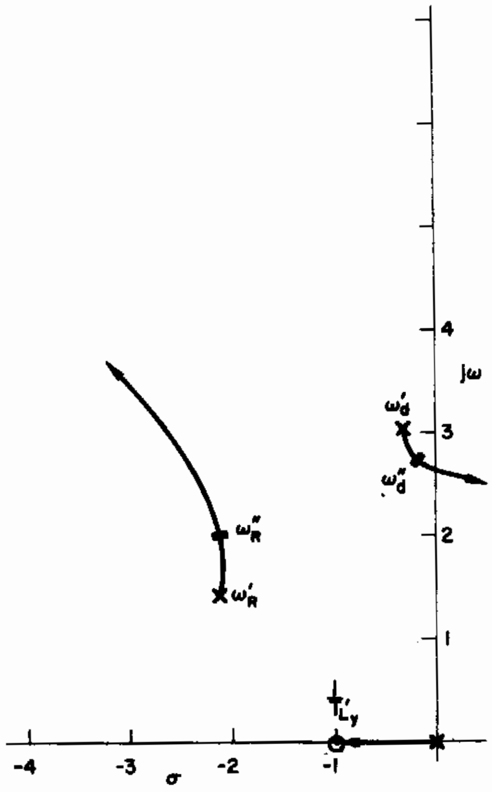

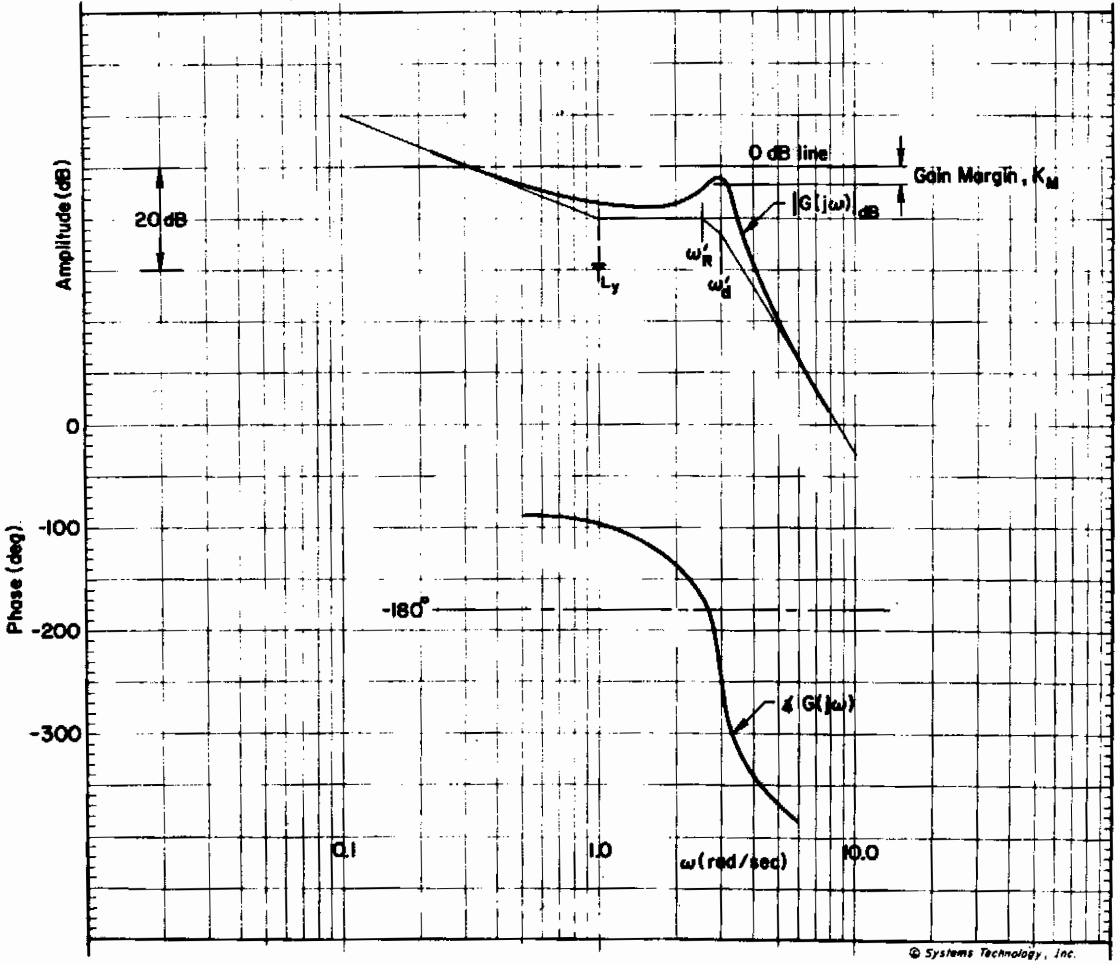

Figure A-26. Lateral Position Control, Translational Augmentation, Unacceptable Dynamics, y, φ → δ_a

It should be recognized that the upper level of the derivatives (i.e., $L_v = 0.16$ and $Y_v \doteq 1.0$) from Ref. 7 are well above the level considered aerodynamically feasible for conventional VTOL's. Furthermore, as noted previously, the configurations are classified as conventional simply because the dynamic characteristics may be approximated in the conventional manner (i.e., $1/T_R \doteq L_p$ and $\omega_d \doteq L_v g/L_p$). To some extent one may question the choice of extremes, however, such gross levels do serve to dramatize otherwise subtle closed-loop control differences which might well be overlooked. Once we identify the gross effect, it is far easier to trace the interaction sequence as the multiloop closures are made. Detailed aspects of the closures showing the effects of the two derivatives are considered generically later in these discussions.

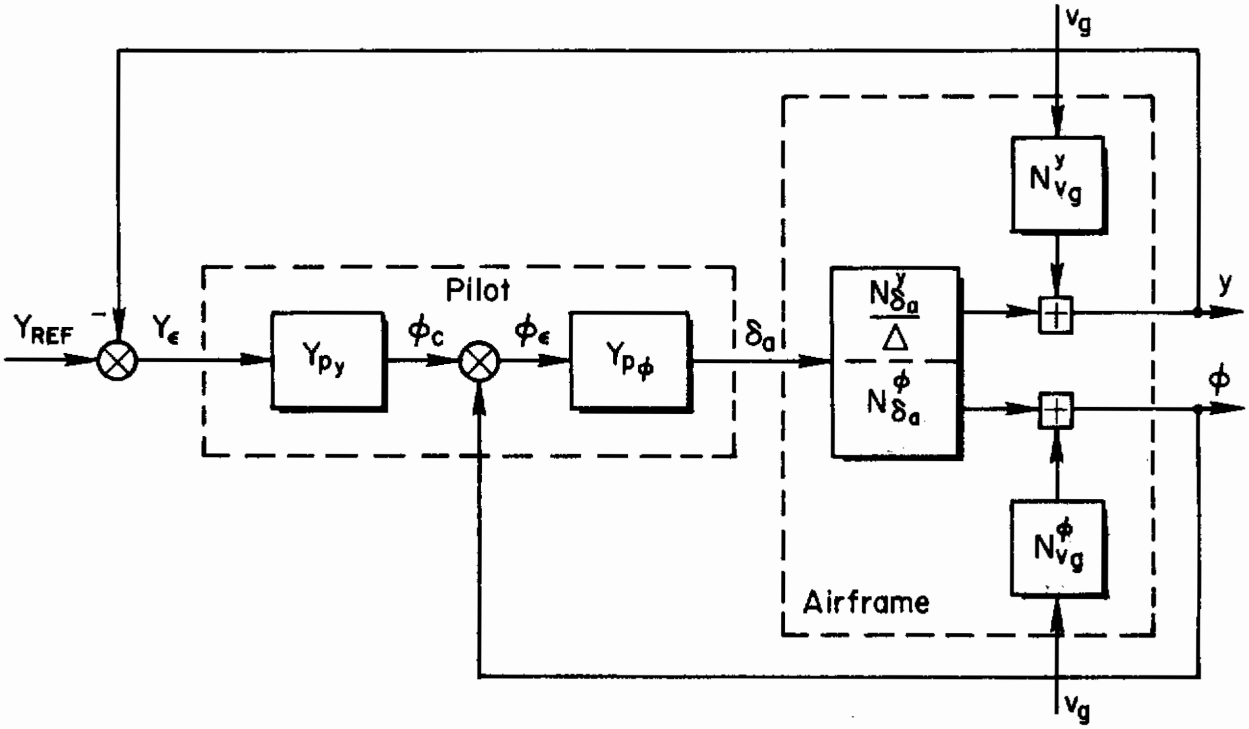

As the starting point, it is worthwhile reviewing the steady-state expressions (i.e., trim values or dc levels) for the rms error which are defined by the level of Y_v and L_v. For example, from the block diagram shown in the sketch the closed-loop expressions are

Roll Attitude

$$\frac{\varphi}{v_g} = \frac{N^{\varphi''}_{v_g}}{\Delta''} = \frac{N^{\varphi}_{v_g} + Y_y Y_\varphi N^{\varphi\,y}_{v_g\delta}}{\Delta + Y_\varphi N^{\varphi}_{\delta} + Y_y Y_\varphi N^{y}_{\delta}}$$

where
$$N^{\varphi}_{v_g} = -L_v s$$

$$N^{\varphi\,y}_{v_g\delta_a} = \frac{Y_v L_\delta}{s}$$

$$N^{\varphi}_{\delta} = L_\delta\left(s - Y_v + \frac{L_v Y_\delta}{L_\delta}\right)$$

$$N^{y}_{\delta} = \frac{Y_\delta}{s}\left(s^2 - L_p s + g\frac{L_\delta}{Y_\delta}\right)$$

$$N^{y}_{v_g} = -\frac{Y_v}{s}\left(s^2 - L_p s + g\frac{L_v}{Y_v}\right)$$

$$N^{y\,\varphi}_{v_g\delta} = \frac{-Y_v L_\delta}{s}$$

$$\Delta = s(s - Y_v)(s - L_p) - gL_v = 0$$

$$\frac{\varphi}{v_g} = \frac{-L_v s + Y_y Y_\varphi\left(\frac{Y_v L_\delta}{s}\right)}{s(s - Y_v)(s - L_p) - gL_v + Y_\varphi L_\delta\left(s - Y_v + \frac{L_v Y_\delta}{L_\delta}\right) + Y_y Y_\varphi\left[\frac{Y_\delta}{s}\left(s^2 - L_p s + \frac{gL_\delta}{Y_\delta}\right)\right]}$$

when s → 0. Therefore

$$\left.\frac{\varphi}{v_g}\right|_{ss} \doteq \frac{Y_v}{g}$$

Control Input

$$\frac{\delta}{v_g} = \frac{N^{\delta''}_{v_g}}{\Delta''} = \frac{-Y_\varphi\left(N^{\varphi}_{v_g} + Y_y N^{y}_{v_g}\right)}{\Delta''}$$

$$= \frac{-Y_\varphi\left[-L_v s - \frac{Y_y Y_v}{s}\left(s^2 - L_p s + \frac{gL_v}{Y_v}\right)\right]}{s(s - Y_v)(s - L_p) - gL_v + Y_\varphi L_\delta\left(s - Y_v + \frac{L_v Y_\delta}{L_\delta}\right) + Y_y Y_\varphi\left[\frac{Y_\delta}{s}\left(s^2 - L_p s + \frac{gL_\delta}{Y_\delta}\right)\right]}$$

when s → 0

$$\left.\frac{\delta}{v_g}\right|_{ss} = \frac{-K_{p_\varphi}(K_{p_y} g L_v)}{K_{p_y} K_{p_\varphi} g L_\delta}$$

Therefore,

$$\left.\frac{\delta}{v_g}\right|_{ss} = \frac{-L_v}{L_\delta}$$

However, we note that the lateral position trim level is imminently tied to the pilot's compensation level, that is

Lateral Position

$$\frac{Y}{v_g} = \frac{N_{v_g}^{y''}}{\Delta''} = \frac{N_{v_g}^{y} + Y_\varphi N_{v_g \delta_a}^{y \ \varphi}}{\Delta + Y_\varphi N_\delta^\varphi + Y_y Y_\varphi N_\delta^y}$$

$$= \frac{\frac{-Y_v}{s}(s^2 - L_p s + \frac{g L_v}{Y_v}) + Y_\varphi(\frac{-Y_v L_\delta}{s})}{s(s - Y_v)(s - L_p) - g L_v + Y_\varphi L_\delta (s - Y_v + \frac{L_v Y_\delta}{L_\delta}) + Y_y Y_\varphi \frac{Y_\delta}{s}(s^2 - L_p s + \frac{g L_\delta}{Y_\delta})}$$

when $s \rightarrow 0$

$$\left.\frac{Y}{v_g}\right|_{ss} = \frac{-g L_v - Y_\varphi Y_v L_\delta}{Y_y Y_\varphi g L_\delta}$$

Therefore,

$$\left.\frac{Y}{v_g}\right|_{ss} = -\left(\frac{g L_v + K_{p_\varphi} Y_v L_\delta}{K_{p_y} K_{p_\varphi} g L_\delta}\right)$$

and, in fact, the steady-state level, $Y/v_g|_{ss}$, is inversely proportional to the pilot's position-loop gain, K_{p_y}.

Gust Response Characteristics

Conventional Dynamics, $Y_v \doteq 0$. Typical roll attitude gust response expressions for the conventional dynamics (Config. 1-5, Table A-I) are summarized below and discussed in the following paragraphs. The transfer functions are written in shortened form as follows:

$$[s^2 + 2\zeta_i \omega_i s + \omega_i^2] \rightarrow [\zeta_i , \omega_i]$$

$$A(s + a) \rightarrow A(a)$$

With no outer-loop lead

Case 1

$$\frac{\varphi}{v_g} = \frac{0.01(0.142)(-0.142)[0.998, 10.01]}{(2.55)(21.65)[0.18, 0.191][0.165, 3.66]}$$

$$\frac{Y}{v_g} = \frac{0.037(3.507)(21.51)[0.045, 4.625]}{(2.55)(21.65)[0.18, 0.191][0.165, 3.66]}$$

Case 3

$$\frac{\varphi}{v_g} = \frac{0.03(0.135)(-0.132)[0.999, 10.0]}{(3.817)(21.51)[0.273, 0.206][0.169, 3.63]}$$

$$\frac{Y}{v_g} = \frac{0.037(5.037)(21.12)[0.042, 5.903]}{(3.817)(21.51)[0.273, 0.206][0.169, 3.63]}$$

Case 5

$$\frac{\varphi}{v_g} = \frac{0.04(0.171)(-0.177)[0.997, 10.024]}{(1.703)(20.4)[0.273, 0.559][0.212, 3.12]}$$

$$\frac{Y}{v_g} = \frac{0.037(4.565)(19.86)[-0.057, 6.55]}{(1.703)(20.4)[0.273, 0.559][0.212, 3.12]}$$

With outer-loop lead

Case 1 $(1/T_{L_y} = 1)$

$$\frac{\varphi}{v_g} = \frac{0.01(0.594)(-1.37)(4.74)(35.66)}{(2.55)(21.35)[0.518, 1.291][0.04, 2.916]}$$

$$\frac{Y}{v_g} = \frac{0.037(3.507)(21.51)[0.045, 4.625]}{(2.55)(21.35)[0.518, 1.291][0.04, 2.916]}$$

Case 5 $(1/T_{L_y} = 2.5)$

$$\frac{\varphi}{v_g} = \frac{0.04(0.401)(-0.522)(7.26)(14.74)}{(1.703)(20.34)[0.269, 0.937][0.206, 2.89]}$$

$$\frac{Y}{v_g} = \frac{0.037(4.57)(19.86)[-0.057, 6.55]}{(1.703)(20.34)[0.269, 0.937][0.206, 2.89]}$$

The closed-loop regulatory control was evaluated, assuming a random gust represented as the output of a linear filter whose input is white noise (see Ref. 1). The linear filter was of the form

$$v_g = \frac{2\omega_g \sigma_{v_g}}{s + \omega_g}$$

where $\omega_g = 0.5$ rad/sec. Values of the standard deviation for roll attitude and lateral displacement were calculated based on a unity σ_{v_g}.

No Lead in Position Loop. The roll attitude gust transfer function asymptotes for a satisfactory and unacceptable case are shown in Fig. A-27. The most significant differences between systems occur in the frequency region 0.1 rad/sec to 1 rad/sec. The dynamic characteristics in this region are dominated by the low frequency complex pair of poles which resulted from the position-loop closure. For the satisfactory case these poles have a relatively low break frequency which is close to the break frequencies of the real zeros of the gust transfer function. This results in relatively low gains in the critical frequency region, giving rise to the low values of attitude error. For the unsatisfactory case the break frequencies of the dominant poles and zeros are more widely separated, resulting in higher gains in the critical frequency region, giving rise to larger values of attitude error. The corresponding roll attitude power spectrum plot is shown in Fig. A-28. It is apparent that for the satisfactory case the attitude response σ_φ, is small, and the energy is located at much lower frequencies than for the unacceptable case. For the unacceptable case, the major portion of the energy is located in the crossover frequency region of the position loop, $\omega_{c_y} \doteq 1$ rad/sec. This may have a significant effect on pilot opinion since, as the effective bandpass of the input disturbance approaches crossover frequency values, then the pilot may have difficulty recognizing error signals and controlling the vehicle.

It is evident that the location of the pole/zero combinations in the critical frequency region (0.1 to 4.0 rad/sec) is of fundamental importance in determining rms gust errors. The frequency of the dominant mode is mainly determined by the location of the real pole near the origin in the position loop; this pole is displaced farther from the origin as the frequency of the basic vehicle Dutch roll mode increases. The increase in Dutch roll frequency is a direct result of increasing the value of L_v. A large value of L_v, therefore, for the unacceptable cases is the dominant factor in producing the larger roll attitude errors.

Control input power spectrum is shown in Fig. A-29. The distinct peaks from the power spectrum curves can be associated with the dominant modes of the closed-loop system, especially for the unacceptable case.

$$N_{v_g}^{\phi''} = -L_v\left[s+(1/T''_{L_1})\right]\left[s+(1/T''_{L_2})\right]\left[s+\left(\frac{4''}{\tau_e}\right)_{num}\right]^2$$

$$\Delta'' = \left[s^2+2\zeta''_r\omega''_r s+(\omega''_r)^2\right]\left[s^2+\zeta''_d\omega''_d s+(\omega''_d)^2\right]\left[s+\left(\frac{4''}{\tau_e}\right)\right]$$

Unified
Servo
Analysis
Method

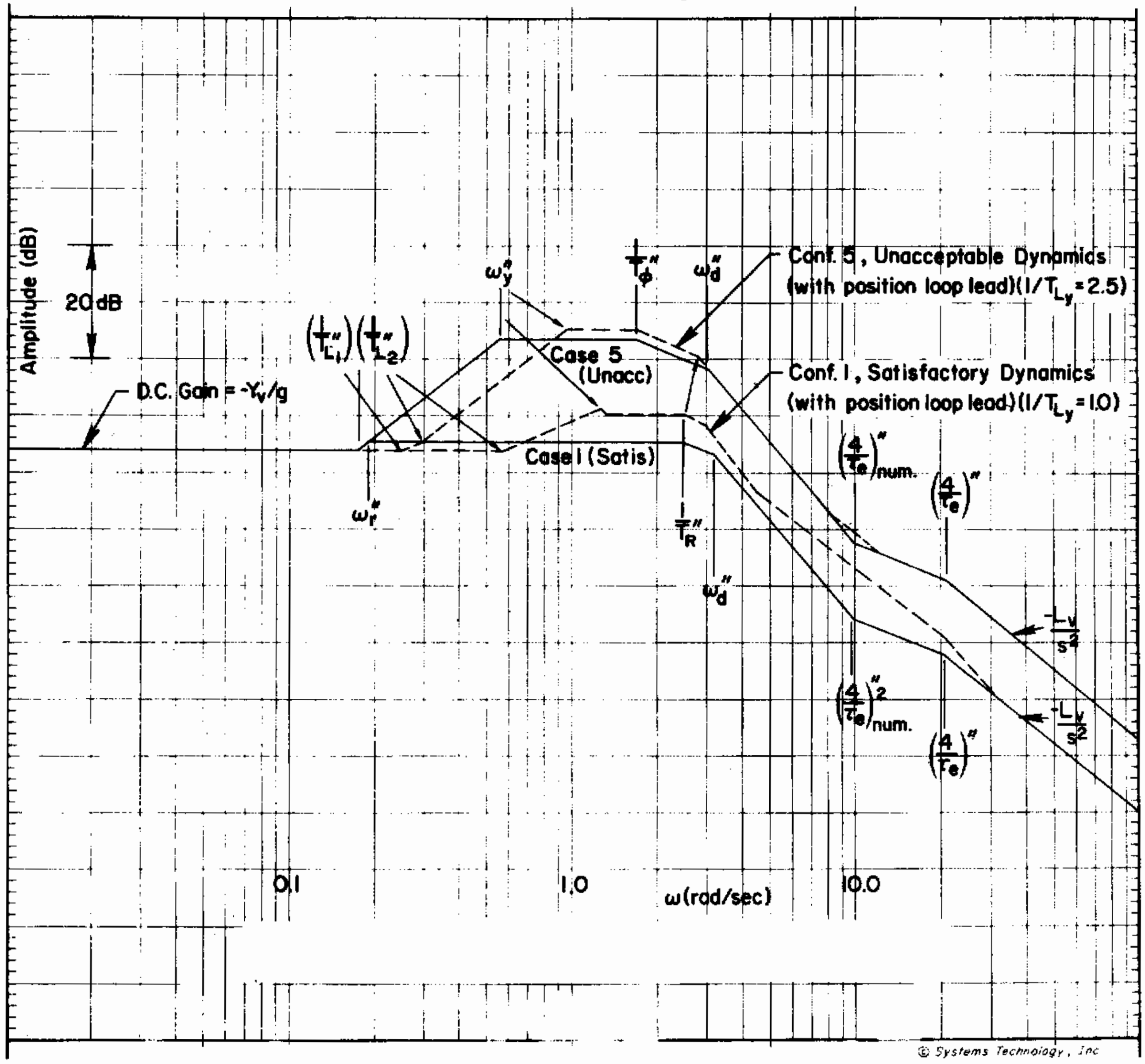

Figure A-27. Roll Attitude Gust Asymptotes $|N_{v_g}^{\varphi''}/\Delta''|$ (without Gust Filter)

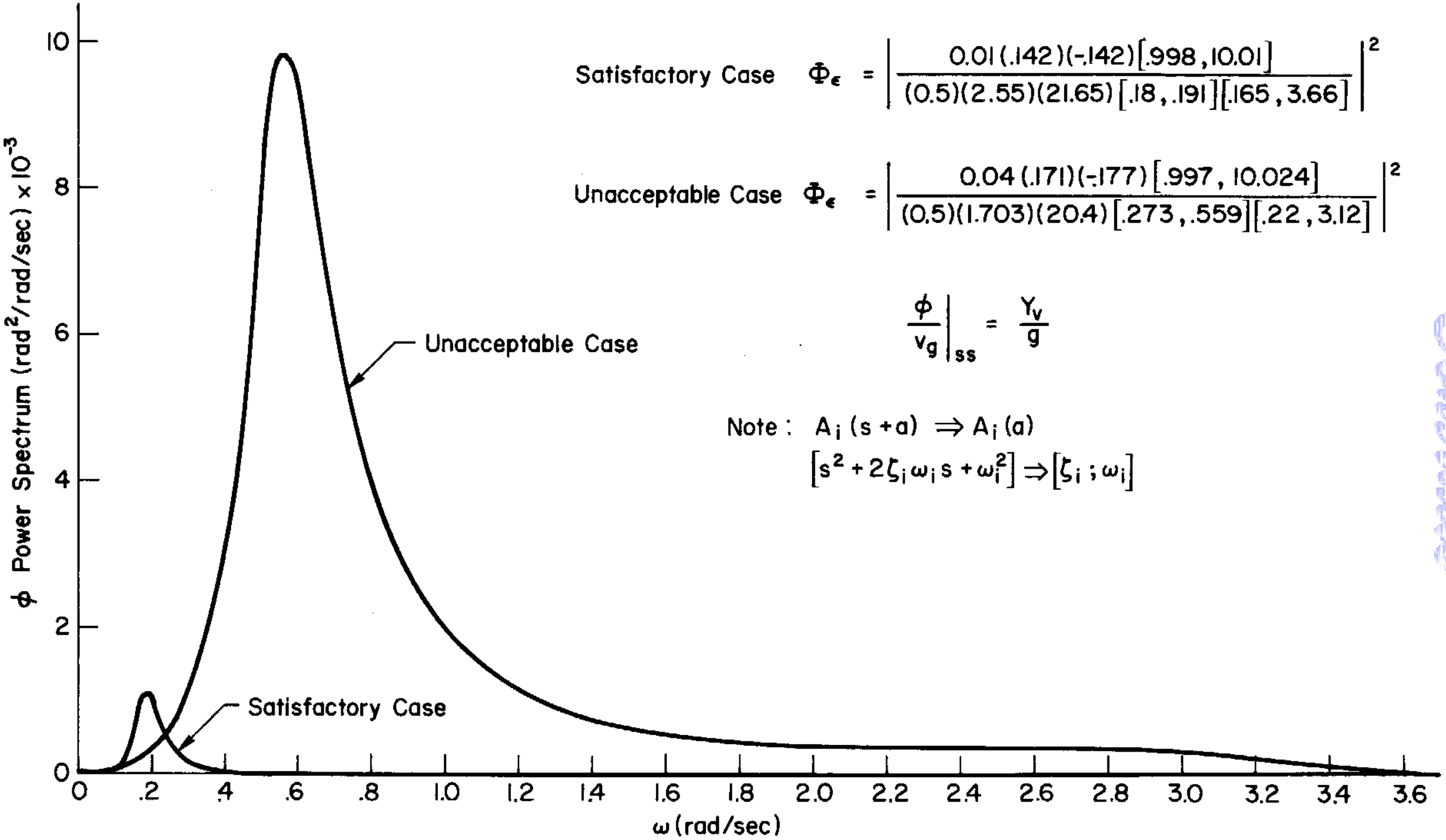

Satisfactory Case $$\Phi_\epsilon = \left| \frac{0.01(.142)(-.142)[.998, 10.01]}{(0.5)(2.55)(21.65)[.18, .191][.165, 3.66]} \right|^2$$

Unacceptable Case $$\Phi_\epsilon = \left| \frac{0.04(.171)(-.177)[.997, 10.024]}{(0.5)(1.703)(20.4)[.273, .559][.22, 3.12]} \right|^2$$

$$\left.\frac{\phi}{v_g}\right|_{ss} = \frac{Y_v}{g}$$

Note : $A_i(s+a) \Rightarrow A_i(a)$

$[s^2 + 2\zeta_i \omega_i s + \omega_i^2] \Rightarrow [\zeta_i ; \omega_i]$

Figure A-28. Roll Attitude Power Spectrum (No Position Loop Lead)

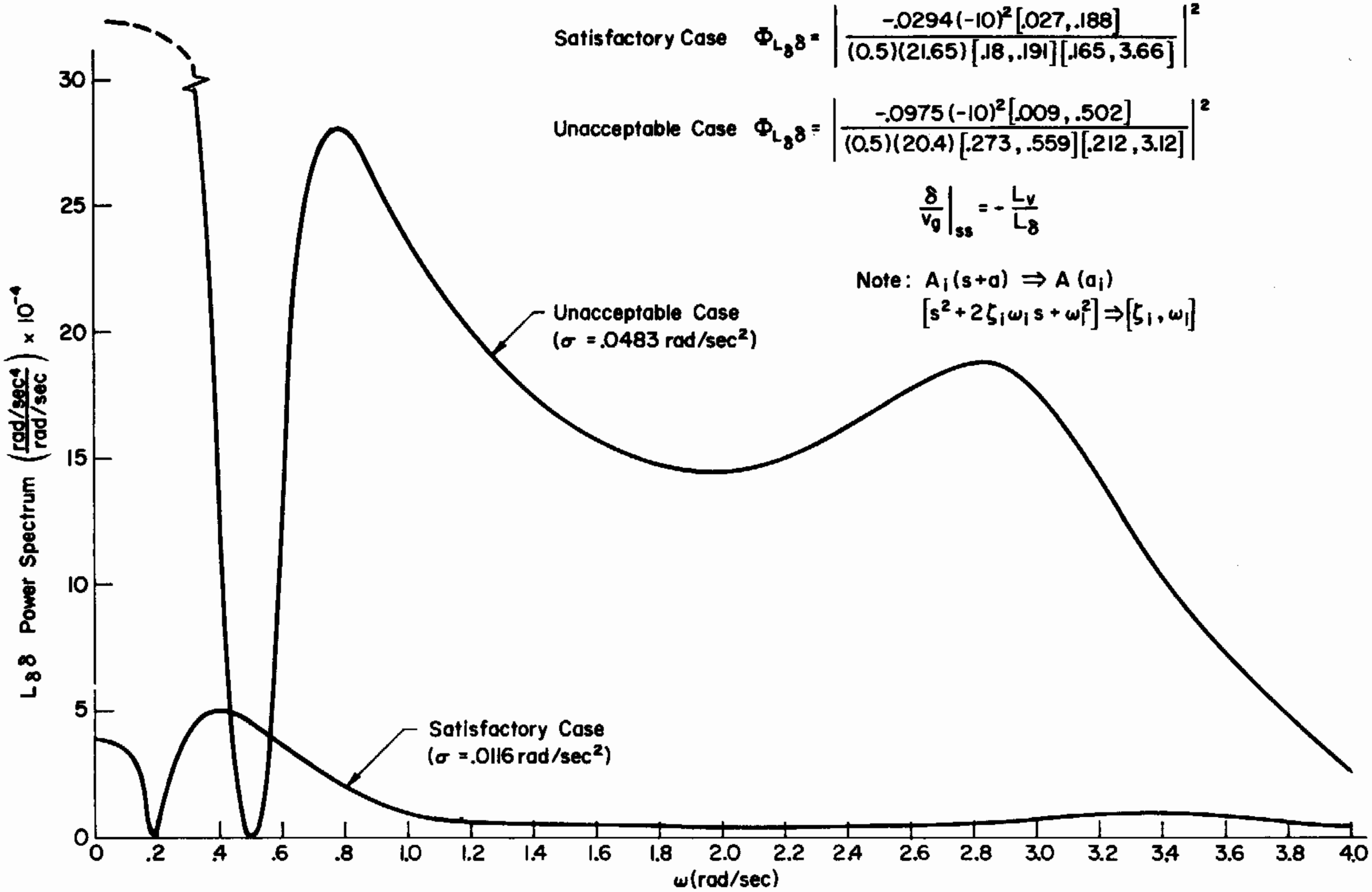

Figure A-29. Control Power Spectrum $\Phi_{L_\delta \delta}$ (No Position Loop Lead)

The gust transfer function asymptotes for lateral displacement (i.e., σ_y error) are shown in Fig. A-30. Differences between satisfactory and unacceptable cases are due to variations in steady-state gain since differences in the break frequencies are small.

Lead Compensation in Position Loop. Effect of lead in the outer loop on system gust response is to increase the attitude errors. Attitude errors have increased, especially for the satisfactory case, although the trend with pilot rating is similar to the cases without lead. Lateral displacement errors have decreased substantially, especially for the satisfactory cases. The reason why pilot lead in the position loop increases the attitude errors is evident from Fig. A-30. The dominant pair of complex poles relocate at higher frequency because of lead, giving rise to higher gain levels (i.e., larger attitude commands).

The corresponding roll attitude power spectrum with position-loop lead is shown in Fig. A-31. The major portion of the gust response energy is still located in the region of position-loop crossover frequency for the unacceptable case. For the satisfactory case, the dominant gust response region has relocated at a much higher frequency, and a larger position-loop lead is required in this case to achieve adequate crossover frequencies. This larger value of lead tends to decrease the damping of the high frequency closed-loop mode and to increase the damping of the low frequency mode. Thus the dominant portion of the roll attitude power spectrum tends to relocate at higher frequencies for the satisfactory case with position-loop lead. For the unacceptable case, the values of position-loop lead are such that the low frequency mode is still dominant in determining the shape of the roll attitude power spectrum. Smaller values of position-loop lead were required for the unacceptable case, primarily because of the higher Dutch roll frequency of the basic vehicle which tended to produce higher crossover frequencies in the position loop. This redistribution of the gust response energy indicates that the pilot has some capacity to alter the system gust response to suit his desires in the satisfactory cases, and that his capacity to do so in the unacceptable cases is severely restricted.

The control input power spectrum is shown in Fig. A-32. Effects of the dominant modes are easily distinguished for the lightly damped modes and less easily distinguished for the heavily damped modes.

Lateral displacement gust asymptotes with position-loop lead again are shown in Fig. A-30 for comparison. Steady-state gain has decreased substantially in both cases with a corresponding decrease in position errors. The unacceptable case exhibits a much lower damping ratio than the satisfactory case. The net effect is to produce larger position errors for the unacceptable case.

$$N_{v_g}^{y''} = -Y_v\left[s+(1/T_{L_1}'')\right]\left[s+(1/T_{L_2}'')\right]\left[s^2+2\zeta_N''\omega_N''s+(\omega_N'')^2\right]$$

$$\Delta'' = \left[s^2+2\zeta_r''\omega_r''s+(\omega_r'')^2\right]\left[s^2+2\zeta_d''\omega_d''s+(\omega_d'')^2\right]\left[s+\left(\frac{4''}{\tau_e}\right)\right]$$

Unified
Servo
Analysis
Method

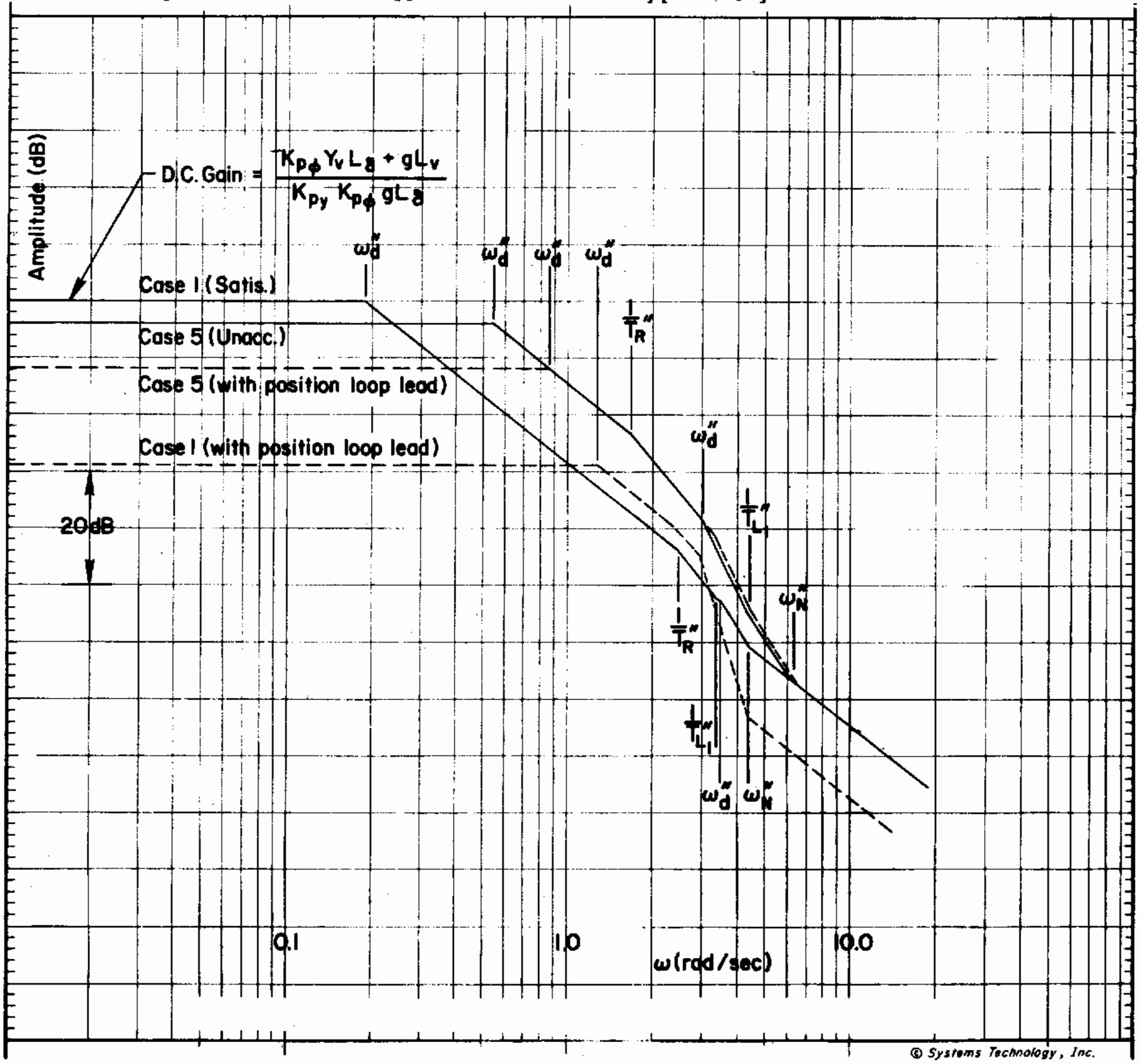

Figure A-30. Lateral Displacement Gust Asymptotes $|N_{v_g}^{y''}/\Delta''|$ (without Gust Filter)

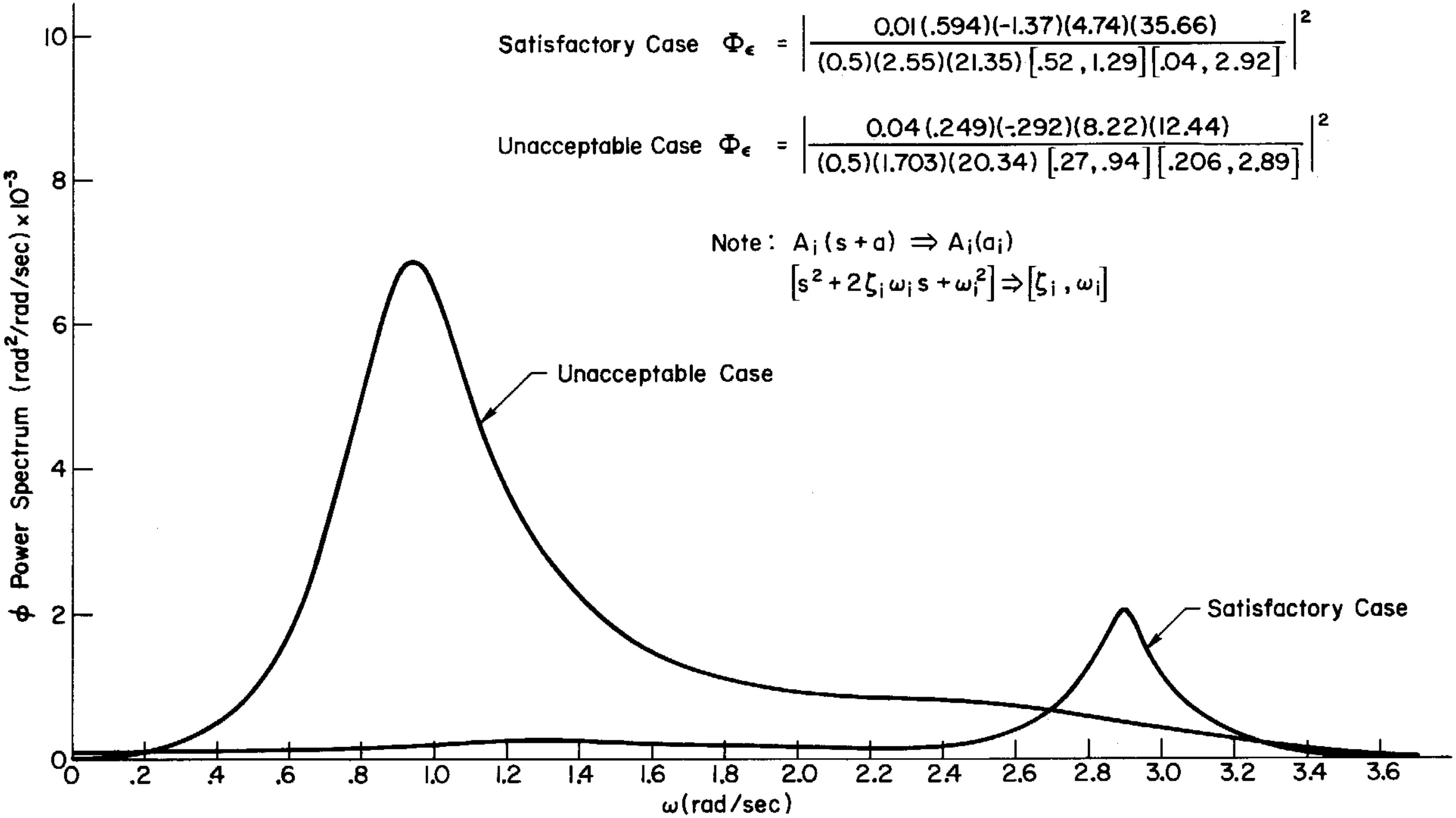

Figure A-31. Roll Attitude Power Spectrum (With Position Loop Lead)

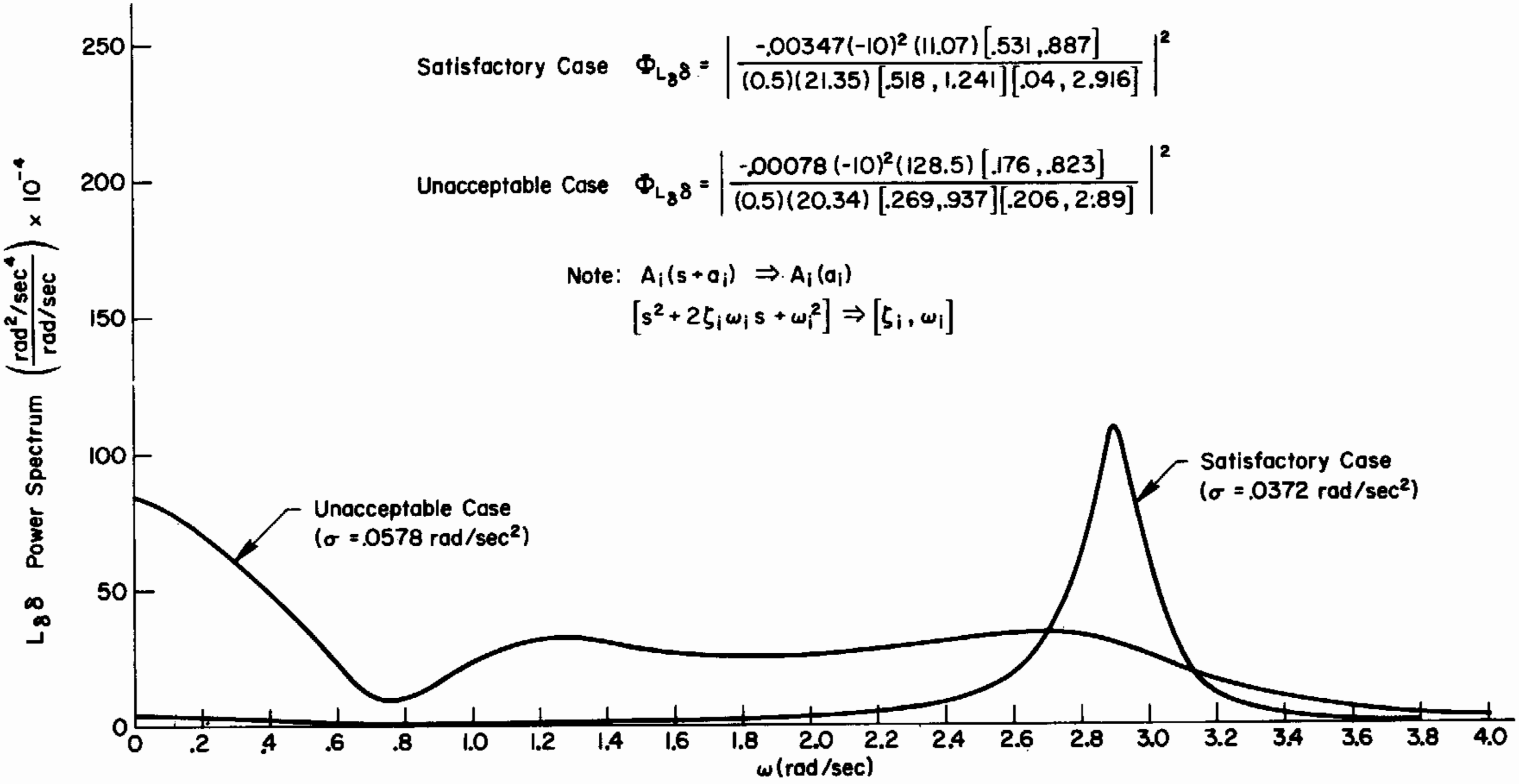

Satisfactory Case $\Phi_{L_\delta \delta} = \left| \dfrac{-.00347(-10)^2(11.07)[.531,.887]}{(0.5)(21.35)[.518,1.241][.04,2.916]} \right|^2$

Unacceptable Case $\Phi_{L_\delta \delta} = \left| \dfrac{-.00078(-10)^2(128.5)[.176,.823]}{(0.5)(20.34)[.269,.937][.206,2:89]} \right|^2$

Note: $A_i(s+a_i) \Rightarrow A_i(a_i)$

$[s^2+2\zeta_i\omega_i s+\omega_i^2] \Rightarrow [\zeta_i,\omega_i]$

Figure A-32. Control Power Spectrum $\Phi_{L_\delta \delta}$ with Position Loop Lead

From the lateral position gust transfer function asymptotes (Fig. A-30), it is clear that the frequency location of the gust response energy is similar for both satisfactory and unacceptable cases. This is another indication that pilot opinion is based on characteristics of the attitude loop where L_v dominates the gust response.

It is evident that the values of attitude and lateral position rms errors are strongly dependent on the amount of pilot lead in the outer loop. Thus rms error values are useful only as a trend indicator when the ground rules are held constant, e.g., when sufficient pilot lead is generated to produce similar crossover frequencies in each case.

A significant feature of the gust response characteristics is that for the satisfactory cases it is possible for the pilot to adjust outer-loop lead so as to obtain a tradeoff between the magnitude of attitude error and the magnitude of position error, depending on his requirements for accomplishing the task (see Fig. A-33). Results shown on Fig. A-33 were obtained by computing σ ratios from the gust response characteristics. For precision hover in a gusty environment he has the capability of generating lead in the Y-loop so as to reduce position errors at the expense of some increase in attitude errors. For the unacceptable cases, the variation of attitude and position errors with pilot lead is much less significant, indicating that he is more limited in his capacity to alter the system gust response to suit his desires. This is another good indication as to why the pilot ratings deteriorate from satisfactory to unacceptable.

In addition, the significant differences in the predicted spectral characteristic between satisfactory and unacceptable case and, likewise, the differences with and without lead, give a good indication of which loop the pilot is emphasizing, and the level of compensation in each. Such information, obtained from an experimental program, could be valuable as a source for checking the predictions of quasi-linear models and generally as a clue to the pilot control problems (e.g., see Ref. 2). However, except as a relative standard, σ_δ does not appear to be a better merit for specification purposes than any other statistical measure (e.g., σ_φ or σ_y).

Effect of Large L_v and Y_v Terms. The primary effect of the L_v and Y_v terms on the gust response features can be illustrated by examination of the closed-loop expressions for φ/v_g and y/v_g calculated for Configurations 22-36 of Table A-VI. We will examine the φ/v_g numerator with both φ and y loops closed first.

$$N_{v_g}^{\varphi''} = N_{v_g}^{\varphi} + Y_y Y_\varphi N_{v_g \delta}^{\varphi\ y} = -L_v s + Y_{p_y} Y_\varphi \frac{Y_v L_\delta}{.\ s}$$

The complete φ/v_g expression after putting in Y_{p_y} and Y_{p_φ} is:

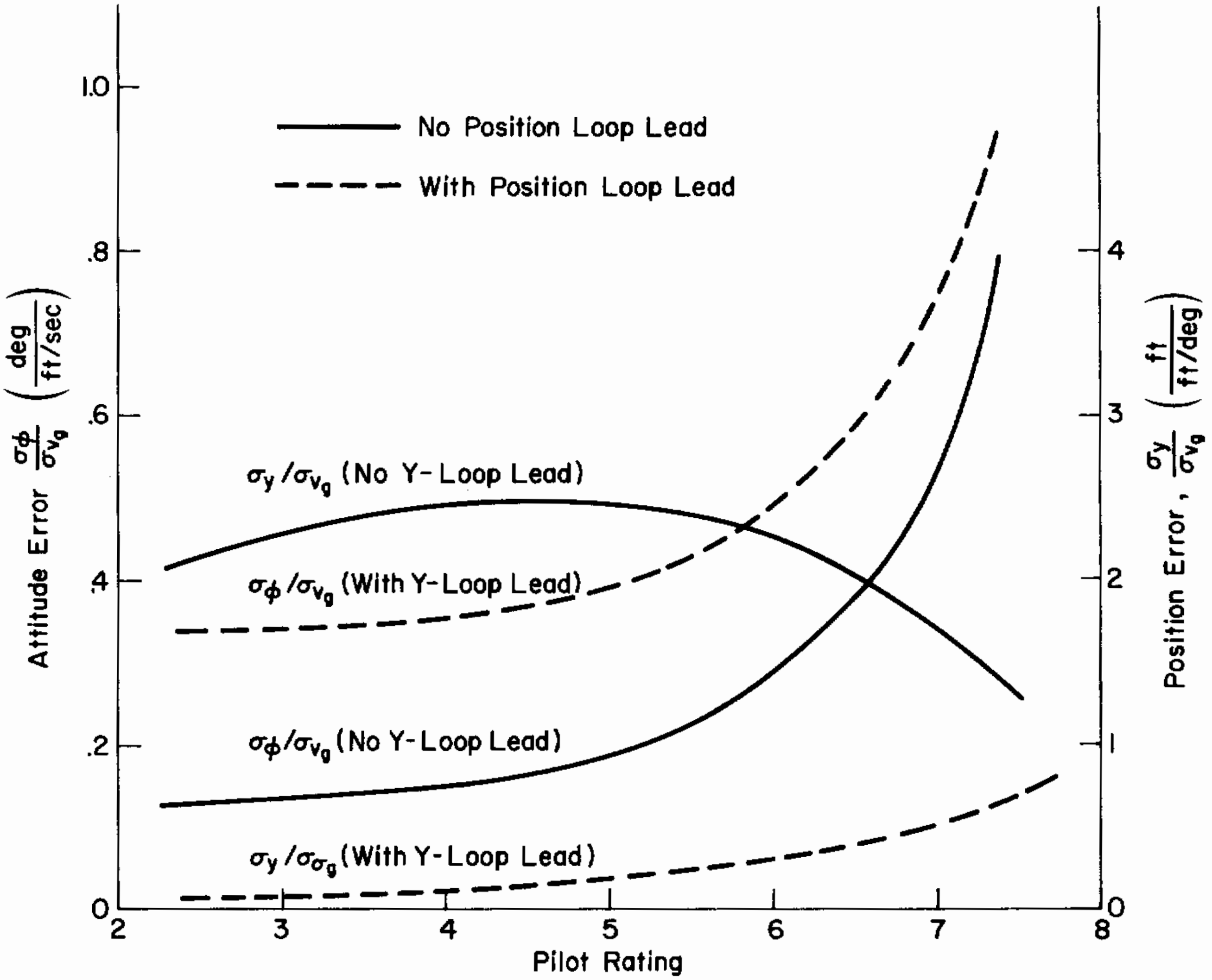

Figure A-33. Estimated Effect of Position-Loop Compensation on Error Performance

$$\frac{\varphi}{v_g} = \frac{-L_v\left[s^2\left(s + \frac{4}{\tau}\right)^2 - \frac{K_{p_y}K_{p_\varphi}T_{L_\varphi}Y_vL_\delta(s + 1/T_{L_\varphi})(s - 4/\tau)^2}{L_v}\right]}{\Delta''}$$

Putting the numerator in root locus form:

$$N^{\varphi''}_{v_g} = -L_v\left[1 - \frac{\overbrace{K_{p_x}K_{p_\varphi}T_{L_\varphi}L_\delta}^{K_{RL}}(s + 1/T_{L_\varphi})(s - 4/\tau)^2 Y_v}{s^2(s + 4/\tau)^2\ L_v}\right]$$

when the effective gain K_{RL} is

① low $K_{RL}Y_v/L_v$

② high $K_{RL}Y_v/L_v$

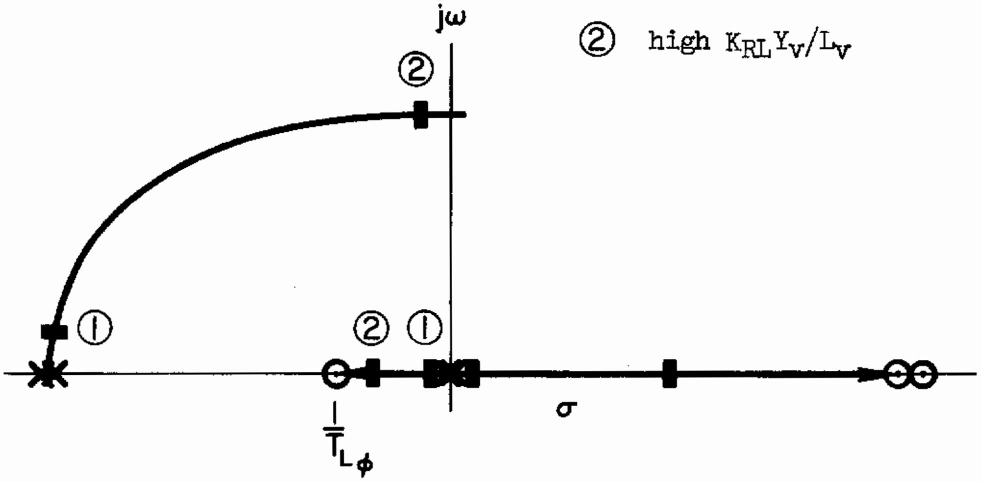

The resultant locus sketched above shows that the zero locations are a function of Y_v/L_v. When the gain Y_v/L_v is large the real axis zeros are large (i.e., $\doteq 1/T_{L_\varphi}$ and $4/\tau$) and about the same magnitude as ω_g or $1/T_y''$. The net result is that the φ/v_g amplitude asymptotes are easily approximated by a second-order expression, $\varphi/v_g \doteq K/(s+\omega_g)^2$, as shown in Fig. A-34. Obviously, then, the value of σ_φ can approximately be obtained from the φ/v_g dc gain. This value is $-Y_v/g$. Since L_v was also shown to affect the φ/v_g transfer function, σ_φ may be proportional to Y_v/L_v. The sketch below shows the roughly linear relation between σ_φ and the Y_v/L_v. For Y_v smaller the zeros are smaller than the denominator poles and the φ/v_g amplitude ratio is peaked. The φ/v_g amplitude ratio asymptotes for a typical configuration as compared to a higher Y_v case is presented in Fig. A-35. The effect is even more pronounced when plotted in cartesian coordinates as in Figs. A-36 and A-37.

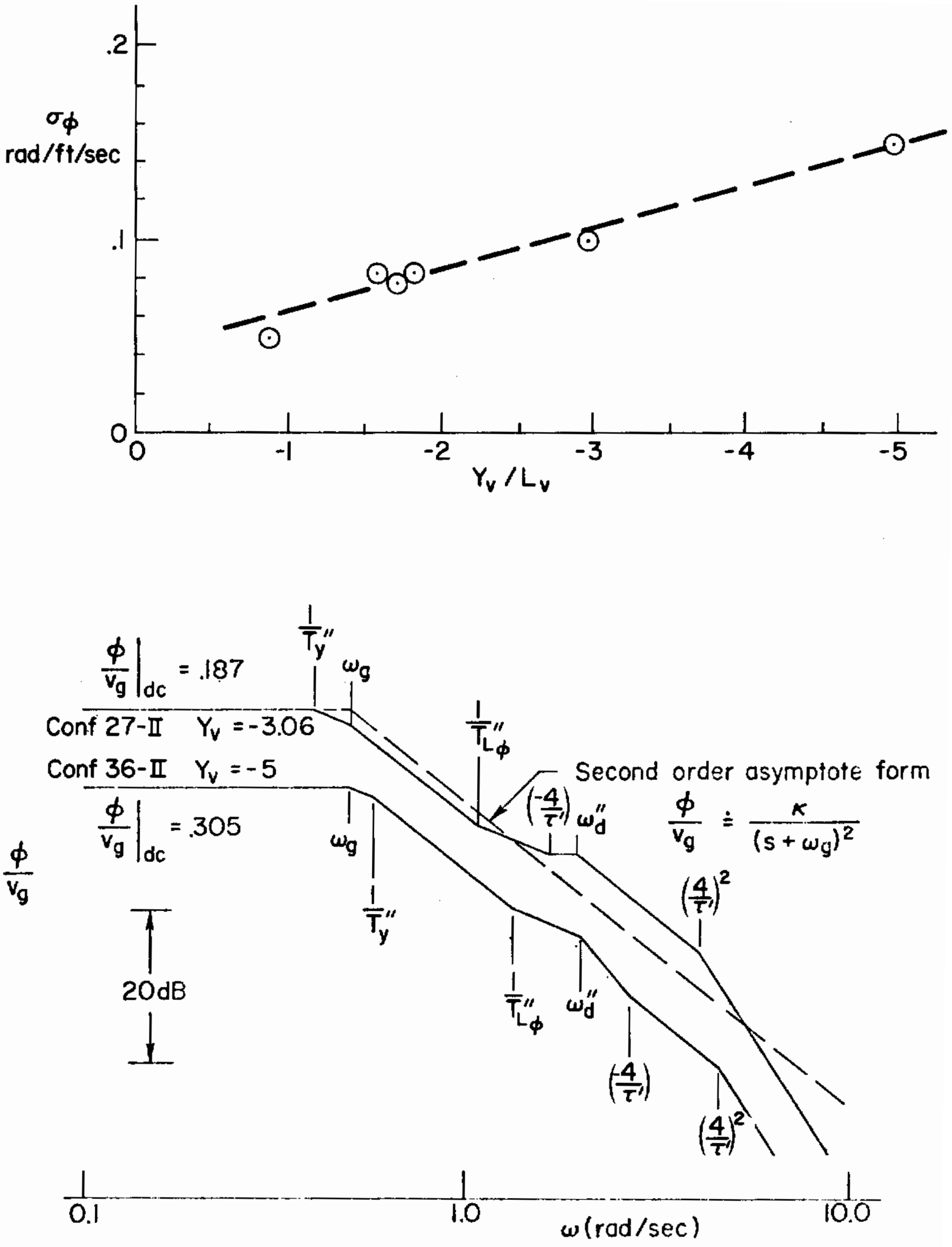

Figure A-34. Roll Attitude Gust Asymptotes

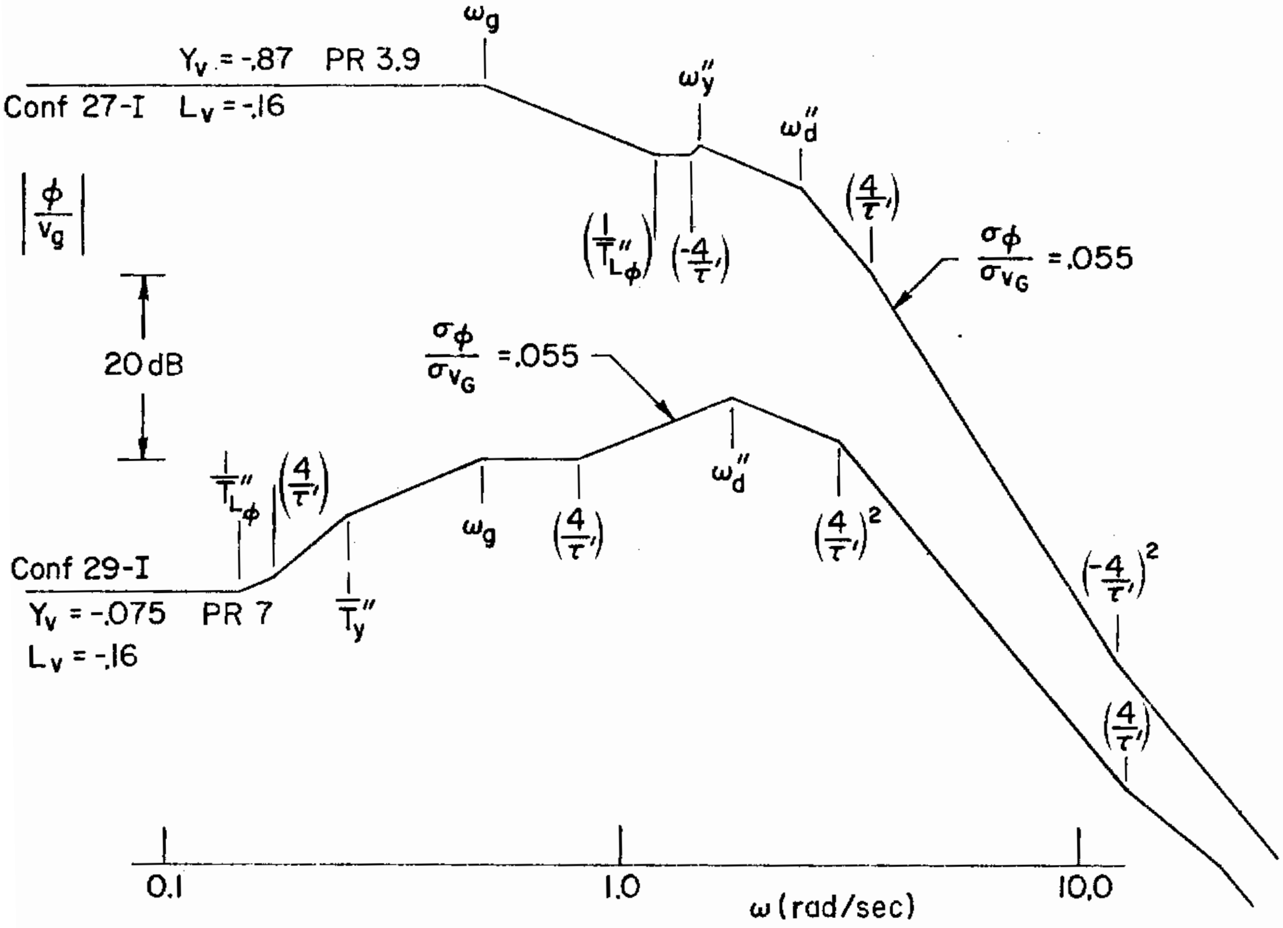

Figure A-35. Roll Attitude Gust Asymptotes
(Comparison between Satisfactory and Unacceptable)

The outer position-loop expression is

$$\frac{Y}{v_g}(s) = \frac{N_{y_{v_g}}''}{\Delta''} = \frac{N_{v_g}^{y} + Y_{p_\varphi} N_{v_g \delta}^{y \varphi}}{\Delta''}$$

$$N_{y_{v_g}}'' = -Y_v\left[\left(s+\frac{4}{\tau}\right)^2\left(s^2 - L_p s + \frac{gL_v}{Y_v}\right) + K_{p_\varphi} T_{L_\varphi} L_\delta \left(s + \frac{1}{T_{L_\varphi}}\right)\left(s - \frac{4}{\tau}\right)^2\right]$$

$$\Delta'' = \left[s^2 + 2\zeta_r''\omega_r''s + (\omega_r'')^2\right]\left[s^2 + 2\zeta_d''\omega_d''s + (\omega_d'')^2\right]\left(s + \frac{1'}{T_x}\right)\left(s + \frac{4''}{\tau}\right)$$

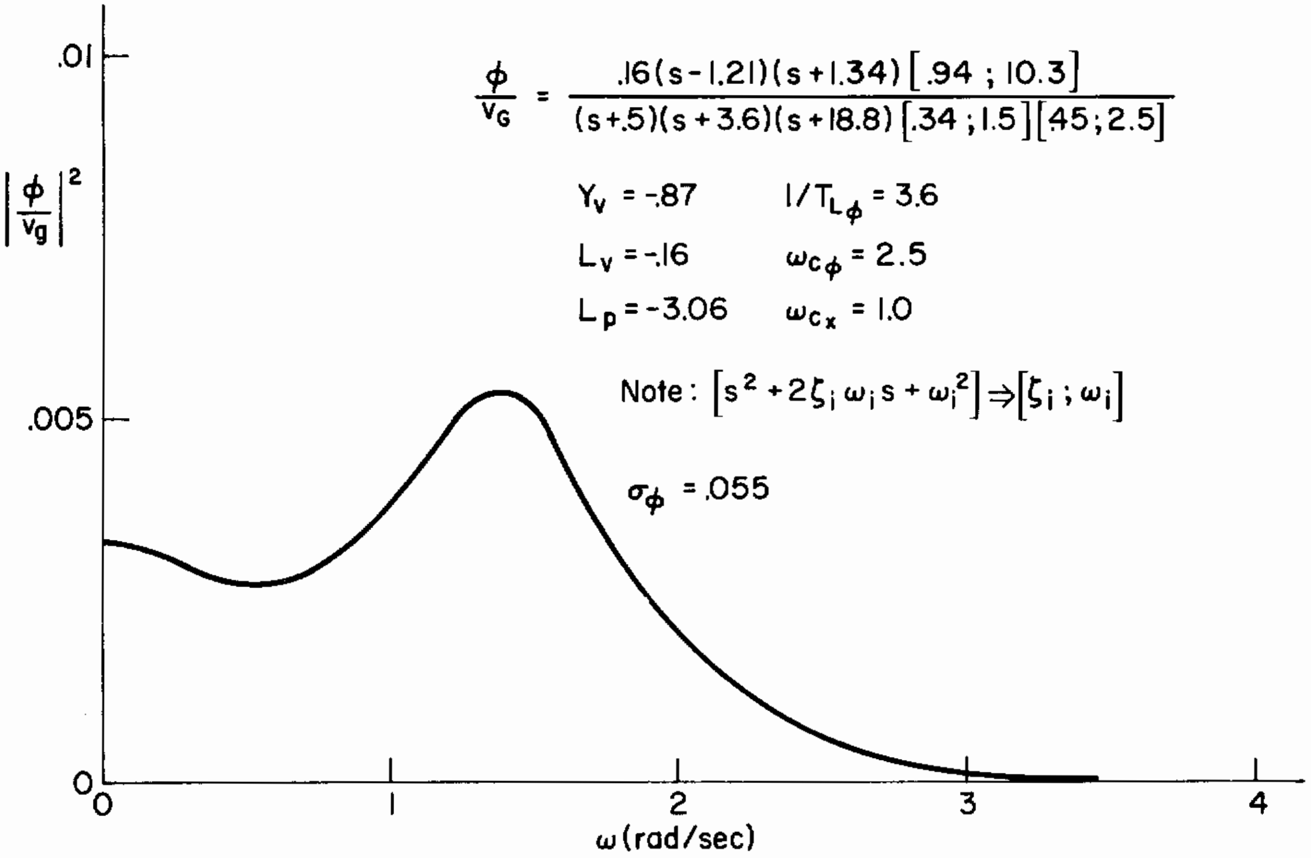

Figure A-36. Roll Attitude Response Spectra (Conf. 27-I)

From identities of Ref. 37 the low frequency gain of the y/v_g transfer function approaches $1/K_{p_y}$. Thus from Table A-X, y/v_g transfer function poles and zeros, it is seen that the zeros are larger than ω_g or $1/T_x'$, so the general asymptotic shape of the spectrum is as sketched below.

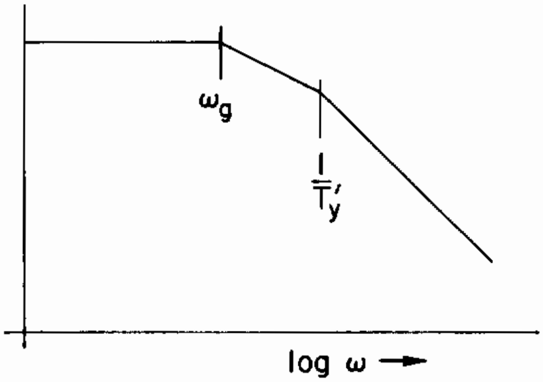

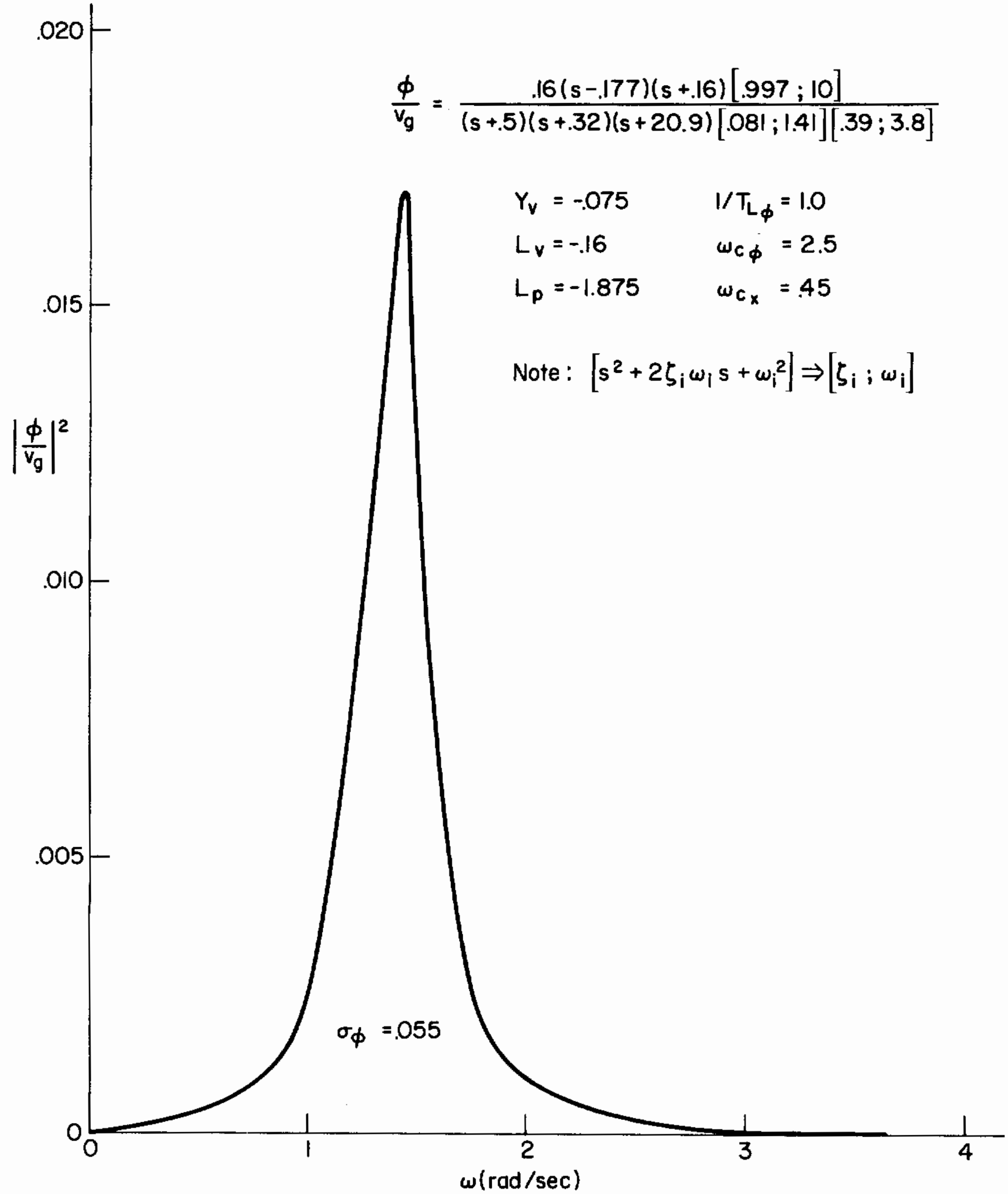

Figure A-37. Roll Attitude Response Spectra (Conf. 29-I)

TABLE A-X

SUMMARY OF GUST RESPONSE CHARACTERISTICS FOR VARIOUS Y_v/L_v RELATIONS

	CONFIG. NO.	PILOT RATING	Y_v/L_v	σ_φ	φ/v_G TRANSFER FUNCTION	CLOSURE CONDITIONS	σ_y
SATISFACTORY	1	PR 3.0	$\frac{5}{0.16}$	0.147	$\frac{0.16(1.31)(-2.72)[0.534\,;\,15.01]}{(0.5)(0.564)(17.86)[0.115\,;\,2][0.93\,;\,4.55]}$	$\frac{1}{T_{L_\varphi}} = 1.5$ $\omega_{c_y} = 1.2$ $\omega_{c_\varphi} = 2.5$	1.4
	2	PR 3.8	$\frac{3}{0.16}$	0.10	$\frac{0.16(1.06)(-1.65)[0.79\,;\,12.0]}{(0.5)(0.41)(17.2)[0.071\,;\,1.93][0.90\,;\,4.04]}$	$\frac{1}{T_{L_\varphi}} = 1.5$ $\omega_{c_y} = 0.7$ $\omega_{c_\varphi} = 2.5$	1.74
	3	PR 3.8	$\frac{0.87}{0.16}$	0.055	$\frac{0.16(1.34)(-1.21)[0.94\,;\,10.3]}{(0.5)(3.6)(18.8)[0.34\,;\,1.5][0.45\,;\,2.5]}$	$\frac{1}{T_{L_\varphi}} = 3.6$ $\omega_{c_y} = 1.0$ $\omega_{c_\varphi} = 2.5$	1.2
UNACCEPTABLE	4	PR 6.9	$\frac{1.87}{0.16}$	0.085	$\frac{0.16(2.81)(-1.38)(7.45)(15.13)}{(0.5)(2.61)(23.6)[0.21\,;\,3.05][0.32\,;\,1.45]}$	$\frac{1}{T_{L_\varphi}} = 1.0$ $\frac{1}{T_{I_y}} = 1.0$ $\omega_{c_\varphi} = 3.0$ $\omega_{c_y} = 0.9$	1.32
	5	PR 7.3	$\frac{0.86}{0.08}$	0.078	$\frac{0.08(1.62)(-0.96)(7.21)(12.13)}{(0.5)(2.02)(19.75)[0.1\,;\,1.2][0.22\,;\,2.65]}$	$\frac{1}{T_{L_\varphi}} = 1.0$ $\frac{1}{T_{I_y}} = 1.0$ $\omega_{c_\varphi} = 2.5$ $\omega_{c_y} = 1.0$	1.75
	6	PR 5.7	$\frac{1.66}{0.16}$	0.082	$\frac{0.16(0.662)(-1.61)[0.857\,;\,11.38]}{(0.5)(0.32)(20.1)[0.08\,;\,2.47][0.66\,;\,2.77]}$	$\frac{1}{T_{L_\varphi}} = 1.0$ $\omega_{c_y} = 0.4$ $\omega_{c_y} = 2.75$	1.92
	7	PR 7.3	$\frac{0.24}{0.08}$	0.050	$\frac{0.08(0.44)(-0.54)[0.965\,;\,10.3]}{(0.5)(0.73)(20)[0.4\,;\,2.91][0.096\,;\,1.48]}$	$\frac{1}{T_{L_\varphi}} = 1.2$ $\omega_{c_y} = 1.0$ $\omega_{c_\varphi} = 2.5$	1.24
	8	PR 6.9	$\frac{0.075}{0.16}$	0.055	$\frac{0.16(0.16)(-0.177)[0.997\,;\,10.0]}{(0.5)(0.32)(20.9)[0.081\,;\,1.42][0.386\,;\,3.81]}$	$\frac{1}{T_{L_\varphi}} = 1.0$ $\omega_{c_y}{}^{*} = 0.45$ $\omega_{c_\varphi} = 2.5$	2.12

Note: $s^2 + 2\zeta_i\omega_i s + \omega_i^2 \Rightarrow [\zeta_i\,,\,\omega_i]$; $A(s+a) \Rightarrow A(a)$

$^{*}\omega_{c_x} = 1.0$ if $1/T_{L_x} = 1.35$ added but σ_y unchanged; $\sigma_\varphi = 0.044$.

TABLE A-X (Concluded)

CONFIG. NO.	σ_y	y/v_g TRANSFER FUNCTION	CLOSURE CONDITIONS	σ_φ
1	1.38	$\frac{-4.93(3.53)(17.57)[0.11\,;\,2.26]}{(0.5)(0.564)(17.85)[0.115\,;\,2.0][0.93\,;\,4.55]}$	$\frac{1}{T_{L_\varphi}} = 1.5 \quad \omega_{c_x} = 1.2$ $\omega_{c_\varphi} = 2.05$	0.147
2	1.74	$\frac{-3.06(3.95)(17.0)[0.19\,;\,2.29]}{(0.5)(0.41)(17.2)[0.071\,;\,1.93][0.902\,;\,4.04]}$	$\frac{1}{T_{L_\varphi}} = 1.5 \quad \omega_{c_x} = 0.7$ $\omega_{c_\varphi} = 2.0$	0.10
3	1.2	$\frac{-0.87(4.88)(18.47)[0.063\,;\,3.73]}{(0.5)(3.6)(18.8)[0.34\,;\,1.5][0.45\,;\,2.5]}$	$\frac{1}{T_{L_\varphi}} = 3.6 \quad \omega_{c_x} = 1.0$ $\omega_{c_\varphi} = 2.5$	0.052
4	1.32	$\frac{-1.875(2.43)(23.53)[0.1\,;\,3.665]}{(0.5)(2.61)(23.55)[0.21\,;\,3.05][0.32\,;\,1.45]}$	$\frac{1}{T_{L_\varphi}} = 1.0 \quad \frac{1}{T_{I_x}} = 1.0 \quad \tau = 0.33$ $\omega_{c_\varphi} = 3.0 \quad \omega_{c_x} = 0.9$	0.085
5	1.75	$\frac{-0.86(2.36)(19.72)[0.05\,;\,3.33]}{(0.5)(2.02)(19.75)[0.1\,;\,1.2][0.22\,;\,2.65]}$	$\frac{1}{T_{L_\varphi}} = 1.0 \quad \frac{1}{T_{I_x}} = 1.0$ $\omega_{c_\varphi} = 2.5 \quad \omega_{c_x} = 1.0$	0.078
6	1.92	$\frac{-1.66(2.17)(19.99)[0.106\,;\,3.52]}{(0.5)(0.32)(20.06)[0.08\,;\,2.47][0.66\,;\,2.77]}$	$\frac{1}{T_{L_\varphi}} = 1.0 \quad \omega_{c_x} = 0.4$ $\omega_{c_\varphi} = 2.75$	0.085
7	1.24	$\frac{-0.24(3.3)(19.9)[-0.004\,;\,4.53]}{(0.5)(0.73)(20.0)[0.401\,;\,2.91][0.096\,;\,1.48]}$	$\frac{1}{T_{L_\varphi}} = 1.2 \quad \omega_{c_x} = 1.0$ $\omega_{c_\varphi} = 2.5$	0.050
8	2.12	$\frac{-0.075(4.9)(20.0)[-0.027\,;\,8.54]}{(0.5)(0.32)(20.9)[0.081\,;\,1.42][0.386\,;\,3.81]}$	$\frac{1}{T_{L_\varphi}} = 1.0 \quad \omega_{c_x} = 0.45$ $\omega_{c_\varphi} = 2.5$	0.055

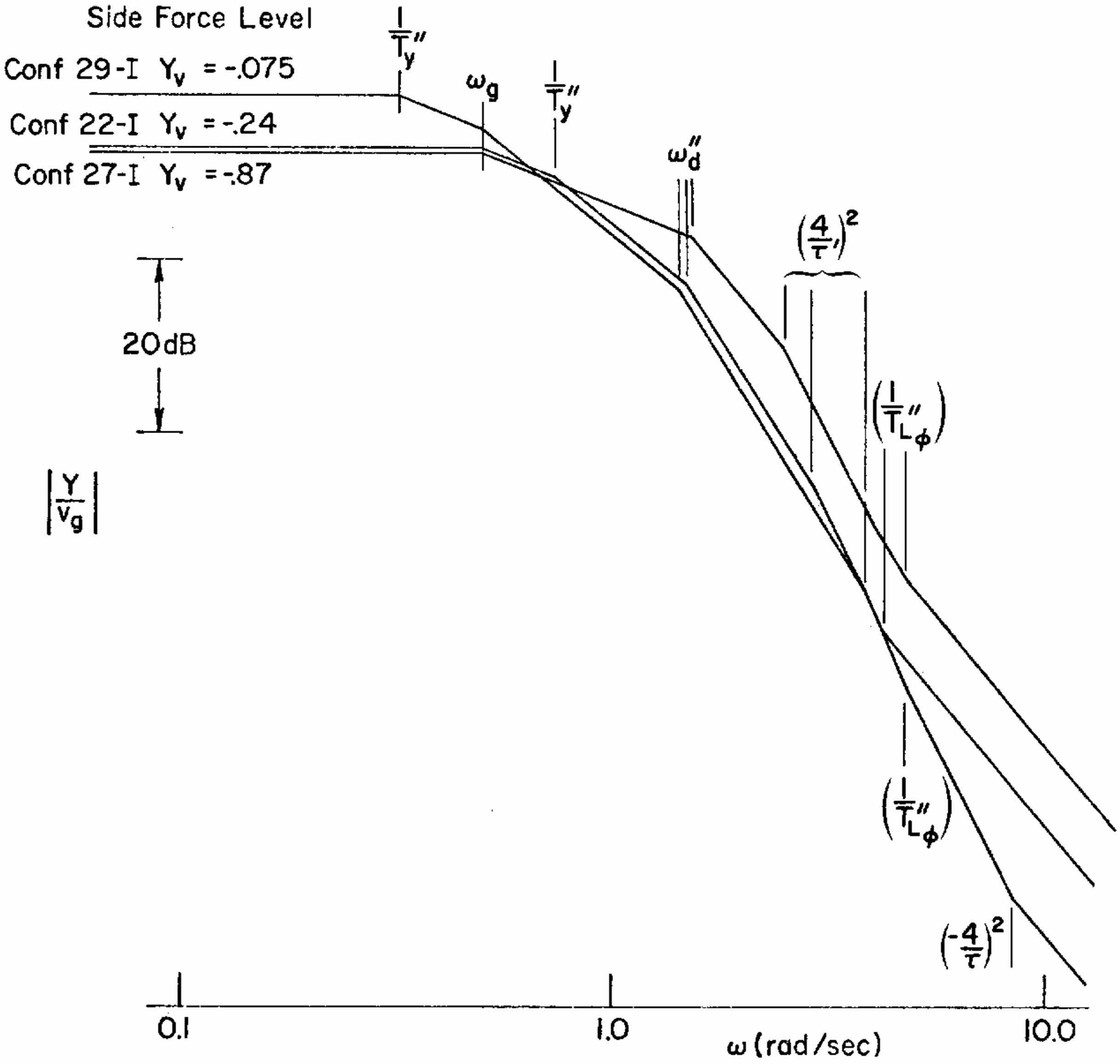

Figure A-38. Lateral Position Asymptotes
for Various Levels of Y_v

Figure A-38 is the actual asymptotic plots of y/v_g for typical cases of low Y_v to high Y_v. For the low Y_v case, the decreasing amplitude is more apparent since the frequency of the complex numerator zeros is determined by gL_v/Y_v. With a low L_v and high Y_v case the y/v_g would not approach $1/K_{p_y}$. But for our cases where ω_g and $1/T_y'' \ll$ numerator frequency the approximation is good and

$$\left.\frac{y}{v_g}\right|_{dc} \doteq \frac{L_v(1+K_\varphi)}{K_{p_y}K_{p_\varphi}L_\delta} \propto \frac{\sigma_y}{\sigma_{v_g}}$$

From the above relation the effects of Y_v and pilot gains on σ_y can be shown. In any two systems with identical characteristic equations, K_φ increases as Y_v increases for ω_{c_y} = const (i.e., $K_\varphi = K_{p_\varphi} L_\delta Y_v / g L_v$) and therefore σ_y will increase with K_φ from the previous relation. By increasing K_{p_φ} or K_{p_y} (increasing crossover frequency) σ_y can be reduced.

An outer-loop gain increase is the key parameter for reducing σ_y since K_{p_y} and ω_{c_y} are in direct proportion and thus increasing ω_{c_y} increases $y/v_g|_{dc}$.

The typical spectra of y/v_g are presented in Figs. A-39 and A-40. The satisfactory ratings have a very rapid decrease in power with frequency whereas the unacceptable cases (Fig. A-40) contain peaks near the outer-loop crossover frequency.

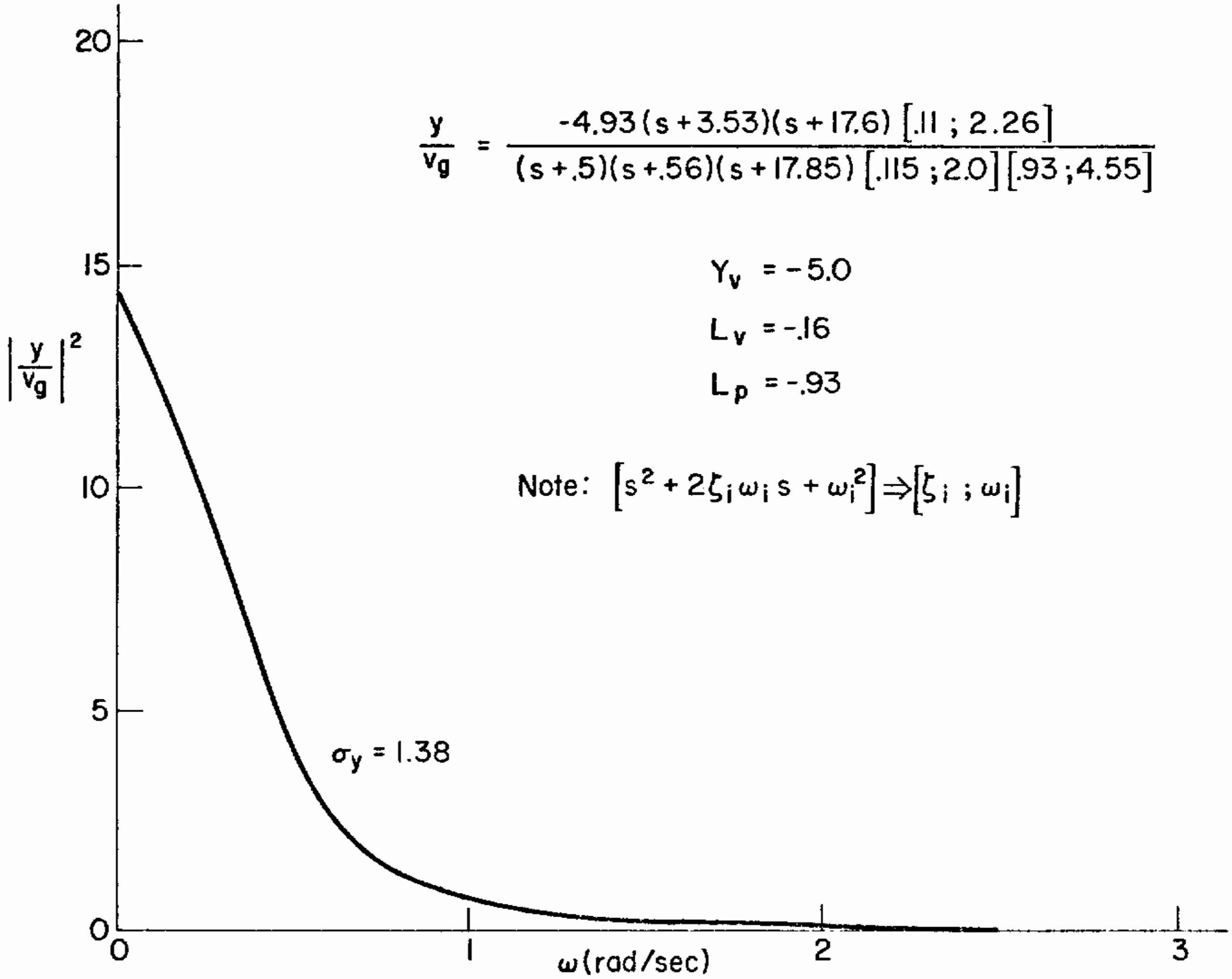

Figure A-39. Lateral Position Response Spectra, Satisfactory Response

$$(\mathrm{II})\quad \frac{y}{v_g} = \frac{-.86(s+2.36)(s+19.72)\,[.05\,;\,3.33]}{(s+.5)(s+2.02)(s+19.75)\,[.1\,;\,1.2]\,[.22\,;\,2.65]}$$

$$(\mathrm{I})\quad \frac{y}{v_g} = \frac{-.24(s+3.3)(s+19.9)\,[-.004\,;\,4.53]}{(s+.5)(s+.73)(s+20)\,[.401\,;\,2.91]\,[.096\,;\,1.48]}$$

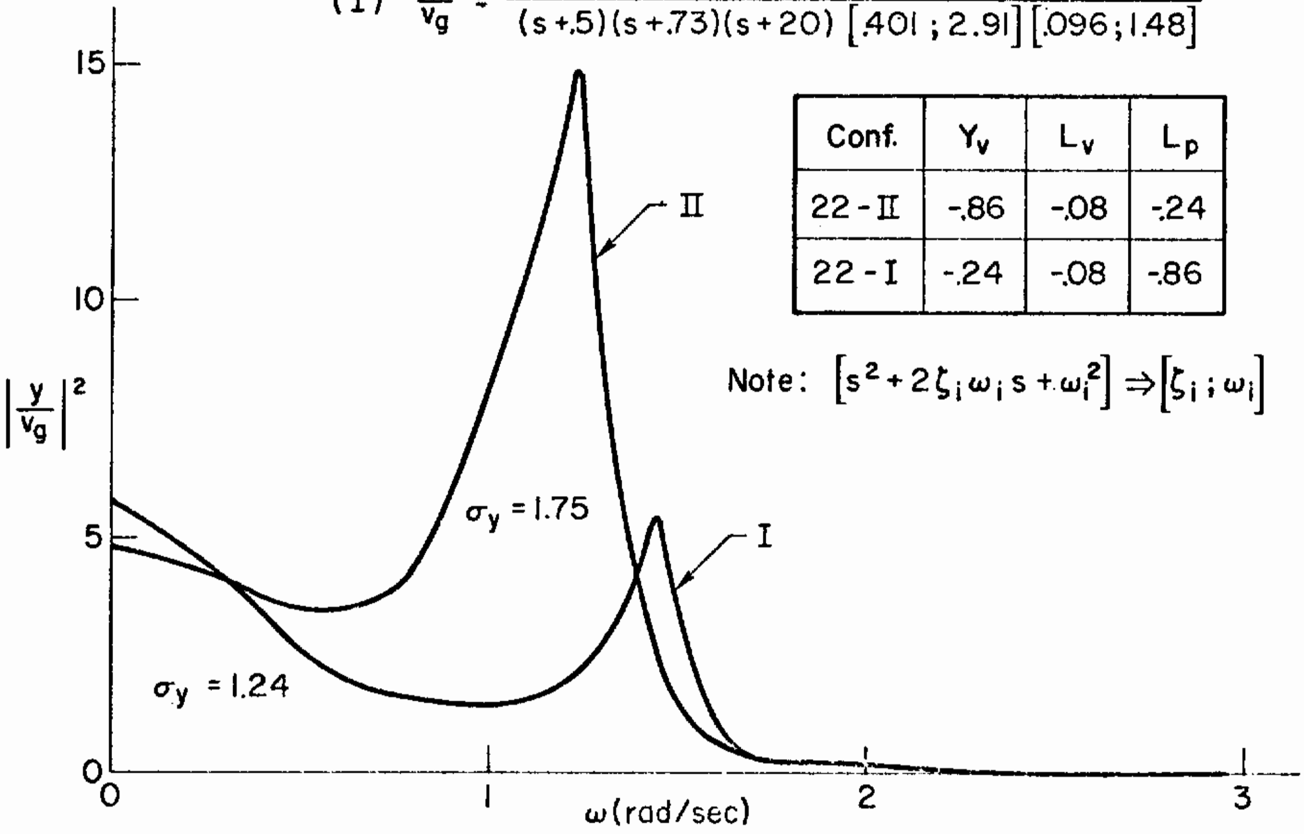

Conf.	Y_v	L_v	L_p
22 - II	-.86	-.08	-.24
22 - I	-.24	-.08	-.86

Note: $[s^2 + 2\zeta_i\omega_i s + \omega_i^2] \Rightarrow [\zeta_i\,;\,\omega_i]$

Figure A-40. Lateral Position Response Spectra, Unacceptable Dynamics

In conclusion, the effects of Y_v and L_v and gust response characteristics appear to relate to the pilot ratings as follows:

1. For large Y_v the ratings are improved as the ratio Y_v/L_v is reduced.
2. There is some evidence that the pilot may need to lag the outer loop in order to reduce σ_y; that is, eliminate the effects of inner-loop leads.
3. The shape of the φ/v_g spectrum also appears important because when φ/v_g becomes peaked due to Y_v/L_v being low, the pilot rating is degraded.

APPENDIX B

EFFECTS OF CONTROL SYSTEM LAGS AND DELAYS ON CLOSED-LOOP SYSTEM

This appendix contains the development of analytical expressions to show the effects of control system lags and high frequency dynamics on the closed-loop pilot/vehicle system.

EFFECTS OF CONTROL LAG

System Sensitivity to T_c

System is

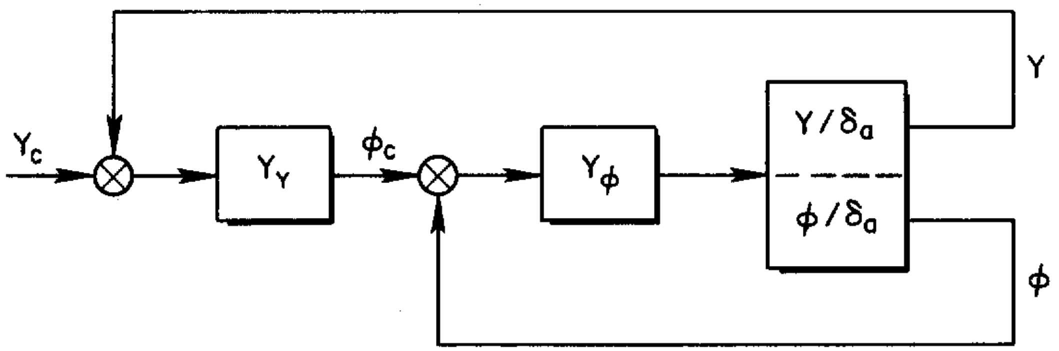

$$\left.\frac{Y}{\varphi_c}\right|_{\varphi \leftarrow \delta} = \frac{Y_\varphi N_\delta^Y}{\Delta + Y_\varphi N_\delta^\varphi} = \frac{Y_\varphi N_\delta^Y}{\Delta'} \tag{B-1}$$

$$\left.\frac{Y}{Y_c}\right|_{\substack{\varphi \leftarrow \delta \\ Y \leftarrow \delta}} = \frac{Y_Y Y_\varphi N_\delta^Y}{\Delta + Y_\varphi N_\delta^\varphi + Y_Y Y_\varphi N_\delta^Y} = \frac{Y_Y Y_\varphi N_\delta^Y}{\Delta''} \tag{B-2}$$

Looking at the Inner Loop

$$\Delta' = \Delta + Y_\varphi N_\delta^\varphi \tag{B-3}$$

Include control lag as part of pilot transfer function, Y_φ

$$\text{where} \qquad Y_\varphi^* = \frac{K_{P_\varphi} T_{L_\varphi}(s + 1/T_{L_\varphi})(s - 4/\tau)^2}{T_c(s + 4/\tau)^2(s + 1/T_c)}$$

$$N_\delta^\varphi = L_{\delta_a}(s + 1/T_{\varphi_1})$$

$$\Delta = (s + 1/T_R)(s^2 + 2\zeta_d\omega_d s + \omega_d^2)$$

$$\therefore \Delta' = \Delta + Y_\varphi^* N_\delta^\varphi = (1/T_R)[\zeta_d\omega_d] + L_\delta K_{P_\varphi} \frac{T_{L_\varphi}}{T_c} \frac{(1/T_{L_\varphi})(-4/\tau)^2(1/T_{\varphi_1})}{(4/\tau)^2(1/T_c)}$$

$$= (s + 1/T_R)(s^2 + 2\zeta_d\omega_d s + \omega_d^2)$$

$$+ \frac{L_\delta K_{P_\varphi} \dfrac{T_{L_\varphi}}{T_c} (s + 1/T_{L_\varphi})(s - 4/\tau)^2(s + 1/T_{\varphi_1})}{(s + 4/\tau)^2(s + 1/T_c)} \qquad \text{(B-4)}$$

$$\Delta' = 0$$

$$\therefore 1 + (s + 1/T_R)(s^2 + 2\zeta_d\omega_d s + \omega_d^2)$$

$$\times \frac{(s + 4/\tau)^2(s + 1/T_c)}{L_\delta K_{P_\varphi} \dfrac{T_{L_\varphi}}{T_c} (s + 1/T_{L_\varphi})(s - 4/\tau)^2(s + 1/T_{\varphi_1})} = 0$$

$$= 1 + T_c(s + 1/T_c) \frac{(s + 1/T_R)(s^2 + 2\zeta_d\omega_d s + \omega_d^2)(s + \tau/4)^2}{L_\delta K_{P_\varphi} T_{L_\varphi}(s + 1/T_{L_\varphi})(s - \tau/4)^2(s + 1/T_{\varphi_1})} = 0$$

$$= 1 + T_c(s + 1/T_c)G(s) = 1 + G(s) + sT_cG(s) = 0$$

$$\therefore 1 + \frac{T_c s G(s)}{1 + G(s)} = 0 \qquad \text{(B-5)}$$

Note that $$\frac{G(s)}{1 + G(s)} = \frac{1}{1 + 1/G(s)}$$

$\therefore$ Equation to be solved is $1 + \dfrac{T_cS}{1 + 1/G(s)} = 0$

where $$1 + \frac{1}{G(s)} = 1 + \frac{L_\delta K_{P_\varphi} T_{L_\varphi}(s + 1/T_{L_\varphi})(s - \tau/4)^2(s + 1/T_{\varphi_1})}{(s + \tau/4)^2(s + 1/T_R)(s^2 + 2\zeta_d\omega_d s + \omega_d^2)}$$

$$= 1 + \frac{Y_\varphi N_\delta^\varphi}{\Delta} = \frac{\Delta + Y_\varphi N_\delta^\varphi}{\Delta} = \frac{\Delta'}{\Delta} \tag{B-6}$$

$\therefore$ Equation to be solved is

$$1 + \frac{T_cS\Delta}{\Delta'} = 0 \tag{B-7}$$

For convenience we rearrange this so that $\sum P > \sum Z$

$$\therefore 1 + \frac{1}{T_c}\frac{\Delta'}{S\Delta} = 0 \tag{B-8}$$

$$1 + KG'(s) = 0 \tag{B-9}$$

where $K = 1/T_c$

and $G'(s) = \Delta'/S\Delta$

Note when T_c is small, gain K is large and roots are close to the zeros of $G'(s)$ which are Δ' which are the original closed-loop roots.

EFFECTS OF HIGH FREQUENCY DYNAMICS

Assume high frequency effects can be approximated by $e^{-\tau s}$ which is equivalent to increasing pilot transport lag.

$$\therefore \quad Y_{\varphi} = -\frac{K_{P_{\varphi}} T_{L_{\varphi}} (s + 1/T_{L_{\varphi}})(s - 2/\tau)}{(s + 2/\tau)} \tag{B-10}$$

$$N^{\varphi}_{\delta} = L_{\delta_a}(s + 1/T_{\varphi_1})$$

$$\Delta = (s + 1/T_R)(s^2 + 2\zeta_d\omega_d s + \omega_d^2)$$

$$\Delta' = \Delta + Y_{\varphi} N^{\varphi}_{\delta} = 0 = (s + 1/T_R)(s^2 + 2\zeta_d\omega_d s + \omega_d^2) - \frac{L_{\delta} K_{P_{\varphi}} T_{L_{\varphi}} (s + 1/T_{L_{\varphi}})(s + 1/T_{\varphi_1})(s - 2/\tau)}{(s + 2/\tau)}$$

$$= \frac{\overbrace{(s + 1/T_R)(s^2 + 2\zeta_d\omega_d s + \omega_d^2)}^{\Delta}(s + 2/\tau) \overbrace{- L_{\delta} K_{P_{\varphi}} T_{L_{\varphi}} (s + 1/T_{L_{\varphi}})(s + 1/T_{\varphi_1})}^{Y^*_{\varphi} N^{\varphi}_{\delta}}(s - 2/\tau)}{(s + 2/\tau)}$$

$$= \Delta(s + 2/\tau) + Y^*_{\varphi} N^{\varphi}_{\delta}(s - 2/\tau)$$

$$= \Delta s + (2/\tau)\Delta + Y^*_{\varphi} N^{\varphi}_{\delta} s - (2/\tau) Y^*_{\varphi} N^{\varphi}_{\delta}$$

$$= (2/\tau)(\Delta - Y^*_{\varphi} N^{\varphi}_{\delta}) + s\,(\Delta + Y^*_{\varphi} N^{\varphi}_{\delta}) = 0$$

$$\therefore \quad 1 + (2/\tau)\left\{\frac{\Delta - Y^*_{\varphi} N^{\varphi}_{\delta}}{s(\Delta + Y^*_{\varphi} N^{\varphi}_{\delta})}\right\} = 0 \tag{B-11}$$

APPENDIX C

STABILITY DERIVATIVES FOR DIRECT FORCE CONTROL COUPLING ANALYSES IN HOVER

The longitudinal stability derivatives and control coupling terms employed in the studies of Section III are contained in this appendix. Tables C-I and C-II list the pertinent data from the experiments by Gallagher (Ref. 16) and Breul (Ref. 17), respectively.

TABLE C-I

DATA FOR CONTROL COUPLING STUDIES BY GALLAGHER, REF. 16

a) Derivatives

DERIVATIVES	CASE 1		CASE 2	
	A	B	A	B
M_u	+0.005	+0.005	+0.043	+0.043
X_δ (g/in.)	0	−2.25*	0	−2.25
$M_\delta \left(\frac{\text{rad/sec}^2}{\text{in.}}\right)$	0.54	0.54	0.54	0.54
M_q (1/sec)	−3.0	−3.0	−3.0	−3.0
X_u	−0.016	−0.016	−0.016	−0.016
Pilot Rating	3.0	4.0	3.5	7.0

*These magnitudes of X_δ are extremely large and can only be envisioned as a longitudinally mounted propeller or jet.

TABLE C-I (Concluded)

b) Transfer Functions

CASE		NUMERATOR	DENOMINATOR, Δ
1	A	$N_\delta^\theta = M_\delta(s+0.016)$	$(s+3.02)[s^2+2(-0.01)(0.23)s+(0.23)^2]$
		$N_\delta^x = 32.2\ M_\delta$	$s\Delta$
	B	$N_\delta^\theta = M_\delta(s-0.65)$	$(s+3.02)[s^2+2(-0.01)(0.23)s+(0.23)^2]$
		$N_\delta^x = M_\delta Y_{p_\theta}(s+0.25)(s+2.75)$	$s\Delta$
2	A	$N_\delta^\theta = M_\delta(s+0.016)$	$(s+3.15)[s^2+2(-0.07)(0.66)s+(0.66)^2]$
		$N_\delta^x = 32.2\ M_\delta$	$s\Delta$
	B	$N_\delta^\theta = M_\delta(s-6.0)$	$(s+3.15)[s^2+2(-0.07)(0.66)s+(0.66)^2]$
		$N_\delta^x = M_\delta Y_{p_\theta}(s+0.25)(s+2.75)$	$s\Delta$

TABLE C-II

DATA FOR CONTROL COUPLING STUDY BY BRUEL, REF. 17

CASE NO.	STABILITY DERIVATIVE	CONTROL TERMS		PILOT RATING RANGE
	M_q sec^{-1}	X_δ ft/sec^2/in.	M_δ rad/sec^2/in.	
1	−0.3	0	0.25	$3 < PR < 5$ (acceptable)
2	−0.3	−1.0	0.25	$3 < PR < 5$ (acceptable)
3	−0.3	−2.0	0.25	$PR > 5$ (unsatisfactory)
4	−1.0	0	0.1	$3 < PR < 5$ (acceptable)
5	−1.0	−1.0	0.1	$PR < 3$ (good)
6	−1.0	−2.0	0.1	$PR > 5$ (unacceptable)

APPENDIX D

SUMMARY OF AERODYNAMIC STABILITY DERIVATIVES FOR LATERAL/DIRECTIONAL STUDIES

The lateral/directional stability and control characteristics of this appendix were utilized in the closed-loop analyses covered in the transition studies of Section IV.

Tables D-I and D-II summarize the XC-142A derivatives and transfer function characteristics used in the generalized studies of closed-loop regulatory and maneuver tasks. These derivatives were derived from material of Ref. 33.

Table D-III provides the dynamic characteristics calculated for each configuration tested in the flight test program of Ref. 22. Similar information for the control coupling study of Ref. 25 is presented in Table D-IV. Only the factors utilized in the analysis are presented.

TABLE D-I

LATERAL/DIMENSIONAL DERIVATIVES FOR THE XC-142

(Note: Data are for body-fixed centerline)

FLIGHT CONDITION

$W = 37,474$ lb $\qquad \gamma_o = 0$

$I_x = 173,000$ slug-ft^2 $\qquad I_z = 267,000$

$I_y = 122,000$ slug-ft^2 $\qquad I_{xz} = 7,000$

	DERIVATIVES		
FLT. COND. / DERIV.	HOVER	60 KTS	120 KTS
Y_v	-0.015	-0.0945	-0.175
Y_{δ_a}[†]	0	0	0
Y_{δ_r}[‡]	0	0.248	0.94
L'_β	-0.00062	-0.715	-1.91
L'_p	-0.235	-0.539	-0.855
L'_r	-0.0335	0.382	0.559
L'_{δ_a}[†]	-0.285	-0.167	-0.193
L'_{δ_r}[‡]	0.0622	-0.0871	0.0913
N'_β	-0.00039	0.218	0.580
N'_p	-0.0062	-0.137	-0.116
N'_r	-0.211	-0.332	-0.565
N'_{δ_a}[†]	-0.0075	-0.0129	-0.0266
N'_{δ_r}[‡]	-0.208	-0.150	-0.132

[†] δ_a inches of lateral stick (includes aileron and differential main prop blade angle); positive δ_a gives negative $\dot{p}$.

[‡] δ_r inches of pedal (includes rudder, aileron, and differential main prop blade angle); positive δ_r gives negative $\dot{r}$.

TABLE D-II

XC-142 LATERAL/DIRECTIONAL TRANSFER FUNCTION FOR THE AILERON AND RUDDER CONTROLS

TRANSFER FUNCTION		BEGIN TRANSITION ($U \doteq 0$ KTS)	MIDTRANSITION ($U \doteq 60$ KTS)	END TRANSITION ($U \doteq 120$ KTS)
Δ	ζ_d	−0.265	−0.0292	0.169
	ω_d	0.225	0.683	0.914
	$1/T_s$	0.1911	0.118	0.124
	$1/T_r$	0.3894	0.886	1.61
$N^{\varphi}_{\delta_a}$	A_{φ}	−0.285	−0.167	−0.193
	ζ_{φ}	(0.0132)	0.411	0.418
	ω_{φ}	(0.2119)	0.555	0.977
$N^{r}_{\delta_r}$	A_r	−0.208	−0.150	−0.132
	$1/T_r$	0.3944	0.863	1.15
	ζ_r	−0.2912	−0.281	−0.066
	ω_r	0.2443	0.557	0.456
$N^{r}_{\delta_a}$	A_r	−0.0075	−0.0129	−0.026
	ζ	0.505	−0.8	−0.454
	ω	0.7713	1.19	0.959
	$1/T_{r_{\delta_a}}$	−0.76	0.8	1.056
$N^{\varphi\ r}_{\delta_a \delta_r}$	A_{φ_r}	0.06	0.024	0.028
	$1/T_{\varphi_r}$	0.015	0.0898	0.148
$N^{r\ \beta}_{\delta_a \delta_r}$	A_{β_r}		−0.00003	−0.0012
	ζ_{β_r}	−1.93	−0.04	0.0
	ω_{β_r}	no roots	15.	6.0
$N^{\varphi\ \beta}_{\delta_a \delta_r}$	$A_{\beta_{\varphi}}$	−0.06	−0.00041	−0.00089
	$1/T_{\varphi_{\beta}}$	no root	59.0	32.0

TABLE D-II (Concluded)

TRANSFER FUNCTION		BEGIN TRANSITION ($U \doteq 0$ KTS)	MIDTRANSITION ($U \doteq 60$ KTS)	END TRANSITION ($U \doteq 120$ KTS)
$N^{\beta}_{\delta_r}$	A_β	0.208	0.00245	0.00464
	$1/T_{\beta_1}$	0.326	−0.308	−0.024
	$1/T_{\beta_2}$	9.52	0.587	1.076
	$1/T_{\beta_3}$	none	62.0	28.77
$N^{y}_{\delta_a}$	A_y	9.17	5.39	6.22
	ζ_y	(0.2119)	0.313	0.325
	ω_y	(0.0132)	0.518	0.857

TABLE D-III

LATERAL/DIRECTIONAL DERIVATIVES AND TRANSFER FUNCTION FACTORS

Flight Conditions: U_o = 50.6 ft/sec; W = 2,900 lb: γ (approach) = 11 deg

Constant Derivatives: Y_{δ_a} = 2.24 (ft/sec^2)/in.; L_{δ_a} = 1.72 (rad/sec^2)/in.;
L_p = −10 1/sec; N_v = 0.02 1/ft-sec
(Derivatives obtained from Ref. 22)

Variable Derivatives:							
L_v 1/ft-sec		−0.01		−0.02		−0.05	
Rating		3-1/2	6-1/2	3-1/2	6-1/2	3-1/2	6-1/2
Y_v 1/sec		−0.029	−0.029	−0.042	−0.042	−0.081	−0.081
Y_{δ_r} (ft/sec^2)/in.		−0.64	−0.48	−0.80	−0.48	−1.12	−0.48
N_r 1/sec		−2.2	−0.7	−3.3	−0.7	−5.7	−0.7
N_{δ_r} (rad/sec^2)/in.		0.8	0.6	1.0	0.6	1.4	0.6
Transfer Function Factors:							
Δ Denom.	$1/T_s$	0.075	0.022	2.95	0.042	5.52	0.097
	$1/T_R$	10.0	10.0	10.0	10.0	10.0	10.0
	ζ_d $(1/T_{d_1})$	(0.609)	0.344	0.707	0.335	0.306	0.311
	ω_d $(1/T_{d_2})$	(1.54)	1.02	0.268	1.04	0.408	1.07
$N_{\varphi\delta_a}$	A_φ	1.72	1.72	1.72	1.72	1.72	1.72
	ζ_φ $(1/T_{\varphi_1})$	(0.683)	0.354	(0.36)	0.35	(0.20)	0.35
	ω_φ $(1/T_{\varphi_2})$	(1.53)	1.01	(2.96)	1.01	(5.52)	1.01
$N_{r\delta_a}$	A_ψ	0.045	0.045	0.045	0.045	0.045	0.045
	ζ_ψ $(1/T_{\psi_1})$	(4.51)	(4.51)	(4.51)	(4.51)	(4.51)	(4.51)
	ω_ψ $(1/T_{\psi_2})$	(5.48)	(5.48)	(5.48)	(5.48)	(5.48)	(5.48)
$N_{r\delta_r}$	A_r	0.8	0.6	1.0	0.6	1.4	0.6
	$1/T_{r_1}$	10.0	10.0	10.0	10.0	10.0	10.0
	ζ_r	0.027	0.027	0.039	0.039	0.061	0.061
	ω_r	0.179	0.179	0.254	0.254	0.401	0.401
$N^{\varphi\ r}_{\delta_a\delta_r}$	A_{φ_r}	1.37	1.03	1.72	1.03	2.41	1.03
	$1/T_{\varphi_r}$	0	0	0	0	0	0

TABLE D-IV

LATERAL/DIRECTIONAL DERIVATIVES AND TRANSFER FUNCTIONS
CONTROL COUPLING STUDY

(Derivatives obtained from Ref. 25)

BASIC CONSTANT DERIVATIVES		
$Y_v = -0.042$	$L_v = -0.02$	$U_o = 50.6$ ft/sec = 30k
$Y_p = -5.45$	$L_p = -4.2$	$N_v = 0.02$
$Y_r = 2.65$	$L_{\delta_a} = 0.67$	$N_r = -3.3$
$Y_{\delta_a} = 1.0$		$N_{\delta_r} = 0.80$
$Y_{\delta_r} = -0.64$		

DENOMINATOR	
$1/T_R = 4.2$ $1/T_s = 3.0$ $\zeta_d = 0.35$ $\omega_d = 0.41$	$\Delta = (s+3.0)(s+4.2)[s^2+2(0.35)(0.41)s+(0.41)^2]$

TABLE D-IV (Continued)

a) Regulatory Control

$$\left.\frac{\psi}{\delta_r}\right]_{\varphi \rightarrow \delta_a}$$

CONTROL FACTOR FOR VARIATIONS IN CROSS COUPLING DERIVATIVES, N_{δ_a} AND L_{δ_r}

Δ Denom.	N_{δ_a}	0.75	0	−0.2	−0.75	0	0	0
	L_{δ_r}	0	0	0	0	1.0	−0.4	−1.2
	$1/T_s$	3.0	3.0	3.0	3.0	3.0	3.0	3.0
	$1/T_R$	4.2	4.2	4.2	4.2	4.2	4.2	4.2
	ζ_d	0.35	0.35	0.35	0.35	0.35	0.35	0.35
	ω_d	0.41	0.41	0.41	0.41	0.41	0.41	0.41
$N^{\varphi}_{\delta_a}$	A_{φ}	0.67	0.67	0.67	0.67	0.67	0.67	0.67
	$1/T_{\varphi_1}$	0.91	0.36	0.24	−0.024	0.36	0.36	0.36
	$1/T_{\varphi_2}$	2.4	2.95	3.1	3.34	2.95	2.95	2.95
$N^{r}_{\delta_r}$	A_r	0.8	0.8	0.8	0.8	0.8	0.8	0.8
	$1/T_r$	4.24	4.24	4.24	4.24	4.27	4.22	4.18
	ζ_r $(1/T_{r_2})$	−0.013	−0.013	−0.013	−0.013	−0.046	0.014	(0.3)
	ω_r $(1/T_{r_3})$	0.39	0.39	0.39	0.39	0.581	0.276	(−0.26)
$N^{\varphi\ r}_{\delta_a \delta_r}$	A_{φ_r}	0.53	0.53	0.53	0.53	0.53	0.53	0.53
	$1/T_{\varphi_r}$	−0.0217	−0.0038	0.0009	0.014	−0.041	0.011	0.041

$$N^{\varphi}_{\delta_a} = A_{\varphi}(s + 1/T_{\varphi_1})(s + 1/T_{\varphi_2})$$

$$N^{\psi}_{\delta_r} = A_r(s + 1/T_r)[s^2 + 2\zeta_r\omega_r s + \omega_r^2]$$

$$N^{\varphi\ r}_{\delta_a \delta_r} = A_{\varphi_r}(s + 1/T_{\varphi_r})$$

$$\left.\frac{\psi}{\delta_r}\right]_{\varphi \rightarrow \delta_a} = \frac{Y_{p_\psi}[N^{r}_{\delta_r} + Y_{p_\varphi} N^{\varphi\ r}_{\delta_a \delta_r}]}{s[\Delta + Y_{p_\varphi} N^{\varphi}_{\delta_a}]}$$

TABLE D-IV (Concluded)

b) Maneuvering Control

$$\left.\frac{\psi}{\delta_a}\right]_{\substack{\varphi \rightarrow \delta_a \\ \beta \rightarrow \delta_r}}$$

Δ Denom.	N_{δ_a}	−0.5	−0.75	0.75	−0.75	0.75
	L_{δ_r}	0.6	0.75	−1.0	0	0.75
	$1/T_s$	3.0	3.0	3.0	3.0	3.0
	$1/T_R$	4.2	4.2	4.2	4.2	4.2
	ζ_d	0.35	0.35	0.35	0.35	0.35
	ω_d	0.41	0.41	0.41	0.41	0.41
$N^{\varphi}_{\delta_a}$	A_{φ}	0.67	0.67	0.67	0.67	0.67
	$1/T_{\varphi_1}$ (ζ_d)	0.087	−0.024	0.83	−0.024	0.83
	$1/T_{\varphi_2}$ (ω_d)	3.22	3.3	2.5	3.3	2.5
$N^{\beta}_{\delta_r}$	A_{β}	−0.0128	−0.0128	−0.0128	−0.0128	−0.0128
	$1/T_{\beta_1}$	−0.36	−0.45	0.67	0	−0.45
	$1/T_{\beta_2}$	4.04	4.0	4.65	4.0	4.0
	$1/T_{\beta_3}$	68.0	69.5	53	66.0	69.5
$N^{r}_{\delta_a}$	A_r	−0.5	−0.75	0.75	−0.75	0.75
	$1/T_{r_1}$	4.04	4.2	4.3	4.2	4.3
	ζ_r $(1/T_{r_2})$	(−0.217)	0.044	−0.043	0.044	−0.044
	ω_r $(1/T_{r_3})$	(0.24)	0.128	0.53	0.128	0.53
$N^{\beta\ \varphi}_{\delta_r \delta_a}$	$A_{\beta\varphi}$	−0.021	−0.0236	0.011	−0.0084	−0.0236
	$1/T_{\beta_\varphi}$	42.0	56.0	−104	67.0	2.23
$N^{\beta\ r}_{\delta_r \delta_a}$	A_{β_r}	−0.0096	−0.010	−0.025	−0.0064	−0.0064
	ζ_{β_r}	−0.35	−0.2	−0.112	0.28	(0)
	ω_{β_r}	7.5	5.7	5.69	7.3	(4.2)

APPENDIX E

CALCULATION OF CLOSED-LOOP RMS GUST RESPONSES FOR LATERAL/DIRECTIONAL MODE

For analytical purposes it is desirable to have a random v-gust input spectrum that is simple in form but adequately representative of the actual gust generator used in the test (see Ref. 26). Such a form, used in Ref. 33 and shown there to be representative of the v-gust generator, is the simple gust spectrum

$$\Phi_{v_g} = \frac{2\omega_g \sigma_{v_g}^2}{\omega^2 + \omega_g^2} \tag{E-1}$$

This corresponds to the passage of white noise through a first-order filter with a transfer function

$$Y_f = \frac{\sqrt{2\omega_g}\ \sigma_{v_g}}{s + \omega_g} \tag{E-2}$$

The gust break frequency ω_g was chosen as 0.5 rad/sec to match the actual case of Ref. 26.

The transfer functions of the above responses to the side gust, v_g, with both the ψ and φ loops closed are given below:

$$\left.\frac{\psi}{v_g}\right]_{\substack{\varphi \to \delta_a \\ \psi \to \delta_r}} = \frac{\overbrace{N^{r}_{v_g} + Y_{p_\varphi} N^{r \cdot \varphi}_{v_g \delta_a}}^{N^{r'}_{v_g}}}{s\Delta''} \tag{E-3}$$

$$\left.\frac{\varphi}{v_g}\right]_{\substack{\varphi \to \delta_a \\ \psi \to \delta_r}} = \frac{\overbrace{sN^{\varphi}_{v_g} + Y_{p_\psi} N^{\varphi\ r}_{v_g \delta_r}}^{N^{\varphi'}_{v_g}}}{\Delta''} \tag{E-4}$$

$$\frac{N_{\delta_r}\delta_r}{v_g} = Y_{p_\psi}\left.\frac{\psi}{v_g}\right]_{\substack{\varphi \to \delta_a \\ \psi \to \delta_r}} \tag{E-5}$$

$$\frac{L_{\delta_a}\delta_a}{v_g} = Y_{p_\varphi}\left.\frac{\varphi}{v_g}\right]_{\substack{\varphi \to \delta_a \\ \psi \to \delta_r}} \tag{E-6}$$

where $$\Delta'' = \frac{s\left(\Delta_{lat} + Y_{p_\varphi}N^{\varphi}_{\delta_a}\right) + Y_{p_\psi}\left(N^{r}_{\delta_r} + Y_{p_\varphi}N^{r\ \varphi}_{\delta_r\delta_a}\right)}{s\left(s + \frac{4}{\tau}\right)^4}$$

$$N^{r}_{v_g} = N_v s^2(s - L_p)$$

$$N^{r\ \varphi}_{v_g\delta_a} = L_{\delta_a}N_v s$$

$$N^{\varphi}_{v_g} = L_v s(s - N_r)$$

$$N_{v_g\delta_r} = N_{\delta_r}L_v s$$

The mean-square values of ψ, φ, $N_{\delta_r}\delta_r$, and $L_{\delta_a}\delta_a$ were calculated from the response spectra:

$$\Phi_\lambda = \left[\frac{\lambda}{v_g}(j\omega)\right]^2 \Phi_{v_g}$$

$$\text{for} \qquad \lambda = \psi,\ \varphi,\ N_{\delta_r}\delta_r,\ \text{or}\ L_{\delta_a}\delta_a \tag{E-7}$$

Φ_{v_g} is the gust spectrum of Eq. E-1 and $\lambda/v_g(j\omega)$ is the transfer function of λ to v_g gust inputs with both φ and ψ loops closed. Equation E-7 can also be written

$$\Phi_\lambda = \left|Y_\lambda(j\omega)\right|^2 \tag{E-8}$$

$$Y_\lambda(j\omega) = \frac{\lambda}{v_g}(j\omega)$$

The mean-squared values were computed by numerically integrating the spectra from Eq. E-8.

APPENDIX F

SYSTEMS SURVEYS SHOWING EFFECTS OF RUDDER COUPLING TERMS, L_{δ_r}, OR MANUAL ATTITUDE CONTROL TASK

This appendix presents the systems surveys showing the effects of rudder coupling terms, L_{δ_r}, or manual attitude control task using the technique $\psi \rightarrow \delta_r$, $\varphi \rightarrow \delta_a$. Three levels of the rolling moment due to rudder, L_{δ_r}, are examined for the case where adverse aileron yaw, N_{δ_a}, is zero. RMS gust responses (σ_ψ and σ_φ) to a side gust for the same cases are also presented. These results illustrate that the rudder coupling term L_{δ_r} (i.e., when $N_{\delta_a} = 0$) does not significantly affect regulatory control.

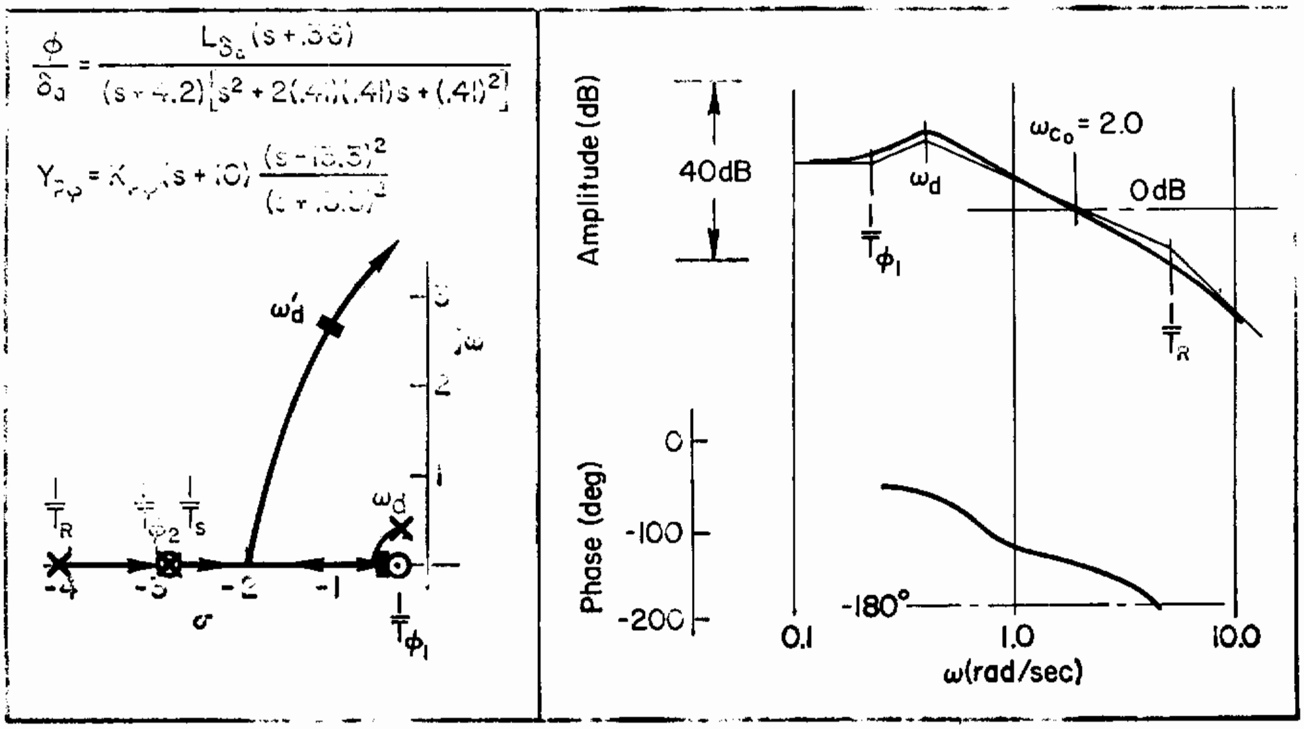

For Both Loops Closed at 2.0 rad/sec

$\sigma_\phi / \sigma_{v_g}$ = .104 rad/ft/sec

$\sigma_\psi / \sigma_{v_g}$ = .154 rad/ft/sec

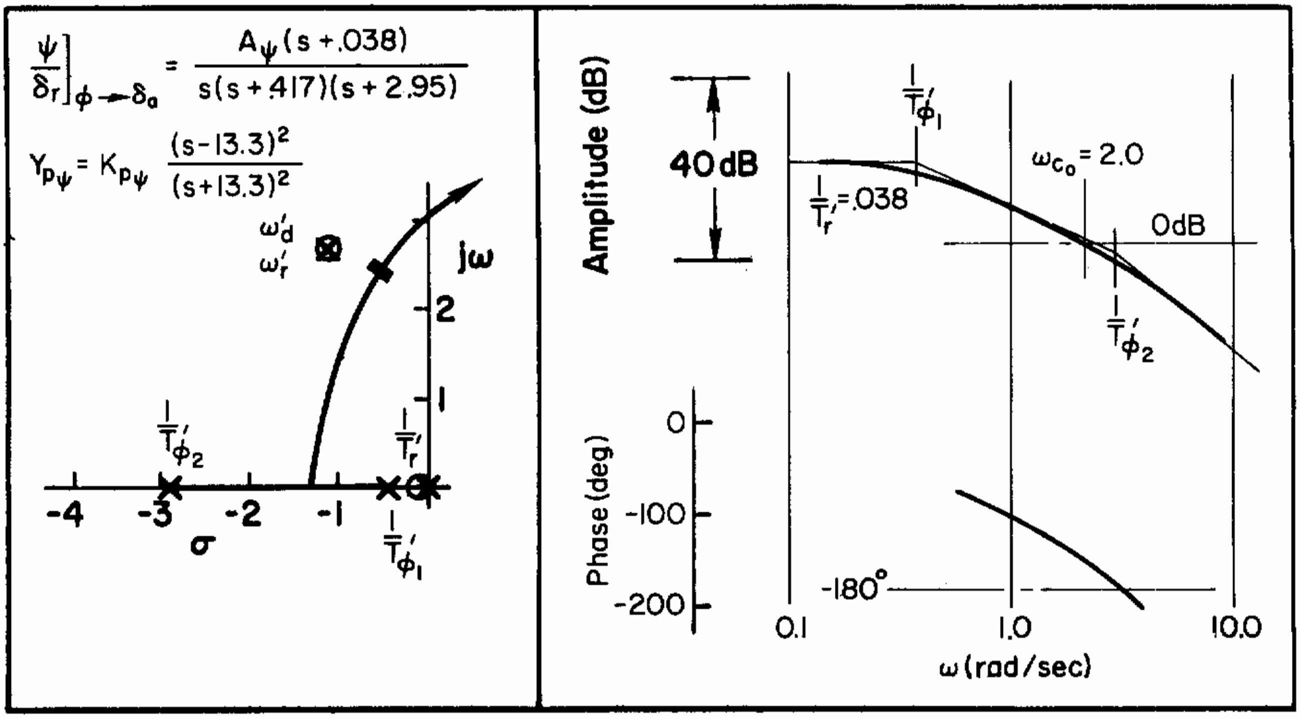

Figure F-1. Heading Closure with Rudder for $N_{\delta_a} = 0$, $L_{\delta_r} = -0.4$ and Pilot Rating of 3-1/2

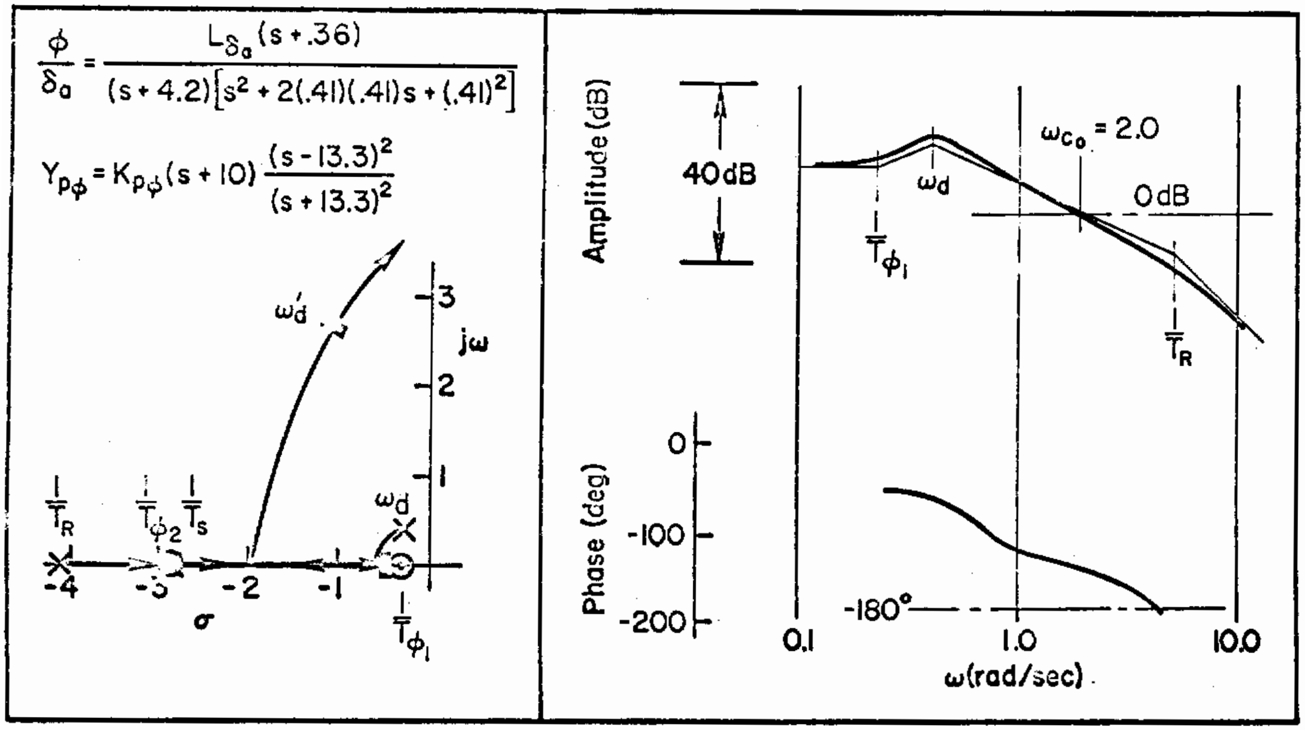

For Both Loops Closed at 2.0 rad/sec

$\sigma_\phi / \sigma_{v_g} = .105$ rad/ft/sec

$\sigma_\psi / \sigma_{v_g} = .154$ rad/ft/sec

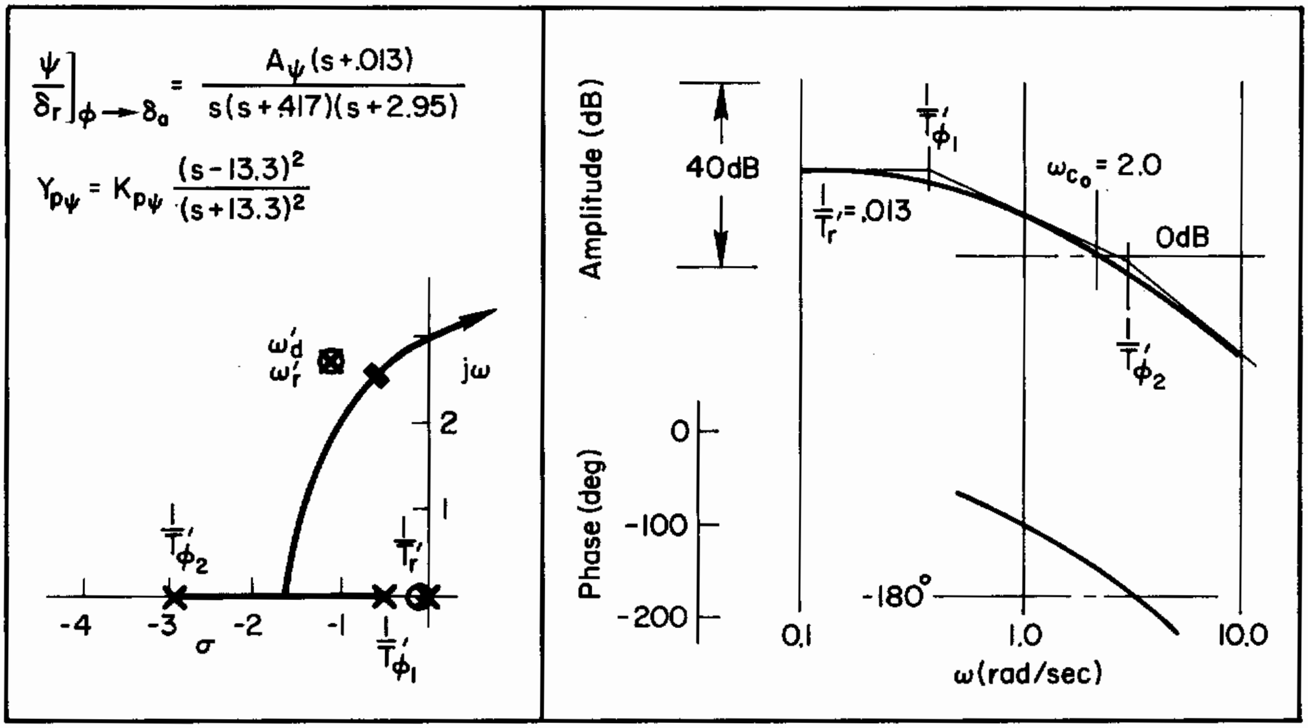

Figure F-2. Heading Closure with Rudder for $N_{\delta_a} = 0$, $L_{\delta_r} = -1.2$ and Pilot Rating of 6-1/2

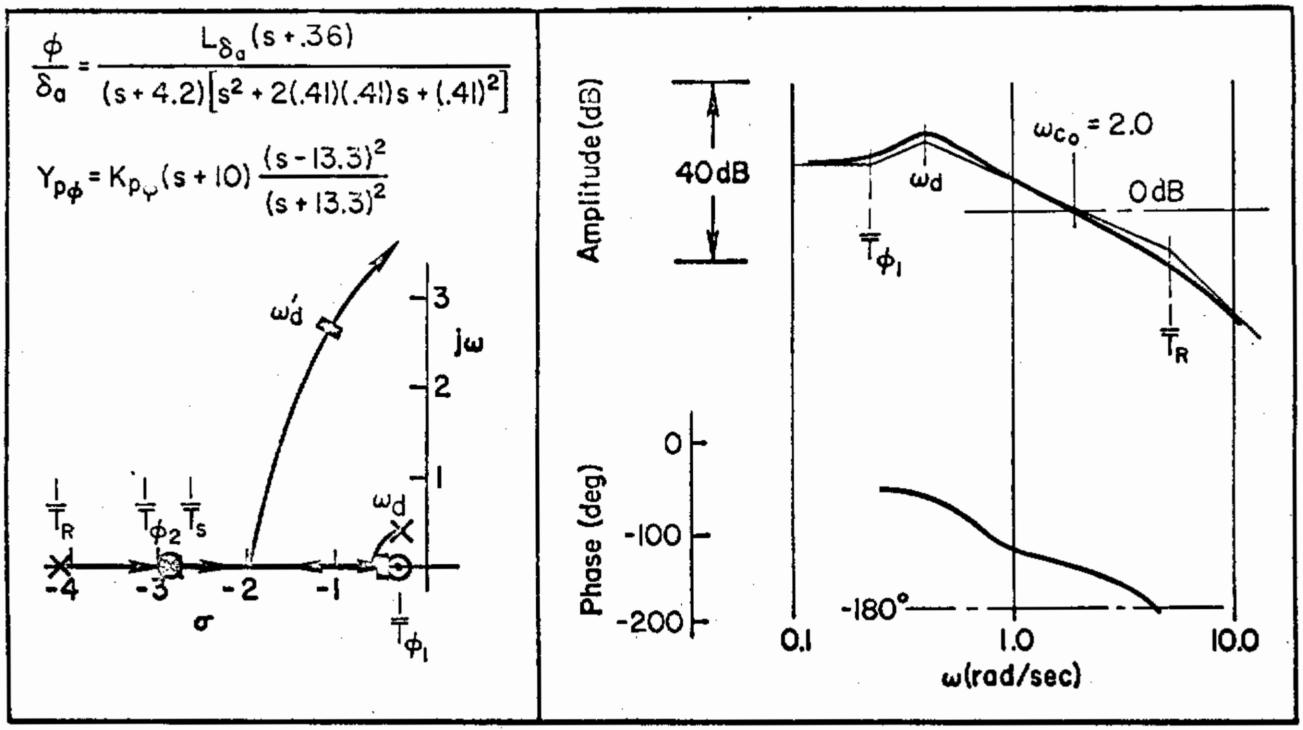

For Both Loops Closed at 2.0 rad/sec

σ_ϕ/σ_{v_g} = .102 rad/ft/sec

σ_ψ/σ_{v_g} = .153 rad/ft/sec

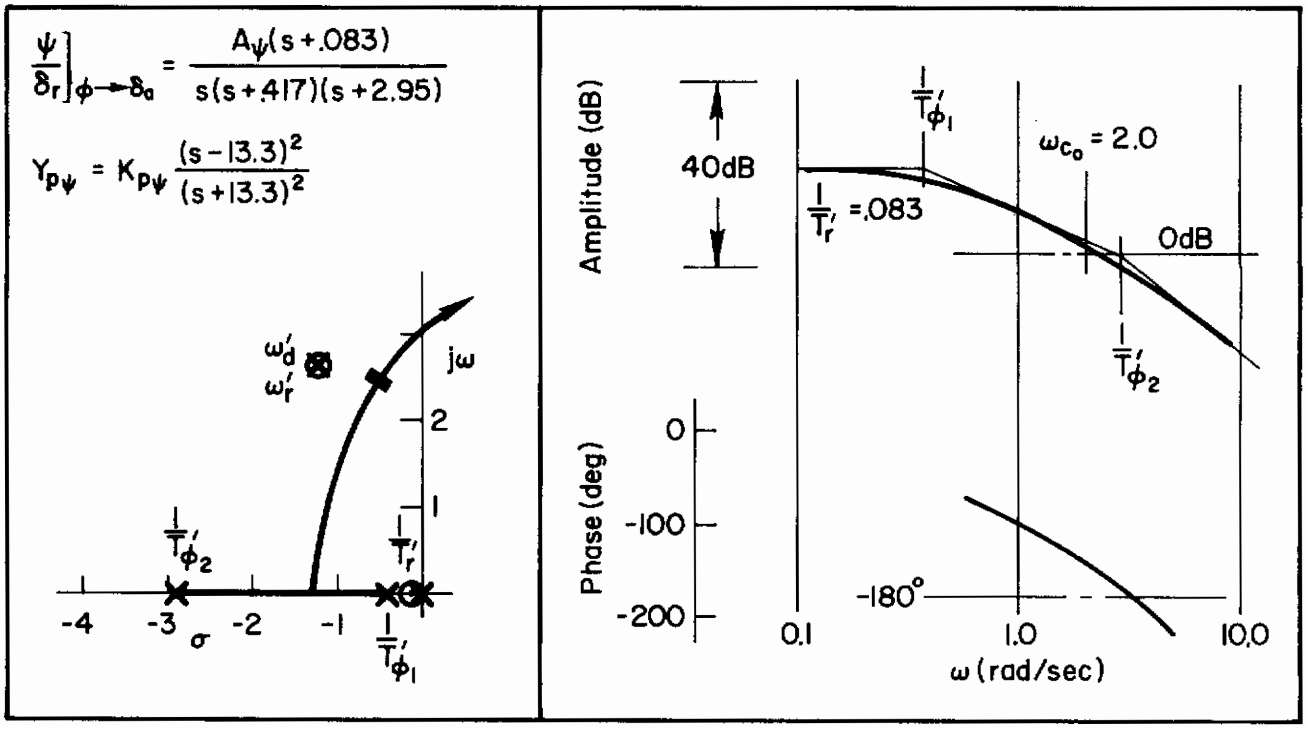

Figure F-3. Heading Closure with Rudder for $N_{\delta_a} = 0$, $L_{\delta_r} = +1.0$ and Pilot Rating of 6-1/2

Unclassified
Security Classification

DOCUMENT CONTROL DATA - R & D

(Security classification of title, body of abstract and indexing annotation must be entered when the overall report is classified)

1. ORIGINATING ACTIVITY *(Corporate author)* Systems Technology, Inc. 13766 S. Hawthorne Blvd. Hawthorne, California 90250	2a. REPORT SECURITY CLASSIFICATION Unclassified 2b. GROUP N/A

3. REPORT TITLE

Analysis of VTOL Handling Qualities Requirements
Part II -- Lateral-Directional Hover and Transition

4. DESCRIPTIVE NOTES *(Type of report and inclusive dates)*
Final Report -- July 1968-January 1970

5. AUTHOR(S) *(First name, middle initial, last name)*
Craig, Samuel J.
Campbell, Anthony

6. REPORT DATE January 1970	7a. TOTAL NO. OF PAGES 224	7b. NO. OF REFS 38
8a. CONTRACT OR GRANT NO. AF33(615)-3736 b. PROJECT NO. 698DC c. Task Nr. 698DC 00 001 d.	9a. ORIGINATOR'S REPORT NUMBER(S) STI TR 181-1 9b. OTHER REPORT NO(S) *(Any other numbers that may be assigned this report)* AFFDL-TR-67-179, Part II	

10. DISTRIBUTION STATEMENT
This document is subject to special export controls and such transmittal to foreign governments or foreign nationals may be made only with prior approval of the Handling Qualities Group, Control Criteria Branch, Air Force Flight Dynamics Laboratory, Wright-Patterson AFB, Ohio 45433

11. SUPPLEMENTARY NOTES N/A	12. SPONSORING MILITARY ACTIVITY AFFDL (FDCC) Wright-Patterson AFB, Ohio 45433

13. ABSTRACT

Analyses of available handling qualities data were performed to determine lateral/directional dynamic requirements for VTOL aircraft in hover and low speed flight.

The basis for this treatment is an examination of the pilot/vehicle as a closed-loop servo system. The quasi-linear pilot describing function is applied. The results of the studies suggest that the primary factors identifying satisfactory and unacceptable hover mode dynamic features are related to the closed-loop deficiencies.

Detailed consideration is made of the control task and piloting functions in transition flight. The results of this generic appraisal are evoked to confirm and justify preliminary lateral/directional requirement for control in transition.

DD FORM 1 NOV 65 1473

Unclassified
Security Classification

Unclassified
Security Classification

14. KEY WORDS	LINK A		LINK B		LINK C	
	ROLE	WT	ROLE	WT	ROLE	WT
VTOL						
Handling Qualities						
Pilot Vehicle Analyses						
Lateral-Directional Hover						
Lateral-Directional Transition						

Unclassified
Security Classification